

Petrological, mineralogical and geochemical
investigations of Late Mesozoic magmatism in
eastern China:
Implications for tectonic evolution and crust-mantle
interaction

Von der Naturwissenschaftlichen Fakultät
der Gottfried Wilhelm Leibniz Universität Hannover
zur Erlangung des Grades
Doktor der Naturwissenschaften
Dr. rer. nat.

genehmigte Dissertation

von

Chao Zhang

geboren am 09.Feb.1982 in Zhenjiang, China

2012

Referent: Prof. Dr. François Holtz
Korreferent: Prof. Dr. Jürgen Koepke
Tag der Promotion: 13 April 2012

Erklärung zur Dissertation

gemäß §6(1) der Promotionsordnung der Naturwissenschaftlichen Fakultät der
Gottfried Wilhelm Leibniz Universität Hannover

für die Promotion zum Dr. rer. nat

Hierdurch erkläre ich, dass die Dissertation mit dem Titel

**“Petrological, mineralogical and geochemical investigations of Late Mesozoic
magmatism in eastern China: Implications for tectonic evolution and crust-
mantle interaction“**

selbstständig verfasst und alle benutzten Hilfsmittel und Quellen sowie
gegebenenfalls die zu Hilfeleistung herangezogene Institutionen vollständig
angegeben wurden.

Die Dissertation wurde nicht schon als Masterarbeit, Diplomarbeit oder andere
Prüfungsarbeit verwendet.

Hannover, den 13 April 2012

Chao Zhang

ACKNOWLEDGEMENTS

Thanks to the acceptance letter from Professor Francois Holtz which arrived at me via faxing on 9 January 2008, I could then have the chance to perform my PhD study at this ideal institute. In the past three years, Francois supervised me of scientific investigation in the fields of geochemistry, petrology and mineralogy and manuscript writing, which made this thesis possible. I am very glad that the door of Francois's office has been always opened, and so that any discussion with him could be carried on at any time. During the time when I met study or living problems, the supports, instructions and encouragements from Francois always helped me to find a way. His large quantities of experience on experimental petrology and geochemistry enlarged my mind in understanding physicochemical principals of magmatic processes, and promoted my motivation in performing experimental researches in future. Now, when I finish the thesis, and my PhD study under the supervision of Prof Holtz appears to be drawing to a conclusion, my first acknowledge is to express my heartfelt thanks and deep appreciation to Professor Holtz for all that he has done for me, as which has definitely changed my life.

Before I came to Hannover, all my geological studies, at the China University of Geosciences (Wuhan), were supervised by Professor Changqian Ma. He introduced me into the amazing geology world, and taught me how to decipher the coded ancient rocks and gorgeous mountains. Referring to this thesis, all the sampling works were completed with his assistance. I also thank him for his advice and support about my proposal of studying abroad. During my stay in Hannover, he also offered his suggestion and encouragement per email frequently.

All the staffs of Institute of Mineralogy, as well as the PhD students, have helped me in many kinds of works, such as sample preparation, microprobe use, geological excursions, scientific discussion and professional conferences. I would like to acknowledge these people: Harald Behrens, Jürgen Koepke, Otto Diedrich, Renat Almeev, Roman Botcharnikov, Anna-Maria Welsch, Alexander Bartels, Wanja Dziony, Svenja Germerott, Clemens Kirchner, Annette Quetscher, Tatiana Shishkina, André Stechern and Paul Eric Wolff. I also thank the secretaries, Kristin Kortlang and Sabine Kropp, for their kind help about various documental stuffs. In addition, special thanks go to Jasper Berndt-Gerdes for allowing and guiding me to use the LA-ICP-MS lab at the University of Münster. I would also like to thank my old friend Roger Mason who just retired from a professorship of petrology, for his generous help of polishing the language of my papers submitted for publishing.

My PhD study in Hannover has been financially supported by the China Scholarship Council (CSC), German Academic Exchange Service (DAAD), and DFG (granted to Prof. Francois Holtz). I would like to express my appreciations to these funds.

At last, I want to thank my parents for their continuous understanding and support. My wife, Mrs. Xiaoyan Li, who is studying geology at University of Freiburg (so far way from Hannover!), have demonstrated by her performances that geological issues can be discussed delightfully and fruitfully between a loving couple.

ABSTRACT

The continent of East China underwent widespread Late Mesozoic coeval tectonic–magmatic events, which have largely contributed to the continental growth and differentiation and principally built the modern panorama of lithospheric structure and terrain landscape. The Late Mesozoic massive magmatism (now represented as intrusive and volcanic rocks) took place in both northern and central part of East China, but these two regions differ from each other in terms of spatio-temporal distribution, magma genesis and evolution, geodynamic regime and style of crust–mantle interaction. The eastern North China Craton, geologically identical to the northern part of East China, has been transformed from a region of thick (~200 km) cold continental lithosphere into thin (80–120 km) hot lithosphere with oceanic characteristics. This great transformation was primarily achieved in the Late Mesozoic, but the responsible geodynamic force and tectonic regime have not been fully understood. Almost synchronously, the central part of East China (mainly the Dabie-Sulu orogen and associated basins) underwent remarkable lithospheric extension and associated magmatism, which gave rise to strong uplift and unroofing of the orogen and formation of polymetallic deposits in the adjacent faulted regions. Investigation using the characteristics of the related magmatism as “petroprobe” of these significant geological events would help us better understanding how the lithospheric part of the “Earth Machine” works.

In this study, the magmatic events and their geochemical characteristics are used to deduce geodynamic processes which are useful to clarify the evolution of the East China continent during late Mesozoic time. This dissertation is composed of three parts which are devoted to discuss the following main petrological and tectonic issues: i) tectonic evolution of North China deciphered using volcanic rocks, ii) partial melting of Dabie orogen roots and crust–mantle interaction, and iii) halogen abundance and distribution in mantle- and crust-derived magmas.

1. Tectonic evolution of North China deciphered using volcanic rocks

Several major volcanic zones are distributed across the eastern North China Craton, from northwest to southeast: the Greater Xing’an Range; Jibei-Liaoxi, Xishan, and Songliao Basins, and the Yanji, Huanghua and Ludong volcanic zones. The spatio-temporal distribution patterns and genetic relationships between these volcanic zones have been poorly understood and is one of the major targets of this study. We performed petrological, geochemical and geochronological investigations of the Late Mesozoic volcanic rocks in the Huanghua volcanic zone (depression basin) within the Bohai Bay Basin, which have not been adequately carried out up to now. Zircon LA-ICP-MS and SHRIMP U-Pb dating show that basic-intermediate volcanic rocks were extruded within the Huanghua volcanic zone in the Early Cretaceous at 118.8 ± 1.0 Ma, prior to the Late Cretaceous acid lavas at 71.5 ± 2.6 Ma. The Early Cretaceous basic and intermediate lavas are characterized by strong enrichments in LREE and LILE and depletions in HREE and HFSE, indicating a volcanic arc origin related to oceanic subduction. Formation ages and geochemical features indicate that the Late Cretaceous acid lavas are products of crustal re-melting in an extensional regime. Combined information from all these volcanic zones shows that subduction-related volcanic rocks were generated in the Jibei-Liaoxi and Xishan volcanic zones during the Early Jurassic, about 60 Ma earlier than their analogues extruded in the Huanghua and Ludong volcanic zones during the Early Cretaceous. This trend also exists in the youngest extension-related volcanism in each of these zones: Early Cretaceous asthenosphere-derived alkaline basalts in the northwest and Late Cretaceous in the southwest. A tectonic model of northwestward subduction and continuous oceanward retreat of the Paleo-Pacific Plate is proposed to explain the migration pattern of both arc-related and post-subduction extension-related volcanic rocks. As the subduction zone continuously migrated, active continental margin and backarc regimes successively were prevailing in different parts of North China during the Late Mesozoic times (J1-K2).

2. Partial melting of Dabie lower continental crust and crust–mantle interaction

The central part of East China mainly consists of the Dabie-Sulu orogen and associated foreland and backland basins, and adjacent areas. The Dabie orogen is characterized by massive intrusive rocks which comprise nearly half of the surface. These magmatic rocks are mostly felsic plutons or batholiths, which are predominantly non-adakitic granitoids with minor adakitic components. Previous studies show that the adakitic granitoids in the central and northern Dabie orogen have low Mg-numbers (<45), and low Cr and Ni concentrations, which indicates no interaction between crustal melts and mantle peridotites, and thus excludes a geodynamic model involving lower-crust delamination. The crust of southern Dabie orogen, which is currently thinner

than the northern counterpart, is an optimal region to check whether or not crustal delamination has taken place beneath the Dabie orogen. In this study, high-Mg adakitic components from the southern Dabie orogen are identified. The rocks with adakitic signatures occur as mafic magmatic enclaves enclosed in a low-Mg adakitic felsic host (Meichuan granodioritic pluton). These two types of magmatic rocks were formed by coeval felsic and mafic magmas during the Early Cretaceous (132±2 Ma, zircon U-Pb age). The adakitic signatures of both the felsic and mafic rocks, such as very high Sr (770-1400 ppm), high Sr/Y ratios (40-130), low Y (3.5-21 ppm) and HREE concentrations are interpreted to be features of the primary magmas, indicating that both of them were generated by partial melting of basaltic protoliths at great depths (>15 kbar). The distinctive major element compositions of the felsic and mafic primary magmas could be attributed to different melting temperatures and melting degrees. The mafic enclaves have distinctively high concentrations of MgO (4.4-5.8 wt.%), Cr (229-374 ppm) and Ni (75-163 ppm), indicating a melt-mantle interaction in which olivine is partly consumed while orthopyroxene and/or pyrope are formed under high-pressure. Modeling suggests that 14% of peridotite relative to melt could have been consumed to elevate the Mg-number of melt to the observed values (55-60), and that transformation from orthopyroxene to pyrope in mantle peridotite could have decreased the Al₂O₃ content from 18-19 wt.% in the initial melts to ~15 wt.% in the resultant mafic melts. Moderate negative zircon εHf(t) and bulk εNd(t) values also indicate contributions from both enriched lithospheric mantle and ancient lower crust. The results suggest that a block with amphibolitic composition of the lower continental crust was delaminated into the lithospheric mantle in the Early Cretaceous, which resulted in partial melting of the delaminated crustal rocks and consequently in melt-mantle interaction. Because a hot lithospheric mantle is a prerequisite for the delamination of the overlying lower crust, we propose that this delamination is attributed to lithospheric extension and asthenospheric upwelling along the Yangtze River fault zone in the late Mesozoic, which could have heated up the lithospheric mantle underneath the neighboring southern Dabie orogen.

3. Halogen abundance and distribution in mantle- and crust-derived magmas

In the central Dabie orogen, besides the predominating granitoid batholiths which were formed by crust-derived felsic magmas, there is the occurrence of coeval minor mafic-ultramafic stocks which were formed by mantle-derived mafic magmas. In this study, analogous mantle-derived magmas have also been identified at the eastern boundary of Dabie orogen (close to the Tan-Lu fault), observable as mafic enclaves in the Liujiawa plutonic complex. Magma mixing is demonstrated by both outcrop-scale textures and microstructures. Major and accessory minerals from the four principal lithological units, i.e. gabbro, two-pyroxene diorite, clinopyroxene diorite and hornblende gabbro, were analyzed by electron microprobe to trace the initial properties of magmatic end-members and magma evolution. The study was focused on the concentrations of halogens (F and Cl) in amphiboles, biotites and apatites from the various lithological units, and on their variation along crystallization path. It is demonstrated by the results that the gabbros and two-pyroxene diorite represent mafic magmas without contamination by crustal material, while the clinopyroxene diorites show clear evidence of mixing between low-F mafic and high-F felsic magmas. The hornblende gabbros contain abundant high-Al amphiboles and may have formed at ~860 °C from water-rich mafic magma. For most amphiboles, log(Cl/OH) shows a systematic negative correlation with Mg-number, confirming the effect of Mg-Cl avoidance. Biotites from gabbro and two-pyroxene diorite show a rough positive correlation between log(Cl/OH) and Mg concentration, whereas the biotites from clinopyroxene diorite show a reverse trend. Negative correlations between Cl and F contents are observable for all analyzed apatites. Quantitative modeling and comparison indicate that over the course of decompression (magma ascent or crustal uplift and erosion); the apatites have not been re-equilibrated in terms of volatile contents. The absolute concentrations of Cl and F in melts coexisting with amphiboles, biotites and apatites have been estimated based on available models and newly developed calculation procedures. The modeling results indicate that Cl concentration in melt remained nearly constant over the course of crystallization, and decreased dramatically at low temperatures, as a result of fluid exsolution. In contrast, F concentration in melt remained above 1000 ppm and has not been strongly affected by fluid exsolution, because of its preferred incorporation into melt rather than fluid. Our results also indicate that halogen concentrations in early high-temperature amphibole can be preserved and that these minerals have the potential to indicate halogen abundance in melt of an early magmatic stage. Based on the distribution characteristics of F in magmatic systems, the partitioning relation of F between amphibole and melt has been tentatively built by data regression, which is qualitatively consistent with the Fe-F avoidance rule but needs further quantitative experimental calibration.

Keywords: subduction, delamination, magmatic process

ZUSAMMENFASSUNG

Der ostchinesische Kontinent wurde im späten Mesozoikum von flächendeckenden magmatischen und tektonischen Ereignissen geprägt, die den Aufbau und die Differentiation der kontinentalen Kruste geprägt haben. Ihre Erforschung trägt zu dem Verständnis der heutigen Lithosphäre bei. In dieser Arbeit werden die mesozoischen magmatischen Gesteine mit Hilfe von geochemischen Methoden charakterisiert um daraus geodynamische Prozesse abzuleiten. Die Ergebnisse tragen zum Verständnis der Entwicklung des ostchinesischen Kontinents im späten Mesozoikum bei. Die hier vorgestellte Studie besteht aus drei Teilen, welche die folgenden petrologischen und tektonischen Aspekte behandelt:

1. Tektonisch Entwicklung Nordchinas entschüsselt mit Hilfe von vulkanischen Gesteinen

Geochronologische und geochemische Daten der vulkanischen Hauptzone im östlichen Nordchinas zeigen, dass der subduktionsbezogener Vulkanismus in den Zonen Jibei-Liaoxi und Xishan während des frühen Juras, ca. 60 Ma früher einsetzte als in den vulkanischen Zonen von Huanghua und Ludong (frühe Kreide). Dementsprechend ist eine Migration des Extensionsvulkanismus in diesen Zonen zu beobachten: frühe kreidezeitliche alkali-reiche Basalte in Nordwesten und späte kreidezeitliche alkali-reiche Basalte im Südwesten. Ein tektonisches Modell für die Nordwest gerichtete Subduktion und den kontinuierlichen Ozean gerichteten Rückzug der Paläo-Pazifischen Platte kann mit Hilfe der Migrationsmuster der vulkanischen Gesteine erstellt werden. Dieses Modell berücksichtigt ebenfalls eine Migration der geodynamischen Prozesse, die typisch für Inselbogen und für post-subduktion Extension sind, gleichzeitig mit der Migration der Subduktionszone im späten Mesozoikum (J1-K2).

2. Partielles Aufschmelzen des Dabie Hauptorogens und Krusten-Mantel Interaktion

Spät mesozoische adakitische Granite mit niedrigen Mg Gehalten treten sowohl im nördlichen als auch im südlichen Gebiet des Dabie Orogens auf, wobei adakitische Diorite mit hohem Mg Gehalt nur im südlichen Teil auftreten. Im Rahmen dieser Arbeit wurde eine typische adakitische dioritische Intrusion, der Meichuan Pluton, untersucht. Mafische Enklaven, die im Diorit vorkommen, haben mittlere SiO₂, hohe MgO, Cr, Ni Konzentrationen. Zirkone haben einen negativen εHf(t) und εNd(t) Wert. Dementsprechend sind klare Mantel-Signaturen in diesen Gesteinen zu finden. Eine mögliche Interpretation für die Entstehung der mafischen Enklaven ist, dass sie Produkte von Teilschmelzprozessen in delaminierten Amphiboliten sind, und dass diese Schmelzen anschließend durch Interaktionen mit Mantelgesteinen geochemische verändert wurden. Petrologische und geochemische Befunde bevorzugen ein geodynamisches Modell in dem die untere kontinentale Kruste während der frühen Kreide in lithosphärischen Mantel delaminiert wurde.

3. Verteilung von Halogeniden in Schmelzen aus dem Mantel und der Kruste

Der plutonische Liujiawa Komplex befindet sich an der östlichen Grenzen des Dabie Orogens. Er besteht aus Gesteinen, die aus Teilschmelzen von Mantel- und Krustengesteinen entstanden sind. Anhand der Texturen im Aufschluss und der Mikrostrukturen ist festzustellen, dass die Gesteine aus Mischungen von unterschiedlichen Schmelzen entstanden sind. Die Konzentrationen von Fluor und Chlor wurde in Amphibolen, Biotiten und Apatiten von verschiedenen Lithologien bestimmt um Rückschlüsse zu dem Verhalten der Volatile während der Entstehung und Kristallisation der Schmelzen schließen zu können. Die F-Gehalte von Amphibolen, Biotiten und Apatiten aus krustalen Schmelzen sind deutlich höher als diese von Mineralen, die in Gesteinen mit Mantelkomponenten vorkommen. Die Cl-Gehalte und die F-Gehalte nehmen mit zunehmender Kristallisation (d.h. mit abnehmender Temperatur und Druck) ab. Dieses Verhalten kann mit einer zunehmenden Entgasung eines Fluid-gesättigten Magmas während der Kristallisation erklärt werden.

Schlagwörter: Subduktion, Delamination, magmatische Prozesse

LIST OF PAPERS

This dissertation is based on the following papers which contribute the three parts of the content.

Part I

1. **Zhang C**, Ma C, Liao Q, Zhang J, She Z. 2011. Implications of subduction and subduction zone migration of the Paleo-Pacific Plate beneath eastern North China, based on distribution, geochronology, and geochemistry of Late Mesozoic volcanic rocks. *International Journal of Earth Sciences*, 100, 1665–1684
2. **Zhang C**, Ma C, Liao Q, Zhang J, Xiao D, Fu L, Wang L. 2009. Geochemistry of Late Mesozoic-Cenozoic volcanic rocks in the Huanghua depression, Bohai Bay: Petrogenesis and implications for tectonic transition. *Acta Petrologica Sinica*, 25(5), 1159–1177 (in Chinese with English abstract)

Part II

3. **Zhang C**, Ma C, Holtz F. 2010. Origin of high-Mg adakitic magmatic enclaves from the Meichuan pluton, southern Dabie orogen (central China): Implications for delamination of the lower continental crust and melt-mantle interaction. *Lithos*, 119, 467–484
4. **Zhang C**, Ma C, Holtz F. 2012. Partial melting of hydrous continental lower crust: discussion on the petrogenesis of C-type adakites from the Dabie orogen. *Geological Journal of China Universities*, 18(1), 41-51 (in Chinese with English abstract)

Part III

5. **Zhang C**, Holtz F, Ma C, Wolff P E, Li X. 2012. Tracing the evolution and distribution of F and Cl in plutonic systems from volatile-bearing minerals: A case study from the Liujiawa pluton (Dabie orogen, China). *Contributions to Mineralogy and Petrology*, acceptable after minor revision

TABLE OF CONTENTS

| | |
|------------------------------------|------|
| Acknowledgements..... | iv |
| Abstract..... | v |
| Zusammenfassung..... | vii |
| List of papers..... | viii |
| List of figures..... | xi |
| List of tables..... | xii |
| Curriculum Vitae (Lebenslauf)..... | 190 |

PART I IMPLICATIONS OF SUBDUCTION AND SUBDUCTION ZONE MIGRATION OF THE PALEO-PACIFIC PLATE BENEATH EASTERN NORTH CHINA - BASED ON DISTRIBUTION, GEOCHRONOLOGY AND GEOCHEMISTRY OF LATE MESOZOIC VOLCANIC ROCKS..... 1

| | |
|--|----|
| 1 ABSTRACT..... | 2 |
| 2 INTRODUCTION | 2 |
| 3 GEOLOGICAL SETTING AND PETROLOGY | 4 |
| 4 ANALYTICAL METHODS | 6 |
| 5 RESULTS..... | 7 |
| 5.1 Zircon U-Pb dating..... | 7 |
| 5.2 Geochemistry..... | 9 |
| 6 DISCUSSION | 14 |
| 6.1 Spatio-temporal distribution of Mesozoic volcanic rocks..... | 14 |
| 6.2 Petrogenesis of Mesozoic volcanic rocks..... | 15 |
| 6.3 Migration of arc-related volcanism..... | 17 |
| 6.4 Migration of extension-related volcanism..... | 19 |
| 6.5 Tectonic model | 19 |
| 7 CONCLUSIONS..... | 23 |
| 8 REFERENCES | 24 |

PART II ORIGIN OF HIGH-MG ADAKITIC MAGMATIC ENCLAVES FROM THE MEICHUAN PLUTON, SOUTHERN DABIE OROGEN (CENTRAL CHINA): IMPLICATIONS FOR DELAMINATION OF THE LOWER CONTINENTAL CRUST AND MELT-MANTLE INTERACTION 36

| | |
|---|----|
| 1 ABSTRACT..... | 37 |
| 2 INTRODUCTION | 38 |
| 3 GEOLOGICAL BACKGROUND | 40 |
| 4 FIELD RELATIONSHIPS AND PETROGRAPHY..... | 41 |
| 5 ANALYTICAL METHODS | 43 |
| 6 ANALYTICAL RESULTS..... | 44 |
| 6.1 Zircon CL images and U-Pb dating..... | 44 |
| 6.2 Zircon Lu-Hf isotopic compositions..... | 46 |
| 6.3 Major and trace elements..... | 47 |
| 6.4 Sr-Nd isotopic compositions | 51 |
| 7 DISCUSSION | 52 |
| 7.1 Nature of the mafic enclaves..... | 52 |
| 7.2 Magma hybridization..... | 53 |
| 7.3 Origin of adakitic rocks | 54 |
| 7.3.1 Origin of low-Mg felsic host..... | 57 |
| 7.3.2 Origin of high-Mg MME | 58 |
| 7.4 Geodynamic implications..... | 61 |
| 8 CONCLUSIONS..... | 65 |
| 9 APPENDIX: PETROGENESIS OF DABIE C-TYPE ADAKITE..... | 65 |

| | |
|--|----|
| 9.1 Dispute about C-type adakite | 65 |
| 9.2 Composition of China lower continental crust | 67 |
| 9.3 Partial melting of lower continental crust | 68 |
| 9.3.1 Melting condition | 68 |
| 9.3.2 Melting degree | 71 |
| 9.4 Discussion on the origin of Dabie C-type adakite | 73 |
| 9.4.1 Comparison between Dabie C-type adakite and experimental melts | 73 |
| 9.4.2 Modeling of K ₂ O content with melting degree | 73 |
| 9.5 Summary | 76 |
| 10 REFERENCES | 77 |

**PART III TRACING THE EVOLUTION AND DISTRIBUTION OF F AND CL IN
PLUTONIC SYSTEMS FROM VOLATILE-BEARING MINERALS: A CASE STUDY FROM
THE LIUJIAWA PLUTON (DABIE OROGEN, CHINA)91**

| | |
|---|-----|
| 1 ABSTRACT | 92 |
| 2 INTRODUCTION | 92 |
| 3 GEOLOGICAL BACKGROUND | 95 |
| 4 SAMPLE DESCRIPTIONS | 96 |
| 4.1 Gabbro (GN) | 97 |
| 4.2 Two-pyroxene diorite (PD) | 98 |
| 4.3 Clinopyroxene diorite (CD) | 99 |
| 4.4 Hornblende gabbro (HG) | 99 |
| 5 ANALYTICAL METHODS | 100 |
| 6 RESULTS | 102 |
| 6.1 Pyroxene | 102 |
| 6.2 Feldspar | 102 |
| 6.3 Amphibole | 103 |
| 6.3.1 Cation distribution | 103 |
| 6.3.2 Halogen distribution | 105 |
| 6.4 Biotite | 106 |
| 6.4.1 Cation distribution | 106 |
| 6.4.2 Halogen distribution | 106 |
| 6.5 Apatite | 108 |
| 6.5.1 Cation distribution | 108 |
| 6.5.2 Halogen distribution | 108 |
| 7 ESTIMATION OF CRYSTALLIZATION CONDITIONS | 110 |
| 7.1 Amphibole | 110 |
| 7.2 Biotite | 111 |
| 7.3 Apatite | 112 |
| 8 CALCULATION PROCEDURE TO DETERMINE PARTITIONING OF CL AND F IN MELT-FLUID SYSTEMS | 113 |
| 8.1 Chlorine | 114 |
| 8.2 Fluorine | 118 |
| 9 ESTIMATION OF CL AND F IN MELTS FROM HYDROUS MINERALS | 121 |
| 9.1 Amphibole-melt-fluid system | 121 |
| 9.2 Biotite-melt-vapor system | 122 |
| 9.3 Apatite-melt-fluid system | 125 |
| 10 DISCUSSION | 130 |
| 10.1 Evolution of F and Cl in melt over the course of crystallization | 130 |
| 10.2 Partitioning of F in amphibole-melt-fluid system | 130 |
| 10.3 Mixing of high-F and low-F magmas | 131 |
| 11 CONCLUDING REMARKS | 132 |
| 12 APPENDIX A: CALCULATION OF H ₂ O SPECIES | 132 |
| 13 APPENDIX B: ESTIMATION OF C _K /C _{NA} IN MELT | 134 |
| 14 REFERENCES | 134 |

List of figures

Part I

| | | |
|-----------|---|----|
| Fig. I-1 | Tectonic sketch of North China..... | 5 |
| Fig. I-2 | Isopachous map of Mesozoic volcanic rocks | 6 |
| Fig. I-3 | Representative CL images of analyzed zircons..... | 8 |
| Fig. I-4 | Zircon U-Pb concordia diagrams..... | 9 |
| Fig. I-5 | Diagrams of major elemental classification of volcanic rocks..... | 10 |
| Fig. I-6 | Diagrams of element abundances plotted versus MgO | 11 |
| Fig. I-7 | Chondrite-normalized REE and N-MORB-normalized patterns..... | 12 |
| Fig. I-8 | Principle Late Mesozoic strata (J1-K2)..... | 13 |
| Fig. I-9 | Variations in trace element and $\epsilon\text{Nd}(t)$ values | 18 |
| Fig. I-10 | Spatio-temporal distribution of Mesozoic volcanic rocks | 20 |

Part II

| | | |
|------------|---|----|
| Fig. II-1 | Geological sketch of the Dabie orogen | 39 |
| Fig. II-2 | Photographs of field relationships between enclaves and host rocks..... | 42 |
| Fig. II-3 | CL images of representative zircons | 45 |
| Fig. II-4 | LA-ICP-MS U-Pb zircon concordia diagrams | 46 |
| Fig. II-5 | Zircon $\epsilon\text{Hf}(t)$ values | 47 |
| Fig. II-6 | Total alkali-silica (TAS) diagram..... | 48 |
| Fig. II-7 | Plots of SiO_2 versus major elements and representative trace elements..... | 49 |
| Fig. II-8 | Chondrite-normalized REE and N-MORB-normalized trace element patterns..... | 50 |
| Fig. II-9 | Initial $^{87}\text{Sr}/^{86}\text{Sr}$ versus $\epsilon\text{Nd}(t)$ ($t=132$ Ma) | 51 |
| Fig. II-10 | Plots of Ba versus Ni and MgO versus Ni..... | 55 |
| Fig. II-11 | Plots of Sr/Y versus Y and SiO_2 versus MgO..... | 56 |
| Fig. II-12 | Geochemical modeling of melt-peridotite interaction..... | 59 |
| Fig. II-13 | Age distribution of Late Mesozoic magmatic rocks | 62 |
| Fig. II-14 | Illustration of the geodynamic model and the origin of the Meichuan pluton..... | 63 |
| Fig. II-15 | Average crustal structure and composition for different tectonic units of China..... | 67 |
| Fig. II-16 | P-T diagram of metamafic rocks at H_2O -undersaturated condition..... | 69 |
| Fig. II-17 | Hypothetical P-T diagram of phase relations in hydrous system..... | 71 |
| Fig. II-18 | Maximum melting degree of metabasalt. | 72 |
| Fig. II-19 | Comparison between the Dabie C-type adakites and some experimental melt..... | 74 |
| Fig. II-20 | Modeling of K_2O content dependent on melt fraction..... | 75 |

Part III

| | | |
|--------------------------|---|-----|
| Fig. III-1 | Position of the Liujiawa pluton in the Dabie orogen..... | 96 |
| Fig. III-2 | Mineral textures of the gabbro (GN)..... | 97 |
| Fig. III-3 | Mineral textures of the two-pyroxene diorite (PD)..... | 98 |
| Fig. III-4 | Mineral textures of the clinopyroxene diorite (CD)..... | 99 |
| Fig. III-5 | Mineral textures of the hornblende gabbro (HG)..... | 100 |
| Fig. III-6 | Amphibole compositions..... | 104 |
| Fig. III-7 | Biotite compositions..... | 107 |
| Fig. III-8 | Apatite compositions..... | 109 |
| Fig. III-9 | Fitting regressions of fluid-melt partitioning coefficients of Cl and F | 120 |
| Fig. III-10 | Modeling of Cl in melt calculated from amphibole compositions..... | 122 |
| Fig. III-11 | Modeling of F and Cl in melt calculated from biotite compositions..... | 124 |
| Fig. III-12 | Modeling of F and Cl in melt calculated from apatite compositions..... | 128 |
| Fig. III-13 | Estimated F and Cl concentration in melt versus temperature..... | 129 |
| Supplementary Fig. III-1 | Time scan of F concentration two Durango apatites..... | 144 |
| Supplementary Fig. III-2 | Pyroxene compositions..... | 144 |
| Supplementary Fig. III-3 | Plagioclase composition..... | 145 |
| Supplementary Fig. III-4 | Nomenclature of amphiboles..... | 146 |
| Supplementary Fig. III-5 | Composition profile of the CD amphibole..... | 147 |

List of tables

Part I

| | |
|--|----|
| Table I-1 LA-ICP-MS U-Pb data of zircons from sample K36-2..... | 30 |
| Table I-2 SHRIMP U-Pb data of zircons from sample F22..... | 31 |
| Table I-3 Elemental compositions of Mesozoic volcanic rocks | 32 |
| Table I-4 Sr and Nd isotopic composition of Late Mesozoic volcanic | 33 |
| Table Supplementary I-1 Supplementary major elemental composition of Late Mesozoic volcanic rocks from Huanghua depression, Bohai Bay Basin..... | 34 |

Part II

| | |
|--|----|
| Table II-1 Zircon U-Pb dating results for the Meichuan pluton..... | 86 |
| Table II-2 Zircon Lu-Hf isotopes for the Meichuan pluton..... | 87 |
| Table II-3 Elemental compositions of the Meichuan pluton..... | 88 |
| Table II-4 Sm-Nd and Rb-Sr isotopic compositions of the Meichuan pluton..... | 90 |

Part III

| | |
|---|-----|
| Table III-1 Estimation of crystallization conditions of amphibole and volatile contents of coexisting melt..... | 141 |
| Table III-2 Estimation of crystallization conditions of biotite and coexisting melt composition..... | 142 |
| Table III-3 Estimation of crystallization conditions of apatite and coexisting melt composition | 143 |
| Supplementary Table III-1 Mineral assemblages of studies rock types from the Liujiawa pluton..... | 148 |
| Supplementary Table III-2 Composition of amphiboles from the Liujiawa pluton..... | 149 |
| Supplementary Table III-3 Composition of biotites from the Liujiawa pluton..... | 171 |
| Supplementary Table III-4 Composition of biotite from the Liujiawa pluton..... | 183 |
| Supplementary Table III-5 Summary of estimation of C_K/C_{Na} in melts..... | 189 |

**Part I Implications of subduction and
subduction zone migration of the Paleo-Pacific
Plate beneath eastern North China - based on
distribution, geochronology and geochemistry of
Late Mesozoic volcanic rocks**

1 Abstract

Several major volcanic zones are distributed across the eastern North China Craton, from northwest to southeast: the Greater Xing'an Range; Jibei-Liaoxi, Xishan, and Songliao Basins, and the Yanji, Huanghua and Ludong volcanic zones. The Huanghua depression within the Bohai Bay Basin, was filled by middle Late Mesozoic volcanic rocks and abundant Cenozoic alkaline basalts. Zircon LA-ICP-MS and SHRIMP U-Pb dating show that basic-intermediate volcanic rocks were extruded in the Early Cretaceous of 118.8 ± 1.0 Ma (weighted mean $^{206}\text{Pb}/^{238}\text{U}$ age), before Late Cretaceous acid lavas at 71.5 ± 2.6 Ma. An inherited zircon from andesite has a Paleoproterozoic core crystallization age of 2424 ± 22 Ma ($^{206}\text{Pb}/^{207}\text{Pb}$ age) indicating that the basement of the Bohai Bay Basin is part of the North China Craton. Early Cretaceous basic and intermediate lavas are characterized by strong enrichments in LREE and LILE and depletions in HREE and HFSE, indicating a volcanic arc origin related to oceanic subduction. Depletion in Zr only occurs in basic and intermediate volcanic rocks, while depletions in Sr and Ti exist only in acid samples, indicating the acid series is not genetically related to the basic-intermediate series. Formation ages and geochemical features indicate that the Late Cretaceous acid lavas are products of crustal remelting in an extensional regime. Combined information from all these volcanic zones shows that subduction-related volcanic rocks were generated in the Jibei-Liaoxi and Xishan volcanic zones during the Early Jurassic, about 60 Ma earlier than their analogues extruded in the Huanghua and Ludong volcanic zones during the Early Cretaceous. This younging trend also exists in the youngest extension-related volcanism in each of these zones: Early Cretaceous asthenosphere-derived alkaline basalts in the northwest and Late Cretaceous in the southwest. A tectonic model of northwestward subduction and continuous oceanward retreat of the Paleo-Pacific Plate is proposed to explain the migration pattern of both arc-related and post-subduction extension-related volcanic rocks. As the subduction zone continuously migrated, active continental margin and backarc regimes successively played their roles in different parts of North China during the Late Mesozoic (J₁-K₂).

2 Introduction

The reactivated Precambrian North China Craton (NCC) has been transformed from a region of thick (~200 km) cold continental lithosphere (Menzies et al. 1993; Griffin et al. 1998) into thin (80~120 km) hot lithosphere with oceanic characteristics (Chi 1988; Fan and Hooper 1989). This great transformation occurred

in the Late Mesozoic and was accompanied by widespread magmatism (Zhai et al. 2004; Wu et al. 2005). However, the mechanism that removed Archean continental lithosphere and the geodynamic setting in which it took place are still not agreed and although many models have been proposed, none have found general acceptance. The models include: delamination of lower crust and mantle (Deng et al. 1996; Gao et al. 1998; Qian et al. 2003; Gao et al. 2004; Wu et al. 2005; Huang et al. 2007; Zhai et al. 2007; Yang and Li 2008), thermo-tectonic destruction of a lithospheric root (Menzies et al. 1993; Menzies and Xu 1998; Griffin et al. 1998; Xu 2001), hydrolytic weakening of subcontinental lithosphere (Niu 2005; Niu 2006), and thinning associated with intracontinental rifting and continental marginal rifting (Ren et al. 2002). There are also many different proposals for tectonic forces that might have driven the thinning process: a global-scale mantle superplume (Jahn et al. 1999; Wilde et al. 2003), subduction of continental lithosphere at the southern boundary of the NCC during collision between South China and North China (Menzies and Xu 1998; Gao et al. 2002), subduction of continental lithosphere at the northern boundary of the NCC during collision between Siberia and the NCC (Meng 2003; Wang et al. 2006a; Guo et al. 2007), and a combination of northward and southward subduction and collision at both boundaries (Zhang et al. 2003; Zhai et al. 2007). None of these theories explain all the data (Wu et al. 2008).

Theories proposing Paleo-Pacific plate subduction give a good explanation of the migration pattern of widespread Late Mesozoic granitoids and volcanic rocks in South China (Zhou and Li 2000; Zhou et al. 2006). After the NCC and South China craton had collided to form a single plate at the T₃/J₁ boundary (Lin and Fuller 1990), a continental margin must have been present to the east of the united East China block and become part of the East Asian continental arc (Şengör and Natal'in 1996). Late Mesozoic subduction of the Paleo-Pacific Plate from the east could have caused lithospheric thinning, tectonic erosion of the NCC and widespread magmatism (Zhao et al. 1994; Wu et al. 2003; Zhao et al. 2004; Sun et al. 2007) as proposed in a recent overview by Wu et al. (2008). More data is needed to determine whether these processes occurred in a backarc setting (Watson et al. 1987; Zheng et al. 2006; Wang et al. 2006a; Xu et al. 2008) or at an active continental margin (Wu et al. 2008) or both, and what were the dominant tectonic regimes. The widespread Late Mesozoic volcanic rocks in the NCC and adjacent areas offer opportunities to obtain relevant tectonic information. Many geochronological and geochemical studies have been carried out on samples from several volcanic zones (Fig. I-1) such as the Greater Xing'an Range (e.g. Zhang et al. 2008c), Songliao Basin (e.g. Wang et al. 2002), Yanji Zone (e.g. Li et al. 2007), Jibei-Liaoxi Zone (e.g. Zhang et al. 2008a; Yang and

Li 2008), Xishan Zone (e.g. Yuan et al. 2006), and Ludong Zone (e.g. Qiu et al. 2002; Zhang et al. 2002) but there have so far been no studies of Mesozoic volcanic rocks in the Bohai Bay Basin.

In this paper, we present zircon U-Pb dates and geochemical data that constrain the timing of volcanism and petrogenesis of Mesozoic volcanic rocks from the Huanghua depression in the Bohai Bay Basin, attempt to discover a spatio-temporal distribution pattern, and develop a tectonic model invoking subduction of the Paleo-Pacific Plate.

3 Geological setting and petrology

The NCC is bounded by the NE China Fold Belt to the north and Qinling-Dabie-Sulu Orogenic Belt to the south (Fig. I-1) and comprises an eastern and a western Archean block separated by the north-south trending 1.8 Ga Proterozoic Central Orogenic Belt (Zhao et al. 2000), both containing cratonic nuclei of Archean to Paleoproterozoic crystalline basement (Liu et al. 1992; Zhao et al. 2001; Zhai and Liu 2003). The western part of the NCC lacks Mesozoic-Cenozoic volcanism, implying that it has been stable since the Mesozoic and we shall not discuss it further. By contrast, igneous rocks are widespread in the eastern part of the NCC (e.g., Wu et al. 2005). From northwest to southeast, the Mesozoic volcanic zones in the eastern NCC and NE China Fold Belt are: the Greater Xing'an Range, the Jibei-Liaoxi zone of northern Hebei Province and western Liaoning Province, the Xishan zone of the Beijing Municipal Region, the Songliao Basin, the Yanji Zone, the Huanghua Zone of the Huanghua depression inside the Bohai Bay Basin, and the Ludong Zone of eastern Shandong Province (Fig. I-1).

The Bohai Bay Basin in the eastern part of the NCC has the thinnest crust and highest geothermal gradient in eastern China (Liu 1987) and is considered to be an incompletely developed backarc basin because of the nature of Cenozoic volcanic rocks (Zhou and Armstrong 1982). Tertiary basaltic lavas occur all over the Basin (Liu et al. 1986; Gao and Zhang 1995; Zhang et al. 2009a), but Mesozoic volcanic rocks are mostly found in the Huanghua depression near the center. The Mesozoic volcanic rocks here are basic, intermediate and acid lavas and tuffs and breccias, often interbedded with terrigenous sediments. Fig. I-2 summarizes the temporal distribution of Mesozoic volcanic rocks from column sections obtained from representative boreholes through Mesozoic volcanic rocks. Acid volcanics are confined to the Fenghuadian district, while intermediate volcanics are more widely

distributed along with basic components. Because of a lack of fossils in associated sediments and reliable isotopic dating of volcanic rocks, the timing and petrogenesis of Mesozoic volcanism has not so far been well constrained.

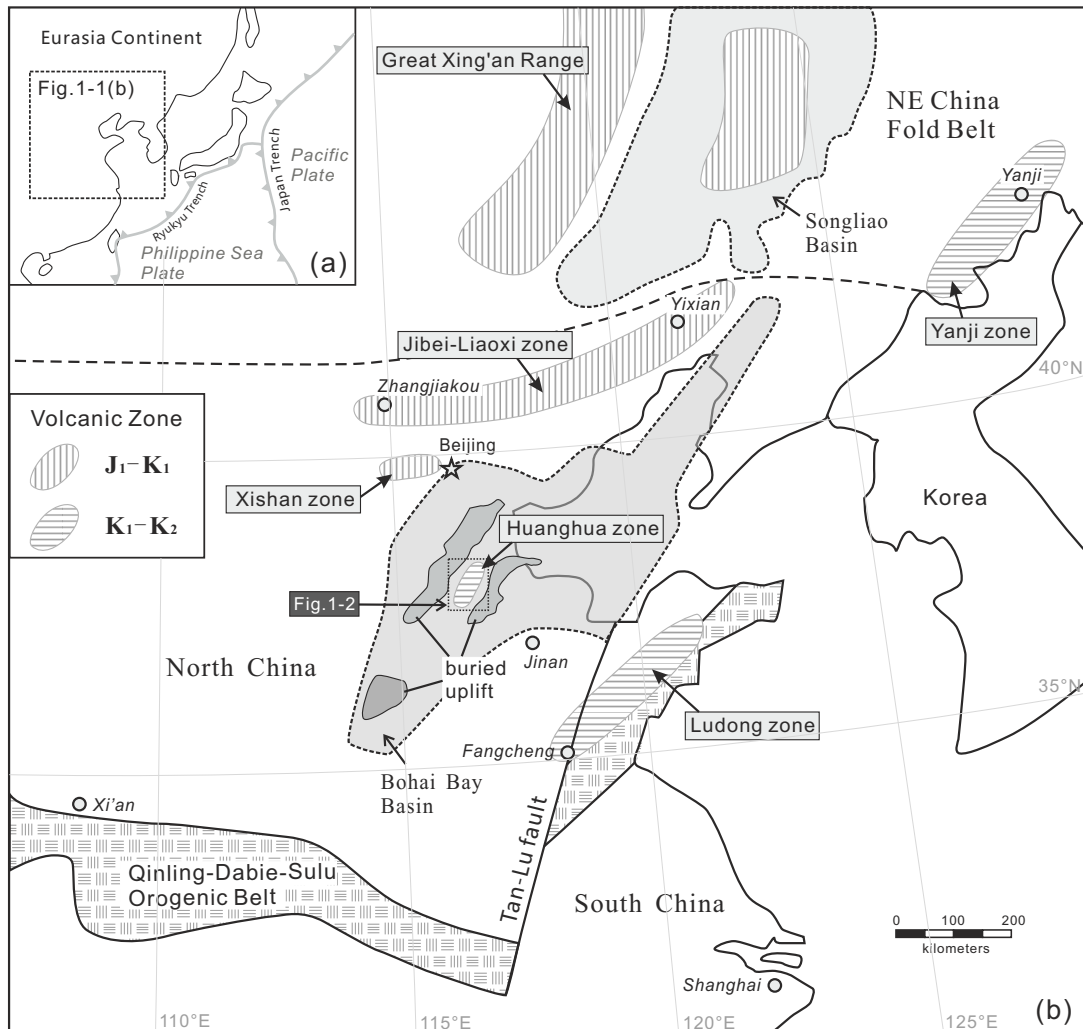


Fig. 1-1 Tectonic sketch of North China, showing the positions of several important volcanic zones.

We have conducted zircon U-Pb dating on two samples, one of andesitic lava (sample K36-2) from borehole Kou36, and one of rhyolitic lava (sample F22) from borehole Feng22. Sample K36-2 has porphyritic texture and no lineation. The phenocrysts are amphibole and biotite and most have suffered secondary alteration giving rise to magnetite and fine-grained muscovite. Sample F22 is also porphyritic with K-feldspar and a few biotite phenocrysts and displays typical rhyolite flow lamination and lineation without secondary alteration. Basaltic lava (sample K12) from borehole Kou12 contains iddingsite phenocrysts almost entirely replacing the original olivine and abundant plagioclase microcrysts, and is cut by numerous tiny

calcite veins visible in thin section. The secondary alteration in samples K36-2 and K12 has had a significant influence on major element compositions but only a small influence on trace elements which will be discussed later.

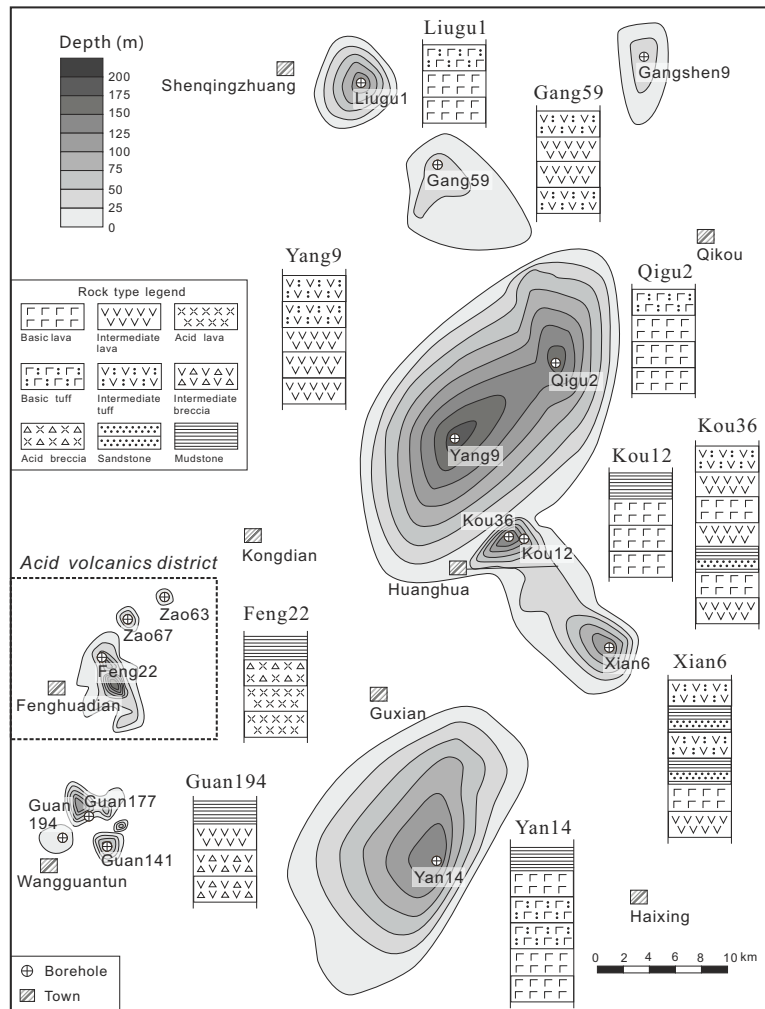


Fig. I-2 Isopachous map of Mesozoic volcanic rocks in the Huanghua depression, Bohai Bay basin. Strata columns of principle borehole are showed (vertical length is not scaled). Note the acid volcanic strata is restricted in the southwest near the Fenghuadian Town, while intermediate and basic volcanics are closely related and often interbedded each other. The distribution and depth are constrained by data of about 80 boreholes which meet Mesozoic volcanic rocks. Because a great number of boreholes in the area do not go through Cenozoic sediments, the actual distribution of Mesozoic volcanic strata might be wider than discovered.

4 Analytical methods

Zircons were separated and hand-picked from crushed rock samples for U-Pb dating and mounted in epoxy resin. Sections were ground down to about 1/3

thickness to expose grain centers, and cathodoluminescence (CL) imaging conducted to reveal the internal structure of zircon grains. Zircon U-Pb dating for sample F22 was performed using a sensitive high-resolution ion microprobe (SHRIMP II) at the Beijing SHRIMP Center, Chinese Academy of Geological Sciences, instrumental condition and analytical procedures given by Wan et al. (2005). Zircons from sample K36-2 were analyzed using Inductively Coupled Plasma-Mass Spectrometry (ICP-MS) Agilent 1700a coupled to a GeoLas 2005 DUV 193 nm UArF laser at the State Key Laboratory of Geological Processes and Mineral Resources, China University of Geosciences (Wuhan), instrumental conditions and analytical procedure described by Yuan et al. (2004). Analyses of major and trace element compositions were performed at the Analytical Institute of Hubei Bureau of Geology and Mineral Resources. Major element oxides were measured using a Regaku 3080E XRF spectrometer, and trace elements were measured with Inductively Coupled Plasma-Atomic Emission Spectrometry (ICP-AES). Relative standard deviation is < 5% for major elements, < 4% for REE and Y, and 5-10% for trace elements. Sr and Nd isotopic analyses were performed at the State Key Laboratory of Geological Processes and Mineral Resources, China University of Geosciences (Wuhan), using a Finnegan MAT-261 multicollector mass spectrometer. Analyses of NBS987 and La Jolla gave $^{87}\text{Sr}/^{86}\text{Sr} = 0.710289 \pm 4$ (2σ) and $^{143}\text{Nd}/^{144}\text{Nd} = 0.511845 \pm 2$ (2σ), respectively. Total procedural Sr and Nd blanks were < 1 ng and < 50 pg, respectively. Detailed analytical procedures for elemental and Sr-Nd isotopic measurements are given by Gao et al. (1999).

5 Results

5.1 Zircon U-Pb dating

Zircon U-Pb isotopic data for samples K36-2 and F22 are listed in Tables I-1 and I-2. The CL images showed that zircons from sample K36-2 were mostly prismatic with rhythmic oscillatory zoning and large length/width ratios, indicating magmatic crystallization. They were usually incomplete and might have crystallized in the volcanic conduit and subsequently been damaged during eruption (Fig. I-3a). One oval zircon grain displayed weak rhythmic oscillatory zoning in the center surrounded by a homogenous high-luminescence rim, indicating overprinting by high temperature metamorphism on a magmatic core (Vavra et al. 1999). On a U-Pb concordia diagram (Fig. I-4a), 16 analytical spots from 14 prismatic zircon grains formed a cluster close to the concordia curve yielding a weighted mean $^{206}\text{Pb}/^{238}\text{U}$ age of 118.8 ± 1.0 (1σ) Ma that probably represents the crystallization age of the lava. The analytical spot at the center of the oval zircon plotted on the concordia curve

with a $^{206}\text{Pb}/^{207}\text{Pb}$ age of 2424 ± 22 (1σ) Ma, indicating a Paleoproterozoic age of the magmatic protolith and showing that there could have been Archean-Palaeoproterozoic crystalline basement beneath the Bohai Bay Basin. The date is consistent with the peak of crystallization ages in NCC Archean and Palaeoproterozoic basement (Gao et al. 2004), indicating that the Bohai Bay Basin is indeed part of the NCC.

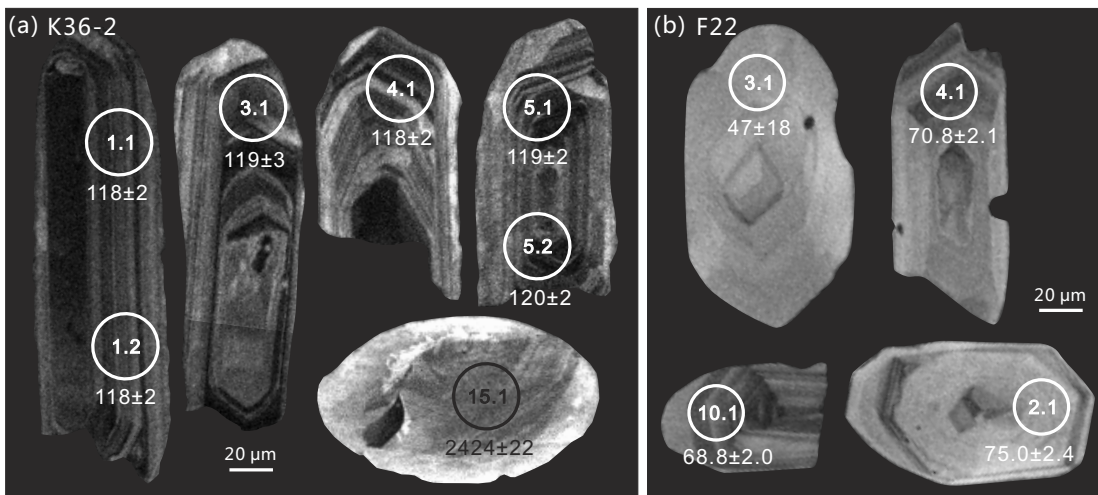


Fig. I-3 Representative CL images of analyzed zircons from (a) K36-2 and (b) F22. The circles and inner figures denote analytical spots and numbers, while the figures under each circle denote respective $^{206}\text{Pb}/^{238}\text{U}$ (Phanerozoic) or $^{206}\text{Pb}/^{207}\text{Pb}$ (Precambrian) ages (Ma).

Most zircon grains from sample F22 showed prismatic texture with rhythmic oscillatory zoning (Fig. I-3b) indicating a magmatic origin. Because the radiogenic ^{207}Pb of some analytic spots was below the detection limit, the U-Pb concordia diagram is presented as total $^{238}\text{U}/^{206}\text{Pb}$ versus total $^{207}\text{Pb}/^{206}\text{Pb}$ (Fig. I-4b). The weighted mean $^{206}\text{Pb}/^{238}\text{U}$ age of 9 spots on 9 zircons was 71.5 ± 2.6 (1σ) Ma, representing the crystallization age of the lava. Analytical spot 3.1 in the outer zone of a zircon grain without clear oscillatory zoning had very low Th and U abundances and yielded a $^{206}\text{Pb}/^{238}\text{U}$ age of 47 ± 18 (1σ) Ma. We infer that it formed by zone-controlled or surface-controlled alteration that has reduced the Th and U abundances and removed the original zircon zoning (Vavra et al. 1999), and so we have excluded this result from the weighted mean age.

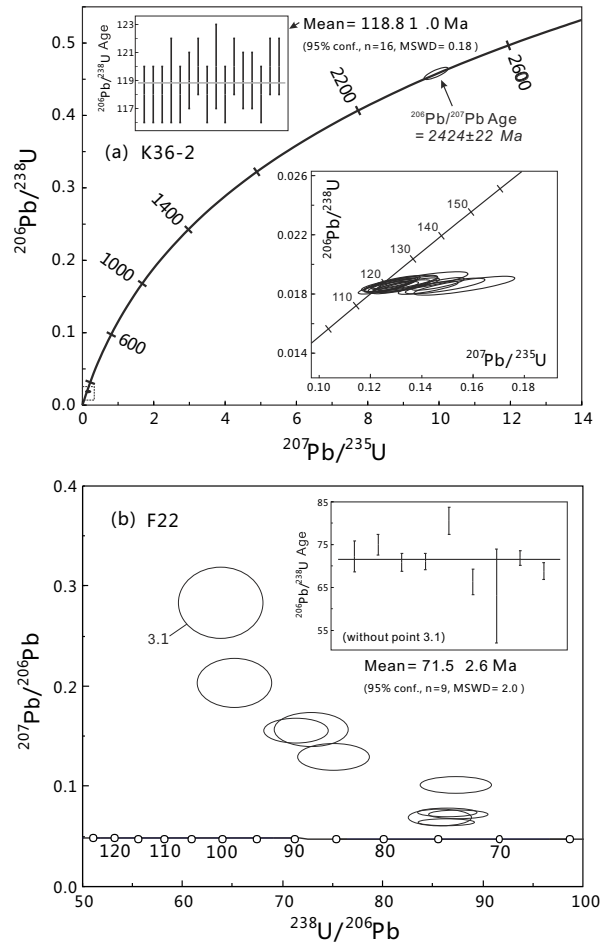


Fig. I-4 Zircon U-Pb concordia diagrams for (a) K36-2 and (b) F22, obtained by LA-ICP-MS and SHRIMP respectively.

5.2 Geochemistry

Chemical compositions of representative volcanic rocks are listed in Table I-3. In a TAS ($\text{Na}_2\text{O}+\text{K}_2\text{O}$ versus SiO_2) diagram (Fig. I-5a), basic and intermediate volcanic rocks generally plot in a continuous series through the basanite, trachybasalt, basaltic trachyandesite, trachyandesite and trachydacite fields, mostly with alkaline affinity. On a K_2O versus SiO_2 binary diagram (Fig. I-5b), the majority of the basic samples are classified as shoshonite but two samples belong to the high-K calc-alkaline series. The intermediate samples belong to both the shoshonite and high-K calc-alkaline series. Sample K12 has the lowest SiO_2 content and plots as basanite but cannot represent the initial major elemental composition because the sample is cut by numerous calcite-forming veins that give rise abnormally to high CaO and CO_2 contents. Sample K36-2 has an uncommonly high alkaline content especially of Na_2O which could be result of input of alkaline liquid during later metasomatism. On the Nb/Y versus Zr/ TiO_2 diagram (Winchester and Floyd 1977, not shown) the basic

and intermediate volcanic rocks plot as an alkali basalt and trachyandesite magma series. This implies that in most samples the contents of mobile elements such as K and Na and immobile high field strength elements (HFSE) such as Nb, Y and Zr have not been greatly affected by later metasomatism. The acid volcanic rocks straddle the alkaline-subalkaline boundary and plot as trachydacite, rhyolite and dacite. In diagrams of various oxides plotted versus MgO (Fig. I-6), basic and intermediate volcanic rocks display consistent patterns, and acid volcanic rocks exhibit distinctive chemical variations, notably very low TiO₂ and P₂O₅ contents. It is therefore unlikely that the acid lavas evolved from the basic or intermediate magmas; more likely they had a different origin.

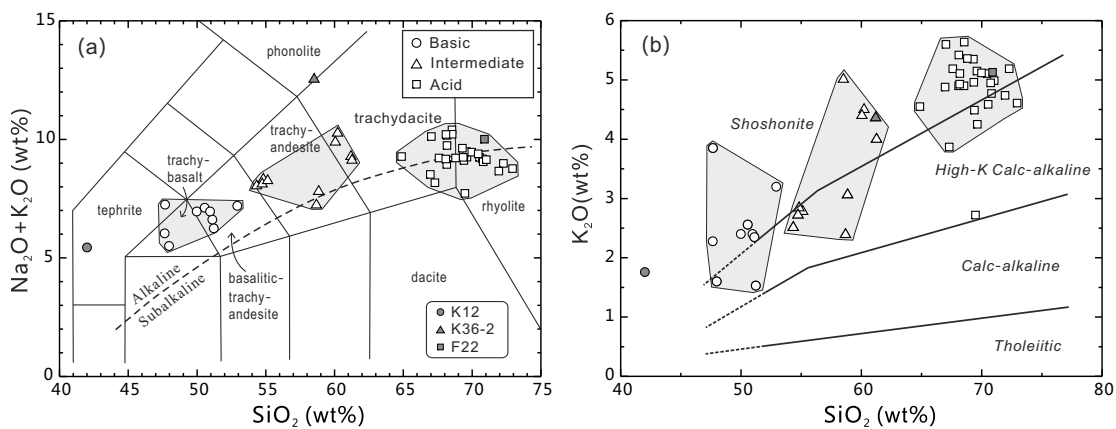


Fig. I-5 Diagrams of major elemental classification of volcanic rocks. (a) Plots of $\text{Na}_2\text{O} + \text{K}_2\text{O}$ versus SiO_2 . The classification of rock types is after Le Bas et al. (1986), and the boundary between alkaline and subalkaline series is after Irvine and Baragar (1971). (b) Plots of K_2O versus SiO_2 . Field boundaries are modified from Peccerillo and Taylor (1976). The data out of Table I-3 are from Gao and Zhang (1995) and listed in Table Supplementary I-1.

Chondrite-normalized rare earth element (REE) and normal mid-ocean-ridge basalt (N-MORB) trace element patterns are shown in Fig. I-7. All the Mesozoic basic, intermediate and acid volcanic rocks from the Huanghua depression have highly enriched light REE (LREE) contents and relatively depleted middle REE (MREE) and heavy REE (HREE), different from those of oceanic island basalt (OIB) and enriched mid-ocean-ridge basalt (E-MORB), and also from Cenozoic basalts of the Huanghua depression. The basic and intermediate samples have higher total REE abundance (321.39-660.26 ppm) and relatively stronger MREE/HREE fractionation ($(\text{Tb}/\text{Lu})_{\text{N}} = 1.62-4.26$) than the acid ones ($\sum \text{REE} = 192.16-320.58$ ppm, $(\text{Tb}/\text{Lu})_{\text{N}} = 1.47-1.99$). The basic and intermediate samples generally show no evident Eu anomalies ($\text{Eu}/\text{Eu}^* = 0.75-0.97$), while the some of the acid ones show slight

negative Eu anomalies ($\text{Eu}/\text{Eu}^* = 0.67\text{-}0.84$). Strong enrichment in Rb, Ba and K, and marked depletion in Nb and Ta occur in all samples but Zr depletion occurs only in basic and intermediate samples, while depletions in Sr and Ti exist only in acid ones. These trace element features confirm that the acid series is not genetically related to the basic-intermediate series as revealed by U-Pb dating and major elements.

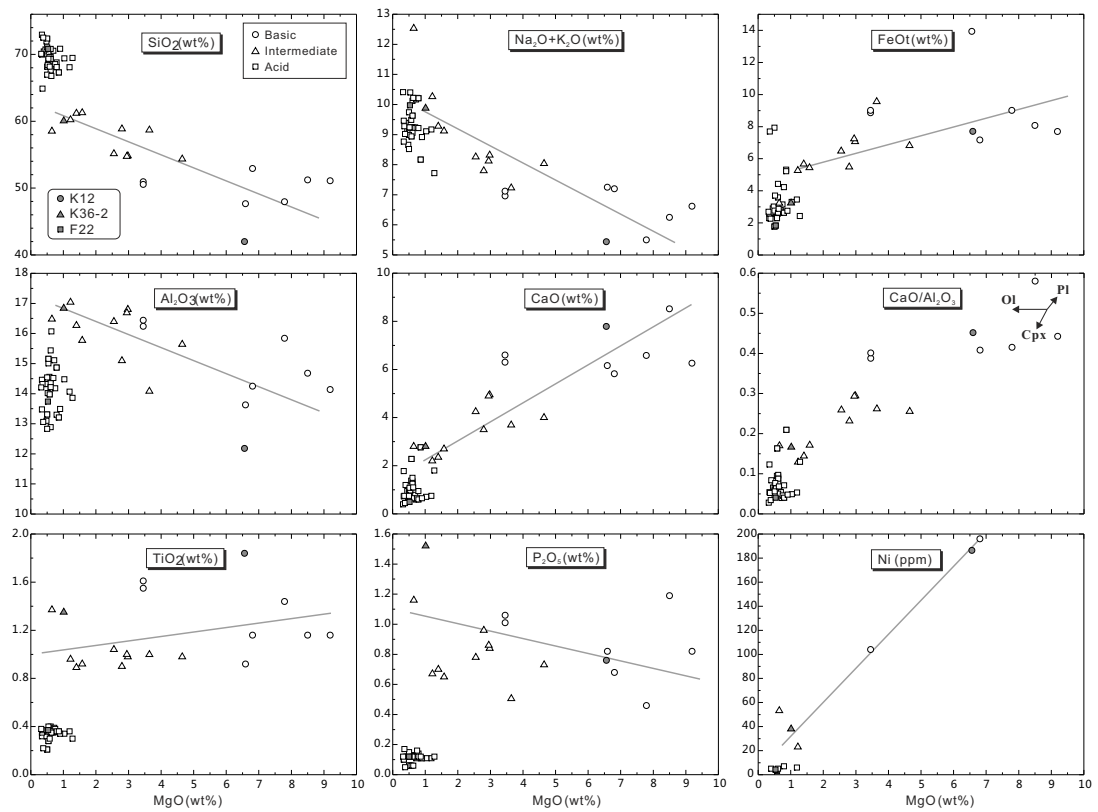


Fig. I-6 Diagrams of element abundances plotted versus MgO for the Mesozoic volcanic rocks in the Huanghua depression. FeOt (total FeO) = $\text{FeO} + 0.9 \cdot \text{Fe}_2\text{O}_3$. The enclosed lines show principle trends for basic to intermediate rocks. The data out of Table I-3 are from Gao and Zhang (1995) and listed in Table Supplementary I-1.

Sr and Nd isotopic compositions of representative volcanic rocks are listed in Table I-4. The initial $^{87}\text{Sr}/^{86}\text{Sr}$ ratios and $\epsilon_{\text{Nd}}(t)$ values were calculated in accordance with zircon U-Pb dates of 118 Ma for intermediate lava (K36-2) and 72 Ma for acid lava (F22). For basic lava (K12) an age of 118 Ma was used on the assumption that it formed synchronously with the intermediate lavas. All the volcanic rocks have homogeneous isotopic ratios with $(^{87}\text{Sr}/^{86}\text{Sr})_i$ ranging from 0.7049 to 0.7066, $(^{143}\text{Nd}/^{144}\text{Nd})_i$ ranging from 0.5115 to 0.5116, and $\epsilon_{\text{Nd}}(t)$ ranging from -17.5 to -17.4. Their EMI-like isotopic character is similar to the enriched Late Mesozoic

lithospheric mantle beneath the central NCC (Zhang et al. 2004) and distinct from Cenozoic asthenosphere-derived basalts (Zhang et al. 2002; Zhang et al. 2009a).

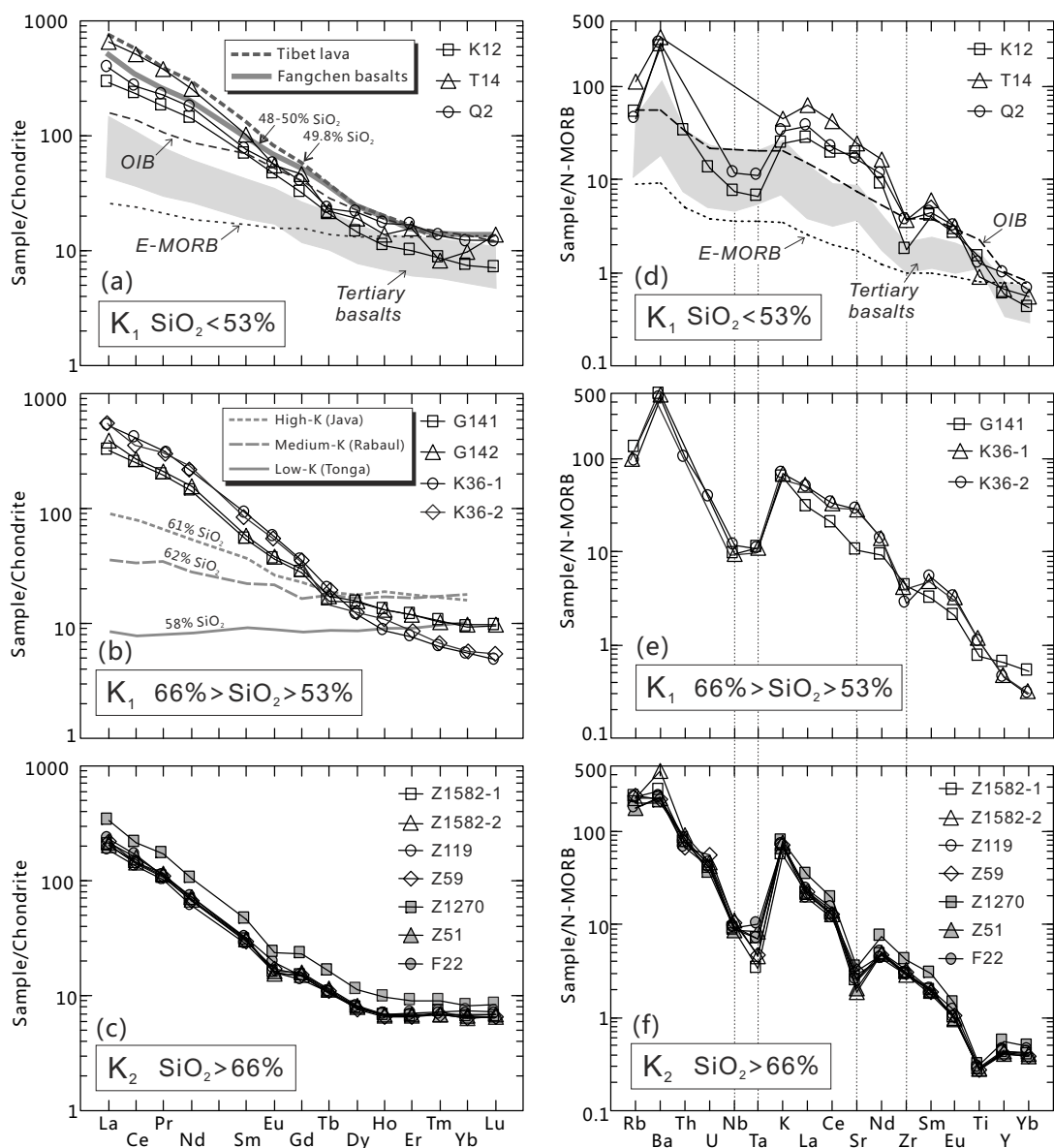


Fig. I-7 Chondrite-normalized REE patterns (a-c) and N-MORB normalized spidergrams (d-f) for Mesozoic volcanic rocks in the Huanghua depression, Bohai Bay basin. Compositions of chondrite, N-MORB, E-MORB and OIB are from Sun and McDonough (1989). Tertiary basalts from the Huanghua depression (Zhang et al. 2009a), Cenozoic Tibet post-collisional lava (Turner et al. 1996), Later Cretaceous Fangcheng basalts from the Ludong volcanic zone (Zhang et al. 2002) and three common types of volcanic arc lavas, i.e. high-K (Java), medium-K (Rabaul) and low-K (Tonga) andesites (Gill 1981) are shown for comparison.

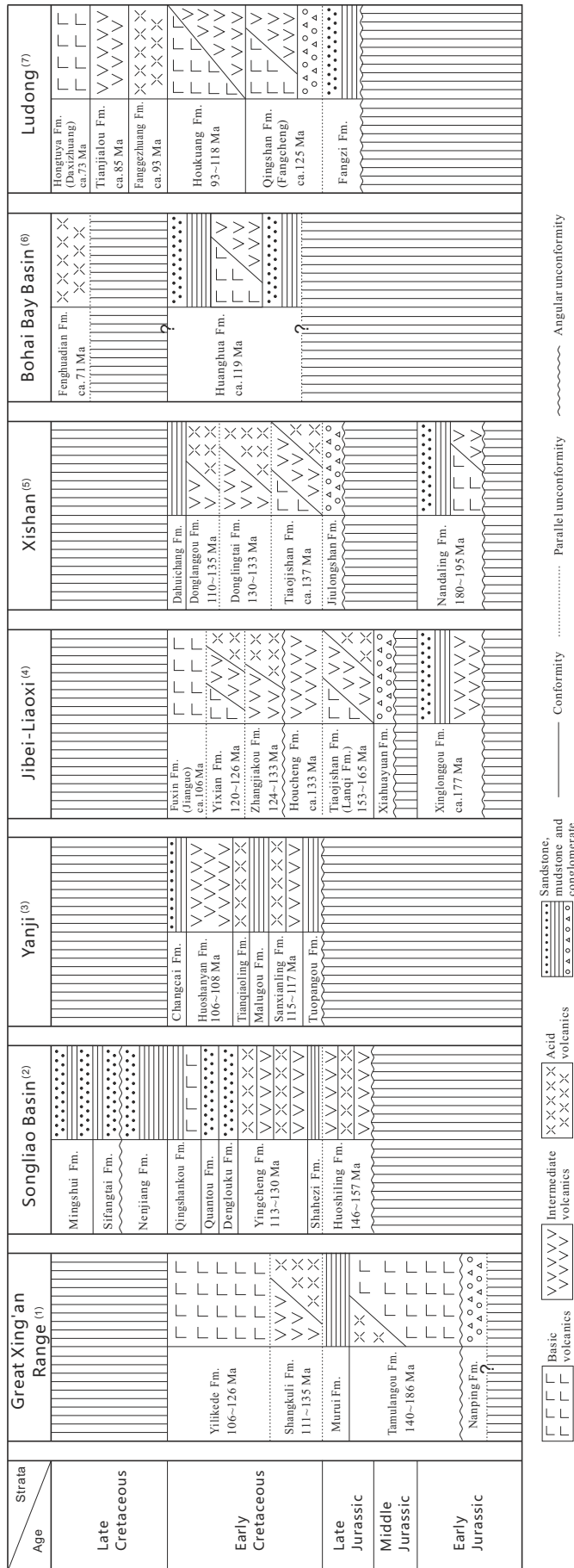


Fig. 1-8 Principle Late Mesozoic strata (J1-K2) in several important volcanic zones. Data sources: (1) Wang et al. (2006), Zhang et al. (2008); (2) Tan et al. (1989), Wang et al. (2002, 2009); Zhang et al. (2009b); (3) Li et al. (2007); (4) Davis et al. (2001), Li et al. (2001), Zhang et al. (2003), Niu et al. (2004), Yang et al. (2006), Yang and Li (2008), Zhang et al. (2008a, b); (5) Li et al. (2004b), Yuan et al. (2006); (6) this study; (7) Qiu et al. (2002), Yan et al. (2003), Ling et al. (2007), Zhang and Sun (2002), Tang et al. (2008).

6 Discussion

6.1 Spatio-temporal distribution of Mesozoic volcanic rocks

Magmatic zircons from sample K36-2 yielded a weighted mean $^{206}\text{Pb}/^{238}\text{U}$ age of 118.8 ± 1.0 Ma, indicating that intermediate volcanic lava was extruded in Early Cretaceous times. SHRIMP zircon dating of sample F22 obtains a result of 71.5 ± 2.6 Ma, which reveals that the acid lava formed much later in the Late Cretaceous. This zircon U-Pb age is similar to a K-Ar date of 75.8 ± 2.0 Ma for rhyolite lava obtained by Zhang 1989 (unpublished report, see Gao and Zhang 1995), but quite different from Early Cretaceous ages (128.2 ± 40.5 Ma) acquired from a Sm-Nd pseudo-isochron on several individual whole-rock samples (Gao and Zhang 1995). As shown in Fig. I-2, the acid volcanic rocks only occur in a limited area near Fenghuadian Town and do not coexist with other types of volcanic rocks. In contrast, basic and intermediate volcanic rocks are widely distributed and often interbedded with each other, showing a close relationship. We conclude that the basic and intermediate lavas could have formed contemporaneously in the Early Cretaceous, and they might be evolved products from a common primary magma, supported by their similar geochemical features stated above. It is also possible that the Late Cretaceous acid volcanic rocks could represent another distinct episode of volcanic activity that only has an acid component, as evidenced by their distinctive ages, distribution and geochemical characteristics.

The major volcanic zones in North China and adjacent areas (Fig. I-1) appear to be composed of similar types of volcanic rocks but erupted at different times over different durations (Fig. I-8, references in caption) showing a younging trend from northwest to southeast. Volcanic activity began in the northwestern part of NE China Fold Belt and North China in the Early Jurassic (ca. 180-195 Ma) with eruption of basalt of the Tamulangou Formation in the Greater Xing'an Range, andesite and dacite of the Xinglonggou Formation in the Jibei-Liaoxi Zone, and basalt and andesite of the Nandaling Formation in the Xishan Zone. Mesozoic volcanism represented by basalt of the Yilikede Formation (ca. 106 Ma) in the Greater Xing'an Range, Jianguo alkaline basalt of the Fuxin Formation (ca. 106 Ma) in the Jibei-Liaoxi Zone and alkaline intermediate-acid lavas of the Donglanggou Formation (ca. 110 Ma) in the Xishan Zone ceased almost simultaneously in the three zones at the end of the Early Cretaceous. From Late Jurassic to Early Cretaceous (ca. 157-113 Ma), volcanism represented by intermediate-acid lavas occurred in the Songliao Basin. Much later, volcanic activity started in the Early Cretaceous (ca. 120 Ma) in the Huanghua Zone and in the Ludong Zone where it is represented by basaltic

andesite and andesite. It ceased approximately at the same time in both zones near the end of the Late Cretaceous (ca. 71-73 Ma) with rhyolite of the Fenghuadian Formation and alkaline basalt of the Hongtuya Formation, respectively. There was Mesozoic volcanic activity with a limited duration in the Yanji Zone during the Early Cretaceous (ca. 106-117 Ma).

6.2 Petrogenesis of Mesozoic volcanic rocks

The basic lavas from the Huanghua depression have low SiO₂, but significant MgO and Ni contents (Fig. I-6) implying that fractionation of olivine caused a major decrease of MgO and Ni but did not increase SiO₂. Partial melts from mantle sources are normally basaltic (Wilson 1989) while partial melts from basaltic oceanic crust or lower continental crust are granitic or granodioritic (e.g., Rapp et al. 1991). High-degree partial dehydration melting of basaltic oceanic crust or lower continental crust under sufficiently high temperatures (ca. 1100 °C) can produce intermediate and even mafic melts (e.g., Rapp and Watson 1995) but these magmas are of much higher Na₂O and lower MgO contents than mantle-derived basic lavas. This suggests that our basic lavas are unlikely to be products of partial melting of basaltic crust, but favor a mantle-derivation origin. As shown in the chondrite-normalized REE patterns and N-MORB normalized spidergrams (Fig. I-7a, d), the basic lavas are strongly enriched in LREE and LILE such as Rb, Ba, K and Sr, but depleted in HFSE such as Nb, Ta, Zr and Ti. These trace elemental signatures are similar to subduction-related arc lavas which are generally formed by partial melting of a mantle wedge assisted by slab-derived aqueous fluids (Hofmann 1988; Wilson 1989).

Andesitic melt with high MgO and low alkalis could be produced by a small proportion of partial melting of hydrous mantle peridotite at ~30 km depth, as revealed by melting experiments (Green and Ringwood 1980) but this does not explain the large proportion of andesitic lavas from the Huanghua depression (Fig. I-2) or their low MgO and high alkali contents (Fig. I-6). Intermediate melts can also be generated by partial melting of a subducted oceanic slab with a garnet-bearing residue but little plagioclase in the source (Rapp and Watson 1995). Slab-originated lavas could have MORB-like Sr-Nd isotopic features (Martin 1999) and high MgO from interaction with peridotite during their ascent through the overlying mantle wedge (Rapp et al. 1999). The geochemistry of the Mesozoic intermediate volcanic rocks from the Huanghua depression is similar to slab-originated adakite in some aspects such as high Sr/Y and La/Yb ratios, but they have lower MgO and Mg#, and Sr-Nd isotopic compositions with an EMI affinity which effectively rule out a slab-

melting origin. The intermediate volcanic rocks have higher SiO₂, Na₂O+K₂O, Th and U, but lower MgO, FeO_t, CaO, TiO₂ and Ni contents than the basic rocks, agreeing well with fractionation of olivine, pyroxene and magnetite. The negative correlation between CaO/Al₂O₃ and MgO in the basalt-andesite series also indicates that the intermediate lavas could be residual melts derived from basic lavas via fractionation of olivine and clinopyroxene (Fig. I-6). As REE are mainly contained in accessory phases such as monazite, zircon, apatite and allanite (Watt and Harley 1993; Bea 1996) and the partition coefficients of REE for olivine, pyroxene and magnetite are always less than 1 (Nielsen 2006), fractional crystallization of these mafic minerals would not cause notable variations in REE abundances, which is in accordance with the observed similarities of REE patterns of intermediate and basic volcanic rocks (Fig. I-7a, b). Finally, possible crustal contamination during magma ascent is indicated by the inherited Precambrian zircon crystal. Thus we suggest that the intermediate lavas evolved from basic lavas by fractionation of mainly olivine and pyroxene, and possibly slight crustal assimilation. This idea is supported by the close interbedded relationship between basic and intermediate lavas.

Compared with ordinary arc tholeiitic to calc-alkaline series, the basic and intermediate volcanic rocks from the Huanghua depression are characterized by strong enrichments in alkaline elements (Fig. I-5), LREE (Fig. I-8) and LILE (e.g., Rb and Ba), similar to Cenozoic post-collisional lavas of Tibet (Turner et al. 1996) and the Early Cretaceous Fangchen basalts from the Ludong volcanic zone (Zhang et al. 2002). Their highly enriched Nd isotope values ($\epsilon_{Nd}(t) = \sim -18$, Table I-4) have an EMI affinity, similar to Late Mesozoic gabbros in the Taihangshan region, central NCC (Zhang et al. 2004). This indicates that the source was unlikely to be depleted mantle, but probably ancient enriched lithospheric mantle which suffered metasomatism or influx of silicic melts. The silicic melts could have been high in LILE and low in HFSE and radiogenic Nd isotope because they were derived by partial melting of ancient lower crust (Zhang et al. 2004). This interaction between ancient lithospheric mantle and crust implies early subduction prior to the Late Mesozoic volcanism.

Rhyolite can be generated by two alternative mechanisms: partial melting of crust when heated by mantle-derived magma (e.g., Hochstein et al. 1993) or evolution of basaltic magma via fractional crystallization and/or crustal assimilation (e.g., McCulloch et al. 1994). The Late Cretaceous acid lavas from the Huanghua depression are characterized by high SiO₂, but low MgO, FeO_t, CaO, TiO₂, Al₂O₃, P₂O₅ and Ni contents. Diagrams of element abundances plotted versus MgO (Fig. I-6)

especially for Al_2O_3 , TiO_2 , FeO and P_2O_5 , usually show that the acid lavas occupy isolated compositional fields and show independent evolution trends from basic and intermediate lavas. The data field of Th/La versus Ta/La for acid lavas overlaps the field of lower continental crust (LCC), showing a genetic relationship (Fig. I-9b). Low Al_2O_3 content (mostly $< 15\%$), negative Sr anomaly and a flat HREE pattern (Fig. I-7) indicate that partial melting occurred in the presence of a plagioclase-rich but garnet-free residue, implying a low depth (< 10 kbar) of melt generation (Rapp and Watson 1995). We therefore suggest that the Late Cretaceous acid lavas were generated by remelting of lower continental crust at a shallow level caused by heating by an unknown coeval mantle-derived magma, because of the relatively young isotopic ages and limited distribution of the acid volcanics.

6.3 Migration of arc-related volcanism

The spatio-temporal distribution of Late Mesozoic volcanic rocks indicates migration of arc-related volcanism from northwest to southeast. In the Jibei-Liaoxi volcanic zone Mesozoic volcanism started at ca. 180 Ma as high-Mg adakitic andesite in the Xinglonggou Formation (Fig. I-8), generated by partial melting of a subducted oceanic slab and subsequent interaction with mantle peridotite (Li 2006; Yang and Li 2008). In the Xishan volcanic zone, basalt and andesite of the Nandaling Formation represent the onset of volcanism in the Early Jurassic, with evidence of fluid-related enrichment of certain elements during partial melting (Fig. I-9) that could be related to subduction (Li et al. 2004a). In the Greater Xing'an Range, subduction of the Paleo-Pacific Plate is the most likely geodynamic regime to explain Mesozoic volcanism although geochemical evidence for partial melting of hydrated mantle wedge has not yet been obtained (Zhang et al. 2008c). In the Huanghua volcanic zone, basic-intermediate lavas were erupted in the Early Cretaceous (ca. 120 Ma) and their metasomatic geochemical features support a volcanic arc origin (Fig. I-9a). Although the Early Cretaceous Fangcheng basalt of the Qingshan Formation in the Ludong volcanic zone lacks obvious volcanic-arc affinity, it might have been generated by partial melting of enriched lithospheric mantle caused by extensive interaction with a crust-derived melt (Zhang et al. 2002). We suggest that northward subducted continental crust above northwestward subducted oceanic crust might have blocked fluid derived by dehydration of the subducted slab from entering the mantle wedge because of the location of the Ludong volcanic zone is close to the Sulu continental collision orogen.

Granitoids found in South Korea formed mainly in three episodes (Sagong et

al. 2005): Triassic (248-210 Ma), Jurassic (197-158 Ma), and Cretaceous-Early Tertiary (110-50 Ma). The Cretaceous granites are volcanic-plutonic complexes with arc-related calc-alkaline affinities (Poulet et al. 1994), indicating the presence of a volcanic arc. In Southwest Japan, volcanic arc-related magmatism started at ca. 100 Ma with the emplacement of Ryoke Granitoids (Kutsukake 2002) about 10 Ma later than similar arc-related magmatism in South Korea. Additionally, calc-alkaline mafic rocks from the Ryoke Belt (Southwest Japan) are in the age range of 71-86 Ma, which also show an eastward younging trend (Nakajima et al. 2005).

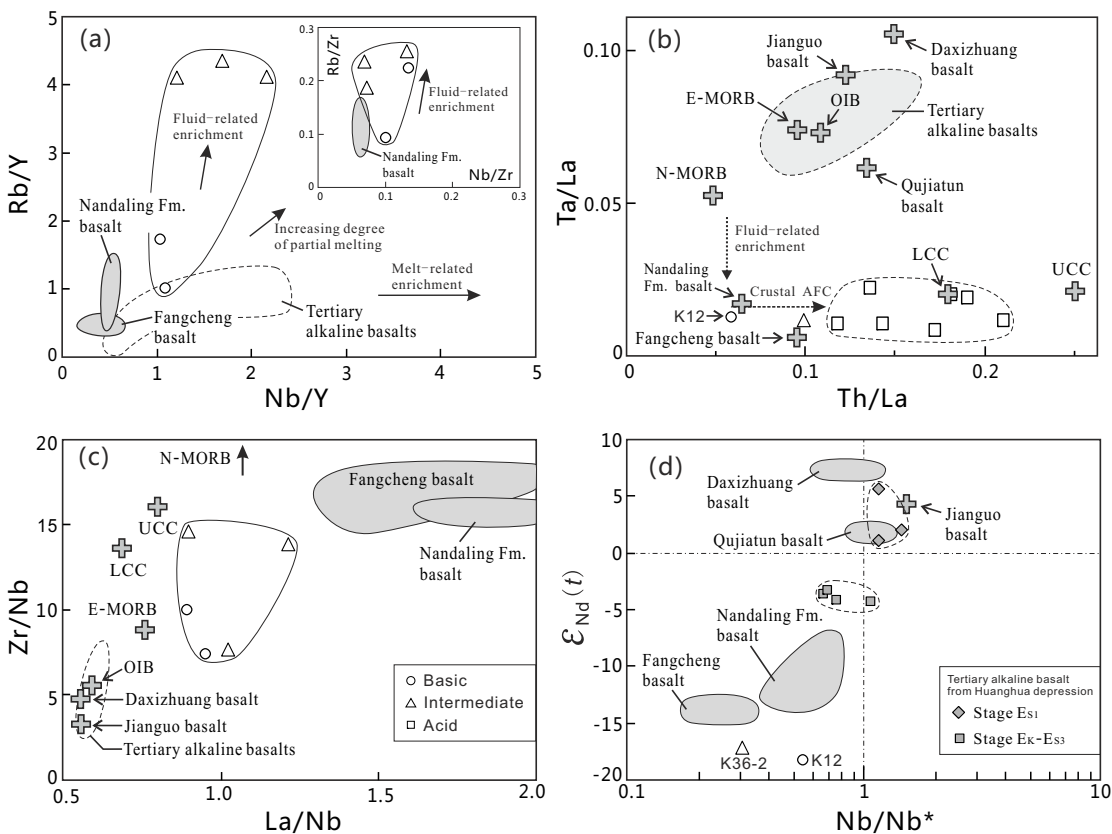


Fig. I-9 Variations in trace element and $\epsilon_{Nd}(t)$ values of representative Mesozoic-Cenozoic basalts in the NCC. (a) Nb/Y versus Rb/Y (inserted Nb/Zr versus Rb/Zr); (b) Th/La versus Ta/La; (c) La/Nb versus Zr/Nb; (d) Nb/Nb* versus $\epsilon_{Nd}(t)$. Trends associated with fluid-related enrichment, melt-related enrichment and increasing degree of partial melting are from Kepezhinskias et al. (1996). Nb/Nb* indicating HFSE fractionation modified from the method of Salters and Shimizu (1988) is calculated as $(Nb)_N \times 2 / ((U)_N + (K)_N)$. $\epsilon_{Nd}(t)$ values are calculated with formation ages of respective rocks. N-MORB, E-MORB and OIB are from Sun and McDonough (1989). Lower and upper continental crust (LCC and UCC) are from Rudnick and Gao (2003). Nandaling Formation basalt, Fangcheng basalt, Jianguo basalt, Daxinzhuang basalt and Qujiatun basalt are from Li et al. (2004a), Zhang et al.

(2002, 2003), Yan et al. (2003) and Wang et al. (2006b) respectively. The Tertiary alkaline basalts from Huanghua depression are after Zhang et al. (2009a).

In a word, the spatio-temporal distribution of arc-related volcanism in East Asia shows a southeastward migration pattern which implies a progressive retreat of the subduction zone.

6.4 Migration of extension-related volcanism

The spatio-temporal distribution of extension-related volcanism displays southeastward migration in North China and the NE China Fold Belt. Alkaline basalts, basaltic andesite or rhyolite in the Jibei-Liaoxi and Xishan Zones and the Early Cretaceous Songliao Basin, the later Yanji, Huanghua and Ludong volcanic zones and the Liaodong peninsula related to lithospheric extension also exhibit an eastward migration pattern. The Jianguo alkaline basalt of the Fuxin Formation in the Jibei-Liaoxi Zone erupted at ca. 106 Ma and is derived from the asthenosphere, indicating that there was an extensional regime in greatly thinned lithosphere by the late Early Cretaceous (Zhang et al. 2003). The youngest volcanic rocks in the Xishan Zone, basaltic andesite and andesite of the Donglanggou Formation are high in alkalis indicating an extensional regime (Li et al. 2004b). In the Songliao Basin, Early Cretaceous intermediate lavas of the Yingcheng Formation are characterized by E-MORB-like Sr-Nd isotopic ratios and lack of depletion of HFSE (Wang et al. 2006b; Zhang et al. 2009b) similar to Cenozoic asthenosphere-derived basalts, also indicating an extensional regime and thinned lithosphere. The Late Cretaceous Daxizhuang alkaline basalt (Hongtuya Formation) in the Ludong Zone and the Qujiatun basalt in the Liaodong peninsula are also derived from an asthenospheric magma source (Yan et al. 2003; Wang et al. 2006c) indicating similar petrogenesis and tectonic regime to the Early Cretaceous Jianguo basalt in the Jibei-Liaoxi Zone (Fig. I-9 b-d), showing that the lithospheric thinning and extension were achieved later there. Even later in the southern part of Siberia, Korea and Southwest Japan intraplate alkaline basalts and continental rift tholeiites started to erupt from Late Cenozoic times (Chashchin et al. 2007; Choi et al. 2006; Pouclet et al. 1994). The migration of extension-related volcanic activity could be explained by delamination of a lithospheric root and post-subduction slab break-off, as discussed below.

6.5 Tectonic model

Many different models have been proposed to account for Late Mesozoic

lithospheric thinning, destruction of the NCC and widespread magmatism as explained in the introduction. Triassic collision between South China and North China has been suggested as a likely trigger (Menzies et al. 1993; Xu 2001; Gao et al. 2002) but continental collision accompanied by northward subduction could not have formed the northeast-striking Mesozoic volcanic zones because they postdate the Triassic collision by at least 50 Ma. Early-Middle Jurassic continental collision between Siberia and Mongolia-North China is an alternative model (Meng 2003; Wang et al. 2006a) that does not explain the widely distributed Mesozoic volcanism far away from the collisional suture.

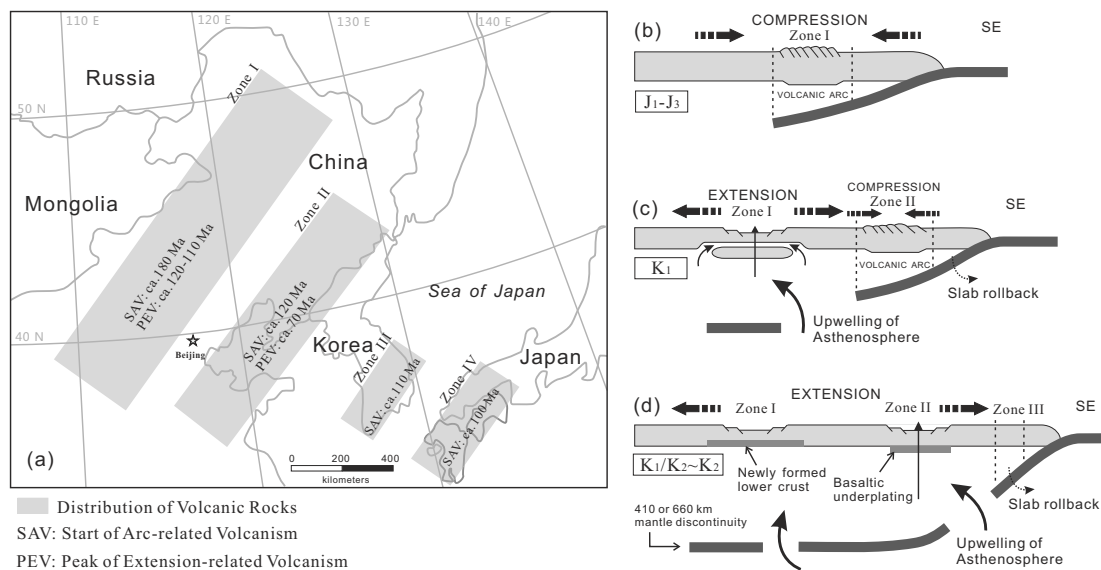


Fig. 1-10 (a) Spatio-temporal distribution of Mesozoic volcanic rocks in the East Asia. Zone I includes the Great Xing'an Range, Jibei-Liaoxi and Xishan zones. Zone II includes the Yanji, Liaodong peninsula, Huanghua and Ludong zones. (b-d) Cartons of principle tectonic scenarios accounting for the generation of seaward migration of mainly two types of volcanic rocks. See text for explanation.

A tectonic model incorporating a slab window generated by subduction of the Kula/Pacific ridge in the Late Cretaceous (Kinoshita 2002) has been invoked to explain Cretaceous-Tertiary magmatism in Southwest Japan (Kinoshita 1995, 2002). Heat flux from the mantle through the window could have induced high-temperature (ca. 850 °C) metamorphism at a shallow crustal depth (Brown 1998). Using a similar model, Kim et al. (2005) interpreted the Jurassic granitoids in South Korea as products of subduction of the Farallon/Izanagi ridge. Since the Farallon, Izanagi and Kula Plates continued to shift north or northeast (Maruyama 1997), slab window effects caused by subduction of oceanic ridges should have migrated northward or

northeastward (Kinoshita 1995, 2002; Kim et al. 2005). Ling et al. (2009) employed a similar model to explain Cretaceous magmatism along the Lower Yangtze River fault zone in central East China. But this model does not agree with our observations in North China presented above that show southeastward migration of both arc- and extension-related volcanism, implying that ridge subduction had little effect on Late Mesozoic tectonomagmatic events. This discrepancy could be explained by transform plate shift nearly perpendicular to the subduction direction preventing the migration of the slab window inland, restricting it only to regions close to the continental margin. The opening of an oceanic ridge has been shown to spread from trench to inland as subduction continues (Thorkelson 1996) and if this is the case transform shift between the relevant oceanic plates along the boundary of the Eurasian Continent (Maruyama 1997) would migrate a slab window northeastward away from North China. On this view, it is reasonable to exclude slab window as the dominating tectonic model for North China.

Subduction of a Paleo-Pacific Plate is another candidate invoked to account for Late Mesozoic tectonomagmatic events in North China (Zhao et al. 1994; Wu et al. 2003; Zhao et al. 2004; Sun et al. 2007; Wu et al. 2008) but the models proposed are too general to be tested in detail. Instead, we advance a model involving subduction and retreat of a Paleo-Pacific Plate and post-subduction slab break-off to explain the southeastward migration of arc- and extension-related volcanism (Fig. I-10a), preceding crustal compression (Davis et al. 2001) and later lithospheric extension (Zhai et al. 2004).

From Early to Late Jurassic times (ca. 180-150 Ma, Fig. I-10b), northwestward subduction of Paleo-Pacific Plate caused the eruption of arc-related calc-alkaline volcanic rock series along the Greater Xing'an Range, Jibei-Liaoxi and Xishan Zone (Zone I in Fig. I-10a). A flat subduction zone composed of moderately old oceanic crust (Gutscher et al. 2000) could explain the Xinglonggou high-Mg adakitic andesite derived from an oceanic slab (Li 2006; Yang and Li 2008). Extensive Jurassic accretionary complexes along the eastern margin of the East Asian continent indicate that subduction of Paleo-Pacific Plate has occurred since the Early Jurassic (Isozaki 1997; Maruyama 1997; Wu et al. 2007). A syn-subduction compressional regime could have been present (Davis et al. 2001; Zhang et al. 2007; Hu et al. 2009) as evidenced by pervasive NNE-NE oriented fault-fold systems (Zhao et al. 1994, 2004) as well as angular unconformities under the Xiahuayuan Formation in the Jibei-Liaoxi Zone and under the Jiulongshan Formation in the Xishan Zone (Fig. I-8). It is generally believed that this crustal compression was

accompanied by extensive thickening, which could have encouraged subsequent delamination of a lithospheric root in the Early Cretaceous (Wu et al. 2003; Meng 2003; Wang et al. 2006a; Wu et al. 2008).

In middle Early Cretaceous times (ca. 130-120 Ma, Fig. I-10c), a deeply subducted oceanic slab broke off beneath Zone I, leading to local upwelling of asthenosphere similar to a backarc regime. Decompressional partial melting of uplifted asthenosphere could have generated OIB-type intracontinental basalts such as the Jianguo alkaline basalt of the Fuxin Formation (Zhang et al. 2003). At the same time, previously thickened crust was drastically thinned by lithospheric extension accompanied by gravitational delamination (Gao et al. 1998; Zhai et al. 2004) producing voluminous A-type granites and erosion of metamorphic core complexes (Wu et al. 2005). It is worthy of mention that abundant hydrous liquid derived by dehydration of oceanic slab appears to have been added to the lithospheric mantle. This would weaken the uppermost mantle by hydration and facilitate its delamination together with an overlying eclogitized crustal root (Sleep 2005). Heated by the upwelling asthenosphere, ancient lithospheric mantle was partially melted to produce basaltic melts (e.g., Chen et al. 2004) which made both a thermal and a material contribution to the simultaneous granitoids (e.g., Qian et al. 2003). At the same time, pervasive thermo-mechanical and chemical erosion at the lithosphere-asthenosphere interface transformed former cold refractory lithospheric mantle into hot fertile lithosphere (Menzies et al. 1993; Xu 2001). Slab rollback induced by slab break-off increased the subduction angle and caused the trench to retreat backwards (Elsasser 1971) and consequently, the volcanic arc migrated southeastward along the Liaodong-Huanghua-Ludong zone (Zone II in Fig. I-10c).

From late Early Cretaceous to Late Cretaceous (Fig. I-10d), eastern North China and the NE China Fold Belt were dominated by crustal extension comparable with a backarc environment (Watson et al. 1987; Zheng et al. 2006; Wang et al. 2006a; Xu et al. 2008). Mantle-derived magmas were able to underplate continental crust and form new basaltic lower crust. Slab break-off gave rise to upwelling of asthenosphere and consequent generation of OIB-type basalts especially in Zone II, such as the Daxizhuang alkaline basalt in the Ludong Zone and the Qujiatun basalt in the Liaodong peninsula (Yan et al. 2003; Wang et al. 2006c). Continuing slab rollback moved the volcanic arc zone further southeastward into Korea and Southwest Japan (Zone III and IV in Fig. I-10a) where abundant arc-related plutonic and volcanic igneous rocks were generated (Pouclet et al. 1994; Kutsukake 2002). It is worth pointing out that this Cretaceous subduction event must have been

independent of the Triassic-Jurassic subduction along the East Asian margin (de Jong et al. 2009; Park et al. 2009) and could have been followed by Kula/Pacific ridge subduction in the Late Cretaceous (Kinoshita 2002).

This model includes a stagnant detached oceanic slab in the mantle transition zone that could still be a magma source, encouraging deep dehydration and convective circulation, and driving intraplate volcanism and continental rifting (Tatsumi et al. 1990). The presence of the slab is supported by seismic tomography across East Asia (Lei and Zhao 2005; Zhu and Zheng 2009) and geochemistry of Cenozoic intraplate Changbaishan basalts in northeastern China (Kuritani et al. 2009). Until the Tertiary alkaline basalts were quite widely erupted in eastern China (Zhou and Armstrong 1982; Basu et al 1991) including the Bohai Bay Basin (Zhang et al. 2009a), indicating continuous enhanced lithospheric extension and asthenospheric upwelling.

7 Conclusions

Andesitic lava closely associated with basaltic lava and basic-intermediate volcanic rocks in the Huanghua depression of the Bohai Bay Basin were extruded in the Early Cretaceous, as indicated by LA-ICP-MS zircon U-Pb ages (118.8 ± 1.0 Ma). SHRIMP zircon U-Pb dating of acid lava that occurs only in a restricted part of the area has a Late Cretaceous extrusion date (71.5 ± 2.6 Ma). The Early Cretaceous basic-intermediate lavas are characterized by strong enrichment in LREE and LILE and depletion in HREE and HFSE, indicating a volcanic arc origin related to oceanic subduction. The intermediate lavas are interpreted as partial melts from the basic lavas that evolved by olivine and pyroxene fractionation possibly accompanied by crustal assimilation, evidenced by an inherited Paleoproterozoic zircon (core 2424 ± 22 Ma). The Late Cretaceous acid lavas are probably products of crustal melting in an extensional regime.

Late Mesozoic arc-related volcanic events in the NCC and adjacent areas show a younging trend towards the Pacific Ocean that has also been found in asthenosphere-derived alkaline basalts and other lithospheric extension-related volcanic rocks. Southeastward retreat of northwestward subduction of the Paleopacific Plate beneath East Asia could be the geodynamic mechanism responsible. As the subduction zone migrated, active continental margin and backarc tectonic regimes played successive roles in different parts of North China during the Late Mesozoic (J_1 - K_2).

8 References

- Basu AR, Wang J, Huang W, Xie G, Mitsunobu T (1991) Major element, REE and Pb, Nd, and Sr isotopic geochemistry of Cenozoic volcanic rocks of eastern China: Implications for origin from suboceanic-type mantle reservoirs. *Earth Planet Sci Lett* 105:149–169
- Bea F (1996) Residence of REE, Y, Th and U in granites and crustal protoliths: implications for the chemistry of crustal melts. *J Petrol* 37:521–552
- Brown M (1998) Unpairing metamorphic belts: P-T paths and a tectonic model for the Ryoke Belt, southwest Japan. *J Metamorph Geol* 16:3–22
- Chashchin AA, Martynov YA, Rasskazov SV, Maksimov SO, Brandt IS, Saranina EV (2007) Isotopic and Geochemical Characteristics of the Late Miocene Subalkali and Alkali Basalts of the Southern Part of the Russian Far East and the Role of Continental Lithosphere in Their Genesis. *Petrology* 15: 575–598
- Chen B, Jahn BM, Arakawa Y et al (2004) Petrogenesis of the Mesozoic intrusive complexes from the southern Taihang Orogen, North China Craton: elemental and Sr–Nd–Pb isotopic constraints. *Contrib Mineral Petrol* 148:489–501
- Chi JS (1988) The study of Cenozoic basalts and upper mantle beneath eastern China. China University of Geosciences Press, Wuhan, pp 225 (in Chinese)
- Choi SH, Mukasa SB, Kwon ST, Andronikov AV (2006) Sr, Nd, Pb and Hf isotopic compositions of late Cenozoic alkali basalts in South Korea: Evidence for mixing between the two dominant asthenospheric mantle domains beneath East Asia. *Chem Geol* 232: 134–151
- Davis GA, Zheng Y, Wang C et al (2001) Mesozoic tectonic evolution of the Yanshan fold and thrust belt, with emphasis on Hebei and Liaoning provinces, northern China. *GSA Memoir* 194:171–198
- de Jong K, Kurimoto C, Ruffet G (2009) Triassic $^{40}\text{Ar}/^{39}\text{Ar}$ ages from the Sakaigawa unit, Kii Peninsula, Japan: implications for possible merger of the Central Asian Orogenic Belt with large-scale tectonic systems of the East Asian margin. *Int J Earth Sci* 98:1529–1556
- Deng JF, Zhao HL, Mo XX et al (1996) Continental root/plume structure in China: key to the continental geodynamics. Geological Publishing House, Beijing, pp 1–110 (in Chinese with English Abstract)
- Elsasser WM (1971) Sea-floor spreading as thermal convection. *J Geophys Res* 76:1101–1112
- Fan QC, Hooper PR (1989) The mineral chemistry of ultramafic xenoliths of eastern China: Implications for upper mantle composition and the paleogeotherms. *J Petrol* 30:1117–1158
- Gao S, Ling W, Qiu Y, Lian Z, Hartmann G, Simon K (1999) Contrasting geochemical and Sm–Nd isotopic compositions of Archean metasediments from the Kongling high-grade terrain of the Yangtze craton: evidence for cratonic evolution and redistribution of REE during crustal anatexis. *Geochim Cosmochim Acta* 63:2071–2088
- Gao S, Rudnick RL, Carlson RW, McDonough WF, Liu YS (2002) Re–Os evidence for replacement of ancient mantle lithosphere beneath the North China Craton. *Earth Planet Sci Lett* 198:307–322
- Gao S, Rudnick RL, Yuan HL et al (2004) Recycling lower continental crust in the North China craton. *Nature* 432:892–897
- Gao S, Zhang BR, Jin ZM, Kern H, Luo TC, Zhao ZD (1998) How mafic is the lower continental crust? *Earth Planet Sci Lett* 161:101–117
- Gao ZY, Zhang LC (1995) Igneous rocks and oil pools. Northwest University Press, Xi'an, pp 1–73 (in Chinese with English abstract)
- Gill JB (1981) Orogenic andesites and plate tectonics. Springer-Verlag, Berlin, pp 390
- Green DH, Ringwood AE (1967) The genesis of basaltic magmas. *Contrib Mineral Petrol* 15:103–190
- Griffin WL, Zhang A, O'Reilly SY, Ryan CG (1998) Phanerozoic evolution of the lithosphere beneath the Sino-Korean Craton. In: Flower M, Chung SL, Lo CH, Lee TY (eds) *Mantle Dynamics and Plate Interactions in East Asia* Mantle Dynamics and Plate Interactions in East Asia. AGU Geodynamics 27:107–126
- Guo F, Fan WM, Li XY, Li CW (2007) Geochemistry of Mesozoic mafic volcanic rocks from the Yanshan belt in the northern margin of the North China Block: relations with post-collisional lithospheric extension. In: Zhai MG, Windley BF, Kusky TM, Meng QR (eds) *Mesozoic sub-continental lithospheric thinning under eastern Asia*. *Geol Soc London Spe Pub* 280:101–129
- Gutscher MA, Maury R, Eissen JP, Bourdon E (2000) Can slab melting be caused by flat subduction? *Geology* 28:535–538
- Hochstein MP, Smith IEM, Regnauer-Lieb K et al (1993) Geochemistry and heat transfer processes in Quaternary rhyolitic systems of the Taupo Volcanic Zone, New Zealand. *Tectonophysics* 223:213–235

- Hofmann AW (1988) Chemical differentiation of the Earth: the relationship between mantle, continental crust, and oceanic crust. *Earth Planet Sci Lett* 90:297–314
- Hu J, Zhao Y, Liu X, Xu G (2009) Early Mesozoic deformations of the eastern Yanshan thrust belt, northern China. *Int J Earth Sci*. doi:10.1007/s00531-009-0417-5
- Huang F, Li SG, Yang W (2007) Contributions of the lower crust to Mesozoic mantle-derived mafic rocks from the North China Craton: implications for lithospheric thinning. In: Zhai MG, Windley BF, Kusky TM, Meng QR (eds) *Mesozoic sub-continental lithospheric thinning under eastern Asia*. *Geol Soc London Spe Pub* 280:55–75
- Irvine TN and Baragar WRA (1971) A guide to the chemical classification to the common volcanic rocks. *Canad J Earth Sci* 8:523–548
- Isozaki Y (1997) Jurassic accretion tectonics of Japan. *Isl Arc* 6:25–51
- Jahn BM, Wu F, Lo CH, Tsai CH (1999) Crust-mantle interaction induced by deep subduction of the continental crust: geochemical and Sr-Nd isotopic evidence from post-collisional mafic-ultramafic intrusions of the northern Dabie complex, central China. *Chem Geol* 157:119–146
- Kepezhinskas P, Defant M, Drummond M (1996) Progressive enrichment of island arc mantle by melt-peridotite interaction inferred from Kamchatka xenoliths. *Geochim Cosmochim Acta* 60:1217–1229
- Kim SW, Oh CW, Choi SG, Ryu IC, Itaya T (2005) Ridge subduction-related Jurassic plutonism in and around the Okcheon metamorphic belt, South Korea, and implications for Northeast Asian tectonics. *Int Geol Rev* 47:248–269
- Kinoshita O (1995) Migration of igneous activities related to ridge subduction in Southwest Japan and the East Asian continental margin from the Mesozoic to the Paleogene. *Tectonophysics* 245:25–35
- Kinoshita O (2002) Possible manifestations of slab window magmatisms in Cretaceous southwest Japan. *Tectonophysics* 344:1–13
- Kuritani T, Kimura JI, Miyamoto T et al (2009) Intraplate magmatism related to deceleration of upwelling asthenospheric mantle: Implications from the Changbaishan shield basalts, northeast China. *Lithos* 112:247–258
- Kutsukake T (2002) Geochemical characteristics and variations of the Ryoke granitoids, southwest Japan: Petrogenetic implications for the plutonic rocks of a magmatic arc. *Gondwana Res* 5:355–372
- Le Bas NJ, Le Maitre RW, Streckeisen A, Zanettin B (1986) A chemical classification of volcanic rocks based on the total alkali-silica diagram. *J Petrol* 27:459–469
- Lei J, Zhao D (2005) P-wave tomography and origin of the Changbai intraplate volcano in Northeast Asia. *Tectonophysics* 397:281–295
- Li CW, Guo F, Fan WM et al (2007) Ar-Ar Geochronology of Late Mesozoic Volcanic Rocks from the Yanji Area, NE China and tectonic implications. *Sci Chin D* 50:505–518
- Li PX, Cheng ZW, Pang QQ (2001) The horizon and age of the Confuciusornis in Beipiao, Western Liaoning. *Acta Geol Sin* 75:1–14 (in Chinese with English abstract)
- Li WP (2006) Geochemical characteristics of the early Jurassic dacites of the Xinglonggou Formation in Beipiao area, western Liaoning province. *Acta Petrol Sin* 22:1608–1616 (in Chinese with English abstract)
- Li XY, Fan WM, Guo F et al (2004a). Modification of the lithospheric mantle beneath the northern North China Block by the Paleo-Asian Ocean: geochemical evidence from mafic volcanic rocks of the Nandaling Formation in the Xishan area, Beijing. *Acta Petrol Sin* 20:557–566 (in Chinese with English abstract)
- Li XY, Fan WM, Guo F et al (2004b) Genesis of Donglanggou Formation potassic volcanics in Xishan, Beijing: Implications for geodynamic mechanism. *Geochimica* 33:353–360 (in Chinese with English abstract)
- Lin J, Fuller M (1990) Palaeomagnetism, North China and South China Collision, and the Tan-Lu Fault. *Phil Trans R Soc Lond (A)* 331:589–598
- Ling M, Wang F, Ding X et al (2009) Cretaceous ridge subduction along the Lower Yangtze River Belt, eastern China. *Econ Geol* 104:303–321
- Ling WL, Xie XJ, Liu XM et al (2007) Zircon U-Pb dating on the Mesozoic volcanic suite from the Qingshan Group stratotype section in eastern Shandong Province and its tectonic significance. *Sci China D* 50:813–824
- Liu DY, Nutman AP, Compston W, Wu JS, Shen QH (1992) Remnants of ≥ 3800 Ma crust in the Chinese part of the Sino-Korean craton. *Geology* 20:339–342
- Liu GD (1987) The Cenozoic rift system of the North China Plain and the deep internal process. *Tectonophysics* 133:277–285

- Liu RX, Qiu CY, Chen WJ et al (1986) The Potassium-Argon dating of Cenozoic volcanic rocks in North China. In: Institute of Geology, China Seismological Bureau (eds) *Research on Recent Crustal Movement*. Seismological Press, Beijing, pp 128–136 (in Chinese with English abstract)
- Luo JL, Gao ZY (1998) Discussion on the origin and geochemical characteristics of the Mesozoic volcanic sequences in Fenghuadian Area, Hebei Province. *Acta Petrol Sin* 14:108–116 (in Chinese with English abstract)
- Martin H (1999) Adakitic magmas: modern analogues of Archean granitoids. *Lithos* 46:411–429
- Maruyama S (1997) Pacific-type orogeny revised: Miyashiro-type orogeny proposed. *Isl Arc* 6:91–120
- McCulloch MT, Keyser TK, Woodhead J et al (1994) Pb-Sr-Nd-O isotopic constraints on the origin of rhyolites from the Taupo Volcanic Zone of New Zealand: evidence for assimilation followed by fractionation of basalt. *Contrib Mineral Petrol* 115:303–312
- Meng QR (2003) What drove late Mesozoic extension of the northern China-Mongolia tract? *Tectonophysics* 369:155–174
- Menzies MA, Fan WM, Zhang M (1993) Palaeozoic and Cenozoic lithosphere and the loss of >120 km of Archean lithosphere, Sino-Korean craton, China. In: Prichard HM, Alabaster T, Harris NBW, Neary CR (eds) *Magmatic Processes and Plate Tectonic*. Geol Soc London Spe Pub 76:1–81
- Menzies MA, Xu YG (1998) Geodynamics of the North China Craton. In: Flower MFJ, Chung SL, Lo CH, Lee TY (eds) *Mantle dynamics and plate interactions in East Asia*. Geophysical Monograph: American Geophysical Union 27:155–165
- Nakajima T, Kamiyama H, Williams IS, Tani K (2005) Mafic rocks from the Ryoke Belt, southwest Japan: implications for Cretaceous Ryoke/San-yo granitic magma genesis. *Geol Soc Am Special Paper* 389:249–263
- Nielsen R (2006) Geochemical Earth Reference Model (GERM) partition coefficient (Kd) database. <http://www.geo.oregonstate.edu/people/faculty/nielsenr.htm>
- Niu BG, He ZJ, Song B et al (2004) SHRIMP geochronology of volcanics of the Zhangjiakou and Yixian Formation, Northern Hebei province, with a discussion on the age of the Xing'anling Group of the Great Hinggan mountains and volcanic strata of the south-eastern coastal area of china. *Acta Geol Sin* 78:1214–1228
- Niu YL (2005) Generation and evolution of basaltic magmas: Some basic concepts and a hypothesis for the origin of the Mesozoic-Cenozoic volcanism in eastern China. *Geol J China Univ* 11:9–46
- Niu YL (2006) Continental lithospheric thinning results from hydration weakening, not “delamination”, and is a special consequence of plate tectonics. <http://www.mantleplumes.org/Hydration.html>. Accessed 28 May 2006
- Park Y, Kim S, Kee WS, Jeong YJ, Yi K, Kim J (2009) Middle Jurassic tectono-magmatic evolution in the southwestern margin of the Gyeonggi Massif, South Korea. *Geosci J* 13:217–231
- Peccerillo A, Taylor SR (1976) Geochemistry of Eocene calc-alkaline volcanic rocks from the Kastamonu area, Northern Turkey. *Contrib Mineral Petrol* 58:63–81
- Poulet A, Lee JS, Vidal P, Cousens B, Bellon H (1994) Cretaceous to Cenozoic volcanism in South Korea and in the Sea of Japan: magmatic constraints on the opening of the back-arc basin. *Geol Soc London Spe Pub* 81:169–191
- Qian Q, Chung SL, Lee TY, Wen DJ (2003) Mesozoic high-Ba-Sr granitoids from North China: geochemical characteristics and geological implications. *Terra Nova* 15:272–278
- Qiu JS, Xu XS, Lo QH (2002) Potash-rich volcanic rocks and lamprophyres in western Shandong Province: ⁴⁰Ar-³⁹Ar dating and source tracing. *Chin Sci Bull* 47:91–99
- Rapp RP, Shimizu N, Norman MD et al (1999) Reaction between slab-derived melts and peridotite in the mantle wedge: experimental constraints at 3.8 GPa. *Chem Geol* 160:335–356
- Rapp RP, Watson EB (1995) Dehydration melting of metabasalt at 8–32-Kbar: implications for continental growth and crust–mantle recycling. *J Petrol* 36:891–931
- Rapp RP, Watson EB, Miller CF (1991) Partial melting of amphibolite eclogite and the origin of Archean trondhjemites and tonalites. *Precam Res* 51:1–25
- Ren J, Tamaki K, Li S, Junxia Z (2002) Late Mesozoic and Cenozoic rifting and its dynamic setting in Eastern China and adjacent areas. *Tectonophysics* 344:175–205
- Rudnick RL, Gao S (2003) The composition of the continental crust. In: Rudnick RL (ed) *The crust. Treatise on Geochemistry*, Elsevier, Oxford, pp 3:1–64
- Sagong H, Kwon S-T, Ree JH (2005) Mesozoic episodic magmatism in South Korea and its tectonic implication. *Tectonics* 24:TC5002–TC5007
- Salter VJM, Shimizu N (1988) World-wide occurrence of HFSE-depleted mantle: *Geochim Cosmochim Acta* 52:2177–2182
- Şengör AMC, Natal'in BA (1996) Paleotectonics of Asia: fragments of a synthesis. In: Yin A,

- Harrison TM (eds) The tectonic evolution of Asia. Cambridge Univ Press, Cambridge, pp 486–641
- Sleep NH (2005) Evolution of continental lithosphere. *Annu Rev Earth Planet Sci* 33:369–393
- Sun SS, McDonough WE (1989) Chemical and isotopic systematic of oceanic basalts: Implication for mantle composition and processes. In: Saunders AD and Norry MJ (eds) *Magmatism in the Ocean Basin*. Geol Soc London Spe Pub 42:313–345
- Sun WD, Ding X, Hu YH, Li XH (2007) The golden transformation of the Cretaceous plate subduction in the west Pacific. *Earth Planet Sci Lett* 262:533–542
- Tan ZF, Zhang QF, Yuan ZX (1989) Neocathaysian structural system in East China. China University of Geosciences Press, Wuhan, pp 209 (in Chinese)
- Tang JF, Liu YL, Wang QF (2008) Geochronology of Mesozoic volcanic rocks in Shandong province. *Acta Petrol Sin* 24:1333–1338 (in Chinese with English abstract)
- Tatsumi Y, Maruyama S, Nohda S (1990) Mechanism of backarc opening in the Japan Sea: role of asthenospheric injection. *Tectonophysics* 181:299–306
- Thorkelson DJ (1996) Subduction of diverging plates and the principles of slab window formation. *Tectonophysics* 255:47–63
- Turner S, Arnaud N, Liu J et al (1996) Post-collision, shoshonitic volcanism on the Tibetan Plateau: implications for convective thinning of the lithosphere and the source of ocean island basalts. *J Petrol* 37:45–71
- Vavra G, Schmid R, Gebauer D (1999) Internal morphology, habit and U-Th-Pb microanalysis of amphibolite-to-granulite facies zircons: geochronology of the Ivrea Zone (Southern Alps). *Contrib Mineral Petrol* 134:380–404
- Wan YS, Li RW, Wilde SA et al (2005) UHP metamorphism and exhumation of the Dabie orogen, China: evidence from SHRIMP dating of zircon and monazite from a UHP granitic gneiss cobble from the Hefei basin. *Geochim Cosmochim Acta* 69:4333–4348
- Wang F, Zhou XH, Zhang LC et al (2006a) Late Mesozoic volcanism in the Great Xing'an Range (NE China): Timing and implications for the dynamic setting of NE Asia. *Earth Planet Sci Lett* 251:179–198
- Wang PJ, Chen FK, Chen SM, Siebel W, Satir M (2006b) Geochemical and Nd-Sr-Pb isotopic composition of Mesozoic volcanic rocks in the Songliao basin, NE China. *Geochim J* 40:149–159
- Wang PJ, Gao YF, Ren YG, Liu WZ, Zhang JG (2009) $^{40}\text{Ar}/^{39}\text{Ar}$ age and geochemical features of mugearite from the Qingshankou Formation: Significances for basin formation, hydrocarbon generation and petroleum accumulation of the Songliao Basin in Cretaceous. *Acta Petrol Sin* 25:1178–1190 (in Chinese with English abstract)
- Wang PJ, Liu WZ, Wang SX, Song WH (2002) $^{40}\text{Ar}/^{39}\text{Ar}$ and K/Ar dating on the volcanic rocks in the Songliao basin, NE China: constraints on stratigraphy and basin dynamics. *Int J Earth Sci* 91:331–340
- Wang W, Xu WL, Ji WQ, Yang DB, Pei FP (2006c) Late Mesozoic and Paleogene basalts deep-derived xenocrysts in eastern Liaoning Province, China: Constraints on nature of lithospheric mantle. *Geol J Chin Univ* 12:30–40 (in Chinese with English abstract)
- Watson MP, Hayward AB, Parkinson DN, Zhang ZM (1987) Plate tectonic history, basin development and petroleum source rock deposition onshore China. *Mar Pet Geol* 4:205–225
- Watt GR, Harley SL (1993) Accessory phase controls on the geochemistry of crustal melts and restites produced by dehydration melting. *Contrib Mineral Petrol* 125:100–111
- Wilde SA, Zhou X, Nemchin AA, Sun M (2003) Mesozoic crust-mantle interaction beneath the North China craton: A consequence of the dispersal of Gondwanaland and accretion of Asia. *Geology* 31:817–820
- Wilson M (1989) *Igneous petrogenesis: a global tectonic approach*. Chapman & Hall, London, p466
- Winchester J, Floyd P (1977) Geochemical discrimination of different magma series and their differentiation products using immobile elements. *Chem Geol* 20:325–343
- Wu FY, Ge WC, Sun DY et al (2003) Discussion on the lithospheric thinning in eastern China. *Earth Sci Front* 10:51–60 (in Chinese with English abstract)
- Wu FY, Lin JQ, Wilde SA, Zhang XO, Yang JH (2005) Nature and significance of the Early Cretaceous giant igneous event in eastern China. *Earth Planet Sci Lett* 233:103–119
- Wu FY, Xu YG, Gao S, Zheng JP (2008) Lithospheric thinning and destruction of the North China Craton. *Acta Petrol Sin* 24:1145–1174 (in Chinese with English abstract)
- Wu FY, Yang JH, Lo CH et al (2007) The Heilongjiang Group: A Jurassic accretionary complex in the Jiamusi Massif at the western Pacific margin of northeastern China. *Isl Arc* 16:156–172
- Xu YG (2001) Thermo-tectonic destruction of the Archean lithospheric keel beneath the Sino-Korean

- craton in China: evidence, timing and mechanism. *Phys Chem Earth (A)* 26:747–757
- Xu YG, Blusztajn J, Ma JL, Suzuki K, Liu JF, Hart SR (2008) Late Archean to early Proterozoic lithospheric mantle beneath the western North China craton: Sr-Nd-Os isotopes of peridotite xenoliths from Yangyuan and Fansi. *Lithos* 102:25–42
- Yan J, Chen JF, Xie Z et al (2003) Mantle xenoliths from Late Cretaceous basalt in eastern Shandong Province: New constraint on the timing of lithospheric thinning in eastern China. *Chin Sci Bull* 48: 2139–2144
- Yang JH, Wu FY, Shao JA et al (2006) In-situ U-Pb dating and Hf isotopic analyses of zircons from volcanic rocks of the Houcheng and Zhangjiakou Formations in the Zhang-Xuan area, Northeast China. *J Chin Univ Geosci* 31:71–80 (in Chinese with English abstract)
- Yang W, Li SG (2008) Geochronology and geochemistry of the Mesozoic volcanic rocks in Western Liaoning: Implications for lithospheric thinning of the North China Craton. *Lithos* 102:88–117
- Yuan HL, Gao S, Liu XM et al (2004) Accurate U–Pb age and trace element determinations of zircon by laser ablation-inductively coupled plasma mass spectrometry. *Geostand Newslett* 28:353–370
- Yuan HL, Liu XM, Liu YS et al (2006) Geochemistry and U-Pb zircon geochronology of Late-Mesozoic lavas from Xishan, Beijing. *Sci Chin D* 49:50–67
- Zhai MG, Fan QC, Zhang HF, Sui H, Shao J (2007) Lower crustal processes leading to Mesozoic lithospheric thinning beneath eastern North China: Underplating, replacement and delamination. *Lithos* 96:36–54
- Zhai MG, Liu WJ (2003) Paleoproterozoic tectonic history of the North China craton: a review. *Precam Res* 122:183–199
- Zhai MG, Zhu RX, Liu JM et al (2004) Time range of Mesozoic tectonic regime inversion in eastern North China Block. *Sci Chin D* 47:151–159
- Zhang C, Ma CQ, Liao QA et al (2009a) Geochemistry of Late Mesozoic-Cenozoic volcanic rocks in the Huanghua depression, Bohai Bay: Petrogenesis and implications for tectonic transition. *Acta Petrol Sin* 25:1159–1177 (in Chinese with English abstract)
- Zhang FQ, Cheng XG, Chen HL et al (2009b) Zircon chronological and geochemical constraints on the Late Mesozoic volcanic events in the southeastern margin of the Songliao Basin, NE China. *Acta Petrol Sin* 25:39–54 (in Chinese with English abstract)
- Zhang H, Guo WM, Liu XM (2008a) Constraints on the late Mesozoic regional angular unconformity in West Liaoning-North Hebei by LA-ICP-MS dating. *Progress in Natural Science* 18:1395–1402
- Zhang H, Wang MX, Liu XM (2008b) Constraints on the upper boundary age of the Tiaoishan Formation volcanic rocks in West Liaoning-North Hebei by LA-ICP-MS dating. *Chin Sci Bull* 53:3574–3584
- Zhang HF, Sun M, Zhou MF, Fan WM, Zhou XH, Zhai MG (2004) Highly heterogeneous Late Mesozoic lithospheric mantle beneath the North China Craton: evidence from Sr-Nd-Pb isotopic systematics of mafic igneous rocks. *Geol Mag* 141:55–62
- Zhang HF, Sun M, Zhou X et al (2002) Mesozoic lithosphere destruction beneath the North China Craton: evidence from major-, trace-element and Sr-Nd-Pb isotope studies of Fangcheng basalts. *Contrib Mineral Petrol* 144:241–253
- Zhang HF, Sun M, Zhou X et al (2003) Secular evolution of the lithosphere beneath the eastern North China Craton: evidence from Mesozoic basalts and high-Mg andesites. *Geochim Cosmochim Acta* 67:4373–4387
- Zhang JH, Ge WC, Wu FY et al (2008c) Large-scale Early Cretaceous volcanic events in the northern Great Xing'an Range, Northeastern China. *Lithos* 102:138–157
- Zhang YQ, Dong SW, Zhao Y et al (2007) Jurassic tectonic of North China: a synthetic view. *Acta Geol Sin* 81:1462–1480 (in Chinese with English abstract)
- Zhao GC, Cawood PA, Wilde SA et al (2000) Metamorphism of basement rocks in the central zone of the North China Craton: Implications for Paleoproterozoic tectonic evolution. *Precam Res* 103:55–88
- Zhao GC, Wilde SA, Cawood PA et al (2001) Archean blocks and their boundaries in the North China Craton: lithological, geochemical, structural and P-T path constraints and tectonic evolution. *Precam Res* 107:45–73
- Zhao Y, Xu G, Zhang SH et al (2004) Yanshanian movement and conversion of tectonic regimes in East Asia. *Earth Sci Front* 11:319–328 (in Chinese with English abstract)
- Zhao Y, Yang ZY, Ma XH (1994) Geotectonic transition from paleoasian system and Plaeotethyan system to Paleopacific active continental margin in eastern Asia. *Sci Geol Sin* 29:105–119 (in Chinese with English abstract)
- Zheng JP, Griffin WL, O'Reilly SY et al (2006) Mineral chemistry of peridotites from Paleozoic, Mesozoic and Cenozoic lithosphere: constraints on mantle evolution beneath Eastern China. *J*

Petrol 47:2233–2256

- Zhou X, Sun T, Shen W, Shu L, Niu Y (2006) Petrogenesis of Mesozoic granitoids and volcanic rocks in South China: A response to tectonic evolution. *Episodes* 29:26–33
- Zhou XH, Armstrong RL (1982) Cenozoic volcanic rocks of eastern China - secular and geographic trends in chemistry and strontium isotopic composition: *Earth Planet Sci Lett* 59:301–329
- Zhou XM, Li WX (2000) Origin of Late Mesozoic igneous rocks in southeastern China: Implications for lithosphere subduction and underplating of mafic magmas: *Tectonophysics* 326:269–287
- Zhu RX, Zheng TY (2009) Destruction geodynamics of the North China craton and its Paleoproterozoic plate tectonics. *Chin Sci Bull* 54:3354–3366

Table I-1 LA-ICP-MS U-Pb data of zircons from sample K36-2

| Spot | Element (ppm) | | | Ratios corrected for common Pb | | | | | | Age (Ma) | | | | | | |
|------|---------------|------|----------|--------------------------------|-----------------------------------|------------|----------------------------------|------------|----------------------------------|------------|----------------------------------|------------|------|----|------|----|
| | Th | U | Total Pb | Th/U | $^{207}\text{Pb}/^{206}\text{Pb}$ | 1 σ | $^{207}\text{Pb}/^{235}\text{U}$ | 1 σ | $^{206}\text{Pb}/^{238}\text{U}$ | 1 σ | $^{206}\text{Pb}/^{238}\text{U}$ | 1 σ | | | | |
| 1.1 | 80 | 855 | 70.91 | 0.09 | 0.05005 | 0.00233 | 0.12795 | 0.00582 | 0.01855 | 0.00027 | 0.00771 | 0.00040 | 122 | 5 | 118 | 2 |
| 1.2 | 66 | 569 | 46.82 | 0.12 | 0.04926 | 0.00263 | 0.12510 | 0.00654 | 0.01842 | 0.00028 | 0.00593 | 0.00036 | 120 | 6 | 118 | 2 |
| 2.1 | 101 | 475 | 40.14 | 0.21 | 0.05612 | 0.00318 | 0.14252 | 0.00775 | 0.01842 | 0.00029 | 0.00573 | 0.00007 | 135 | 7 | 118 | 2 |
| 3.1 | 267 | 1085 | 94.52 | 0.25 | 0.06120 | 0.00527 | 0.15665 | 0.01301 | 0.01856 | 0.00042 | 0.00572 | 0.00010 | 148 | 11 | 119 | 3 |
| 4.1 | 105 | 783 | 65.20 | 0.13 | 0.05143 | 0.00216 | 0.13089 | 0.00520 | 0.01846 | 0.00025 | 0.00581 | 0.00007 | 125 | 5 | 118 | 2 |
| 5.1 | 73 | 769 | 64.09 | 0.10 | 0.05243 | 0.00329 | 0.13446 | 0.00825 | 0.01860 | 0.00032 | 0.00799 | 0.00055 | 128 | 7 | 119 | 2 |
| 5.2 | 60 | 642 | 53.80 | 0.09 | 0.05012 | 0.00249 | 0.12988 | 0.00631 | 0.01880 | 0.00028 | 0.00698 | 0.00039 | 124 | 6 | 120 | 2 |
| 6.1 | 178 | 339 | 30.00 | 0.52 | 0.05834 | 0.00412 | 0.14912 | 0.01028 | 0.01854 | 0.00035 | 0.00617 | 0.00025 | 141 | 9 | 118 | 2 |
| 7.1 | 92 | 366 | 31.96 | 0.25 | 0.05310 | 0.00530 | 0.13776 | 0.01343 | 0.01882 | 0.00045 | 0.00880 | 0.00057 | 131 | 12 | 120 | 3 |
| 8.1 | 71 | 674 | 57.90 | 0.11 | 0.05174 | 0.00304 | 0.13188 | 0.00757 | 0.01849 | 0.00031 | 0.00778 | 0.00047 | 126 | 7 | 118 | 2 |
| 9.1 | 28 | 343 | 28.57 | 0.08 | 0.05089 | 0.00389 | 0.13134 | 0.00983 | 0.01872 | 0.00036 | 0.00738 | 0.00071 | 125 | 9 | 120 | 2 |
| 10.1 | 35 | 572 | 47.20 | 0.06 | 0.04982 | 0.00271 | 0.12780 | 0.00680 | 0.01861 | 0.00030 | 0.00707 | 0.00056 | 122 | 6 | 119 | 2 |
| 11.1 | 80 | 722 | 60.73 | 0.11 | 0.05680 | 0.00277 | 0.14633 | 0.00679 | 0.01868 | 0.00028 | 0.00581 | 0.00007 | 139 | 6 | 119 | 2 |
| 12.1 | 224 | 1373 | 114.37 | 0.16 | 0.04959 | 0.00245 | 0.12680 | 0.00612 | 0.01855 | 0.00029 | 0.00610 | 0.00027 | 121 | 6 | 118 | 2 |
| 13.1 | 53 | 682 | 57.19 | 0.08 | 0.05211 | 0.00317 | 0.13449 | 0.00785 | 0.01872 | 0.00032 | 0.00588 | 0.00013 | 128 | 7 | 120 | 2 |
| 14.1 | 114 | 954 | 79.85 | 0.12 | 0.05011 | 0.00237 | 0.12939 | 0.00598 | 0.01873 | 0.00028 | 0.00645 | 0.00029 | 124 | 5 | 120 | 2 |
| 15.1 | 132 | 167 | 408.56 | 0.79 | 0.15705 | 0.00360 | 9.91612 | 0.22277 | 0.45803 | 0.00553 | 0.12864 | 0.00255 | 2427 | 21 | 2431 | 24 |

Table I-2 SHRIMP U-Pb data of zircons from sample F22

| Spot | Th (ppm) | U (ppm) | Th/U | % ²⁰⁶ Pb _c | ²⁰⁶ Pb* | Total ²³⁸ U/ ²⁰⁶ Pb | ±% | Total ²⁰⁷ Pb/ ²⁰⁶ Pb | ±% | ²⁰⁷ Pb* / ²⁰⁶ Pb* | ±% | ²⁰⁷ Pb* / ²³⁵ U | ±% | ²⁰⁶ Pb* / ²³⁸ U | ±% | Age (Ma) | |
|------|-------------|------------|------|----------------------------------|--------------------|--|-----|---|-----|--|----|--|----|--|-----|-------------------------------------|-----|
| | | | | | | | | | | | | | | | | ²⁰⁶ Pb/ ²³⁸ U | 1σ |
| 1.1 | 51 | 74 | 0.72 | 17.85 | 0.871 | 72.9 | 3.4 | 0.157 | 7.2 | | | | | 0.01127 | 5.1 | 72.2 | 3.6 |
| 2.1 | 186 | 152 | 1.27 | 12.02 | 1.73 | 75.1 | 3.2 | 0.1301 | 6.7 | 0.033 | 34 | 0.053 | 34 | 0.01171 | 3.3 | 75.0 | 2.4 |
| 3.1 | 39 | 32 | 1.26 | 53.63 | 0.431 | 63.9 | 4.4 | 0.283 | 8.3 | | | | | 0.0073 | 39 | 47 | 18 |
| 4.1 | 1048 | 384 | 2.82 | 5.34 | 3.85 | 85.8 | 2.5 | 0.0701 | 7.7 | 0.027 | 56 | 0.041 | 56 | 0.01104 | 3.0 | 70.8 | 2.1 |
| 5.1 | 1020 | 600 | 1.76 | 4.27 | 5.96 | 86.4 | 2.3 | 0.0746 | 3.8 | 0.040 | 28 | 0.062 | 28 | 0.01107 | 2.7 | 71.0 | 1.9 |
| 6.1 | 342 | 146 | 2.42 | 10.22 | 1.76 | 71.4 | 3.0 | 0.1551 | 5.3 | 0.077 | 28 | 0.134 | 29 | 0.01257 | 4.0 | 80.5 | 3.2 |
| 7.1 | 501 | 229 | 2.26 | 9.75 | 2.25 | 87.3 | 2.7 | 0.1021 | 5.5 | | | | | 0.01034 | 4.5 | 66.3 | 3.0 |
| 8.1 | 94 | 67 | 1.45 | 35.89 | 0.887 | 65.3 | 3.8 | 0.203 | 8.0 | | | | | 0.0098 | 17 | 63 | 11 |
| 9.1 | 1399 | 958 | 1.51 | 3.24 | 9.54 | 86.3 | 2.3 | 0.0649 | 3.1 | 0.0389 | 19 | 0.060 | 19 | 0.01121 | 2.4 | 71.9 | 1.7 |
| 10.1 | 1107 | 641 | 1.79 | 6.03 | 6.29 | 87.5 | 2.3 | 0.0731 | 3.8 | 0.024 | 59 | 0.035 | 60 | 0.01074 | 2.9 | 68.8 | 2.0 |

Pb_c and Pb* indicate the common and radiogenic portions, respectively.

Table I-3 Elemental compositions of Mesozoic volcanic rocks in the Huanghua depression, Bohai Bay Basin

| Sample | K12 | T14 | Q2 | G141 | G142 | K36-1 | K36-2 | Z1582-1 | Z1582-2 | Z119 | Z59 | Z1270 | Z51 | F22 |
|--------------------------------|----------------|----------------|----------------|----------------|----------------|----------------|----------------|----------------|----------------|----------------|----------------|----------------|----------------|----------------|
| Borehole No. | Kou12 | Tang14 | Qigu2 | Guan141 | Guan142 | Kou36-1 | Kou36-2 | Zaol1582-1 | Zaol1582-2 | Zaol119 | Zaol59 | Zaol1270 | Zaol51 | Feng22 |
| Depth(m) | 1990 | 2241 | 2331 | 3304 | 2380 | 1685 | 1686 | 2989 | 3022 | 3096 | 2982 | 2858 | 3026 | 2942 |
| Era | K ₁ | K ₁ | K ₁ | K ₁ | K ₁ | K ₁ | K ₁ | K ₂ | K ₂ | K ₂ | K ₂ | K ₂ | K ₂ | K ₂ |
| Rock type | Te | BTA | BTA | T | TA | TA | P | T | T | R | R | T | T | R |
| Data source | (1) | (2) | (2) | (2) | (2) | (2) | (1) | (3) | (3) | (3) | (3) | (3) | (3) | (1) |
| SiO ₂ (wt%) | 42.00 | 52.93 | 50.95 | 60.22 | 55.14 | 60.06 | 58.52 | 67.59 | 68.10 | 71.04 | 70.44 | 67.03 | 68.08 | 70.90 |
| TiO ₂ | 1.84 | 1.16 | 1.61 | 0.96 | 1.04 | 1.35 | 1.37 | 0.35 | 0.36 | 0.35 | 0.35 | 0.40 | 0.36 | 0.37 |
| Al ₂ O ₃ | 12.18 | 14.25 | 16.24 | 17.04 | 16.40 | 16.84 | 16.48 | 14.35 | 14.87 | 14.32 | 14.16 | 15.44 | 14.07 | 13.80 |
| Fe ₂ O ₃ | 6.54 | 5.81 | 7.64 | 4.36 | 3.52 | 1.27 | 0.64 | 2.90 | 1.17 | 1.68 | 1.89 | 1.94 | 0.98 | 0.62 |
| FeO | 8.05 | 1.94 | 1.99 | 1.34 | 3.31 | 2.10 | 2.65 | 1.82 | 1.58 | 1.11 | 0.85 | 0.96 | 2.58 | 1.27 |
| MnO | 0.19 | 0.09 | 0.22 | 0.10 | 0.08 | 0.08 | 0.04 | 0.04 | 0.02 | 0.03 | 0.03 | 0.05 | 0.03 | 0.03 |
| MgO | 6.56 | 6.81 | 3.45 | 1.22 | 2.55 | 1.01 | 0.65 | 0.61 | 0.79 | 0.50 | 0.40 | 0.61 | 1.19 | 0.54 |
| CaO | 7.79 | 5.82 | 6.30 | 2.20 | 4.25 | 2.80 | 2.80 | 1.10 | 0.60 | 1.00 | 1.20 | 1.50 | 0.75 | 0.51 |
| Na ₂ O | 3.68 | 4.00 | 4.56 | 5.76 | 5.48 | 5.48 | 7.52 | 4.03 | 4.79 | 4.16 | 4.28 | 4.52 | 4.27 | 4.88 |
| K ₂ O | 1.76 | 3.20 | 2.40 | 4.50 | 2.78 | 4.40 | 5.01 | 5.19 | 5.42 | 4.99 | 5.11 | 5.60 | 4.90 | 5.13 |
| P ₂ O ₅ | 0.76 | 0.68 | 1.06 | 0.67 | 0.78 | 1.52 | 1.16 | 0.12 | 0.12 | 0.12 | 0.12 | 0.12 | 0.11 | 0.12 |
| H ₂ O ⁺ | 2.95 | 2.40 | 0.46 | 0.80 | 1.82 | 1.04 | 1.00 | 0.98 | 0.92 | 0.50 | 0.42 | 1.08 | 1.20 | 1.43 |
| H ₂ O ⁻ | n.d. | 1.22 | 1.68 | n.d. | n.d. | n.d. | n.d. | 0.31 | 0.30 | 0.23 | 0.17 | 0.45 | 0.48 | n.d. |
| CO ₂ | 5.17 | n.d. | n.d. | 0.12 | 0.66 | 1.06 | 0.43 | n.d. | n.d. | n.d. | n.d. | n.d. | n.d. | 0.14 |
| L.O.I | 3.79 | n.d. | 2.98 | 1.65 | n.d. | 2.62 | 1.13 | n.d. | n.d. | 1.02 | 1.41 | 0.56 | 0.69 | 1.24 |
| Total | 99.47 | 100.31 | 98.56 | 99.29 | 97.81 | 99.01 | 98.27 | 99.39 | 99.04 | 100.03 | 99.42 | 99.70 | 99.00 | 99.74 |
| Mg# | 46 | 63 | 41 | 29 | 41 | 36 | 26 | 20 | 35 | 25 | 22 | 29 | 38 | 34 |
| Nb (ppm) | 17.32 | n.d. | 27 | 22 | n.d. | 21 | 27.24 | 20 | 26 | 22 | 24 | 21 | 20 | 21.19 |
| Zr | 129.1 | 275 | 269 | 320 | n.d. | 289 | 205.9 | 214 | 215 | 214 | 224 | 310 | 242 | 222.5 |
| Y | 16.7 | 18.5 | 27.4 | 18.1 | 17.8 | 12.41 | 12.6 | 11.7 | 12.1 | 12.2 | 11.4 | 15.4 | 11.6 | 12.7 |
| Ta | 0.86 | n.d. | 1.46 | 1.46 | n.d. | 1.30 | 1.41 | 0.44 | 0.60 | 0.92 | 0.62 | 0.92 | 1.10 | 1.31 |
| Rb | 29 | 62 | 25 | 74 | n.d. | 54 | 51.6 | 131 | 128 | 128 | 134 | 113 | 98 | 100 |
| Sr | 1699 | 2173 | 1455 | 929 | n.d. | 2457 | 2548.6 | 222 | 168 | 262 | 284 | 313 | 188 | 231.3 |
| Ba | 1662.8 | 2100 | 1829 | 3081 | n.d. | 2665 | 2746.3 | 1722 | 2745 | 1426 | 1375 | 1250 | 1431 | 1447.4 |
| U | 0.62 | n.d. | n.d. | n.d. | n.d. | n.d. | 1.79 | 1.84 | 2.16 | 2.1 | 2.6 | 1.66 | 1.98 | 1.94 |
| Th | 4.00 | n.d. | n.d. | n.d. | n.d. | n.d. | 12.19 | 9 | 11 | 9 | 8 | 10 | 10 | 8.11 |
| Pb | 14.91 | n.d. | n.d. | n.d. | n.d. | n.d. | 34.01 | n.d. | n.d. | n.d. | n.d. | n.d. | n.d. | 19.55 |
| Hf | 3.54 | n.d. | n.d. | n.d. | n.d. | n.d. | 6.05 | n.d. | n.d. | n.d. | n.d. | n.d. | n.d. | 6.22 |
| V | 190 | 165 | 157 | 83 | n.d. | 148 | 129 | 41 | 39 | 36 | 33 | 33 | 25 | 18 |
| Cr | 143.9 | 328 | 236 | 237 | n.d. | 295 | 131.4 | 30 | 13 | 21 | 22 | 19 | 13 | 10.1 |

| | | | | | | | | | | | | | | |
|----------------------|--------|--------|--------|--------|--------|--------|--------|--------|--------|--------|--------|--------|--------|--------|
| Co | 49.7 | 40.0 | 28.0 | 12 | n.d. | 6 | 6.7 | 7 | 5 | 4 | 3 | 4 | 7 | 3.3 |
| Ni | 186.4 | 196 | 104 | 23 | n.d. | 38 | 53.3 | 7 | 5 | 3 | 5 | 4 | 6 | 4.2 |
| La (ppm) | 68.02 | 154.7 | 92.34 | 75.61 | 92.08 | 130.3 | 124.11 | 52.32 | 52.27 | 47.29 | 55.91 | 85.11 | 55.18 | 59.80 |
| Ce | 142.3 | 311.9 | 165.1 | 151.6 | 164.1 | 221.2 | 250.7 | 93.7 | 95.1 | 88.8 | 95.3 | 142.2 | 104.7 | 110.6 |
| Pr | 17.33 | 35.77 | 21.55 | 18.52 | 20.17 | 28.5 | 28.47 | 11.12 | 11.74 | 10.47 | 11.33 | 17.56 | 11.64 | 11.35 |
| Nd | 65.7 | 118.3 | 83.0 | 66.2 | 73.7 | 105 | 98.4 | 34.0 | 34.8 | 30.9 | 34.2 | 53.5 | 36.6 | 36.1 |
| Sm | 10.50 | 15.62 | 11.59 | 8.31 | 8.98 | 12.19 | 13.75 | 5.04 | 5.1 | 4.66 | 4.95 | 7.73 | 5.19 | 5.24 |
| Eu | 2.68 | 3.20 | 3.25 | 2.10 | 2.23 | 3.03 | 3.32 | 1.01 | 0.98 | 1.01 | 1.08 | 1.47 | 1.02 | 1.22 |
| Gd | 6.53 | 9.46 | 8.2 | 5.67 | 6.09 | 6.76 | 7.23 | 3.30 | 3.40 | 3.09 | 3.41 | 5.11 | 3.57 | 3.33 |
| Tb | 0.79 | 0.83 | 0.88 | 0.59 | 0.64 | 0.51 | 0.75 | 0.42 | 0.47 | 0.43 | 0.45 | 0.67 | 0.46 | 0.43 |
| Dy | 3.65 | 4.9 | 5.42 | 3.85 | 3.93 | 3.18 | 3.03 | 2.16 | 2.27 | 2.2 | 2.08 | 3.11 | 2.22 | 2.16 |
| Ho | 0.62 | 0.78 | 0.97 | 0.74 | 0.75 | 0.58 | 0.49 | 0.41 | 0.42 | 0.42 | 0.4 | 0.59 | 0.41 | 0.42 |
| Er | 1.67 | 2.56 | 2.79 | 1.98 | 1.97 | 1.36 | 1.27 | 1.17 | 1.23 | 1.19 | 1.17 | 1.61 | 1.20 | 1.27 |
| Tm | 0.22 | 0.21 | 0.34 | 0.27 | 0.26 | 0.17 | 0.16 | 0.20 | 0.19 | 0.19 | 0.19 | 0.25 | 0.19 | 0.20 |
| Yb | 1.27 | 1.68 | 2.05 | 1.60 | 1.65 | 0.91 | 0.92 | 1.20 | 1.24 | 1.27 | 1.17 | 1.50 | 1.18 | 1.38 |
| Lu | 0.18 | 0.35 | 0.30 | 0.24 | 0.25 | 0.13 | 0.12 | 0.18 | 0.19 | 0.19 | 0.18 | 0.23 | 0.18 | 0.20 |
| ΣREE | 321.39 | 660.26 | 397.78 | 337.30 | 376.76 | 513.82 | 532.72 | 206.27 | 209.41 | 192.16 | 211.82 | 320.58 | 223.73 | 233.70 |
| (La/Yb) _N | 36.12 | 62.08 | 30.37 | 31.86 | 37.62 | 96.54 | 90.77 | 29.39 | 28.42 | 25.10 | 32.22 | 38.25 | 31.53 | 29.23 |
| (Tb/Lu) _N | 2.94 | 1.62 | 2.00 | 1.68 | 1.74 | 2.67 | 4.26 | 1.59 | 1.69 | 1.54 | 1.70 | 1.99 | 1.74 | 1.47 |
| Eu/Eu* | 0.92 | 0.75 | 0.97 | 0.89 | 0.87 | 0.93 | 0.92 | 0.71 | 0.68 | 0.77 | 0.76 | 0.67 | 0.69 | 0.84 |

Rock type: T, Trachyte; R, Rhyolite; TA, Trachyandesite; P, Phonolite; Te, Tephrite; BTA, Basaltic trachyandesite; B, Basalt. Data source: (1) this study; (2) Gao and Zhang (1995); (3) Luo and Gao (1998). Mg# = $[100 \times \text{molar Mg}/(\text{Mg}+\text{Fe})]$; Eu/Eu* = $\text{Eu}_N/(\text{Sm}_N \times \text{Gd}_N)^{0.5}$. n.d. = not determined.

Table I-4 Sr and Nd isotopic composition of representative Late Mesozoic volcanic rocks from the Huanghua depression, Bohai Bay Basin

| Sample | Rock type | $^{87}\text{Sr}/^{86}\text{Sr}$ | $^{87}\text{Rb}/^{86}\text{Sr}$ | $^{143}\text{Nd}/^{144}\text{Nd}$ | $^{147}\text{Sm}/^{144}\text{Nd}$ | $(^{87}\text{Sr}/^{86}\text{Sr})_i$ | $(^{143}\text{Nd}/^{144}\text{Nd})_i$ | $\epsilon_{\text{Nd}(0)}$ |
|--------|--------------|---------------------------------|---------------------------------|-----------------------------------|-----------------------------------|-------------------------------------|---------------------------------------|---------------------------|
| K12 | Basic | 0.705009 | 0.0494 | 0.511618 | 0.0966 | 0.7049 | 0.5115 | -18.4 |
| K36-2 | Intermediate | 0.705383 | 0.0585 | 0.511652 | 0.0844 | 0.7053 | 0.5116 | -17.5 |
| F22 | Acid | 0.707837 | 1.251 | 0.511619 | 0.0879 | 0.7066 | 0.5116 | -18.2 |

Table Supplementary I-1 Supplementary major elemental composition of Late Mesozoic volcanic rocks from Huanghua depression, Bohai Bay Basin*

| Sample | K12-1 | T5 | T10-1 | T10-2 | GSS5 | QG2-1 | QG2-2 | G103-1 | G103-2 | G141-2 | G141-2 | G142-1 | G177-1 | G177-2 | Z55-1 | Z55-2 | Z59-1 | |
|--------------------------------|--------|--------|--------|--------|-----------|--------|--------|----------|--------------|----------|----------|----------|----------|----------|-------|--------|--------|--------|
| Bore No. | Kou12 | Tai5 | Tai10 | Tai10 | Gangshen5 | Qigu2 | Qigu2 | Guant103 | Guant103 | Guant141 | Guant141 | Guant142 | Guant177 | Guant177 | Zao55 | Zao55 | Zao55 | |
| Depth(m) | 2227.0 | 2227.0 | 2242.0 | 2346.0 | 3296.0 | 2314.2 | 2327.2 | 3400.6 | 3408.0 | 3312.6 | 3400.0 | 2380.1 | 2310.3 | 2310.3 | | | | 3016.0 |
| Rock type | Basic | | | | | | | | Intermediate | | | | | | | | | |
| SiO ₂ | 47.64 | 47.67 | 51.22 | 51.11 | 47.97 | 50.55 | 49.98 | 54.34 | 58.68 | 61.19 | 61.27 | 58.85 | 54.82 | 54.74 | 69.48 | 67.30 | 69.63 | |
| TiO ₂ | 1.94 | 0.92 | 1.16 | 1.16 | 1.44 | 1.55 | 1.65 | 0.98 | 1.00 | 0.89 | 0.92 | 0.90 | 0.98 | 1.00 | 0.30 | 0.36 | 0.36 | |
| Al ₂ O ₃ | 14.15 | 13.63 | 14.68 | 14.14 | 15.84 | 16.44 | 16.60 | 15.64 | 14.08 | 16.27 | 15.77 | 15.10 | 16.80 | 16.69 | 13.86 | 13.21 | 14.48 | |
| Fe ₂ O ₃ | 5.94 | 5.95 | 2.73 | 3.91 | 3.47 | 7.24 | 8.00 | 1.83 | 6.27 | 4.16 | 4.34 | 2.54 | 3.92 | 3.87 | 0.80 | 3.33 | 1.69 | |
| FeO | 4.85 | 2.35 | 5.62 | 4.18 | 5.89 | 2.50 | 1.96 | 5.17 | 3.92 | 1.93 | 1.54 | 3.20 | 3.54 | 3.76 | 1.71 | 2.32 | 1.06 | |
| MnO | 0.09 | 0.12 | 0.11 | 0.12 | 0.17 | 0.16 | 0.22 | 0.07 | 0.08 | 0.08 | 0.10 | 0.08 | 0.11 | 0.11 | 0.03 | 0.04 | 0.02 | |
| MgO | 6.97 | 6.59 | 8.50 | 9.19 | 7.79 | 3.45 | 3.45 | 4.65 | 3.64 | 1.40 | 1.58 | 2.80 | 2.98 | 2.95 | 1.28 | 0.86 | 0.61 | |
| CaO | 6.84 | 6.16 | 8.52 | 6.26 | 6.58 | 6.60 | 6.30 | 4.00 | 3.69 | 2.35 | 2.70 | 3.50 | 4.95 | 4.90 | 1.80 | 2.77 | 1.35 | |
| Na ₂ O | 3.76 | 3.40 | 4.72 | 4.27 | 3.90 | 4.56 | 4.56 | 5.53 | 4.84 | 4.92 | 5.12 | 4.74 | 5.48 | 5.40 | 5.00 | 4.30 | 5.00 | |
| K ₂ O | 2.28 | 3.85 | 1.53 | 2.35 | 1.60 | 2.56 | 2.40 | 2.51 | 2.39 | 4.36 | 4.00 | 3.06 | 2.84 | 2.72 | 2.72 | 3.87 | 4.25 | |
| P ₂ O ₅ | 0.82 | 0.82 | 1.19 | 0.82 | 0.46 | 1.01 | 1.06 | 0.73 | 0.51 | 0.70 | 0.65 | 0.96 | 0.84 | 0.86 | 0.12 | 0.11 | 0.13 | |
| CO ₂ | 1.35 | 6.96 | | 0.66 | 0.94 | 0.26 | 0.46 | 1.47 | | 0.12 | 0.22 | 0.44 | 0.19 | 0.21 | 1.34 | | | |
| H ₂ O ⁺ | 3.57 | 1.88 | | 2.04 | 3.55 | 1.62 | 1.68 | 3.41 | | 0.92 | 1.08 | 2.24 | 1.00 | 2.06 | 0.70 | | 0.60 | |
| H ₂ O ⁻ | | | | | | | | | | | | | | | | | 0.22 | |
| LOI | | | | | | 2.53 | 2.98 | | 5.24 | | 1.35 | 3.52 | 1.92 | 2.14 | | 3.97 | 1.20 | |
| Total | 100.20 | 100.30 | 99.98 | 100.21 | 99.60 | 101.03 | 101.30 | 100.33 | 104.33 | 100.34 | 100.64 | 101.93 | 100.37 | 101.41 | 99.14 | 102.44 | 100.60 | |

*after Gao and Zhang (1995)

Table Supplementary I-1 Continued

| Sample | Z59-2 | Z59-3 | Z59-4 | Z64 | Z117 | Z131 | Z1517 | Z1514 | Z1563-1 | Z1563-2 | Z1576-1 | Z1576-2 | F22-15-1 | F22-15-2 | F22-15-3 | F22-15-4 | F22-15-5 | F22-15-6 | |
|--------------------------------|--------|--------|--------|--------|--------|--------|---------|---------|---------|---------|---------|---------|----------|----------|----------|----------|----------|----------|-----------|
| Bore No. | | | | Za064 | Za0117 | Za0131 | Za01517 | Za01544 | Za01563 | Za01563 | Za01576 | Za01576 | | | | | | | Feng22-15 |
| Depth(m) | | | | 2999.2 | | | 2829.0 | 2862.5 | 3232.0 | 3241.0 | 3067.0 | | | | | | | | |
| Rock type | Acid | | | | | | | | | | | | | | | | | | |
| SiO ₂ | 69.60 | 70.54 | 70.74 | 72.28 | 69.98 | 69.40 | 69.35 | 69.30 | 68.18 | 68.53 | 71.94 | 72.94 | 70.81 | 68.80 | 66.96 | 68.17 | 68.55 | 64.87 | |
| TiO ₂ | 0.36 | 0.35 | 0.34 | 0.21 | 0.32 | 0.34 | 0.28 | 0.36 | 0.39 | 0.40 | 0.32 | 0.35 | 0.35 | 0.36 | 0.36 | 0.36 | 0.38 | 0.37 | |
| Al ₂ O ₃ | 14.56 | 14.52 | 14.46 | 13.31 | 14.46 | 14.48 | 15.16 | 14.22 | 15.11 | 15.01 | 13.10 | 13.48 | 12.89 | 13.30 | 12.83 | 14.54 | 14.18 | 14.32 | |
| Fe ₂ O ₃ | 1.81 | 1.91 | 1.74 | 0.70 | 1.56 | 1.17 | 1.36 | 1.85 | 1.55 | 1.78 | 1.97 | 2.03 | 2.14 | 1.38 | 4.06 | 1.32 | 1.72 | 2.82 | |
| FeO | 1.02 | 1.10 | 1.34 | 1.14 | 0.90 | 2.26 | 0.61 | 0.98 | 1.31 | 1.08 | 1.25 | 0.75 | 1.66 | 2.99 | 4.28 | 1.58 | 1.60 | 5.16 | |
| MnO | 0.07 | 0.06 | 0.05 | 0.02 | 0.03 | 0.08 | 0.02 | 0.02 | 0.02 | 0.02 | 0.03 | 0.04 | 0.05 | 0.07 | 0.05 | 0.07 | 0.13 | 0.07 | |
| MgO | 0.57 | 0.69 | 0.45 | 0.50 | 0.34 | 1.03 | 0.54 | 0.61 | 0.72 | 0.54 | 0.48 | 0.34 | 0.61 | 0.79 | 0.50 | 0.50 | 0.75 | 0.36 | |
| CaO | 1.38 | 0.79 | 0.95 | 0.75 | 1.78 | 0.71 | 0.97 | 1.25 | 0.60 | 0.65 | 0.68 | 0.73 | 0.65 | 0.95 | 0.60 | 0.85 | 0.65 | 0.75 | |
| Na ₂ O | 4.34 | 4.65 | 4.23 | 3.80 | 4.34 | 4.62 | 4.28 | 4.28 | 5.06 | 5.50 | 3.92 | 4.16 | 4.29 | 3.86 | 3.64 | 4.81 | 4.58 | 4.73 | |
| K ₂ O | 5.15 | 4.59 | 4.95 | 5.19 | 5.12 | 4.49 | 4.96 | 5.35 | 5.11 | 4.90 | 4.74 | 4.61 | 4.77 | 5.36 | 4.88 | 4.93 | 5.64 | 4.55 | |
| P ₂ O ₅ | 0.12 | 0.12 | 0.12 | 0.06 | 0.10 | 0.11 | 0.06 | 0.12 | 0.11 | 0.12 | 0.12 | 0.10 | 0.12 | 0.14 | 0.13 | 0.15 | 0.16 | 0.17 | |
| CO ₂ | 0.45 | 0.25 | 0.24 | | 0.42 | 0.89 | | | | | | 0.10 | 0.26 | 0.31 | 0.54 | 0.33 | 0.26 | 0.35 | |
| H ₂ O ⁺ | | | | 0.96 | | | 1.54 | 0.72 | 0.88 | 0.94 | 0.54 | | 0.87 | 1.06 | 0.58 | 0.83 | 0.46 | 0.82 | |
| H ₂ O ⁻ | 0.55 | 0.54 | 0.50 | 0.54 | 0.45 | 0.83 | 1.03 | 0.17 | 0.18 | 0.21 | 0.18 | 0.38 | 0.22 | 0.32 | 0.41 | 0.30 | 0.26 | 0.25 | |
| LOI | 0.15 | 0.14 | 0.14 | 1.18 | | 0.14 | 1.84 | 0.94 | 0.96 | 1.00 | 0.60 | 0.17 | | | | | | | |
| Total | 100.13 | 100.25 | 100.25 | 100.64 | 99.80 | 100.55 | 102.00 | 100.17 | 100.18 | 100.68 | 99.87 | 100.18 | 99.69 | 99.69 | 99.82 | 98.74 | 99.32 | 99.59 | |

Part II Origin of high-Mg adakitic magmatic enclaves from the Meichuan pluton, southern Dabie orogen (central China): Implications for delamination of the lower continental crust and melt-mantle interaction

1 Abstract

Field observation, petrography and geochemistry of mafic enclaves/dikes and their host felsic rocks from the Meichuan pluton are used to propose a geodynamic model for the southern Dabie orogen, central China. The similar Sr-Nd isotopic ratios [$\epsilon\text{Nd}(t) = -15$, $(^{87}\text{Sr}/^{86}\text{Sr})_i = 0.70550-0.70597$] and zircon Hf isotopic ratios [$\epsilon\text{Hf}(t) = -25$ to -16] indicate that the two types of magmatic rocks were formed by coeval felsic and mafic magmas during the Early Cretaceous (132 ± 2 Ma, zircon U-Pb age). The adakitic signatures of both the felsic and mafic rocks, such as very high Sr (770-1400 ppm), high Sr/Y ratios (40-130), low Y (3.5-21 ppm) and HREE concentrations are supposed to be features of the primary magmas, indicating that both of them were generated by partial melting of basaltic protoliths at great depths (>15 kbar). The distinctive major element compositions of the felsic and mafic primary magmas could be attributable to different melting temperatures and melting degrees. The mafic enclaves/dike have distinctively high concentrations of MgO (4.4-5.8 wt.%), Cr (229-374 ppm) and Ni (75-163 ppm), indicating a melt-mantle interaction in which olivine is partly consumed while orthopyroxene and/or pyrope are formed under high-pressure. Modeling suggests that 14% of peridotite relative to melt could have been consumed to elevate the Mg# of melt to the observed values (55-60), and that transformation from orthopyroxene to pyrope in mantle peridotite could have decreased the Al_2O_3 content from 18-19 wt.% in the initial melts to ~ 15 wt.% in the resultant mafic melts. Moderate negative zircon $\epsilon\text{Hf}(t)$ and bulk $\epsilon\text{Nd}(t)$ values also suggest contributions from both enriched lithospheric mantle and ancient lower crust. The results can best be explained by assuming that a block of amphibolite-composition lower continental crust was delaminated into the lithospheric mantle, leading to the formation of mafic magmas. This delamination is attributed to lithospheric extension and asthenospheric upwelling along the Yangtze River fault zone in the late Mesozoic which could have heated up the lithospheric mantle underneath the neighboring southern Dabie orogen. The strong input of heat triggered the delamination of the overlying thickened lower crust into lithospheric mantle by weakening the uppermost mantle and resulted in melting reactions in the delaminated crustal block to produce hot (~ 1100 °C) intermediate adakitic magmas ($\text{SiO}_2 = 55-60$ wt.%). The ascent of these hot magmas and their underplating below the lower crust induced the generation of high-silica melts ($\text{SiO}_2 = \sim 70$ wt.%) at lower temperature (~ 925 °C or less). Hybridization processes between the two magma types occurred during further ascent and emplacement in the crust, which could have led to the high concentrations of MgO (2.2-3.5 wt.%), Cr (56-226 ppm) and Ni (33-99 ppm) in the host felsic rocks.

2 Introduction

The petrogenesis of adakites has been hotly debated during the last two decades (e.g., Defant et al., 2002; Richard and Kerrich, 2007; Moyen, 2009). Primitive adakitic magma can be derived from partial melting of subducted oceanic crust in convergent margins (Defant and Drummond, 1990; Yogodzinski et al., 1994), but also from deep crustal rocks in intracontinental settings. In the latter case, the protoliths may be underplated basaltic crust (Atherton and Petford, 1993), delaminated lower continental crust (Xu et al., 2002; Gao et al., 2004; Wang et al., 2006; Xu et al., 2006; Wang et al., 2007a; Xu et al., 2008b), ancient lower continental crust (Stevenson et al., 2005; Jiang et al., 2007) or thickened orogenic root (Chung et al., 2003; Wang et al., 2007b; Xu et al., 2007). The composition of high-Mg adakite, including the sub-group of low-silica adakite (LSA, $\text{SiO}_2 < 60$ wt.%, Martin et al., 2005), is generally interpreted as reflecting the interaction between primary melt and mantle peridotite (Kay, 1978; Kelemen, 1995) and has provided important clues for deciphering the mechanisms of Archean crustal growth (Stern and Hanson, 1991) and Phanerozoic continental crust recycling (Gao et al., 2004, 2008).

The recognition of late Mesozoic adakitic granitoids in the Dabie orogen is of importance to the geodynamic interpretation of the region. Adakitic granitoids (>130 Ma) constitute part of the Late Mesozoic “post-collisional” magmatism, generally characterized by very low Y and Yb concentrations, high Sr/Y and La/Yb ratios. They are also characterized by high SiO_2 (>60 wt.%) and low MgO (<2 wt.%) contents, low $\text{Mg}^\#$ values (<45), and low Cr and Ni concentrations, showing an affinity with high-silica adakites (HAS, Martin et al., 2005). These chemical characteristics indicate high melting pressure (>15 kbar) and an over-thickened orogenic root (>50 km, Wang et al., 2007b; Xu et al., 2007), but no interaction between melts and peridotite. The lack of adakitic granitoids younger than 130 Ma was interpreted to indicate that the crust became thinner after 130 Ma (<35 km, Xu et al., 2007). The thinning of the Dabie orogen was interpreted to be due to delamination of lower crust (Gao et al., 1999) or even to delamination of the whole lithospheric mantle (Wang et al., 2007b; Xu et al., 2007). However, high-Mg adakites have not been found yet in the Dabie orogen, which is difficult to reconcile with the delamination model. It should be mentioned that the Chituling diorite, located beside the eastern boundary of the Dabie orogen as a small intrusion (~1 km²), is suspected by us not to be primitive high-Mg adakites as proposed by Huang et al. (2008). This issue is discussed in detail below.

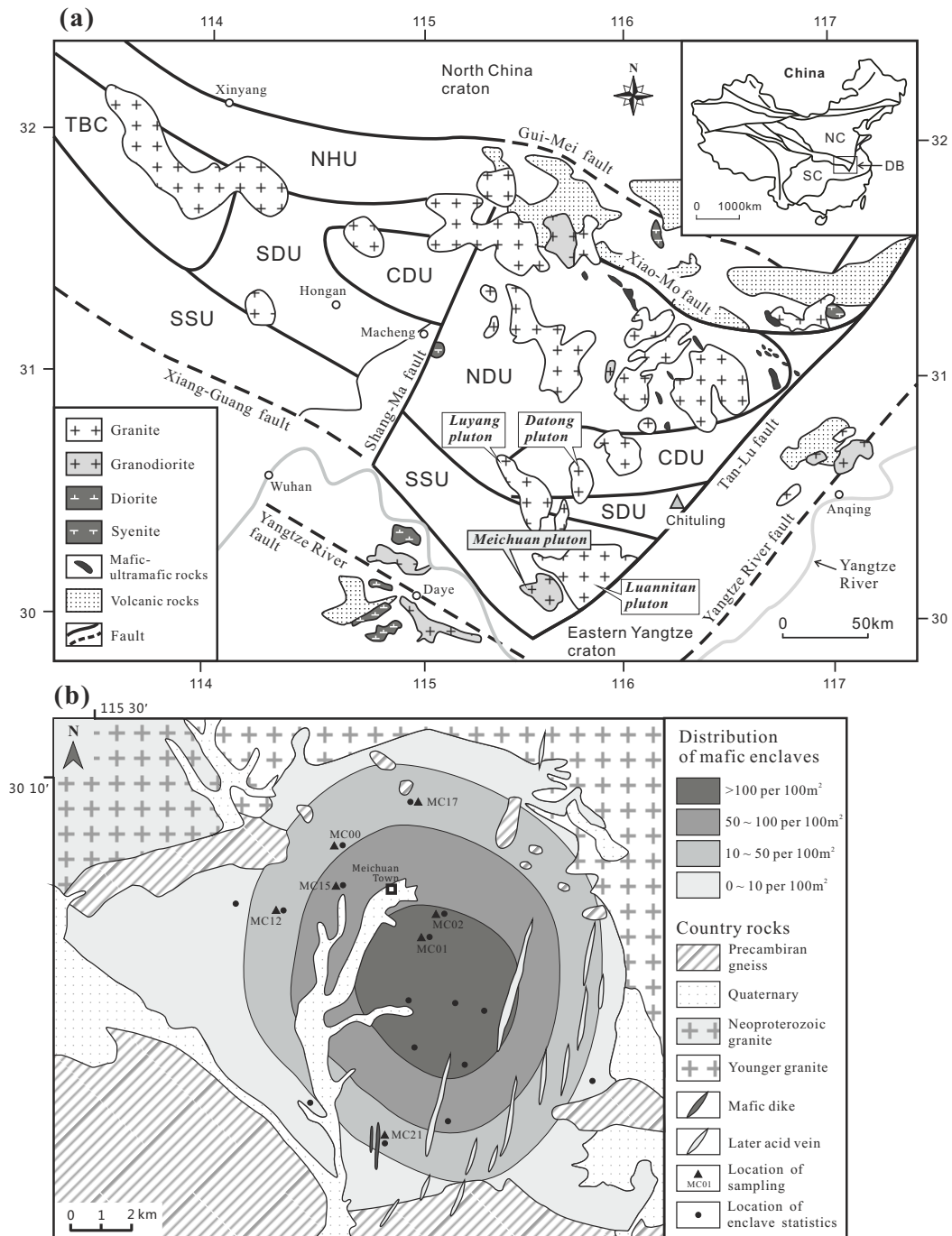


Fig. II-1 (a) Geological sketch of the Dabie orogen. Locations of the Meichuan, Luannitan, Luyang and Datong plutons and the Chituling stock are also shown. Insert denotes the location of the Dabie orogen in China. Abbreviations: DB, Dabie orogen; NHU, North Huaiyang unit; NDU, North Dabie unit; CDU, Central Dabie unit; SDU, South Dabie unit; SSU, Su-Song unit. (b) Simplified geological map of the Meichuan pluton. The distribution density of mafic enclaves is based on the statistics of the number and size of enclaves at outcrops. As the size of enclaves varies widely at different locations, the distribution density is thus estimated on the basis of an assumed average plane size of $10 \times 5 \text{ cm}^2$.

Geophysical studies reveal that the present-day crust of the Dabie orogen is thicker in the North (~42 km) than in the South (~35 km; Wang et al., 1997; Gao et al., 1999; Wang et al., 2000; Sodoudi et al., 2006). This suggests that the southern Dabie is a better site to check if crustal delamination has occurred beneath the Dabie orogen. Furthermore, located south of the Dabie orogen, the Lower Yangtze River magmatic-metallogenic (LYRM) belt along the Yangtze River fault zone is related to a Late Mesozoic lithospheric extension, in which mantle-derived magmatism started ahead of the magmatism in the Dabie orogen (Li et al., 2009 and see below). Thus, both the neighboring LYRM belt and Dabie orogen may have been affected by lithospheric thinning during the same event. As a result, studies on adakitic magmatic rocks located in the southern Dabie orogen could be essential for a better understanding of regional geodynamics during the Late Mesozoic.

In this paper, the petrogenesis of an adakitic plutonic complex of the southern Dabie orogen, the Meichuan pluton, was studied in detail. We present zircon U-Pb ages and Lu-Hf isotopes, bulk major and trace element compositions as well as Sr-Nd isotopes of felsic host rocks and mafic enclaves/dikes. We provide evidence for delamination of the lower continental crust in the southern part of the Dabie orogen and we propose a geodynamic model linking the lithospheric extension along the LYRM belt and the geodynamic evolution in the Dabie orogen.

3 Geological background

The Dabie orogen is part of the Dabie-Sulu orogenic belt, which is regarded as the world's largest ultra high-pressure (UHP) metamorphic terrane. The UHP metamorphic rocks (mostly eclogites) were formed during Triassic northward subduction/collision of the Yangtze craton beneath the North China craton (Hacker et al., 1998, 2000; Ratschbacher et al., 2000). The Dabie orogen is separated from the Qinglin orogen on the western end by the Nanyang Cenozoic basin. On the eastern end, the sinistral Tan-Lu fault shifted the Sulu orogen northward by ~530 km (Okay and Sengor, 1992). The Dabie orogen is generally divided into five petrotectonic units from North to South (Fig. II-1a): (1) the North Huaiyang unit (NHU), composed of low grade metamorphic flysch deposits or passive continental front scraped from the Yangtze craton (Zheng et al., 2005); (2) the North Dabie high-T granulite-facies metamorphic core complex unit (NDU), which was uplifted with two migmatite domes and exhibits middle to lower crustal rocks (Zhang et al., 1996; Wu et al., 2007); (3) the Central Dabie medium-T/UHP metamorphic unit (CDU) where coesite and diamond-bearing eclogites were found (Xu et al., 1992); (4) the South

Dabie lower-T/UHP metamorphic unit (SDU) containing “cold” coesite-bearing eclogites (Li et al., 2004b) and (5) the Su-Song low-T/high-P metamorphic unit (SSU) containing epidote-bearing blueschists with Proterozoic and Triassic isotopic ages (You et al., 1996). These five continuous units are outlined by several large-scale EW-trending faults and are widely intruded by Early Cretaceous granitoids (Ma et al., 1998; Zhao et al., 2005a), consisting of adakites and non-adakites (Ma et al. 2004; Wang et al., 2007b; Xu et al., 2007). Mafic-ultramafic intrusions are emplaced as small stocks in the NDU and the southern margin of the NHU. They show enriched-mantle geochemical affinity, indicating that their mantle protoliths have been previously metasomatised by melts derived from subducted continental crust (Jahn et al., 1999; Huang et al., 2007). The Meichuan pluton lies near the southern margin of the Dabie orogen, tectonically inside the SSU, closely neighboring the Daye area of the LYRM belt. It covers an area of about 184 km². The country rocks mostly consist of the Qijiaoshan Formation, which is a suite of Precambrian supracrustal rocks composed primarily of muscovite-albite schist, muscovite-quartz schist, albite-amphibole schist and plagioclase amphibolite. A younger granitic pluton, the Luannitan pluton, intrudes the Meichuan pluton in the eastern margin (Fig. II-1a).

The LYRM belt is located to the South of the Dabie orogen and belongs to the northern margin of the Yangtze craton (Fig. II-1a). It is characterized by large polymetallic deposits (Cu-Fe-Au, Mo, Zn, Pb, and Ag) and is one of the economically most important metallogenic zones in China (Zhai et al., 1996). As shown by geophysical studies, there is a concealed translithospheric fault (Yangtze River fault) tracing the whole metallogenic belt (Chang et al., 1991). Abundant studies have shown that most Cu-Fe-Au-Mo deposits in the LYRM belt are genetically related to Early Cretaceous magmatism (e.g., Wang et al., 2007a; Li et al., 2008). The Daye district is the westernmost part of the LYRM belt, and is intruded by several dioritic and granodioritic plutons. Compared to most large-sized granitoid plutons in the Dabie orogen, they have three distinctive features: (1) an earlier peak of occurrence at ~140Ma; (2) more mafic compositions and (3) distinctive Sr-Nd-Hf isotopes (discussed below).

4 Field relationships and petrography

The Meichuan pluton is mainly composed of massive medium-grained quartz monzodiorite, quartz diorite and granodiorite, containing occasional plagioclase phenocrysts. The rock-forming minerals of host rocks are plagioclase (35-50%), K-feldspar (20-35%), quartz (5-15%), biotite (5-10%) and hornblende (~5%). The

accessory mineral assemblages generally include titanite, magnetite, apatite and zircon. Some plagioclases show weak continuous normal zoning (An_{24} to An_{13}). Occasionally, some plagioclase megacrysts in diorites contain corroded Ab-rich oligoclase core ($Ab_{83}An_{15}$) mantled by antiperthite. The antiperthite mantle consists of K-feldspar lamellae (Or_{94}) and an oligoclase matrix ($Ab_{71}An_{28}$).

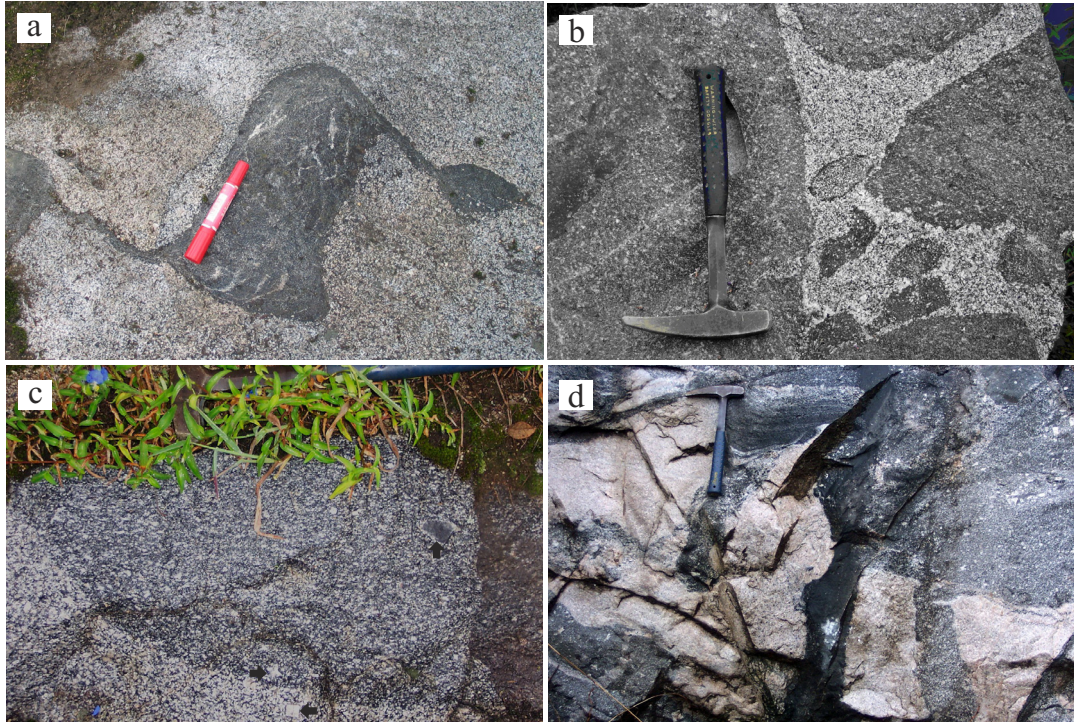


Fig. II-2 Photographs of field relationships between enclaves and host rocks. (a) A big enclave connects two other smaller ones with narrow veins, showing a dextral shearing during magma emplacement. (b) Several large enclaves partly replaced by the felsic host. Note the central ovoid-shaped small one which is almost completely replaced but still shows a dark boundary. (c) A centimeter-sized foreign xenolith with metamorphic texture is enclosed in a coarse-grained mafic enclave, surrounded by a chilled light felsic margin (upward-pointing arrow). Near the lower right boundary of this enclave, a plagioclase megacryst in the host (left-pointing arrow) resembles the one in the enclave (right-pointing arrow), but the former is euhedral and mantled by fine-grained mafic minerals, while the latter is corroded into a fragmentary form with a serrate margin. (d) Part of the contact between felsic hosts (granitic back vein) and mafic dikes. Note that the dark fine-grained dike without phenocrysts is gradually transformed into a light to dark medium-grained dike with abundant plagioclase phenocrysts. To the left, residual shadows of a partly digested mafic dike can be observed.

Mafic magmatic enclaves (MME) are widespread throughout the pluton but most abundant in the center with a density of more than 100 enclaves per 100m² (Fig. II-1b). The MME are lenses or ovoid in shape and are generally distributed as swarms with sharp contacts to the host. Some large enclaves exhibit more variable shapes, indicating shearing deformation (Fig. II-2a) and breakdown process producing daughter enclaves (Fig. II-2b). These large medium-grained enclaves usually have no sharp boundaries with the host (e.g. Fig. II-2c) and foreign xenoliths and plagioclase phenocrysts can be found near the boundary. Most enclaves have dioritic to tonalitic compositions with fine- to medium-grained doleritic textures. Enclaves contain less quartz and more hornblende and biotite than the felsic host. K-feldspar is rare in most enclaves, but is abnormally abundant in enclave MC01-2. The proportions of plagioclase (Ab₇₀₋₈₅), hornblende and biotite vary widely in the range of 30-60%, 5-15% and 10-30%, respectively. Sample MC17-4 is the only one with extraordinarily high proportions of hornblende (~30 %) and may represent a cumulate-rich enclave. Accessory minerals include iron oxides, titanite, apatite, zircon and allanite. The apatite appears in swarms in the matrix or as inclusions enclosed in plagioclase grains, and display euhedral acicular habit, indicative of magma quenching (Wyllie et al., 1962; Vernon, 1983).

Two synplutonic microdioritic composite dikes were observed in the southern part of the pluton (Fig. II-1b) and they are considered to be genetically related to the MME because of their similar composition. The mafic dikes are about 6 meters wide and strike N-S. Along the dike boundaries, rock textures can change strongly at the meter scale, varying from dark fine-grained to light dark medium-grained (Fig. II-2d). The dark fine-grained parts have chilled texture (no phenocryst) and a sharp contact with the felsic host. In contrast, the light dark medium-grained dikes have a transitional boundary with felsic host and contain abundant plagioclase phenocrysts. Furthermore, in some places, only residual shadows of mafic dikes which have been mostly digested by host magma can be observed.

5 Analytical Methods

Zircon U-Pb dating of a host rock (sample MC00-1) and a mafic dike (sample MC21-3) was conducted using an ICP-MS (Agilent 1700a) coupled to a GeoLas 2005 DUV 193 nm UArF laser at the State Key Laboratory of Geological Processes and Mineral Resources, China University of Geosciences (Wuhan, China), following the conventional procedures described by Yuan et al. (2004). The common lead correction was made after the method given by Andersen (2002), while the isotopic

ratios and element concentration of zircons were calculated using GLITTER (ver. 4.0, Macquarie University). The concordia ages and diagrams were obtained using the ISOPLOT program of Ludwig (2003). Errors for individual analyses are quoted at 1σ level, whereas the errors for weighted mean ages are quoted at 2σ level (95% confidence).

In-situ zircon Lu-Hf isotopic analyses were conducted mostly on the dated spots using an excimer laser (193 nm, ArF) ablation system attached to a Neptune MC-ICP-MS at the Institute of Geology and Geophysics, Chinese Academy of Sciences, Beijing. A laser repetition rate of 10 Hz at 100 mJ was used for ablating zircons and the spot diameters were 63 μm . Isobaric interference of ^{176}Lu on ^{176}Hf was corrected base on the measured ^{175}Lu value. The $^{176}\text{Yb}/^{172}\text{Yb}$ value of 0.5887 and mean β_{Yb} value obtained during Hf measurement on the same spot was used for interference correction of ^{176}Yb on ^{176}Hf . The detailed analytical technique was described by Wu et al. (2006). During analyses, the $^{176}\text{Hf}/^{177}\text{Hf}$ and $^{176}\text{Lu}/^{177}\text{Hf}$ ratios of the standard zircon 91500 were 0.282310 ± 15 (2σ , $n=20$) and 0.00031, respectively, similar to those measured using the solution method (e.g., 0.282306 ± 9 , Woodhead et al., 2004).

The Analysis of major, trace and rare earth element compositions was conducted at the Analytical Institute of the Hubei Bureau of Geology and Mineral Resources. Major element oxides were measured using a Regaku 3080E XRF spectrometer. Trace element and rare earth element (REE) were measured by ICP-AES. Relative standard deviation is $< 5\%$ for major elements, $< 4\%$ for REE and Y, and 5-10% for trace elements. Analyses of international standard reference samples were reported by Gao et al. (1991).

Rb-Sr and Sm-Nd isotopic compositions were measured using a Finnigan MAT-262 thermal ionization mass spectrometer (TIMS) in the Laboratory for Radiogenic Isotope Geochemistry, Institute of Geology and Geophysics, Chinese Academy of Sciences (Beijing, China). The procedures of chemical separation and measurement were described in detail by Chen et al. (2000). Raw data obtained were calculated using the Isoplot program (Ludwig 2003), giving $2\sigma_{\text{m}}$ errors.

6 Analytical results

6.1 Zircon CL images and U-Pb dating

Cathodoluminescence (CL) images show that zircons from the felsic host

(MC00-1) are prismatic and euhedral crystals with rhythmic oscillatory zoning and weakly luminescent narrow margins (Fig. II-3a-d). Their length/width ratios are generally 2:1 to 3:1. Some zircons seem to contain enclosed cores (Fig. II-3b, c), but this could not be confirmed by the U-Pb data (Table II-1). Ten spot analyses yielded concordant $^{206}\text{Pb}/^{238}\text{U}$ ages ranging from 129 ± 1 Ma to 134 ± 1 Ma with a weighted mean of 131.8 ± 1.0 Ma (95% conf., MSWD=2.0, Fig. II-4a). Six points analyses that gave discordant U-Pb isotopic ratios are not shown on the concordia diagram (see the suffix of Table II-1). These analytical points are in altered zones of zircons (e.g., Fig II-3d) and are probably affected by hydrothermal alteration (Vavra et al., 1999).

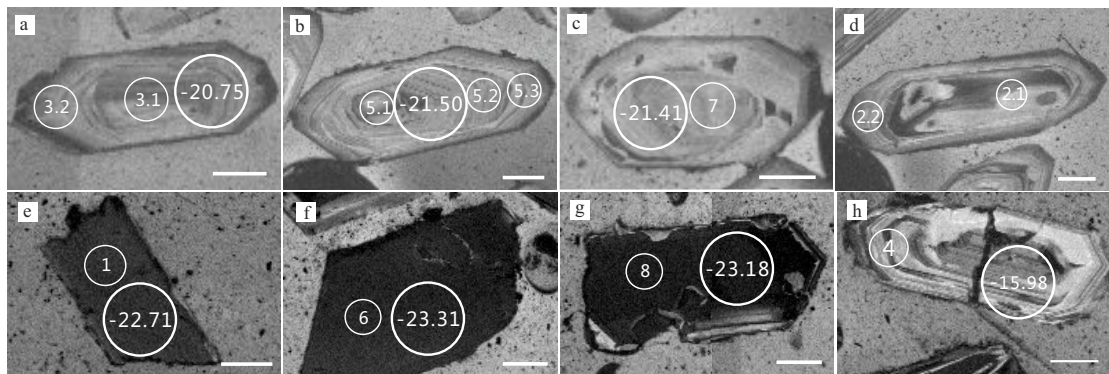


Fig. II-3 CL images of representative zircons from the felsic host rock MC00-1 (a-d) and the mafic dike MC21-3 (e-h). Small circles and inner figures are analytical spots and numbers (see Table II-1). Big circles show analytical spots of in-situ Lu-Hf isotopic analysis, and the figures inside are the corresponding $\epsilon_{\text{Hf}}(t)$ values. Note the zircon with chaotic nebulitic core in (d), which yields discordant U-Pb data owing to possible hydrothermal alteration. Similar zircon grains were avoided during Hf isotopic analysis. Note the light rims with narrow but good rhythmic zoning in (g), which is an overgrowth on the dark core with irregular interfaces. This zircon has a patchy texture of subrounded holes, indicating a dissolution process. The zircon grain in (h) has distinctive CL image and $\epsilon_{\text{Hf}}(t)$ value compared with other zircons from the mafic dike, but resembles the zircons from the felsic host. It is thus considered to be a xenolithic zircon introduced by magma hybridization from the felsic host magma. Scale bars are 40 μm .

Except for one zircon which has a CL pattern similar to those from the felsic host (Fig. II-3h), most zircons from the mafic dike (MC21-3) are subhedral, elongated crystals that have homogeneous CL images with weak-luminescence and rare oscillatory zoning (Fig. II-3e-g). This kind of CL pattern might be a common feature of zircons from intermediate to basic igneous rocks that underwent rapid crystallization, such as dacite (Zeck and Williams 2002), basalt (Li et al., 2004a) and

mafic magmatic enclave (Yang et al., 2007). The CL patterns and high concentrations of Th (792-3104 ppm) and U (558-1057 ppm) are distinct from those of zircons from the felsic host, and thus indicate a different origin for the two types of zircons. In addition, some zircons from the mafic dike with dark cores have relatively light rims with narrow but good rhythmic zoning and irregular interfaces were observed between the cores and the rims (Fig. II-3g). This feature is interpreted to result from resorption and subsequent growth, suggesting that those zircons were incorporated in and interacted with low Th-U magmas, probably the felsic host-forming magmas. Ten spot analyses on dark cores yielded concordant $^{206}\text{Pb}/^{238}\text{U}$ ages ranging from 130 ± 1 Ma to 135 ± 1 Ma with a weighted mean of 132.4 ± 0.5 Ma (95% confidence, MSWD=1.1, Fig. II-4b). Three analytical points were rejected for the same reason as proposed for the felsic host.

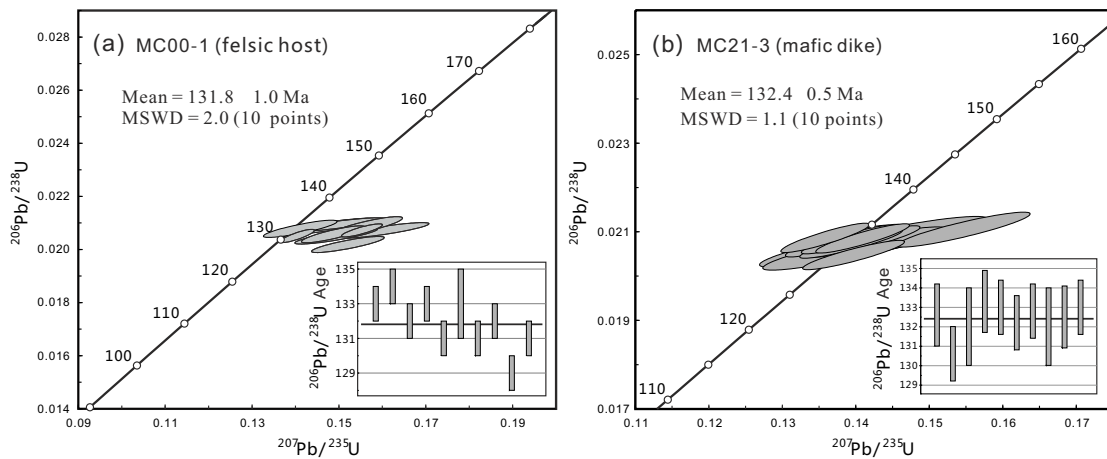


Fig. II-4 LA-ICP-MS U-Pb zircon concordia diagrams for the felsic host rock MC00-1 (a) and the mafic dike MC21-3 (b). Ellipse dimensions and error bars are 2σ .

6.2 Zircon Lu-Hf isotopic compositions

Twenty six Lu-Hf spot analyses were performed on 26 zircon grains selected from the felsic host (MC00-1) and twenty five spot analyses on 25 zircon grains from the mafic dike (MC21-3). Zircon grains with chaotic textures in CL images were not analyzed for Lu-Hf isotopes. Results show variable Hf isotopic compositions, with $^{176}\text{Hf}/^{177}\text{Hf}$ ranging from 0.282047 to 0.282227 and $\epsilon_{\text{Hf}}(t)$ values from -22.8 to -16.4 (weighted average = -20.3) for the felsic host, and $^{176}\text{Hf}/^{177}\text{Hf}$ ranging from 0.281996 to 0.282240 and $\epsilon_{\text{Hf}}(t)$ values from -24.8 to -21.1 for the mafic dike (Table II-2, Fig. II-5). The special zircon enclosed in the mafic dike, whose CL image is distinct from others in the group but similar with zircons from the felsic host (Fig. II-3h), has the highest $\epsilon_{\text{Hf}}(t)$ value for all the measured zircons, indicating its affinity with the felsic

host rather than the mafic dike.

Statistically, the zircons from the mafic dike have lower $\epsilon_{\text{Hf}}(t)$ values (weighted average = -22.84) and correspondingly older two-stage “crust” Hf model ages (T_{DM2} , average = 2.61 Ga) than those from the felsic host, while $\epsilon_{\text{Hf}}(t)$ and T_{DM2} of the latter are -20.3 and 2.47 Ga, respectively (Table II-2). The high T_{DM2} values suggest a significant contribution of Precambrian crustal basement to their protoliths.

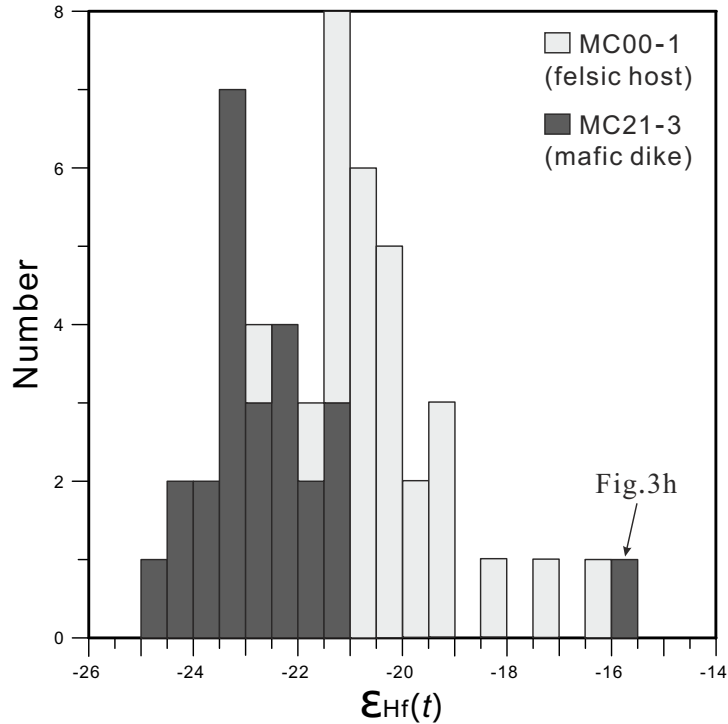


Fig. II-5 Zircon $\epsilon_{\text{Hf}}(t)$ values for the felsic host (MC00-1) and the mafic dike (MC21-3). Note that the highest $\epsilon_{\text{Hf}}(t)$ value was for the magma hybridization-introduced zircon shown in Fig. II-3h.

6.3 Major and trace elements

The major and trace element compositions of selected samples of felsic host rocks, MME, mafic dike and neighboring disturbed mafic dike are listed in Table II-3, including four analyses from previous work. Most samples are subalkaline based on the total alkalis-silica (TAS) diagram (Fig. II-6). The SiO_2 contents of the felsic host rocks vary from 64.6 to 69.6 wt.%. Distinct from the majority of the felsic host, sample MC17-2 is much lower in SiO_2 (58.7 wt.%) and thus classified as monzonite. The MME are intermediate ($\text{SiO}_2=55.5-61.0$ wt.%), corresponding to monzodiorite, monzonite and diorite. Sample MC17-4, which is collected from the vicinity of sample MC17-2, is of gabbroic composition. The mafic dike and host-mixed part (i.e.

labeled as “mixture” in all figures) are chemically similar and plot close to the boundary of the monzonite and diorite fields in the TAS diagram. In most variation diagrams of element abundances versus SiO₂ (Fig. II-7), the felsic host rocks, MME, mafic dike and mixture approximately form continuous trends, except for MC01-2 and MC17-4. The felsic host and MME are both high in Mg[#] [molar Mg/(Mg + Fe²⁺ + Fe³⁺)] with values of 50-60 and 52-61, respectively. Compared with the felsic host, MME and mafic dike generally have high CaO, FeO*, MgO, P₂O₅, V, Cr and Ni concentrations, but low Th and Ba concentrations. Notably, enclave MC01-2 has high concentrations of K₂O, Rb and Ba, but low concentrations of Na₂O, CaO, Al₂O₃ and Sr, consistent with the high contents of biotite and coarse-grained K-feldspar but relatively small amount of plagioclase observed in thin section. Enclave MC17-4 is enriched in hornblende and biotite, explaining its relative depletion in Na₂O, Al₂O₃ and Sr, as well as enrichment in MgO, FeO*, Ti, and Zr (Fig. II-7).

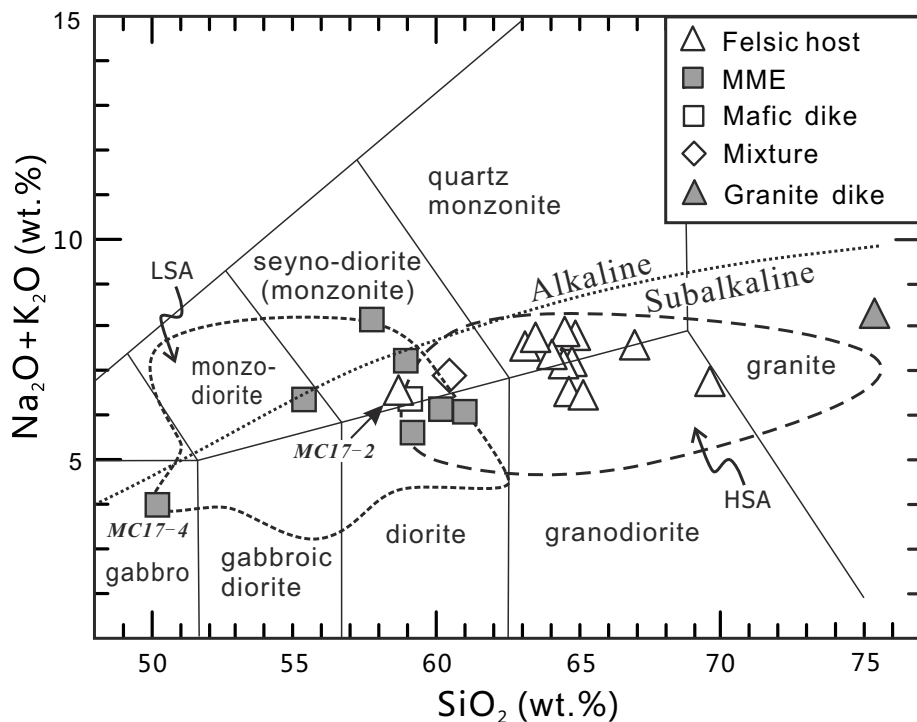


Fig. II-6 Total alkali-silica (TAS) diagram (after Le Bas et al., 1986). The boundary between alkaline and subalkaline series is after Irvine and Baragar (1971), and the fields of low-silica adakites (LSA) and high-silica adakites (HSA) are after Martin et al. (2005).

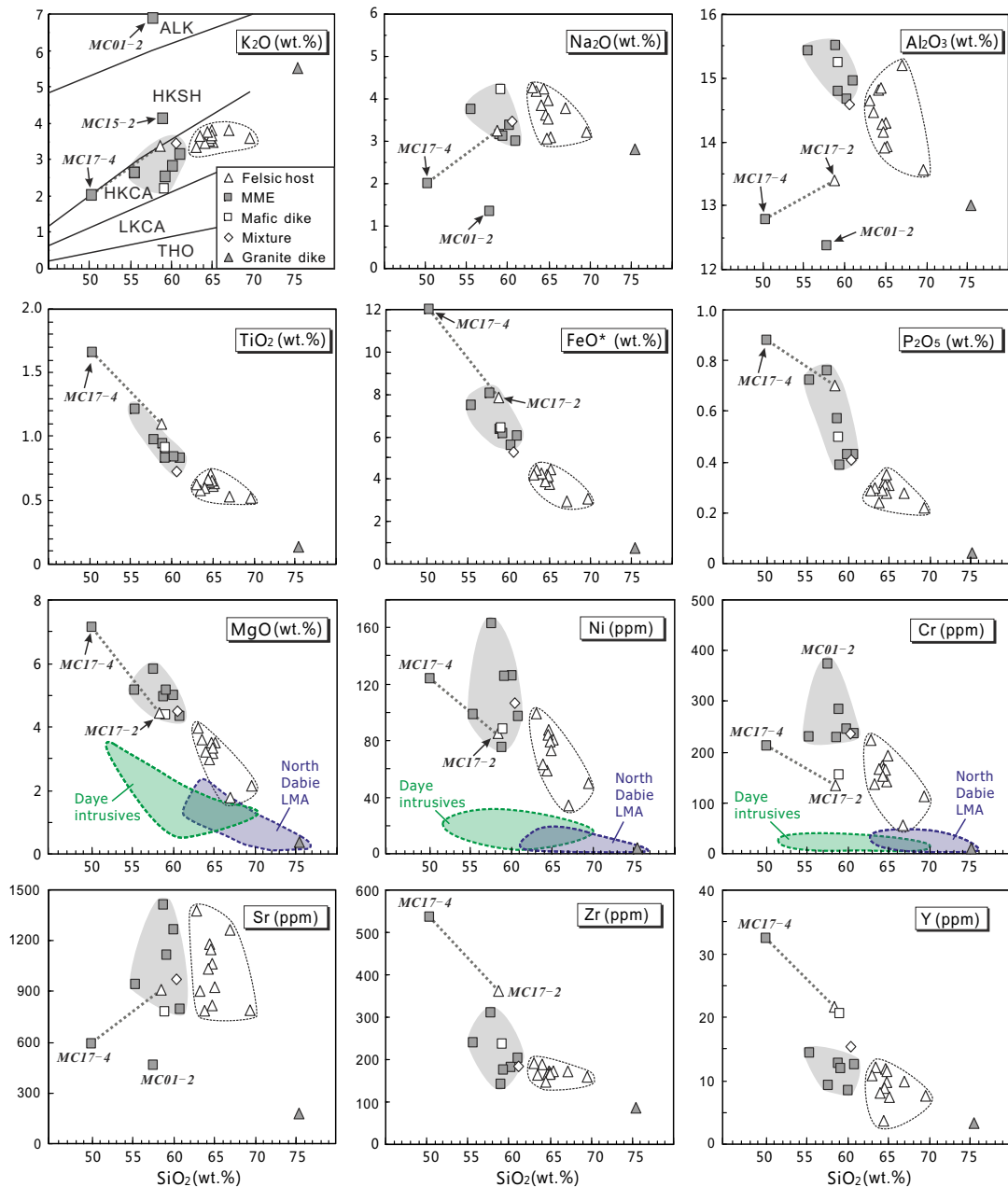


Fig. II-7 Plots of SiO₂ versus major elements and representative trace elements. Abbreviations: THO, tholeiitic; LKCA, low-K calc-alkaline; HKCA, high-K calc-alkaline; HKSH, high-K shoshonitic; ALK, alkaline. Field boundaries are according to Rickwood (1989). The mafic enclave MC17-4 and the felsic host rock MC17-2, connected with a dotted line, were sampled closely at the outcrop. Between them is a transition zone (about 1-meter wide) in which petrography varies gradually. FeO* denotes total iron calculated as FeO. The fields for the Daye intrusives and North Dabie low-Mg adakitic (LMA) granitoids are from Li et al. (2009), Wang et al. (2007b) and Xu et al. (2007).

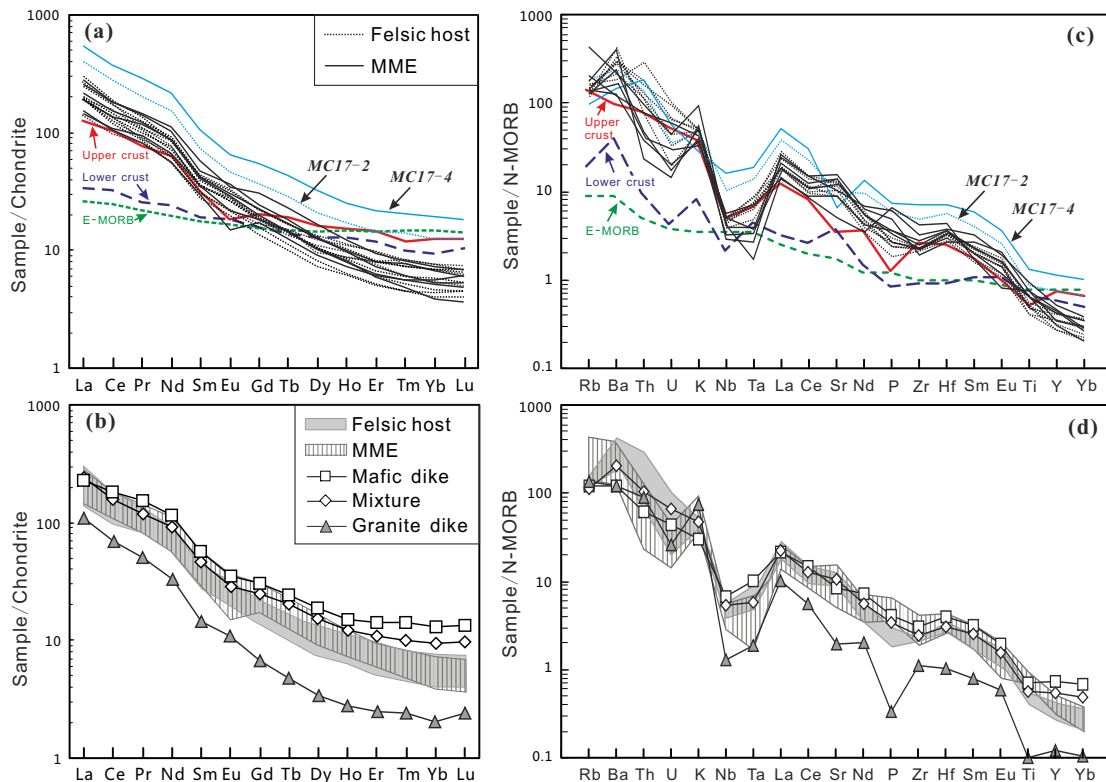


Fig. II-8 Chondrite-normalized REE patterns (a, b) and N-MORB-normalized trace element patterns (c, d). The chondrite values are from McDonough and Sun (1995) and the N-MORB values are from Sun and McDonough (1989).

Chondrite-normalized REE patterns are shown in Fig. II-8 (a-b). Both felsic and mafic rocks have high total REE abundances (148-539 ppm), while the granite dike MC21-2 has the lowest REE content. Most felsic host rocks and MME have parallel REE patterns with high LREE/HREE ratios $[(La/Yb)_N = 27-65]$, while the ratios of the mafic dike and disturbed dike are lower $[(La/Yb)_N = 18-25]$. All the samples have higher LREE/HREE ratios than those of average upper $[(La/Yb)_N = 15.5]$ and lower continental crust $[(La/Yb)_N = 5.3]$ (Rudnick and Gao, 2003). There is no marked negative Eu anomalies for most samples ($Eu/Eu^* = 0.83-1.10$), except for sample MC01-2 ($Eu/Eu^* = 0.66$). As shown in the normal mid-ocean-ridge basalt (N-MORB)-normalized trace element patterns (Fig. II-8 (c-d)), all the samples are enriched in large-ion lithophile elements (LILE, such as Rb, Ba, Sr) and LREE, and depleted in high-field strength elements (HFSE, such as Nb, Ta, P, Ti), with subparallel patterns for felsic host, MME and mafic dike. Ba is enriched relative to Rb and Th. All the samples differ significantly from lower continental crust (Rudnick and Gao, 2003) and enriched MORB (Sun and McDonough, 1989) due to their high LREE and LILE concentrations as well as low HREE and HFSE concentrations. The depletion in HFSE is extremely strong for the granite dike (MC21-2), which could be

caused by fractionation of mafic minerals (i.e., amphibole and biotite). The remarkable P depletion could be result of apatite fractionation.

6.4 Sr-Nd isotopic compositions

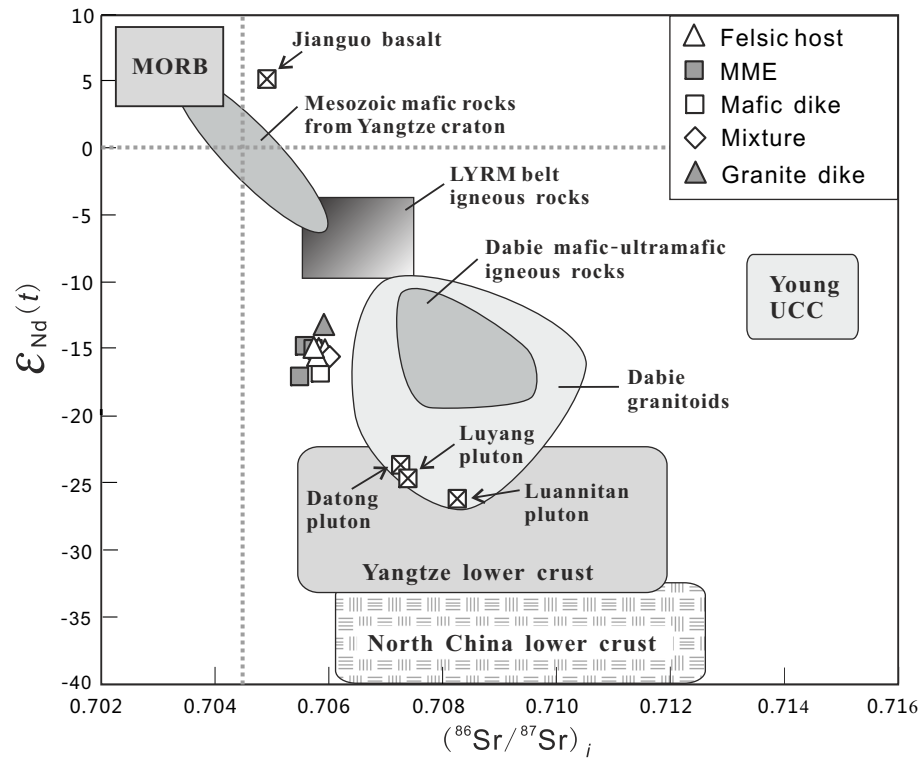


Fig. II-9 Initial $^{87}\text{Sr}/^{86}\text{Sr}$ versus $\epsilon_{\text{Nd}}(t)$ ($t=132$ Ma) plots showing the difference in Sr-Nd isotopic compositions between the Meichuan pluton and other references. Data sources: Dabie granitoids (Ma et al., 1998; Wei et al., 2001; Zhang et al., 2002; Chen et al., 2002; Wang et al., 2007b; Xu et al., 2008); Dabie mafic-ultramafic igneous rocks (Jahn et al., 1999; Wang et al., 2005); LYRM belt igneous rocks (Li et al., 2009), including Early Cretaceous dioritic intrusives and volcanic rocks in the Daye area, volcanic rocks in the Luzong area and mafic intrusions in the Tongling and Ningwu areas; Mesozoic mafic rocks from the Yangtze craton (Wang et al., 2005); Jianguo Mesozoic basalt (Zhang et al., 2003); young upper continental crust (UCC, Taylor and McLennan, 1985); lower crust of Yangtze and North China (Jahn et al., 1999); Datong, Luyang and Luannitan plutons (Zhang, unpublished data; see their positions in Fig. II-1).

Rb-Sr and Sm-Nd isotopic compositions are listed in Table II-4. The initial $^{87}\text{Sr}/^{86}\text{Sr}$ ratios and $\epsilon_{\text{Nd}}(t)$ values have been calculated at 132 Ma corresponding to the zircon U-Pb ages. The nine investigated samples exhibit homogeneous isotopic

compositions, with $(^{87}\text{Sr}/^{86}\text{Sr})_i$ ranging from 0.7055 to 0.7060, $(^{143}\text{Nd}/^{144}\text{Nd})_i$ ranging from 0.51160 to 0.51170, and $\epsilon_{\text{Nd}}(t)$ values ranging from -13.4 to -17.0. Depleted mantle model ages (T_{DM}) calculated using the model of DePaolo (1981) are 1.6~1.8 Ga for the felsic host and 1.8~2.0 Ga for the MME and mafic dike. As shown in the $(^{87}\text{Sr}/^{86}\text{Sr})_i$ versus $\epsilon_{\text{Nd}}(t)$ diagram (Fig. II-9), the Sr-Nd isotopic ratios of the Meichuan pluton are distinctive from both the Yangtze and North China lower crust (Jahn et al., 1999), as well as from typical values for young upper continental crust (Taylor and McLennan 1985). The $\epsilon_{\text{Nd}}(t)$ values overlap those of the Early Cretaceous Dabie granitoids (Ma et al., 1998; Zhang et al., 2002; Chen et al., 2002), Dabie mafic-ultramafic rocks (Jahn et al., 1999; Wang et al., 2005) and North Dabie Precambrian orthogneiss (not shown, Ma et al., 2000), but are lower than those of igneous rocks from the LYRM belt (Li et al., 2009). Their $(^{87}\text{Sr}/^{86}\text{Sr})_i$ values are lower than those of Late Mesozoic igneous rocks and Precambrian gneisses from the Dabie orogen, but similar to those of LYRM igneous rocks. Notably, the Sr-Nd isotopic compositions of the Meichuan samples are distinctive from those of other southern Dabie granitoid plutons, such as the Datong, Luyang and Luannitan plutons.

7 Discussion

7.1 Nature of the mafic enclaves

There are different hypotheses for the genesis of mafic enclaves coexisting within felsic host rocks: (1) restite from melting; (2) disrupted fine-grained margin of plutons; (3) disrupted cumulate; and (4) a blob of coeval magma. Sample MC17-4 contains abundant euhedral biotites and hornblendes (>30%), and large titanite and allanite grains, consistent with the description of mafic aggregates by Barbarin (2005). It is characterized by low contents of Na_2O and Al_2O_3 , very high REE abundances, but strong depletions in Rb, Sr, Ba and Pb compared to other enclaves, which can be explained by accumulation of mafic minerals (biotite and hornblende) and removal of plagioclase (Figs. II-7 and II-8).

Apart from sample MC17-4, the compositions and textures of the other mafic enclaves indicate that they have been formed by rapid crystallization of blobs of coeval mafic magmas and possible subsequent hybridization with felsic magmas. This interpretation is supported by the following observations: (1) the enclaves are much more mafic than the felsic host and cannot be formed from the disrupted fine-grained margin of plutons (Didier and Barbarin, 1991); (2) typical igneous textures can be observed, including mineral flow foliation exhibited by parallel alignment of plagioclase phenocrysts surrounded by small biotite; and (3) abundant acicular

apatites in the matrix indicating chilling of the mafic magma against the felsic host magma (Wyllie et al., 1962; Vernon, 1983).

The U-Pb dating results indicate that zircons in the mafic dike and felsic host crystallized simultaneously. Nevertheless, compared with the zircons from the felsic host, the ones from the mafic dike have higher concentrations of U (558-1057 ppm) and Th (792-3104 ppm), and lower radiogenic Hf ratios ($^{176}\text{Hf}/^{177}\text{Hf} = 0.28208\text{-}0.28223$), indicating that the sources of the two coeval magmas are different.

7.2 Magma hybridization

To avoid misunderstanding, we use *hybridization* in this paper to refer to a process involving both chemical and mechanical mixing. The term mingling here is used to define mechanical mixing, while diffusion is the principal process for chemical mixing between MME and felsic host.

Various theoretical and experimental studies have revealed that hybridization between mafic and felsic magmas depend on the contrasts of mass, density and rheology between them (Sparks and Marshall 1986; van der Laan and Wyllie 1993). Dispersed enclaves (Fig. II-2b) are evidence that magma mingling took place locally, indicating that physical contrasts between enclaves and host are not too large to prevent at least partial hybridization. The occurrences of MME and mafic dikes correspond to hybridization between mafic and felsic magmas at different stages of crystallization of felsic host magma (Barbarin, 2005). In the center of the pluton, slow cooling and crystallization resulted in abundant MME coexisting with felsic host. However, near the boundary of the pluton, rapid cooling and crystallization of felsic host allowed the mafic magmas to fill fractures as dikes.

Our geochemical data allow us to discuss to what extent hybridization has contributed to the homogenization of the whole pluton. The main question which needs to be solved is whether there are two different magma sources for mafic and felsic rocks. As shown in Fig. II-7, there are clear correlations between SiO_2 and Al_2O_3 , TiO_2 , FeO^* , MgO , Ni and Cr , consistent with a mixing trend between two endmembers. It is thus proposed that the high MgO , Ni and Cr concentrations of the felsic rocks may result from binary hybridization between a mafic endmember and a primitive low-Mg felsic endmember (similar to the North Dabie low-Mg adakites). However, for Sr , Zr and to a lesser extent Y , the mafic and felsic rocks have similar concentrations and there is no correlation with SiO_2 (Fig. II-7) or MgO , implying that

the high Sr/Y ratios are primitive features of both the mafic and felsic magmatic rocks. In-situ zircon Hf isotopic analysis has been used successfully to indentify the nature of magmatic protoliths (e.g., Griffin et al., 2000) and hybridization processes between mafic enclaves and felsic hosts (e.g., Yang et al., 2007; Chen et al., 2008). In this case, the zircon $\epsilon_{\text{Hf}}(t)$ values vary continuously from -25 for the mafic dike to up to -16 for the felsic host, implying a possible hybridization between discrete sources. Notably, the zircon enclosed in the mafic dike which has the highest $\epsilon_{\text{Hf}}(t)$ value of -16, could be grouped with the zircons from the felsic host because of its bright CL image (Fig. II-3h) and very low Th and U concentrations (Table II-1), indicating that the homogenization of zircon Hf isotopes did not occur after crystallization. It further implies that all the zircons from sample MC00-1 with mixing-featured $\epsilon_{\text{Hf}}(t)$ values crystallized during or after the hybridization process. On the other hand, homogenization may have also occurred for Sm-Nd and Rb-Sr isotopes, because isotopic diffusion is faster than chemical interdiffusion (Baker, 1989; Lesher, 1990, 1994). This might explain why the mafic and felsic rocks have nearly identical bulk Nd and Sr isotopic compositions (Fig. II-9).

In summary, both mingling and mixing processes could have played a role in the generation of the mafic enclaves and felsic host rocks.

7.3 Origin of adakitic rocks

Most MME, mafic dike and felsic host rocks of the Meichuan pluton are characterized by high SiO₂ (≥ 56 wt.%), Sr (460-1405 ppm) and LREE, low Y (9-14 ppm) and HREE, and thus high Sr/Y (48-148, Fig. II-11a) and La/Yb (40-83) ratios, as well as no significant negative Eu anomaly, consistent with an adakitic signatures (Defant and Drummond 1990).

The adakitic signatures of volcanic rocks or intrusions can be generated by several mechanisms: (1) fractionation of mafic minerals (mainly amphibole and/or pyroxene) in mafic non-adakitic magmas (e.g. Castillo et al., 1999); (2) mixing between mantle-derived mafic magma and crust-derived felsic magma (Guo et al., 2007; Streck et al., 2007), (3) partial melting of a subducted oceanic slab (Kay 1978; Yogodzinski et al., 1994), and (4) partial melting of delaminated lower continental crust (Xu et al., 2002; Gao et al., 2004).

Firstly, although fractional crystallization processes could have occurred locally, they could not dominate the whole geochemical system. MME and mafic

dike are characterized by high $Mg^{\#}$ values (51-61) and high MgO (4.4-7.2 wt.%), Cr (155-374 ppm) and Ni (75-126 ppm) concentrations, which are higher than those of mantle-derived granodiorites from the Daye area which are interpreted to be generated by fractionation process (Fig. II-7, Li et al., 2009). As shown in the diagrams of Ba versus Ni (Fig. II-10a) and MgO versus Ni (Fig. II-10b), except for minor magnetite, fractionation of mafic minerals has been negligible for most Meichuan samples, but could have controlled the formation of Daye intrusives (Li et al., 2009) and Chituling diorites (Huang et al., 2008). In contrast to the observations made for the Meichuan pluton, the Chituling diorites have moderate Y abundance and Sr/Y ratio (Huang et al., 2008), near the overlap of adakite and classical island arc rocks (inset of Fig. II-11a), which could be acquired by fractionation of a small quantity of hornblende and/or pyroxene, consistent with the fractionation trends shown in Fig. II-10. The fractionated phases could also have formed the coexisting synchronous pyroxene-hornblende gabbros which are enclosed in the host diorites, in contrast to previous interpretations (Huang et al., 2008).

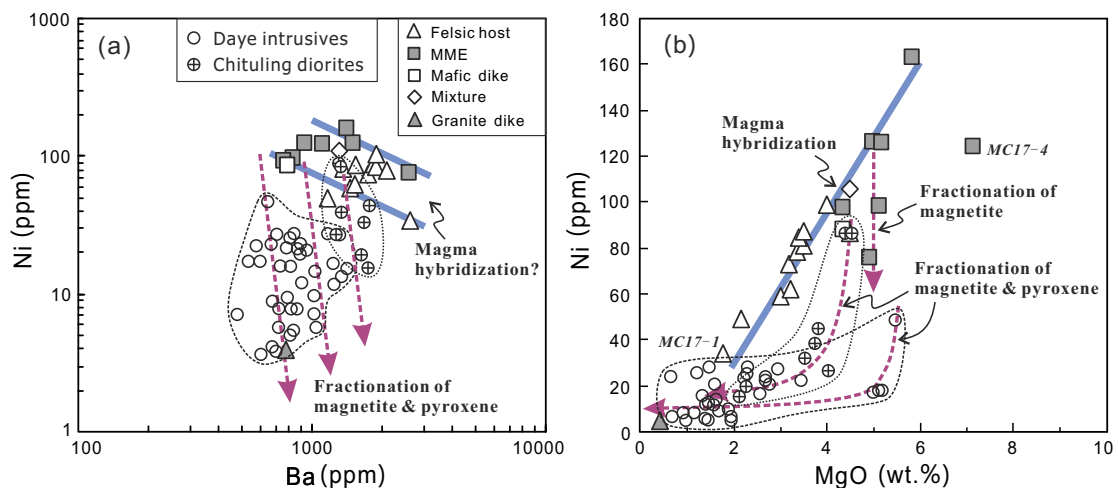


Fig. II-10 Plots of Ba versus Ni (a) and MgO versus Ni (b), indicating that the generation of the Meichuan rocks is not dominated by the fractionation of mafic minerals. The data for the Daye intrusives and the Chituling diorites are from Li et al. (2009) and Huang et al. (2008), respectively.

Secondly, a magma mixing mechanism can be ruled out as well, because potential regional mantle-derived mafic and ultramafic magmatic rocks do not bear adakitic signatures. In detail, scattered early Cretaceous mafic-ultramafic intrusive in the Dabie orogen have low Sr (mostly 200-500 ppm), high Y (mostly 15-30 ppm) and thus low Sr/Y ratios (mostly 8-40) (Jahn et al., 1999; Wang et al., 2005), as do the most mafic intrusive from the Daye area (i.e., Yinzu gabbro-diorite, Sr/Y = 24-28, Wang et al., 2004).

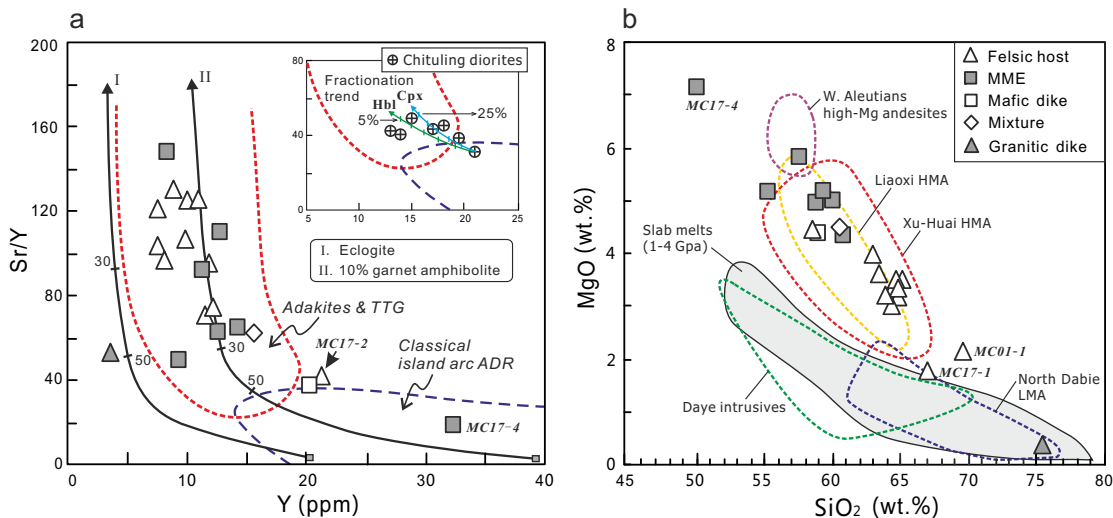


Fig. II-11 Plots of Sr/Y versus Y (a) and SiO₂ versus MgO (b). Values for the Chituling diorites are plotted in the insert for comparison (inset), showing they could be formed by the fractionation of hornblende (Hbl, up to 5 wt.%) and/or clinopyroxene (Cpx, up to 25 wt.%). For andesitic magmas, $K_{Sr}^{Hbl} = 0.4$, $K_Y^{Hbl} = 11.3$, $K_{Sr}^{Cpx} = 0.28$, $K_Y^{Cpx} = 2.4$ (Ewart and Griffin, 1994). The fields of adakites and trondjemite-tonalite-granodiorite (TTG) and classical island arc andesite-dacite-rhyolite (ADR) are after Atherton and Petford (1993). Partial melting curves for basalt, leaving a residue of eclogite and 10% garnet amphibolite, are after Drummond and Defant (1990). Data references: slab melts (1-4 Gpa), Sen and Dunn (1994), Rapp and Watson (1995); North Dabie LMA granitoids, Wang et al. (2007) and Xu et al. (2007); Daye intrusives, Li et al. (2009); Liaoxi HMA andesites, Gao et al. (2004); Xu-Huai HMA granitoids, Xu et al. (2006); W. Aleutians high-Mg andesites, Yogodzinski et al. (1994).

Moreover, high K₂O/Na₂O ratios (0.7-1.3), negative Nb and Ta anomalies (Fig. II-8) and negative $\epsilon_{Nd}(t)$ values are distinctive from oceanic crust-derived adakitic melts, which usually have low K₂O/Na₂O ratios (~0.5), absence of anomalies in Nb and Ta, and positive $\epsilon_{Nd}(t)$ values (Defant and Drummond, 1990). As a result, these geochemical features, as well as very negative $\epsilon_{Hf}(t)$ values of zircons, indicate an affinity with “potassium-rich adakite” (Rapp et al., 2002) and a likely derivation from lower continental crust (Defant et al., 2002).

Moyen (2009) recently emphasized that adakitic signatures (high Sr/Y and La/Yb ratios) might be generated by partial melting not only of metabasalts (amphibolites mostly) at high pressure (>15 kbar), but also possibly of metapelites and metagreywackes at low pressure (<10 kbar). For the Meichuan pluton, the compositional features, especially their low K₂O (2-4 wt.%) and high TiO₂ (>5 wt.%),

are far from that of partial melts of metapelites ($K_2O > 4.5$ wt.%, Skjerlie and Patiño Douce, 1995) and metagreywackes ($TiO_2 < 5$ wt.%, Montel and Vielzeuf, 1997). In addition, metapelites and metagreywackes have been rarely found in the Dabie metamorphic basement, while amphibolites are widely distributed as a major phase (Ma et al., 2000). As a result, amphibolites have been generally taken as possible protoliths for the widely distributed granitoids in the Dabie orogen (Zhang et al., 2002; Wang et al., 2007b; Xu et al., 2007). Assuming that amphibolites are the most likely protoliths for the Meichuan pluton, and based on the results of melting experiments (see review of Moyen, 2009), we propose that the primary magmas for both the felsic and mafic rocks were derived by partial melting of amphibolites at depths greater than 15 kbar.

Inasmuch as the two rock types with different major element compositions (especially SiO_2) could have been derived from an identical protolith (amphibolite), the melting degree and condition should be different for the two rock types. Dehydration melting experiments of basaltic amphibolites by Sen and Dunn (1994) revealed that the formation of intermediate adakitic melts ($SiO_2 = 55-60$ wt.%) requires very high temperature (1050-1150 °C at 20 kbar), while high-silica adakitic melts ($SiO_2 = \sim 70$ wt.%) may be generated at lower temperature (925 °C at 15 kbar or 900 °C at 20 kbar). Additionally, abundances of Al, Ti and P of dehydration partial melts increase as melting temperature increases, while K_2O content decreases (Sen and Dunn, 1994; Rapp and Watson, 1995). The element composition variations with temperature are attributable to changes in modal proportions of the residual phases (Rapp and Watson, 1995). We thus propose that the MME-forming magmas which have low SiO_2 and K_2O but high Al_2O_3 , TiO_2 and P_2O_5 contents compared to the felsic host rocks (Table II-3, Fig. II-7) have likely been formed at a higher temperature (~ 1100 °C) whereas the latter formed at a lower temperature (~ 925 °C).

7.3.1 Origin of low-Mg felsic host

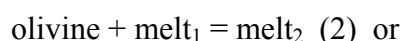
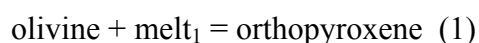
As discussed above, the geochemical composition of the felsic rocks can not be explained by fractional crystallization of mantle-derived melts (Fig. II-10a-b). A hybridization process involving mafic and felsic magmas is better suited to explain the decrease of SiO_2 and increase of MgO, Ni and Cr of the felsic host rocks. As shown in Fig. II-12a, modeling of $Mg^{\#}$ - SiO_2 variation suggests that binary hybridization between high-Mg mafic and high-silica magmas could form the felsic host as confirmed by the hybridization trends shown in Fig. II-10a-b. In the calculation, sample MC12-2 was chosen as the mafic endmember, while two adakitic granites were chosen as possible high-silica endmembers (see caption of Fig. II-12

for detail). Consequently, we propose that the primitive felsic magmas could have high SiO₂ but low MgO, Ni and Cr contents, resembling the low-Mg adakitic (LMA) granitoids in the North Dabie (Wang et al., 2007b; Xu et al., 2007). In addition, detailed discussion on the petrogenesis of Dabie low-Mg (C-type) adakitic rocks are given in the appendix.

7.3.2 Origin of high-Mg MME

Besides adakitic features, the MME are also characterized by very high MgO, Ni and Cr contents (Fig. II-7) and medium SiO₂ content, similar to the high-Mg andesites in the western Aleutians (Yogodzinski et al., 1994), as well as the high-Mg adakitic (HMA) andesites in the Liaoxi area and HMA granitoids in the Xu-Huai area inside the North China craton (Gao et al., 2004; Xu et al., 2006), but distinctive from the LMA granitoids in the North Dabie (Wang et al., 2007b; Xu et al., 2007). Thus, the mafic enclaves could be classified as HMA (Fig. II-11b). Experimental studies have suggested that interaction between low-Mg adakitic melts and mantle peridotite is the most process to form HMA (Rapp et al., 1999), consistent with the explanation for natural rocks (Kay, 1978). Here we prefer a mechanism involving high-pressure partial melting of delaminated lower continental crust and subsequent melt-mantle interaction based on the following evidence.

Geophysical studies reveal that the current crust of the southern Dabie orogen is about 35 km thick (Wang et al., 1997, 2000; Sodoudi et al., 2006), much thinner than the estimated melting depth (>50 km) for the derivation of the adakites from mafic lower crust (Moyen, 2009). The thinning process is explained by delamination of mafic orogenic root (lower continental crust), which could provide favorable conditions for the interaction of adakitic melt with mantle peridotite. As shown by experimental results (Rapp et al., 1999), possible reactions between a SiO₂ saturated (crustal derived) melt and mantle peridotite could be:



Reaction (1) has been proved to work in the situation of low melt/peridotite ratios (~1/1), in which melts are fully consumed. For reaction (2), high melt/peridotite ratios (> 2/1) are needed. At modest melt/peridotite ratios (~2/1),

reaction (3) works generally and produces high-Mg silicic melt with orthopyroxene as a solid phase. Furthermore, reaction (3) may represent a significant mechanism which could contribute to the enrichment of lithospheric mantle (Kelemen, 1998). This reaction also works well in explaining the interaction between adakitic melts derived from partial melting of delaminated North China lower plutonic crust and overlying mantle peridotite (Gao et al., 2008; Xu et al., 2008b), which actually produced mantle-pressure clinopyroxene cores equilibrated with adakitic melts and resulted in a transformation from primary peridotite into olivine-free pyroxenite (Gao et al., 2008).

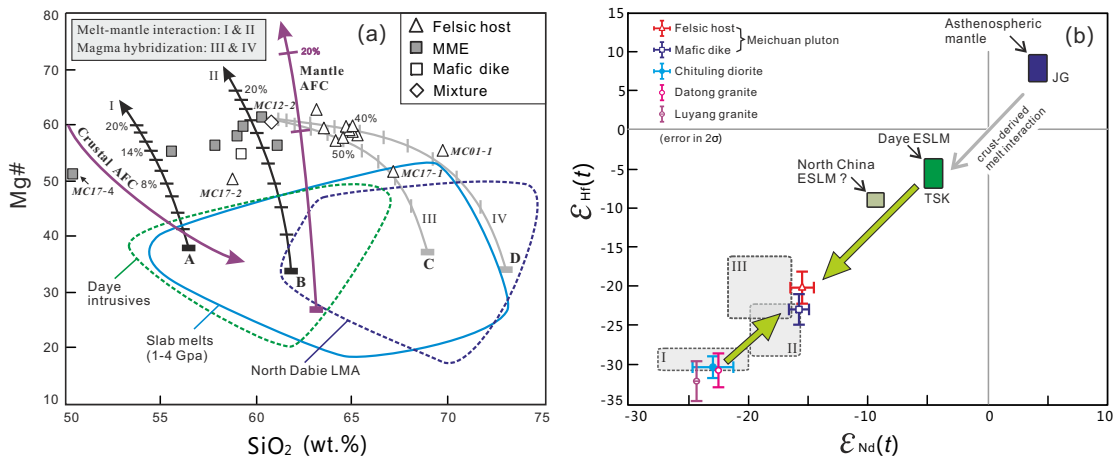
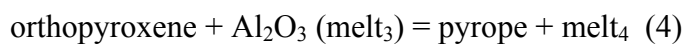


Fig. II-12 Geochemical modeling of melt-peridotite interaction based on SiO₂ and Mg# values (a) and plots of ε_{Hf}(t) versus ε_{Nd}(t) (b). The modeling results shown by the solid lines are for reaction (3). See text for explanation. Starting members for melt-mantle interaction: A (SiO₂ = 56.37 wt.%, Al₂O₃ = 19.11 wt.%, MgO = 2.57 wt.%, Mg# = 38) for an experimental slab melt generated at 1075 °C and 22kbar (Rapp and Watson, 1995); B (SiO₂ = 61.8 wt.%, Al₂O₃ = 16.31 wt.%, MgO = 1.26 wt.%, Mg# = 34) for a North Dabie low-Mg adakite (Wang et al., 2007b). High-silica endmembers for the hybridization calculation: C (SiO₂ = 68.95 wt.%, MgO = 0.65 wt.%, FeO* = 1.96, Mg# = 37) and D (SiO₂ = 72.94 wt.%, MgO = 0.44 wt.%, FeO* = 1.52, Mg# = 34) for North Dabie low-Mg adakites (Wang et al., 2007b). Trends of crustal AFC and mantle AFC are after Stern and Kilian (1996). Data references: Jianguo (JG) late Cretaceous alkali basalt (derived from asthenospheric mantle), Zhang et al. (2003) and Yang et al. (2006); North China ESLM, Chen et al. (2008); Tongshankou (TSK) granodiorite (derived from the Daye ESLM), Li et al. (2008); North Dabie adakitic hornblende quartz-monzonite (I), adakitic granite (II) and non-adakitic granite (III), Xu et al. (2008); Chituling diorite, Huang et al. (2008) for ε_{Nd}(t) and Zhang (unpublished data) for ε_{Hf}(t); Datong adakitic granite and Luyang non-adakitic granite in the southern Dabie orogen, Zhang (unpublished

data). The Hf isotopes for the JG basalt were determined on a bulk sample and those for other rock on zircons using an in-situ technique.

In order to constrain the melt-mantle interaction quantitatively, we modeled it using reaction (3) and major element concentrations ($\text{SiO}_2\text{-Mg}^\#$). We assumed that the lithospheric mantle beneath the Dabie orogen and the LYRM belt had been metasomatised before late Mesozoic (Jahn et al., 1999; Li et al., 2009). Thus, a suitable starting peridotite for modeling melt-mantle interactions is a harzburgite composed of 85% olivine (Fo_{92}) and 15% orthopyroxene ($\text{En}_{92}\text{Fs}_{08}$; Xu et al., 2008b; Gao et al., 2004, 2008). The product orthopyroxene resulting from the transformation of olivine after melt-mantle interaction is assumed to have the composition $\text{En}_{92}\text{Fs}_{08}$. Modeling results show that the Meichuan mafic samples could be generated by the interaction between ~14% harzburgite and low-Mg adakitic monzonitic melts (Fig. II-12a). In the calculation, two possible melt compositions are used, one is an experimental slab melt ($\text{SiO}_2=56$ wt.%, denoted as A in Fig. II-12a) and the other is a North Dabie low-Mg adakitic granite ($\text{SiO}_2=62$ wt.%, denoted as B in Fig. II-12a). In addition, the modeled interaction trends are approximately parallel to the mantle AFC trend calculated by Stern and Kilian (1996), in which the mantle mass-assimilation/fractionation ratio was 2 and the fractionating phases were assumed to be 80% amphibole + 20% clinopyroxene. Fig. II-12a also shows that crustal AFC process could not be responsible for the generation of mafic enclave-forming magmas.

Furthermore, melt-harzburgite interaction experiments at 3.8 GPa reveal that garnet (pyrope) is a major phase in the residue (Rapp et al., 1999), because garnet becomes a stable phase in pyroxenite at depths greater than 45 km (Hirschmann and Stolper, 1996). As a result, Al_2O_3 content of the initial low-Mg melt may be decreased in the product melt after reaction with peridotite. The contributing process could be expressed by the reaction:



Using reaction (4), a further melt-mantle interaction involving ~20% of orthopyroxene could decrease the Al_2O_3 content of initial melts from ~19.1 wt.% to ~15.2 wt.%. This might explain why the Meichuan MME are relatively low in Al_2O_3 compared to high-pressure amphibolite-derived melts in experiments ($\text{Al}_2\text{O}_3 = 18\text{-}19$ wt.%, Rapp and Watson, 1995; Sen and Dunn, 1994).

The melt-mantle interaction process could have also contributed to the isotopic compositions of the Meichuan pluton. As shown in Fig. II-12b, the Nd and Hf isotopic ratios of the Meichuan mafic samples could be a result of mixing between enriched lithospheric mantle and ancient lower crust, which are represented by enriched sublithospheric mantle (ESLM)-derived Tongshankou granodiorite in the Daye area (Li et al., 2008) and lower continental crust-derived Datong adakitic granite (~135 Ma, Zhang, unpublished data) in the southern Dabie orogen, respectively. Since lithospheric mantle usually has extremely low Sr and Hf concentrations compared to silicic melts (e.g., Xu et al., 2008b), the proportion of harzburgite involved in the melt-mantle interaction to produce the resultant Sr-Hf isotopic composition must be quite large. This melt/peridotite ratio is certainly much lower than the calculated result using major elements (equation 3 and 4). Such a decoupling between major elements and isotopic ratios can become realistic if the integrated reaction interface between melt and minerals in the mantle is large. This situation occurs if melts move along narrow pathways at a grain scale in the mantle (Moyen, 2009). Furthermore, isotopic exchange between phases is far more effective than elemental equilibrium during melt movement along interfaces, because isotopic diffusion is much faster than interdiffusion of elements between minerals and melts (Baker, 1989; Leshner, 1990, 1994). As a result, melt-mantle interaction could shift the isotopic composition of melts significantly towards the value of the involved lithospheric mantle, exhibiting element-isotope decoupling. Similar mechanisms have been proposed for other examples, such as the high-Mg[#] adakitic andesites in the Andean Austral Volcanic Zone (Stern and Kilian, 1996), the Liaoxi high-Mg adakitic andesites in the North China craton (Gao et al., 2004) and the Dexing high-Mg adakitic porphyries in the South China craton (Wang et al., 2006).

Based on the discussions above, we propose that the MME and mafic dike-forming magmas were generated by partial melting of mafic delaminated lower continental crust and subsequent melt-mantle interaction.

7.4 Geodynamic implications

Deep subduction/collision of continents generally leads to over-thickening of the orogenic root (Leech, 2001), which could increase the density of the mafic lower crust due to eclogitization (Kay and Kay, 1991) and cause asthenospheric upwelling when the dense eclogite root detaches (Anderson 2005). However, the mechanism leading to the formation of Late Mesozoic (155-110 Ma) large-scale magmatism in the Dabie orogen is unlikely related to continental subduction (Hacker et al., 1998) or

fast exhumation of eclogite to crustal level in the late Trias (Hacker et al., 2000), because the interval between these events and the Mesozoic magmatism in the Dabie orogen is much longer than that between delamination and consequent asthenospheric upwelling (~10 Ma, Jull and Kelemen, 2001). As a result, the mechanism and driving force responsible for the partial melting of the lithospheric mantle (Jahn et al., 1999; Wang et al., 2005) and crustal reworking (Wang et al., 2007b; Xu et al., 2007) in the Dabie orogen has been debated and is still ambiguous.

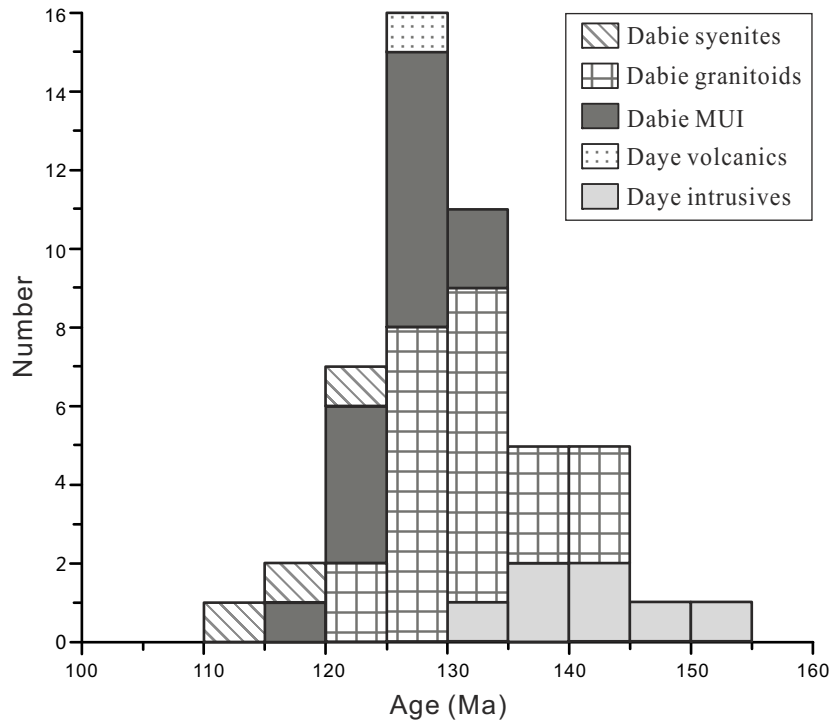


Fig. II-13 Age distribution of Late Mesozoic magmatic rocks in the Dabie orogen and the neighboring Daye area. As Sm-Nd and Rb-Sr isochron ages often prove unreliable, only in-situ zircon U-Pb dating (SHRIMP or LA-ICP-MS) and ⁴⁰Ar-³⁹Ar plateau ages are used. Data sources: Dabie syenites (Chen et al., 2009; Li, unpublished data); Dabie granitoids (Xie et al., 2006b; Wang et al., 2007b; Zhao et al 2005a; Xu et al., 2007; Zhang unpublished data); Dabie mafic-ultramafic intrusives (MUI, Jahn et al., 1999; Wang et al., 2005; Zhao et al., 2005b); Daye volcanics (Xie et al., 2006a); Daye intrusives (Li et al., 2008, 2009).

The compilation of previous studies shows that the various magmatic rocks in the Dabie orogen and its southern neighboring Daye area have lithological and distribution correlations with age (Fig. II-13). The earliest magmatism was recorded by diorites in the Daye area, such as the Yinzu diorite-gabbro complex (151.8±2.7 Ma) and the Lingxiang diorite (141.1±0.7 Ma) (Li et al., 2008), with an occurrence

peak at ~140 Ma, which coincides with the Cu-Fe-Au deposit-related magmatism in the whole LYRM belt (e.g., Wu et al., 2008). Slightly later, extensive granitoid magmatism took place all over the Dabie orogen, together with minor contemporaneous scattered mafic-ultramafic intrusives. It was emphasized by Ma et al. (2004) and Xu et al. (2007) that deformed adakitic granitoids were generated prior to undeformed non-adakitic granitoids, implying a quick lithospheric extension and crust thinning process at ~130 Ma. Minor syenite and A-type granite (e.g., Chen et al., 2009) were emplaced afterwards in the NHU and NDU as the last phase of large-scale magmatism and regional extension (Fig. II-1a). This magmatism sequence clearly exhibits a migrating trend from the LYRM belt to the Dabie orogen, which provides an important clue to investigate the geodynamic setting for the two connected areas.

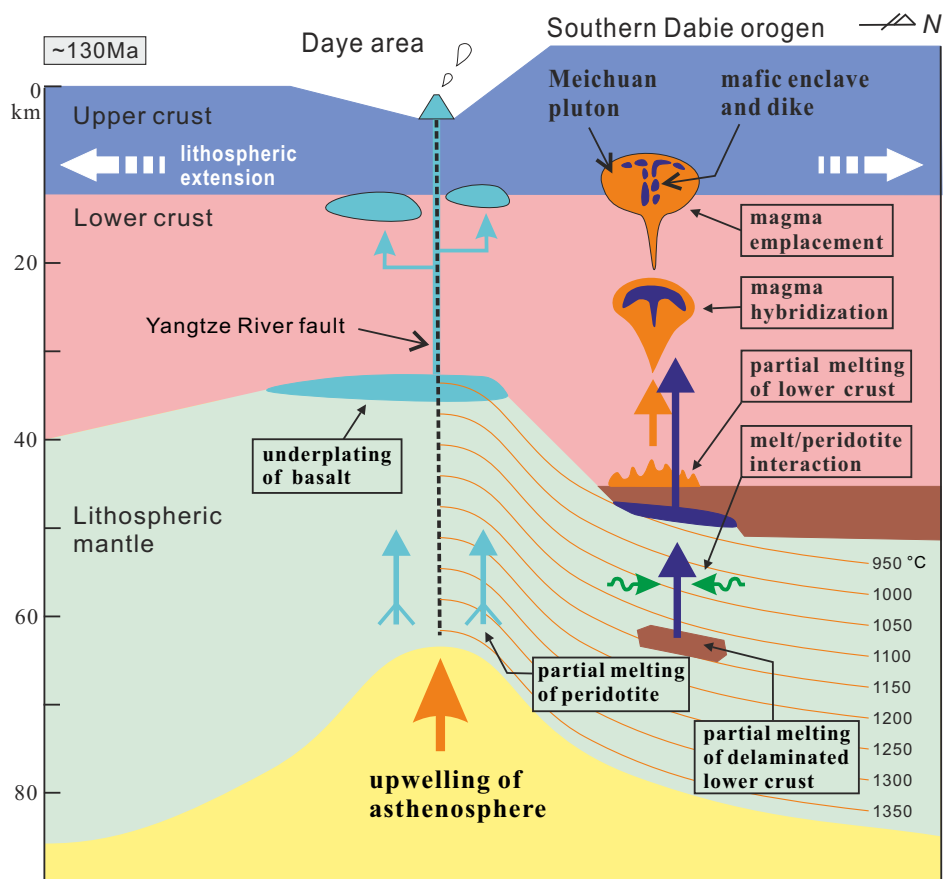


Fig. II-14 A cartoon illustrating the suggested geodynamic model and the origin of the Meichuan pluton. See text for explanation.

We suggest that the lithospheric extension and asthenospheric upwelling along the Yangtze River fault firstly resulted in partial melting of mantle peridotite, and this enabled the lower crust of the southern Dabie orogen to delaminate into the

lithospheric mantle (Fig. II-14). The crust of Dabie orogen was thickened by Triassic continental collision and subsequent upward extrusion of UHP slices (Hacker et al., 2000). The orogenic crust should have maintained its great thickness (>50 km) until ~130 Ma, as evidenced by the lower crust-derived adakitic granitoids in the North Dabie (Wang et al., 2007b; Xu et al., 2007) and southern Dabie (e.g., the Datong pluton, Fig. II-1a, Zhang, unpublished data). Crustal thickening would transform the mafic lower crust into eclogite, whose density is higher than that of peridotite by 0.2-0.4 kg/m³ (Rudnick and Fountain, 1995). However, the viscosity of the mantle has to be sufficiently low to allow effective viscous motions, such as crustal delamination (Jull and Kelemen, 2001). Numerical modeling by Jull and Kelemen (2001) further indicates that high temperatures (>700 °C) for the uppermost mantle are required for the delamination of a denser lower crust within a time scale of 10Myr, due to the negative correlation between viscosity and temperature of the mantle peridotite. As a result, hot tectonic settings, such as lithospheric extension, might be more favorable for delamination of lower crust.

For the Dabie orogen, the absence of crust- or mantle-originated magmatism during the period 230~145Ma indicates a cold setting at that time, which explains why the thickened lower crust may have been preserved for so long. From ~150 Ma, lithospheric extension and asthenospheric upwelling dominated the tectonic setting along the Yangtze River fault zone (including the Daye area), which raised the temperature of the upper mantle above the solidus. As a result, various mantle-derived magmas could ascend and form the mafic intrusions in the Daye area (Li et al., 2009). Basaltic underplating under the crust as revealed by deep seismic reflection profiling across the LYRM belt (Lü et al., 2005) also suggests extensive partial melting of lithospheric mantle. Within a short time (<10 Ma), the lithospheric mantle beneath the southern Dabie orogen was also heated and weakened by heat transfer from the neighboring Daye area, which made the overlying eclogitized lower crust able to sink. The delaminated blocks could then be heated up to produce partial melts under a high-pressure with garnet-rich residues. As mentioned before, the temperature required for the generation of intermediate adakitic melts (SiO₂ = 55-60 wt.%) is about 1100 °C at 20 kbar (Sen and Dunn, 1994). Although partial melting of the delaminated crustal block may have started at less than 1100 °C, most of the generated melt fraction may have been produced at such a high temperature. The absence of synchronous mantle-derived magmatic rocks in the southern Dabie orogen implies that no partial melting of lithospheric mantle occurred, suggesting that the P-T conditions here have never crossed the solidus of anhydrous peridotite (~1300 °C at 20 kbar, Takahashi and Kushiro, 1983; Robinson et al., 1998). Based

on the above constraints, we propose a schematic diagram of the mantle thermal structure beneath the LYRM belt and the neighboring southern Dabie orogen (Fig. II-14).

After removal of the delaminated crustal blocks, the melts further interacted with ambient peridotites during ascent, which incorporated abundant Mg, Cr and Ni and raised $^{143}\text{Nd}/^{144}\text{Nd}$ and $^{176}\text{Hf}/^{177}\text{Hf}$ ratios in the melts. Afterwards, the hot high-Mg adakitic melts underplated the in-situ lower crust, providing heat for partial melting of the lower crust (at ~ 925 °C in water-absent conditions) by which high-silica adakitic melts could have formed. Hybridization between the high-Mg mafic melts and the low-Mg felsic melts may take place before final magmatic emplacement.

8 Conclusions

Felsic host and enclosed MME and mafic dikes of the Meichuan pluton formed coevally and crystallized at 132 ± 2 Ma. The MME and mafic dikes-forming magmas were likely derived by partial melting of delaminated lower continental crust (amphibolite composition), which further interacted with ambient peridotites during ascent. The resultant hot magma with high-Mg adakitic signatures underplated beneath the in-situ lower crust and heated the latter to produce high-silica low-Mg adakitic melts. Afterwards, these two types of magmas rose up together and hybridized with each other during emplacement. It is suggested that the heat supplied by the strong upwelling of asthenosphere in the neighboring Daye modified the thermal and rheological structure of the lithospheric mantle beneath the southern Dabie orogen, allowing the delamination of the dense orogenic root. In contrast, the northern Dabie had a relatively cool upper mantle, which was not hot enough for the delamination of overlying lower crust, because it was located far from the hot center (i.e., Yangtze River fault zone). This might explain the absence of high-Mg adakites in the northern Dabie orogen as well as the preservation of a thicker crust.

9 Appendix: Petrogenesis of Dabie C-type adakite

9.1 Dispute about C-type adakite

The term adakite was originally coined to represent felsic melt deriving from young subducted oceanic slab, which was first observed on the Adak Island at the western end of the Aleutian ridge (Kay, 1978; Defant and Drummond, 1990).

Compared with normal island-arc magmas which are believed to form by partial melting of fluid-metasomatized mantle wedge, these adakites have higher SiO₂ and Al₂O₃ contents, and are rich in large ion lithophile elements (LILE, especially Sr) and light rare earth elements (LREE), but depleted in high field strength elements (HFSE) and heavy rare earth elements (HREE, especially Y). Shortly later, high Sr/Y and La/Yb ratios were demonstrated in identifying adakites (Defant et al., 1991; Defant and Drummond, 1993) and utilized in many case studies (e.g. Stern and Kilian, 1996; Yogodzinski and Kelemen, 1998; Chung et al., 2003). In addition, because of the compositional similarities between adakite and Archean high-Al TTG, hot debates were aroused concerning subduction and Archean tectonics (Martin, 1999; Smithies, 2000; Smithies and Champion, 2000; Martin and Moyen, 2002; Martin et al., 2005; Moyen and Stevens, 2006).

Against the oceanic-type adakite (richer in Na than K), the continental-type (C-type) adakite was termed by Zhang et al. (2001a), which initially refers a series of the Late Mesozoic granitoids from East China (including the Dabie orogen) characterized by adakite-like trace element compositions (e.g., low Y and high Sr/Y), as well as distinctive geochemical features from normal oceanic-type adakites: higher K₂O content and K/Na ratio, lower Al₂O₃ content (<18 wt%), Mg# (<50), εNd(t) and Y/Yb ratio. Zhang et al. (2001b) proposed that these adakite-like granitoids were derived by re-melting of thickened continental lower crust (>50 km), and further inferred that an East-China plateau once existed in Late Mesozoic. Afterward, this view attracted abundant discussion and criticism (Ge et al., 2002; Zhang et al., 2003; Xu and Ma, 2003; Zhang et al., 2004; Zhai, 2004; Xiao et al., 2004; Wang, 2007; Wang and Chen, 2010; Huang and He, 2010; Zhang, 2011; Xiong et al., 2011). A consensus has been reached that *adakite* should not be restricted in the subduction environments and can be formed by partial melting of lower crust in an intracontinental regime (Defant et al., 2002; Rapp et al., 2002; Kay and Kay, 2002; Castillo, 2006).

Because the structure and composition of oceanic crust are generally uniform, adakites from island arcs tend to form with certain mechanisms as revealed by previous geochemical studies. However, the continental crust is much more complex than oceanic crust, which leads to various interpretations of origin of adakite-like rocks that formed within continents, such as mineral fractional crystallization (especially amphibole, Moyen, 2009; Zhang et al. 2011). As a result, some researchers suggested that the term adakite should be only used in environments of oceanic subduction. In addition, the felsic continental crust is an optimal site for the

MASH (melting-assimilation-storage-homogenization) process of magmas, which could result in strong modification of geochemical features of primitive magmas and lead to misinterpretation of the origin of final magmatic rocks (e.g. multi-interpretation of the Andes adakites, Kay and Kay, 2002; Richards and Kerrich, 2007).

9.2 Composition of China lower continental crust

Determination (or estimation) of the source rock is the base of other discussions concerning adakitic magmatism. The lower crust of East China is likely basaltic andesite in composition, rather than basalt. Gao et al. (1998a) demonstrated that the upper part of lower crust has a lower P-wave velocity ($V_p = \sim 6.7$ km/s) than that of the lower part of lower crust ($V_p = \sim 7.1$ km/s), which indicates that they are respectively andesitic and basaltic. As shown in Fig. II-15, the Dabie-Sulu orogen has an andesitic composition in the upper part of lower crust and a basaltic composition in the lower part of lower crust which are of similar thickness, while the upper part is thicker than the lower part in North China craton, Yangtze craton, Inner Mongolia-Hingan orogen, Qilian orogen and Tibetan plateau. If it is assumed that the upper/lower part ratio is 1:1~3:1, an average SiO_2 content of 54~57 wt% for the lower crust could be obtained (Gao et al., 1998a; Gao et al., 1998b), which is slightly higher than the value estimated by Rudnick and Gao (2003) for the average earth continental crust (53.4 wt% SiO_2).

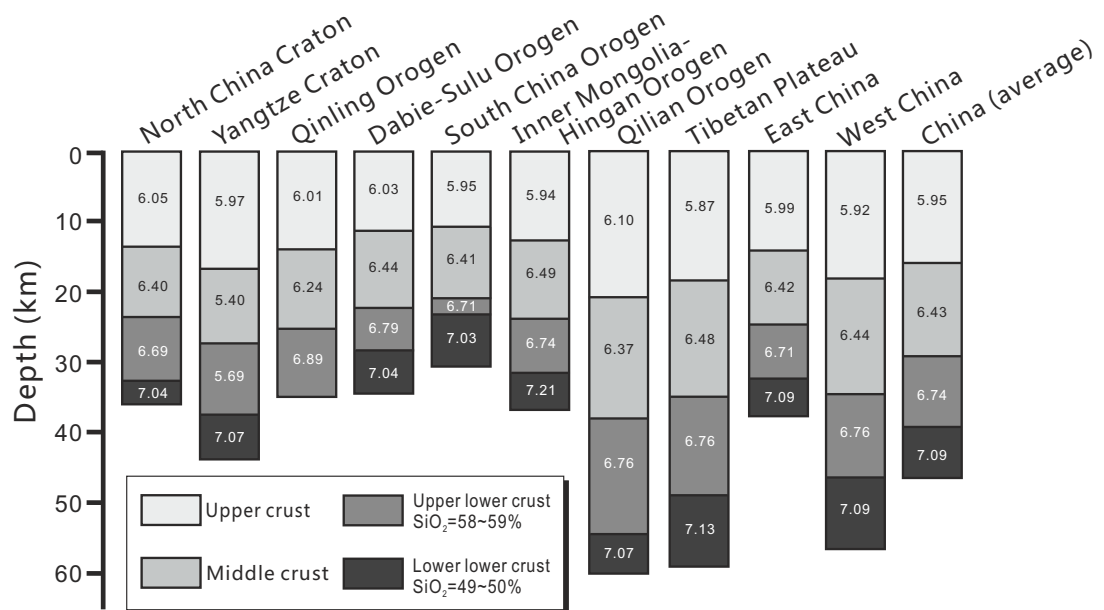


Fig. II-15 Average crustal structure and composition for different tectonic units of China. The values in the figure are V_p values; the lower continental crust is

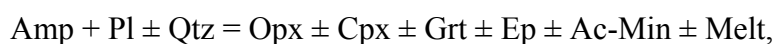
composed of upper and lower parts, which compositionally correspond to felsic and mafic granulite, respectively; after Gao et al. (1998a, b)

Water has critical effect on the partial melting of source rocks (Campbell and Taylor, 1983), as well as the magma migration and intrusion (Holtz and Johannes, 1994; Baker, 1998). The water content of a bulk rock largely determines the maximum melting degree, i.e. fertility of source rock (Clemens and Vielzeuf, 1987). For the lower continental crust, water primarily exists as OH in hydrous minerals rather than inter-grain free fluid. Amphibole is the most important hydrous mineral in the lower continental crust, because it exists in rocks of various compositions within wide pressure and temperature ranges ($P < 2.6$ GPa, $T < 1000$ °C, Vielzeuf and Schmidt, 2001). As indicated by numerous case studies, dehydration of amphibole is the key process of partial melting of amphibole-bearing source rocks. For many partial melting experiments, the mode amount of amphiboles of starting materials (metamorphic alkaline basalt or tholeiitic basalt) is 45-76 wt% (Beard and Lofgren, 1991; Rapp et al., 1991; Rushmer, 1991; Wolf and Wyllie, 1991; Sen and Dunn, 1994; Wolf and Wyllie, 1994; Patino Douce and Beard, 1995; Rapp and Watson, 1995). If it is assumed that H₂O content of amphibole is generally ~2 wt% (possible Cl, F and O substitutions of OH are omitted), the bulk rock H₂O content is consequently within the range of 0.9-1.5 wt%.

9.3 Partial melting of lower continental crust

9.3.1 Melting condition

In order to explain the melting mechanism of subducted oceanic crust and lower continental crust, as well as the origins of Archean TTG and adakite, many researchers did dehydration (fluid-absent or vapor-absent) melting of hydrous metabasic rocks (Beard and Lofgren, 1991; Rapp et al., 1991; Rushmer, 1991; Winther and Newton, 1991; Wolf and Wyllie, 1991; Pawley and Holloway, 1993; Wolf and Wyllie, 1993; Sen and Dunn, 1994; Patino Douce and Beard, 1995; Rapp and Watson, 1995; Liu et al., 1996; Springer and Seck, 1997; Johannes and Koepke, 2001; Lopez and Castro, 2001; Foley et al., 2002; Skjerlie and Patino Douce, 2002; Rapp et al., 2003; Xiong et al., 2005; Zhou et al., 2005; Xiao and Clemens, 2007; Nair and Chacko, 2008). The revealed melting reaction can be approximated by the following equation:



in which accessory minerals (Ac-Min) include rutile, titanite, ilmenite, while garnet and epidote ($P \geq 10$ kbar) and rutile ($P \geq 16$ kbar) form under high pressures. When the melts are extracted from the melting zones, the residual mineral assemblages compose the granulite or eclogite (Fyfe, 1973; Hacker, 1990; Rushmer, 1993). These experimental results have been widely applied to interpret the origin of natural adakitic rocks, as discussed in numerous case studies (see Moyen, 2009). However, we should be aware of the uncertainties from tectonic regime (crustal thermal structure), varieties of source rock and sub-liquidus evolution.

Dehydration of hydrous minerals under fluid-absent conditions have been proved to be the principal mechanism of generating felsic magmas for the lower continental crust (Brown and Fyfe, 1970; Clemens and Vielzeuf, 1987; Beard and Lofgren, 1989), which is also valid for the oceanic crust (Foley et al., 2002; Rapp et al., 2003; Koepke et al., 2004; Koepke et al., 2007). Currently the thermodynamic data of silicate melt are not sufficient, which obstacles thermodynamic modeling of equilibrations involving minerals, melts and fluids (Powell and Holland, 2008), i.e. equilibrations of partial melting of metabasic rocks.

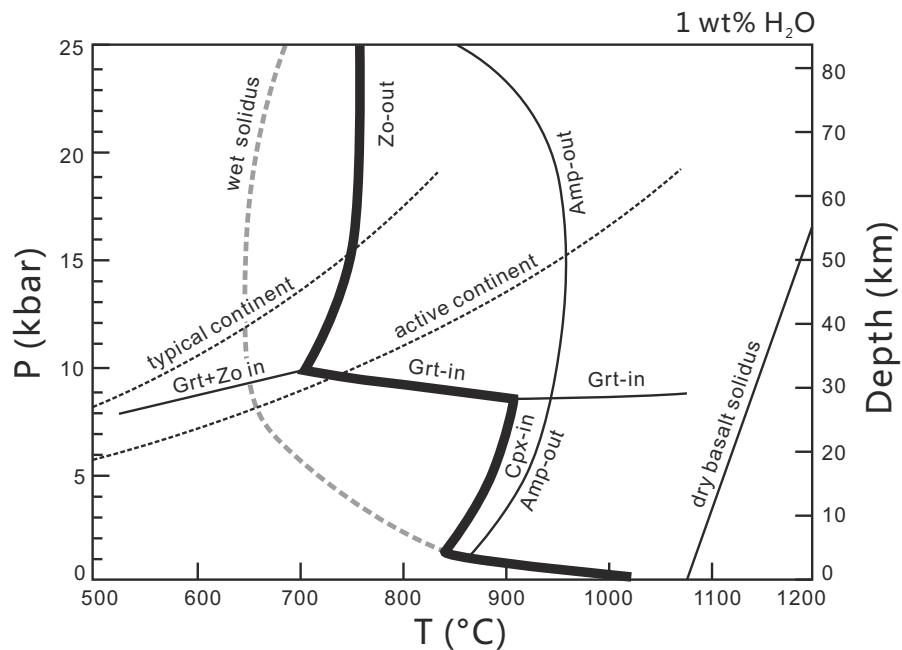


Fig. II-16 P-T diagram of metamafic rocks at H₂O-undersaturated condition. Water-undersaturated solidus and stable fields of minerals are from Vielzeuf and Schmidt (2001); dry basalt solidus is from Lambert and Wyllie (1972); geothermal gradients of typical and active continent are from Winter (2010); at $P = 1.5$ kbar, the amphibole-out is of about 950 °C; mineral abbreviations: Amp – amphibole, Cpx – Ca-rich pyroxene, Grt – garnet, Zo – zoisite

Drummond and Defant (1990) performed trace element modeling of partial melting of MORB, and indicated that the resultant melts would be compositionally similar to adakite and high-Al TTG (low Y and high Sr/Y ratio) if garnet consists 10-25 wt% of the residue (eclogite or garnet amphibolite). Consequently, experimental constraints on the stable P-T conditions of garnet during partial melting of metabasic rocks are crucial for estimating the forming pressure of adakites. Dehydration melting experiments of amphibolite under high pressures (Winther and Newton, 1991; Wolf and Wyllie, 1991; Wolf and Wyllie, 1993; Sen and Dunn, 1994; Wolf and Wyllie, 1994; Patino Douce and Beard, 1995; Rapp and Watson, 1995) demonstrated that garnet is stable within 0.9-1.4 GPa ($T = 800-1000\text{ }^{\circ}\text{C}$). Fig. II-16 shows the P-T diagram of metabasic compositions with 1 wt% H_2O , which is equal to 50 wt% amphibole in the mode.

As mentioned above, garnet and plagioclase as melting residues control the extent of depletion of HREE and Y in the partial melts of amphibolite. However, the proportion of garnet in the residue is dependent on several parameters, such as source rock composition, pressure, temperature and reaction time (achievement of equilibrium). The growth of garnet is generally slower than other coexisting minerals, and thus the state of garnet might be away from equilibrium in garnet-producing experiments (e.g. Wolf and Wyllie, 1994; Xiong et al., 2005). However, geological events are normally in the time scale of million years, which make actual partial melting processes definitely more close to thermodynamic equilibria than experiments performed in laboratories which are in the time scale of hours and days. As result, at the same condition of pressure and temperature, the same source rock could produce more garnet than that indicated by experiments. Based on their own partial melting experiments, Nair and Chacko (2008) concluded that pressures above 1.5 GPa (~50 km depth) are required for generating 20-30 wt% garnet in the residual assemblage. However, other experiments performed by Wolf and Wyllie (1994), Springer and Seck (1997) and Wolke (1996) indicated that pressures between 1.0-1.2 GPa are also adequate for generating the same quantities of garnet. In addition, the stability of plagioclase is highly affected by the H_2O activity in the melt; at higher H_2O activity the plagioclase is less stable. Because H_2O activity increases with decreasing pressure and increasing water content (Burnham, 1979), the stability of plagioclase is not only dependent on pressure, but also on water content. Consequently, it is out of question that partial melting of amphibolites could generate adakite-like magmas at pressure of 1.0-1.2 GPa, coexisting with garnet-bearing (20-30 wt% in the residue) and plagioclase-poor residual assemblage.

9.3.2 Melting degree

The maximum degree (F_{\max}) of partial melting of hydrous metabasic rocks is dependent on the water content of the bulk system (Clemens, 2005). To simplify the discussion, amphibole is taken exclusively as the hydrous mineral. In practical cases, when temperature is within the solidus and liquidus of amphibole, the resultant melt fraction is between zero and F_{\max} . In the following discussion on the melting degree of amphibolites, the theory and method of Clemens and Vielzeuf (1987) are used to estimate the F_{\max} , which is based on H_2O activity model and independent of melting reaction.

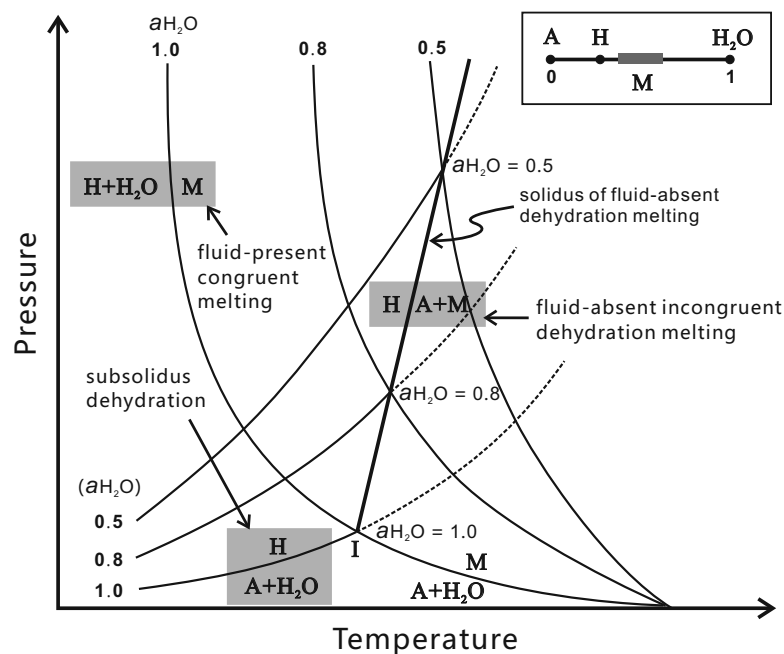


Fig. II-17 Hypothetical P - T diagram of phase relations in hydrous system. Fluid consists of H_2O and CO_2 , and activity of water is dependent on their ratio; A – anhydrous mineral, H – hydrous mineral, M – hydrous melt; reactions $H+H_2O=M$ and $A+H_2O=M$ are considered to have the same dP/dT slope; the dashed lines represent metastable extensions from subsolidus reaction $H=A+H_2O$; the invariant points (I) at conditions of different a_{H_2O} (0.5, 0.8 and 1.0 are noted) determine the geometry of reaction $H=A+M$ (fluid-absent melting); the upper right inset denotes a_{H_2O} of different phases; after Clemens and Vielzeuf (1987)

Fig. II-17 shows an ideal melting relationship of a hydrous system, in which only one hydrous mineral is supposed to exist. The P - T conditions of subsolidus dehydration reaction, fluid-present congruent melting and fluid-absent incongruent dehydration melting are all dependent on H_2O activity. The P - T position of fluid-

absent dehydration melting is determined by the interaction of the reaction lines of fluid-present congruent melting and of subsolidus dehydration reaction if they have equal H_2O activities (Eggler, 1973; Clemens and Vielzeuf, 1987). Based on the model of H_2O activity in silicate melt and related experimental data, Clemens and Vielzeuf (1987) calculated F_{max} values of different rock types. Fig. II-18 shows the relation of water content and F_{max} for metabasic rocks. When the hydrous mineral (i.e. amphibole) is decomposed completely (at 950 °C and 10 kbar, see Fig. II-16), the maximum degree of partial melting is achieved. If it is considered that lower limit of melt fraction for being effectively extracted to form large intrusives is about 20 vol% (Arzi, 1978; Vigneresse et al., 1996; Rosenberg and Handy, 2005), the water content of magma source should be above 0.8 wt% (equal to >40 wt% amphibole in protolith). Furthermore, as mentioned before, the composition of lower continental crust contains generally 50-60 wt% SiO_2 , which constrains the amphibole content of 40-60 wt% (equal to 0.8-1.2 wt% H_2O in the protolith) and consequently F_{max} of 20-27 vol% (15-21 wt%; assuming melt density = 2.2 g/cm³, residue density = 3.2 g/cm³).

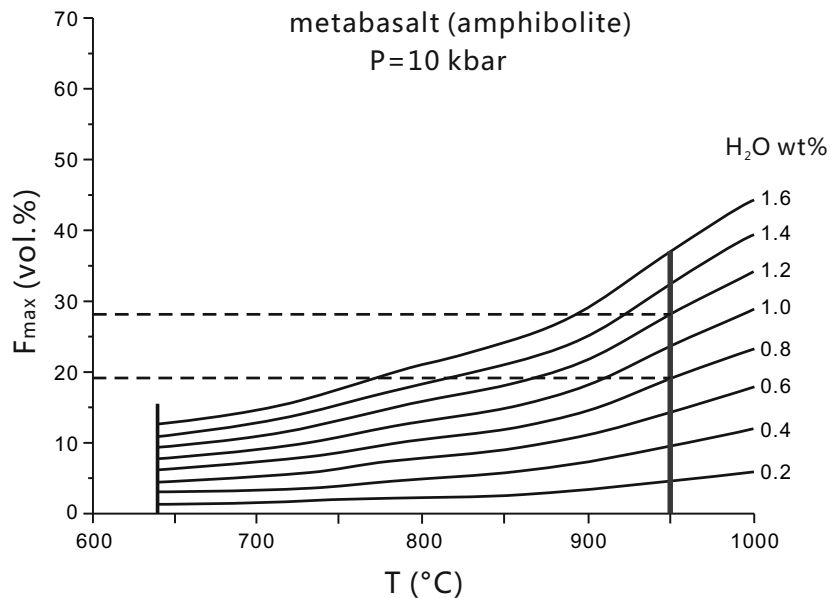


Fig. II-18 Maximum melting degree of metabasalt as a function of temperature and water content of the source rock at 10 kbar. If temperature is raised up to about 950 °C, all amphibole could be decomposed (see Fig.2), and the source rocks with water content of 0.8~1.6 wt% (equivalent to 40~80 wt% amphibole) could give rise to melt of maximum fraction of 20~37 vol% (equally 15-30 wt%); after Clemens and Vielzeuf (1987)

9.4 Discussion on the origin of Dabie C-type adakite

9.4.1 Comparison between Dabie C-type adakite and experimental melts

It has been proposed that partial melting of low-K metabasic rocks can hardly produce high-K calc-alkaline felsic melts (e.g. Roberts and Clemens, 1993). The C-type adakitic rocks from the Dabie orogen are rich SiO₂ (63-75 wt%) and K₂O (3.5-5 wt%), i.e. mainly high-K calc-alkaline series. As shown in Fig. II-19a partial melting of low-K metabasic rocks (K₂O <0.5 wt%) in experiments can only produce melts with a K₂O content lower than 2.5 wt%, i.e. low-K tholeiitic and calc-alkaline series. It is thus indicated that the protoliths of the Dabie C-type adakites are likely calc-alkaline or high-K calc-alkaline series rather than low-K tholeiitic series, which is similar to the estimation for North China C-type adakites (Xiong et al., 2011). In the diagram of K₂O content of experimental melt plotted versus melt fraction (Fig. II-19b), it can be noted that other than K₂O content of source rock, melting degree exerts an important effect on the potassium enrichment of partial melts: K₂O content of melt decreases strongly with increasing melt fraction (melting degree) especially for low melt fractions. This variation trend of K₂O demonstrates that potassium behaviors like highly incompatible elements.

9.4.2 Modeling of K₂O content with melting degree

For felsic melts derived by low-degree partial melting of metabasic rocks, the partition coefficient of K between residual minerals and coexisting melt (M) are: $Kd^{Amp/M} = 0.081$, $Kd^{Plg/M} = 0.10$, $Kd^{Cpx/M} = 0.037$, $Kd^{Opx/M} = 0.0023$, $Kd^{Grt/M} = 0.02$, $Kd^{Qtz/M} = 0.013$ (Nagasawa and Schnetzler, 1971; Nash and Crecraft, 1985). Here the following batch melting relation of trace elements (Rollinson, 1993) is used for quantitative estimation: $C_L = C_O / [F + D \times (1-F)]$, in which C_O and C_L are respectively elemental concentrations in source rock and melt, F is melt fraction. D is the bulk distribution coefficient and calculated as $D = p_1 Kd_1 + p_2 Kd_2 + p_3 Kd_3 + \dots$, where p_1 etc. is normative fraction of the mineral in the residual assemblage with the partition coefficient Kd_1 . When F is smaller than 0.02, the resultant melt could have K₂O content 10 times higher than that of the source rock if the residue is garnet amphibolite (25% garnet + 25% plagioclase + 50% amphibole), and even 25 times higher if the residue is eclogite (50% garnet + 50% clinopyroxene). As a result, the following experimental observations (Fig. II-19b) could be mainly explained by the high incompatibility of potassium: Sen and Dunn (1994) obtained high-K partial melt (K₂O = 5.85 wt%) by melting low-K protolith (K₂O = 0.8 wt%) at high pressure (15 kbar) with garnet amphibolite residue and very low melt fraction ($F = 1.9\%$); Rapp

and Watson (1995) melted low-K high-Al basalt ($K_2O = 0.21$ wt%) at 16 kbar and got high-K melt ($K_2O = 3.08$ wt%) with a very low melting degree ($F = \sim 2\%$); Skjerlie and Patino Douce (2002) melted hydrous eclogite at very high pressures (21-32 kbar) and the resultant melts had K_2O contents (1.12-5.13 wt%) more than 10 to 40 times higher than that of the source rocks ($K_2O = 0.14\%$). Consequently, it cannot be absolutely excluded that high-K calc-alkaline felsic melts could derive from low-K metabasic source rocks. However, if the melting degree increases to above 20%, the K_2O content of resultant melt decreases rapidly (Fig. II-19b).

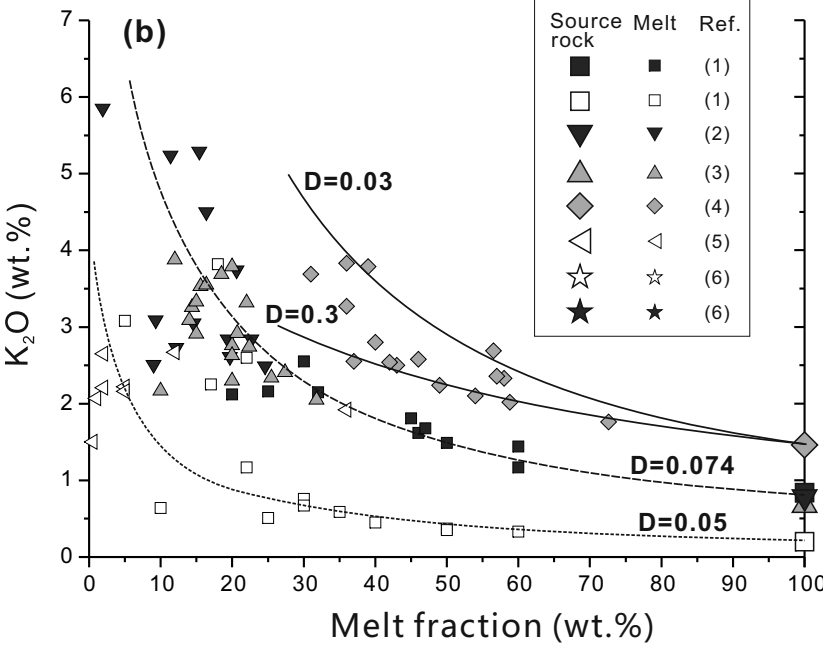
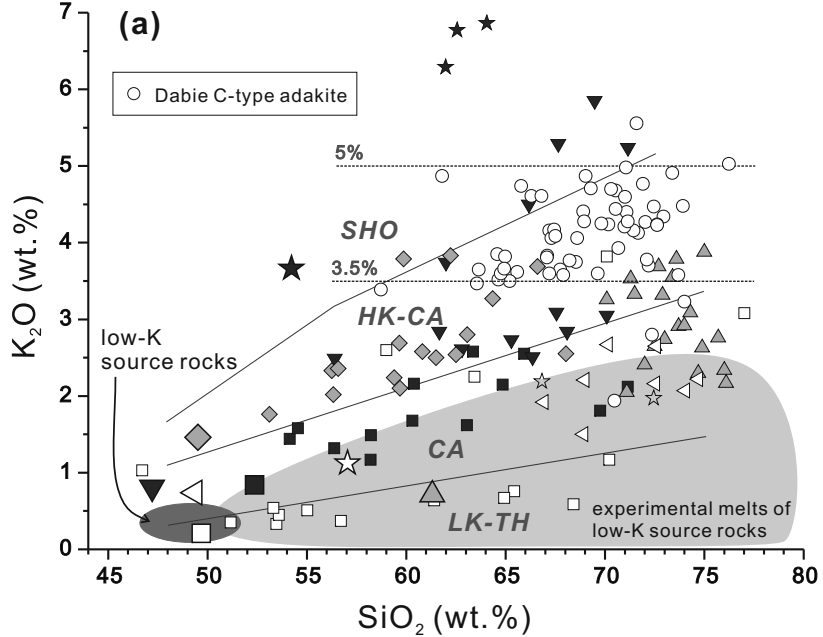


Fig. II-19 Comparison between the Dabie C-type adakites and some experimental melts. (a) SiO₂ versus K₂O diagram; (b) melt fraction versus K₂O diagram; compositions of the Dabie C-type adakites are from Wang et al.(2007), Xu et al.(2007) and Zhao et al.(2007); references of experimental melts: (1) Rapp and Watson (1995), (2) Sen and Dunn (1994), (3) Patino Douce and Beard (1995), (4) Xiong et al. (2005), (5) Zhou et al. (2005), (6) Xiao and Clemens (2007); SHO shoshonitic series, HK-CA high-K calc-alkaline series, CA calc-alkaline series, LK-TH low-K tholeiite series (Rickwood, 1989); low-K source materials can only produce calc-alkaline or low-K tholeiite series melts (references: Beard and Lofgren, 1991; Winther and Newton, 1991; Wolf and Wyllie, 1994; Rapp and Watson, 1995; Lopez and Castro, 2001; Skjerlie and Patino Douce, 2002); D values in (b) are total distribution coefficients used for modeling the K₂O contents of melts

As stated before, although high-K calc-alkaline melts could be generated by partial melting of low-K source rocks with very low melting degrees, effective melt extraction and migration require much higher melt fractions (>20 %, Arzi, 1978; Vigneresse et al., 1996; Rosenberg and Handy, 2005). As a result, very low-degree partial melting could only produce in-situ anatectic rocks (i.e. migmatites), rather than large magmatic intrusives or eruptions. My modeling results (Fig. II-20) show that high-K calc-alkaline melts (3.5-5.0 wt% K₂O, similar to the Dabie C-type adakites, see Fig. II-19a) could be formed by partial melting of high-K calc-alkaline metabasic rocks (1.5 wt% K₂O) with melting degrees of 25%-37% if garnet amphibolite (25% garnet + 25% plagioclase + 50% amphibole) is stable as the residue. If the source rocks are calc-alkaline series, smaller melting degrees decreases are required for generating identical high-K calc-alkaline melts, e.g. $F = 14\sim 23$ wt% for $Co(K_2O) = 1.0$ wt%. If pressure is above the stable field of plagioclase and the residue is eclogite, the required melting degree increases slightly. As a result, 15-35% partial melting of calc-alkaline source rocks (K₂O = 1.0-1.5 wt%) at conditions in which garnet-bearing (~20%) residual assemblage is stable might be the major origin of C-type adakites from the Dabie orogen and North China craton.

As discussed before, the composition of the lower continental crust is generally basaltic andesite (54-57 wt% SiO₂), which constrains the content of amphibole to be less than 60 wt% (bulk water <1.2 wt%). Considering the relation of maximum melting degree and bulk water content (Fig. II-18), one can obtain the F_{max} of 15-21 wt% (note to transform volume into weight). As a result, by comparing this value with Fig. II-20, one can find that source rocks of ~1.0 wt% K₂O might be optimal to generate high-K calc-alkaline melts (3.5-5.0 wt% K₂O).

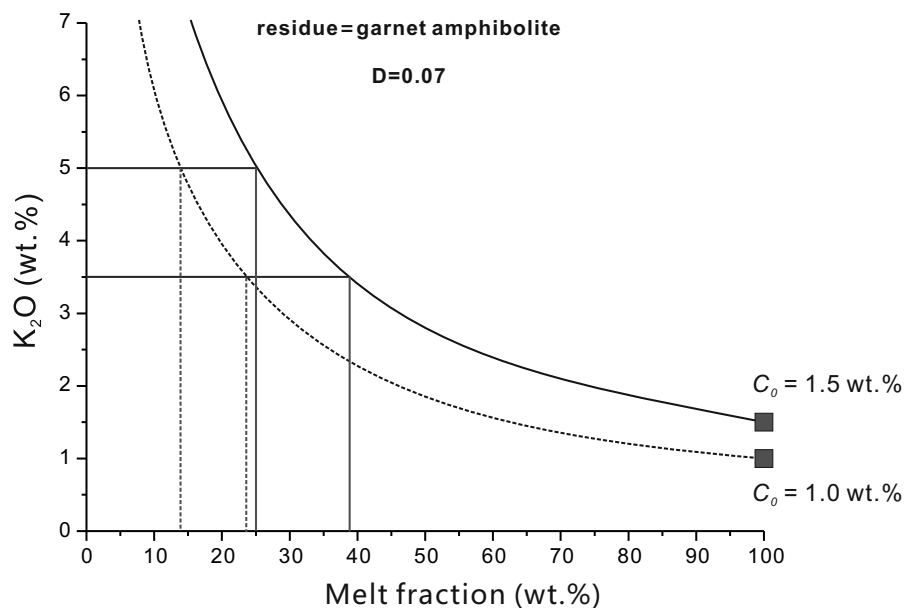


Fig. II-20 Modeling of K_2O content dependent on melt fraction. The D values are total partition coefficients for modeling K_2O content of melts; C_0 values are K_2O contents of source rocks

9.5 Summary

On the basis of continental composition, principals of hydration partial melting of hydrous mafic rocks and published experimental data, we discuss the partial melting mechanism of continental lower crust. By comparing the Dabie C-type adakites and experimental melts, we provide constraints on the magma source, melting conditions (temperature and pressure) and melting degree. Overall, the continental lower crust from the East China, including the Dabie orogen, is basic-intermediate (50~60 wt% SiO_2) and slightly hydrous. Thus, fluid-absent dehydration melting of hydrous minerals is the major mechanism for the continental lower crust generating hydrous felsic melts and anhydrous residue. More than ~20% garnet in the residue could be formed by partial melting of amphibolite at medium pressure (1.0~1.2 GPa, equivalent to 35~40 km), which are generally essential to make the coexisting melt to possess adakitic signatures (especially low Y, high Sr/Y and La/Yb). Based on H_2O activity model and solidus of metamafic rocks, dehydration partial melting which occurs at ~950 °C could lead to a maximum melt proportion of 15~20%, meeting the acquirement of efficient melt segregation. The Dabie C-type adakitic rocks are of high-K calc-alkaline series (3.5~5 wt% K_2O), and it is clear if compared with experimental melts that they cannot derive from low-K protoliths by partial melting with reasonable melting degrees. In the light of the highly-incompatible behavior of K over the course of partial melting, calculation based on

the partition coefficients between melt and possible residues indicates that high-K calc-alkaline melts similar to the Dabie C-type adakitic rocks can be generated by 15~20% (mass basis) partial melting of amphibolites with ~1 wt% K₂O.

10 References

- Andersen, T., 2002. Correction of common lead in U-Pb analyses that do not report 204Pb. *Chemical Geology* 192, 59-79.
- Anderson, D.L., 2005. Large igneous provinces, delamination, and fertile mantle. *Elements* 1, 271-275.
- Arzi A. 1978. Critical phenomena in the rheology of partially melted rocks [J]. *Tectonophysics*, 44(1-4): 173-184.
- Atherton, M.P., Petford, N., 1993. Generation of sodium-rich magma from newly underplated basaltic crust. *Nature* 362, 144-146.
- Baker D R. 1998. Granitic melt viscosity and dike formation. *Journal of Structural Geology*, 20(9-10): 1395-1404.
- Baker, D.R., 1989. Tracer versus trace element diffusion: Diffusional decoupling of Sr concentration from Sr isotope composition. *Geochimica et Cosmochimica Acta* 53, 3015-3023.
- Barbarin, B., 2005. Mafic magmatic enclaves and mafic rocks associated with some granitoids of the central Sierra Nevada batholith, California: nature, origin, and relations with the hosts. *Lithos* 80, 155-177.
- Beard J and Lofgren G. 1991. Dehydration Melting and Water-Saturated Melting of Basaltic and Andesitic Greenstones and Amphibolites at 1, 3, and 6. 9 kb. *Journal of Petrology*, 32(2): 365.
- Beard J S and Lofgren G E. 1989. Effect of Water on the Composition of Partial Melts of Greenstone and Amphibolite. *Science*, 244(4901): 195-197.
- Brown G C and Fyfe W S. 1970. The production of granitic melts during ultrametamorphism. *Contributions to Mineralogy and Petrology*, 28(4): 310-318.
- Burnham C W. 1979. The importance of volatile constituents. In: H S Yoder (Editor), *The evolution of the igneous rocks*. Princeton University Press, Princeton, pp. 439-482.
- Campbell I H and Taylor S R. 1983. No Water, No Granites - No Oceans, No Continents. *Geophysical Research Letters*, 10(11): 1061-1064.
- Castillo, P.R., Janney, P.E., Solidum, R.U., 1999. Petrology and geochemistry of Camiguin Island, southern Philippines: Insights to the source of adakites and other lavas in a complex arc setting. *Contributions to Mineralogy and Petrology* 134, 33-51.
- Chang, Y.F., Liu, X.P., Wu, Y.C., 1991. *The copper-iron belt of the lower and middle reaches of the Changjiang River*. Geological Publishing House, Beijing. 363 pp (in Chinese with English abstract).
- Chen, B., Jahn, B.M., Wei, C.J., 2002. Petrogenesis of Mesozoic granitoids in the Dabie UHP complex, Central China: trace element and Nd-Sr isotope evidence. *Lithos* 60, 67-88.
- Chen, B., Tian, W., Jahn, B.M., Chen, Z.C., 2008. Zircon SHRIMP U-Pb ages and in-situ Hf isotopic analysis for the Mesozoic intrusions in South Taihang, North China craton: Evidence for hybridization between mantle-derived magmas and crustal components. *Lithos* 102, 118-137.
- Chen, F., Hegner, E., Todt, W., 2000. Zircon ages, Nd isotopic and chemical compositions of orthogneisses from the Black Forest, Germany - evidence for a Cambrian magmatic arc. *International Journal of Earth Sciences* 88, 791-802.
- Chen, L., Ma, C.Q., She, Z.B., Mason, R., Zhang, J.Y., Zhang, C., 2009. Petrogenesis and Tectonic Implications of A-type Granites in the Dabie Orogenic Belt, China: Geochronological and Geochemical Constraints. *Geological Magazine* 146, 638-651.
- Chung, S.L., Liu, D.Y., Ji, J.Q., Chu, M.F., Lee, H.Y., Wen, D.J., 2003. Adakites from continental collision zones: Melting of thickened lower crust beneath southern Tibet. *Geology* 31, 1021-1024.
- Clemens J and Vielzeuf D. 1987. Constraints on melting and magma production in the crust. *Earth and Planetary Science Letters*, 86(2-4): 287-306.
- Clemens J D. 2005. Melting of the continental crust: fluid regimes, melting reactions and source-rock fertility. In: B M and A Rushmer Tracy (Editors), *Evolution and Differentiation of the Continental Crust*. Cambridge University Press, Cambridge, pp. 297-331.
- Defant M J and Drummond M S. 1990. Derivation of some modern arc magmas by melting of young subducted lithosphere. *Nature*, 347(6294): 662-665.

- Defant M J and Drummond M S. 1993. Mount St. Helens: Potential example of the partial melting of the subducted lithosphere in a volcanic arc. *Geology*, 21(6): 547-550.
- Defant M J, Kepezhinskas P, Defant M J, et al. 2002. Adakites: some variations on a theme. *Acta Petrologica Sinica*, 18(2): 129-142.
- Defant M J, Richerson P M, Deboer J Z, et al. 1991. Dacite genesis via both slab melting and differentiation: Petrogenesis of La-Yeguada volcanic complex, Panama. *Journal of Petrology*, 32(6): 1101-1142.
- Defant, M.J., Xu, J.F., Kepezhinskas, P., Wang, Q., Zhang, Q., Xiao, L., 2002. Adakites: some variations on a theme. *Acta Petrologica Sinica* 18, 129-142.
- DePaolo, D.J., 1981. Neodymium isotopes in the Colorado Front Range and crust-mantle evolution in the Proterozoic. *Nature* 291, 193-196.
- Didier, J., 1973. *Granites and their Enclaves: The Bearing of Enclave on the Origin of Granites*. Elsevier, Amsterdam. 393 pp.
- Didier, J., Barbarin, B., 1991. The different types of enclaves in granites - Nomenclature. In: Didier J, Barbarin B, eds. *Enclaves and granite petrology*. Elsevier, Amsterdam, pp. 19-23.
- Drummond M S and Defant M J. 1990. A model for trondhjemite-tonalite-dacite genesis and crustal growth via slab melting - Archean to modern comparisons. *Journal of Geophysical Research-Solid Earth and Planets*, 95(B13): 21503-21521.
- Eggler D H. 1973. Principles of melting of hydrous phases in silicate melt, *Carnegie Institute of Washington Year Book*, 491-495.
- Ewart, A., Griffin, W.L., 1994. Application of proton-microprobe data to trace-element partitioning in volcanic rocks. *Chemical Geology* 117, 251-284.
- Foley S, Tiepolo M, Vannucci R. 2002. Growth of early continental crust controlled by melting of amphibolite in subduction zones. *Nature*, 417(6891): 837-840.
- Fyfe W S. 1973. The Granulite Facies, Partial Melting and the Archaean Crust. *Philosophical Transactions of the Royal Society of London. Series A, Mathematical and Physical Sciences*, 273(1235): 457-461.
- Gao S, Luo T-C, Zhang B-R, et al. 1998a. Chemical composition of the continental crust as revealed by studies in East China. *Geochimica Et Cosmochimica Acta*, 62(11): 1959-1975.
- Gao S, Zhang B, Jin Z, et al. 1998b. How mafic is the lower continental crust? *Earth and Planetary Science Letters*, 161(1-4): 101-117.
- Gao, S., Rudnick, R.L., Xu, W.L., Yuan, H.L., Liu, Y.S., Walker, R.J., Puchtel, I.S., Liu, X.M., Huang, H., Wang, X.R., Yang, J., 2008. Recycling deep cratonic lithosphere and generation of intraplate magmatism in the North China Craton. *Earth and Planetary Science Letters* 270, 41-53.
- Gao, S., Rudnick, R.L., Yuan, H.L., Liu, X.M., Liu, Y.S., Xu, W.L., Ling, W.L., Ayers, J., Wang, X.C., Wang, Q.H., 2004. Recycling lower continental crust in the North China Craton. *Nature* 432, 892-897.
- Gao, S., Zhang, B., Jin, Z., Kern, H., 1999. Lower crustal delamination in the Qinling-Dabie orogenic belt. *Science in China (D)* 42, 423-433.
- Gao, S., Zhang, B., Xie, Q., Gu, X., Ouyang, J., Wang, D., Gao, C., 1991. Average chemical compositions of post-Archaean sedimentary and volcanic rocks from the Qinling Orogenic Belt and its adjacent North China and Yangtze Cratons. *Chemical Geology* 92, 261-282.
- Ge X, Li X, Chen Z, et al. 2002. Geochemistry and petrogenesis of Jurassic high Sr/low Y granitoids in eastern China: Constrains on crustal thickness. *Chinese Science Bulletin*, 47(11): 962-968.
- Griffin, W.L., Pearson, N.J., Belousova, E., Jackson, S.E., van Ach-terbergh, E., O'Reilly, S.Y., Shee, S.R., 2000. The Hf isotope composition of cratonic mantle: LAM-MC-ICPMS analysis of zircon megacrysts in kimberlites. *Geochimica et Cosmochimica Acta* 64, 133-147.
- Guo, F., Nakamura, E., Fan, W.M., Kobayoshi, K., Li, C.W., 2007. Generation of Palaeocene adakitic andesites by magma mixing; Yanji Area, NE China. *Journal of Petrology* 48, 661-692.
- Hacker B R. 1990. Amphibolite-facies-to-granulite-facies reactions in experimentally deformed, unpowdered amphibolite. *American Mineralogist*, 75(11-12): 1349-1361.
- Hacker, B.R., Ratschbacher, L., Webb, L., Ireland, T., Walker, D., Dong, S.W., 1998. U/Pb zircon ages constrain the architecture of the ultrahigh-pressure Qinling-Dabie orogen, China. *Earth and Planetary Science Letters* 161, 215-230.
- Hacker, B.R., Ratschbacher, L., Webb, L., McWilliams, M.O., Ireland, T., Calvert, A., Dong, S., Wenk, H.R., Chateigner, D., 2000. Exhumation of ultrahigh-pressure continental crust in east central China: Late Triassic-Early Jurassic tectonic unroofing. *Journal of Geophysical Research* 105, 13339-13364.
- Hirschmann, M.M., Stolper, E.M., 1996. A possible role for garnet pyroxenite in the origin of the "garnet signature" in MORB. *Contributions to Mineralogy and Petrology* 124, 185-208.

- Holtz F and Johannes W. 1994. Maximum and minimum water contents of granitic melts: implications for chemical and physical properties of ascending magmas.; Crustal anatexis and ascent of felsic magmas. *Lithos*, 32(1-2): 149-159.
- Hou Q, Zhang B, Zhang H. 2004. Geochemical characteristics of the amphibolites from Dabie core complex in central East China and their geological implications. *Geological Review*, 50(1): 77-86 (in Chinese with English abstract).
- Huang F and He Y. 2010. Partial melting of the dry mafic continental crust: Implications for petrogenesis of C-type adakites. *Chinese Science Bulletin*, 55(22): 2428-2439.
- Huang F, Li S, He Y. 2011. Comment on "Origin of high-Mg adakitic magmatic enclaves from the Meichuan pluton, southern Dabie orogen (central China): Implications for delamination of the lower continental crust and melt-mantle interaction" by C. Zhang, C.Q. Ma, F. Holtz [*Lithos* 119 (2010) 467-484]. *Lithos*, 125(1-2): 836-838.
- Huang, F., Li, S., Dong, F., He, Y.S., Chen, F., 2008. High-Mg adakitic rocks in the Dabie orogen, central China: Implications for foundering mechanism of lower continental crust. *Chemical Geology* 225, 1-13.
- Huang, F., Li, S., Dong, F., Li, Q., Chen, F., Wang, Y., Yang, W., 2007. Recycling of deeply subducted continental crust in the Dabie Mountains, central China. *Lithos* 96, 151-169.
- Irvine, T.N., Baragaran, W.R.A., 1971. A Guide to the Chemical Classification of the Common Volcanic Rocks. *Canadian Journal of Earth Sciences* 8, 523-548.
- Jahn, B.M., Wu, F.Y., Lo, C.H., Tsai, C.H., 1999. Crust-mantle interaction induced by deep subduction of the continental crust: geochemical and Sr-Nd isotopic evidence from post-collisional mafic-ultramafic intrusions of the northern Dabie complex, central China. *Chemical Geology* 157, 119-146.
- Jiang, N., Liu, Y.S., Zhou, W.G., Yang, J.H., Zhang, S.Q., 2007. Derivation of Mesozoic adakitic magmas from ancient lower crust in the North China craton. *Geochimica et Cosmochimica Acta* 71, 2591-2608.
- Johannes W and Koepke J. 2001. Incomplete reaction of plagioclase in experimental dehydration melting of amphibolite. *Australian Journal of Earth Sciences: An International Geoscience Journal of the Geological Society of Australia*, 48(4): 581 - 590.
- Jull, M., Kelemen, P.B., 2001. On the conditions for lower crustal convective instability. *Journal of Geophysical Research* 106, 6423-6446.
- Kay R W and Kay S M. 2002. Andean adakites: three ways to make them. *Acta Petrologica Sinica*, 18(3): 303-311.
- Kay R W. 1978. Aleutian Magnesian Andesites - Melts from Subducted Pacific Ocean Crust. *Journal of Volcanology and Geothermal Research*, 4(1-2): 117-132.
- Kay, R.W., Kay, S.M., 1991. Creation and destruction of lower continental crust. *Geologische Rundschau* 80, 259-278.
- Kelemen, P.B., 1995. Genesis of high Mg# andesites and the continental crust. *Contributions to Mineralogy and Petrology* 120, 1-19.
- Kelemen, P.B., 1998. Silica enrichment in the continental upper mantle via melt/rock reaction. *Earth and Planetary Science Letters* 164, 387-406.
- Koepke J, Berndt J, Feig S, et al. 2007. The formation of SiO₂-rich melts within the deep oceanic crust by hydrous partial melting of gabbros. *Contributions to Mineralogy and Petrology*, 153(1): 67-84.
- Koepke J, Feig S, Snow J, et al. 2004. Petrogenesis of oceanic plagiogranites by partial melting of gabbros: an experimental study. *Contributions to Mineralogy and Petrology*, 146(4): 414-432.
- Lambert I and Wyllie P. 1972. Melting of gabbro (quartz eclogite) with excess water to 35 kilobars, with geological applications. *The Journal of Geology*, 80(6): 693-708.
- Le Bas, M.J., Le Maitre, R.W., Streckeisen, A., Zanettin, B., 1986. A chemical classification of volcanic rocks based on the total alkali-silica diagram. *Journal of Petrology* 27, 745-750.
- Leech, M.L., 2001. Arrested orogenic development: eclogitization, delamination, and tectonic collapse. *Earth and Planetary Science Letters* 185, 149-159.
- Leshner, C.E., 1990. Decoupling of chemical and isotopic exchange during magma mixing. *Nature* 344, 235-237.
- Leshner, C.E., 1994. Kinetics of Sr and Nd exchange in silicate liquids: Theory, experiments, and applications to uphill diffusion, isotopic equilibration, and irreversible mixing of magmas. *Journal of Geophysical Research* 99, 9585-9604.
- Li, J.W., Zhao, X.F., Zhou, M.F., Ma, C.Q., Zorano, S., Paulo, V., 2009. Late Mesozoic magmatism from the Daye region, eastern China: U-Pb ages, petrogenesis, and geodynamics implications. *Contributions to Mineralogy and Petrology* 157, 383-409.

- Li, J.W., Zhao, X.F., Zhou, M.F., Paulo, V., Ma, C.Q., Deng, X.D., Zorano, S., Zhao, Y.X., Wu, G., 2008. Origin of the Tongshankou porphyry-skarn Cu-Mo deposit, eastern Yangtze craton, Eastern China: geochronological, geochemical, and Sr-Nd-Hf isotopic constraints. *Mineralium Deposita* 43, 315-336.
- Li, X., Su, L., Song, B., Liu, D., 2004a. SHRIMP U-Pb zircon age of the Jinchuan ultramafic intrusion and its geological significance. *Chinese Science Bulletin* 49, 420-422.
- Li, X.P., Zheng, Y.F., Wu, Y.B., Chen, F.K., Gong, B., Li, Y.L., 2004b. Low-T eclogite in the Dabie terrane of China: petrological and isotopic constrains on fluid activity and radiometric dating. *Contributions to Mineralogy and Petrology* 148, 443-470.
- Liu J, Bohlen S R, Ernst W G. 1996. Stability of hydrous phases in subducting oceanic crust. *Earth and Planetary Science Letters*, 143(1-4): 161-171.
- Liu Y, Xu S, Jiang L, et al. 1998. Geochemical characteristics and tectonic settings of amphibolites from the metamorphosed mafic-ultramafic melt in the northern part of the Dabie Shan orogen. *Geotectonica et Metallogenia*, 22(4): 323-331 (in Chinese with English abstract).
- Liu Y, Xu S, Li S, et al. 2004. Rift genesis of banded gneisses and associated amphibolites from the Dabie mountains: Evidence from petrologic geochemistry. *Journal of Mineralogy and Petrology*, 24(1): 1-4 (in Chinese with English abstract).
- Lopez S and Castro A. 2001. Determination of the fluid-absent solidus and supersolidus phase relationships of MORB-derived amphibolites in the range 4-14 kbar. *American Mineralogist*, 86(11-12): 1396.
- Lü, Q., Hou, Z., Yang, Z., Shi, D., 2005. Underplating in the middle-lower Yangtze Valley and model of geodynamic evolution: Constraints from geophysical data. *Science in China (D)* 48, 985-999.
- Ludwig, K.R., 2003. ISOPLOT 3.0: a geochronological toolkit for microsoft excel, Berkeley Geochronology Center. Special publication no. 4.
- Ma, C.Q., Ehlers, C., Xu, C.H., Li, Z.C., Yang, K.G., 2000. The roots of the Dabieshan ultrahigh-pressure metamorphic terrane: constraints from geochemistry and Nd-Sr isotope systematics. *Precambrian Research* 102, 279-301.
- Ma, C.Q., Li, Z.C., Ehlers, C., Yang, K.G., Wang, R.J., 1998. A post-collisional magmatic plumbing system: Mesozoic granitoid plutons from the Dabieshan high-pressure and ultrahigh-pressure metamorphic zone, east-central China. *Lithos* 45, 431-456.
- Ma, C.Q., Yang, K.G., Ming, H.L., Ling, G.C., 2004. The timing of tectonic transition from compression to extension in Dabieshan: Evidence from Mesozoic granites. *Science in China (D)* 47, 453-462.
- Martin H and Moyen J-F. 2002. Secular changes in tonalite-trondhjemite-granodiorite composition as markers of the progressive cooling of Earth. *Geology*, 30(4): 319-322.
- Martin H. 1999. Adakitic magmas: modern analogues of Archaean granitoids. *Lithos*, 46(3): 411-429.
- Martin, H., Smithies, R.H., Rapp, R., Moyen, J.F., Champion, D., 2005. An overview of adakite, tonalite-trondhjemite-granodiorite, TTG, and sanukitoid: relationships and some implications for crustal evolution. *Lithos* 79, 1-24.
- McDonough, W.F., Sun, S.S., 1995. The composition of the Earth. *Chemical Geology* 120, 223-253.
- Montel, J.M., Vielzeuf, D., 1997. Partial melting of metagreywackes, Part II. Composition of minerals and melts. *Contributions to Mineralogy and Petrology* 128, 176-196.
- Moyen J and Stevens G. Experimental constraints on TTG petrogenesis: Implications for Archean geodynamics [M]. *Archean Geodynamics and Environments*, B K, J C Mareschal and C Condie Kent. AGU Geophysical Monograph Series 164, 2006, pp. 149-175.
- Moyen, J.F., 2009. High Sr/Y and La/Yb ratios: The meaning of the “adakitic signature”. *Lithos* 112, 556-574.
- Nagasawa H and Schnetzler C C. 1971. Partitioning of rare earth, alkali and alkaline earth elements between phenocrysts and acidic igneous magma. *Geochimica et Cosmochimica Acta*, 35(9): 953-968.
- Nair R and Chacko T. 2008. Role of oceanic plateaus in the initiation of subduction and origin of continental crust. *Geology*, 36(7): 583-586.
- Nash W and Crecraft H. 1985. Partition coefficients for trace elements in silicic magmas. *Geochimica et Cosmochimica Acta*, 49(11): 2309-2322.
- Okay, A.I., Sengor, A.M.C., 1992. Evidence for intracontinental thrust related exhumation of the ultra-high-pressure rocks in China. *Geology* 20, 411-414.
- Patino Douce A E and Beard J. 1995. Dehydration-melting of biotite gneiss and quartz amphibolite from 3 to 15 kbar. *Journal of Petrology*, 36(3): 707-738.
- Pawley A R and Holloway J R. 1993. Water Sources for Subduction Zone Volcanism: New Experimental Constraints. *Science*, 260(5108): 664-667.

- Powell R and Holland T. 2008. On thermobarometry. *Journal of Metamorphic Geology*, 26(2): 155-179.
- Qian Q. 2001. Adakite: Geochemical characteristics and genesis. *Acta Petrologica et Mineralogica*, 20(3): 297-306 (in Chinese with English abstract).
- Rapp R P, Shimizu N, Norman M D. 2003. Growth of early continental crust by partial melting of eclogite. *Nature*, 425(6958): 605-609.
- Rapp R, Watson E, Miller C. 1991. Partial melting of amphibolite/eclogite and the origin of Archean trondhjemites and tonalites. *Precambrian Research*, 51(1-4): 1-25.
- Rapp R, Xiao L, Shimizu N. 2002. Experimental constraints on the origin of potassium-rich adakites in eastern China. *Acta Petrologica Sinica*, 18(3): 293-302.
- Rapp, R.P., Shimizu, N., Norman, M.D., Applegate, G.S., 1999. Reaction between slab-derived melts and peridotite in the mantle wedge: experimental constraints at 3.8 GPa. *Chemical Geology* 160, 335-356.
- Rapp, R.P., Watson, E.B., 1995. Dehydration melting of metabasalt at 8-32 kbar: implications for continental growth and crust-mantle recycling. *Journal of Petrology* 36, 891-931.
- Rapp, R.P., Xiao, L., Shimizu, N., 2002. Experimental constraints on the origin of potassium-rich adakite in east China. *Acta Petrologica Sinica* 18, 293-311.
- Ratschbacher, L., Hacker, B.R., Webb, L.E., McWilliams, M., Ireland, T., Dong, S.W., Calvert, A., Chateigner, D., Wenk, H.R., 2000. Exhumation of the ultrahigh-pressure continental crust in east central China: Cretaceous and Cenozoic unroofing and the Tan-Lu fault. *Journal of Geophysical Research* 105, 303-338.
- Richards, J.R., Kerrich, R., 2007. Special paper: Adakite-like rocks: their diverse origins and questionable role in metallogenesis. *Economic Geology* 102, 537-576.
- Rickwood, P.C., 1989. Boundary lines within petrologic diagrams which use oxides of major and minor elements. *Lithos* 22, 247-263.
- Roberts M P and Clemens J D. 1993. Origin of high-potassium, talc-alkaline, I-type granitoids. *Geology*, 21(9): 825-828.
- Robinson, J.A.C., Wood, B.J., Blundy, J.D., 1998. The beginning of melting of fertile and depleted peridotite at 1.5 GPa. *Earth and Planetary Science Letters* 155, 97-111.
- Rollinson H R. 1993. Using geochemical data: Evaluation, presentation, interpretation. Longman, Harlow, UK, 352 pp.
- Rosenberg C and Handy M. 2005. Experimental deformation of partially melted granite revisited: implications for the continental crust. *Journal of Metamorphic Geology*, 23(1): 19-28.
- Rudnick, R.L., Fountain, D.M., 1995. Nature and composition of the continental crust: a lower crustal perspective. *Reviews of Geophysics* 33, 267-309.
- Rudnick, R.L., Gao, S., 2003. Composition of the continental crust. In: Rudnick RL, ed. *The crust, Treatise on Geochemistry*, vol 3. Elsevier, pp 1-64.
- Rushmer T. 1991. Partial melting of two amphibolites: contrasting experimental results under fluid-absent conditions. *Contributions to Mineralogy and Petrology*, 107(1): 41-59.
- Rushmer T. 1993. Experimental high-pressure granulites: Some applications to natural mafic xenolith suites and Archean granulite terranes. *Geology*, 21(5): 411.
- Sen, C., Dunn, T., 1994. Dehydration melting of a basaltic composition amphibolite at 1.5 GPa and 2.0 GPa: implication for the origin of adakites. *Contributions to Mineralogy and Petrology* 117, 394-409.
- Skjerlie K and Patiño Douce A. 2002. The fluid-absent partial melting of a zoisite-bearing quartz eclogite from 1.0 to 3.2 GPa; Implications for melting in thickened continental crust and for subduction-zone processes. *Journal of Petrology*, 43(291-314).
- Skjerlie, K., Patiño Douce, A.E., 1995. Anatexis of interlayered amphibolite and pelite at 10 kbar: effect of diffusion of major components on phase relations and melt fraction. *Contributions to Mineralogy and Petrology* 122, 62-78.
- Smithies R H and Champion D C. 2000. The Archean High-Mg Diorite Suite: Links to Tonalite-Trondhjemite-Granodiorite Magmatism and Implications for Early Archean Crustal Growth. *Journal of Petrology*, 41(12): 1653-1671.
- Smithies R H. 2000. The Archean tonalite-trondhjemite-granodiorite (TTG) series is not an analogue of Cenozoic adakite. *Earth and Planetary Science Letters*, 182(1): 115-125.
- Soudouji, F., Yuan, X., Liu, Q., Kind, R., Chen, J., 2006. Lithospheric thickness beneath the Dabie Shan, central eastern China from S receiver functions. *Geophysical Journal International* 166, 1363-1367.
- Sparks, R.S.J., Marshall, L.A., 1986. Thermal and mechanical constraints on mixing between mafic and silicic magmas. *Journal of Volcanology and Geothermal Research* 29, 99-124.

- Springer W and Seck H. 1997. Partial fusion of basic granulites at 5 to 15 kbar: implications for the origin of TTG magmas. *Contributions to Mineralogy and Petrology*, 127(1): 30-45.
- Stern, C.R., Kilian, R., 1996. Role of the subducted slab, mantle wedge and continental crust in the generation of adakites from the Austral volcanic zone. *Contributions to Mineralogy and Petrology* 123, 263-281.
- Stern, R.A., Hanson, G.N., 1991. Archean high-Mg granodiorite: A derivative of light rare earth element-enriched monzodiorite of mantle origin. *Journal of Petrology* 32, 201-238.
- Stevenson, J.A., Daczko, N.R., Clarke, G.L., Pearson, N., Klepeis, K.A., 2005. Direct observation of adakite melts generated in the lower continental crust, Fiordland, New Zealand. *Terra Nova* 17, 73-79.
- Streck, M.J., Leeman, W.P., Chesley, J., 2007. High-magnesian andesite from Mount Shasta: a product of magma mixing and contamination, not a primitive mantle melt. *Geology* 35, 351-354.
- Sun, S.S., McDonough, W.F., 1989. Chemical and isotopic systematics of oceanic basalts: implications for mantle composition and processes. Geological Society, London, Special Publications 42, 313-345.
- Takahashi, E., Kushiro, I., 1983. Melting of a dry peridotite at high pressures and basalt magma genesis. *American Mineralogist* 68, 859-879.
- Taylor, S.R., McLennan, S.M., 1985. *The continental crust: its composition and evolution*. Blackwell, Oxford. 312 pp.
- van der Laan, S.R., Wyllie, P.J., 1993. Experimental interaction of granitic and basaltic magmas and implications for mafic enclaves. *Journal of Petrology* 34, 491-517.
- Vavra, G., Schimid, R., Gebauer, D., 1999. Internal morphology, habit and U-Th-Pb microanalysis of amphibolite-to-granulite facies zircons: geochronology of the Ivrea Zone (Southern Alps). *Contributions to Mineralogy and Petrology* 134, 380-404.
- Vernon, R.H., 1983. Restite, xenoliths and microgranitoid enclaves in granites. *Journal and Proceedings of Royal Society New South Wales* 116, 77-103.
- Vielzeuf D and Schmidt M W. 2001. Melting relations in hydrous systems revisited: application to metapelites, metagreywackes and metabasalts. *Contributions to Mineralogy and Petrology*, 141(3): 251-267.
- Vigneresse J L, Barbey P, Cuney M. 1996. Rheological transitions during partial melting and crystallization with application to felsic magma segregation and transfer. *Journal of Petrology*, 37(6): 1579-1600.
- Walther J V and Orville P M. 1982. Volatile production and transport in regional metamorphism. *Contributions to Mineralogy and Petrology*, 79(3): 252-257.
- Wang Q, Xu J, Zhao Z. 2001. The summary and comment on research on a new kind of igneous rock – adakite. *Advance in Earth Sciences*, 16(2): 201-208 (in Chinese with English abstract).
- Wang Y and Chen S. 2010. The "C-type Adakite": A Concept Based on Misunderstanding? *Bulletin of Mineralogy, Petrology and Geochemistry*, 29(3): 284-292 (in Chinese with English abstract).
- Wang Y. 2007. A discussion on some problems in the research on the Mesozoic potassic igneous rocks in the eastern China. *Geological Review*, 53(2): 198-207 (in Chinese with English abstract).
- Wang, C., Zhang, X., Chen, B., Chen, X., Song, S., Zheng, J., Hu, H., Lou, H., 1997. Crustal structures of Dabieshan orogenic belt. *Science in China (D)* 27, 221-226.
- Wang, C.Y., Zeng, R.S., Mooney, W.D., Hacker, B.R., 2000. A crustal model of the ultrahigh-pressure Dabie Shan orogenic belt, China, derived from deep seismic refraction profiling. *Journal of Geophysical Research* 105, 10857-10869.
- Wang, Q., Wyman, D.A., Xu, J.F., Jian, P., Zhao, Z., Li, C., et al., 2007b. Early Cretaceous adakitic granites in the Northern Dabie Complex, central China: implication for partial melting and delamination of thickened lower crust. *Geochimica et Cosmochimica Acta* 71, 2609-2636.
- Wang, Q., Wyman, D.A., Xu, J.F., Zhao, Z.H., Jian, P., Feng, Z., 2007a. Partial melting of thickened or delaminated lower crust in the middle of eastern China: Implications for Cu-Au mineralization. *Journal of Geology* 115, 149-161.
- Wang, Q., Xu, J.F., Jian, P., Bao, Z.W., Zhao, Z.Z., Li, C.F., Xiong, X.L., Ma, J.L., 2006. Petrogenesis of adakitic porphyries in an extensional tectonic setting, Dexing, South China: implications for the genesis of porphyry copper mineralization. *Journal of Petrology* 47, 119-144.
- Wang, Q., Zhao, Z.H., Bao, Z.W., Xu, J.F., Liu, W., Li, C.F., et al., 2004. Geochemistry and petrogenesis of the Tongshankou and Yinzu adakitic intrusive rocks and the associated porphyry copper–molybdenum mineralization in southeast Hubei, east China. *Resource Geology* 54, 137-152.
- Wang, Y.J., Fan, W.M., Peng, T.P., Zhang, H.F., Guo, F., 2005. Nature of the Mesozoic lithospheric mantle and tectonic decoupling beneath the Dabie Orogen, Central China: Evidence from

- $^{40}\text{Ar}/^{39}\text{Ar}$ geochronology, elemental and Sr-Nd-Pb isotopic compositions of early Cretaceous mafic igneous rocks. *Chemical Geology* 220, 165-189.
- Wannamaker P. 2000. Comment on "The petrologic case for a dry lower crust" by Bruce WD Yardley and John W. Valley. *Journal of Geophysical Research*, 105(B3): 6057-6064.
- Wei, C.J., Zhang, L.F., Wang, S.G., 2001. Mesozoic high-K granitic rocks from the eastern Dabie Mountains, Central China and their geological implications. *Science in China (D)* 44, 525-534.
- Williams Q and Hemley R J. 2001. Hydrogen in the deep earth. *Annual Review of Earth and Planetary Sciences*, 29(1): 365-418.
- Winter J D. 2010. *Principles of Igneous and Metamorphic Petrology*. Pearson Prentice Hall, New Jersey, 702 pp.
- Winther K T and Newton R C. 1991. Experimental melting of hydrous low-K tholeiite: evidence on the origin of Archean cratons. *Bull. geol. Soc. Denmark*, 39(213-228).
- Wolf M and Wyllie P. 1993. Garnet growth during amphibolite anatexis: implications of a garnetiferous restite. *The Journal of Geology*, 101(3): 357-373.
- Wolf M and Wyllie P. 1994. Dehydration-melting of amphibolite at 10 kbar: the effects of temperature and time. *Contributions to Mineralogy and Petrology*, 115(4): 369-383.
- Wolf M B and Wyllie P J. 1991. Dehydration-Melting of Solid Amphibolite at 10 Kbar - Textural Development, Liquid Interconnectivity and Applications to the Segregation of Magmas. *Mineralogy and Petrology*, 44(3-4): 151-179.
- Woodhead, J., Hergt, J., Shelley, M., Eggins, S., Kemp, R., 2004. Zircon Hf-isotope analysis with an excimer laser, depth profiling, ablation of complex geometries, and concomitant age estimation. *Chemical Geology* 209, 121-135.
- Wu, C.L., Dong, S.W., Guo, H.P., Guo, X.Y., Gao, Q.M., Liu, L.G., Chen, Q.L., Lei, M., 2008. Zircon SHRIMP U-Pb dating of intermediate-acid intrusive rocks from Shizishan, Tongling and the deep processes of magmatism. *Acta Petrologica Sinica* 24, 1801-1812 (in Chinese with English Abstract).
- Wu, F.Y., Yang, Y.H., Xie, L.W., Yang, J.H., Xu, P., 2006. Hf isotopic compositions of the standard zircons and baddeleyites used in U-Pb geochronology. *Chemical Geology* 234, 105-126.
- Wu, Y.B., Zheng, Y.F., Zhang, S.B., Zhao, Z.F., Wu, F.Y., Liu, X.M., 2007. Zircon U-Pb ages and Hf isotope compositions of migmatite from the North Dabie terrane in China: constraints on partial melting. *Journal of Metamorphic Geology* 25, 991-1009.
- Wyllie, P.J., Cox, K.G., Biggar, G.M., 1962. The habit of apatite in synthetic systems and igneous rocks. *Journal of Petrology* 3, 238-242.
- Xiao L and Clemens J. 2007. Origin of potassic (C-type) adakite magmas: Experimental and field constraints. *Lithos*, 95(3-4): 399-414.
- Xiao L, Rapp P R, Xu J F. 2004. The role of deep processes controls on variation of compositions of adakitic rocks. *Acta Petrologica Sinica*, 20(2): 219-228 (in Chinese with English abstract).
- Xie, G.Q., Mao, J.W., Li, R.L., Zhou, S.D., Ye, H.S., Yan, Q.R., Zhang, Z.S., 2006a. SHRIMP zircon U-Pb dating for volcanic rocks of the Dasi Formation in southeast Hubei Province, mid-die-lower reaches of the Yangtze River and its implications. *Chinese Science Bulletin* 51, 3000-3009.
- Xie, Z., Zheng, Y.F., Zhao, Z.F., et al., 2006b. Mineral isotope evidence for the contemporaneous process of Mesozoic granite emplacement and gneiss metamorphism in the Dabie orogen. *Chemical Geology* 231, 214-235.
- Xiong X L, Adam J, Green T H. 2005. Rutile stability and rutile/melt HFSE partitioning during partial melting of hydrous basalt: implications for TTG genesis. *Chemical Geology*, 218(3-4): 339-359.
- Xiong X, Liu X, Zhu Z, et al. 2011. Adakitic rocks and destruction of the North China Craton: Evidence from experimental petrology and geochemistry. *SCIENCE CHINA Earth Sciences*, 54(6): 858-870.
- Xu H, Ma C Q. 2003. Constraints of experimental petrology on the origin of adakites, and petrogenesis of Mesozoic K-rich high Sr/Y ratio granitoids in eastern China. *Earth Science Frontiers*, 10(4): 417-427 (in Chinese with English abstract).
- Xu, H.J., Ma, C.Q., Ye, K., 2007. Early Cretaceous granitoids and their implications for the collapse of the Dabie orogen, eastern China: SHRIMP zircon U-Pb dating and geochemistry. *Chemical Geology* 240, 238-259.
- Xu, H.J., Ye, K., Ma, C.Q., 2008a. Early Cretaceous granitoids in the North Dabie and their tectonic implications: Sr-Nd and zircon Hf isotopic evidences. *Acta Petrologica Sinica* 24, 87-103 (in Chinese with English abstract).
- Xu, J.F., Shinjo, R., Defant, M.J., Wang, Q., Rapp, P.T., 2002. Origin of Mesozoic adakitic intrusive rocks in the Ningzhen area of east China: partial melting of delaminated lower continental crust? *Geology* 30, 1111-1114.

- Xu, S.T., Okay, A.L., Ji, S., Sengör, A.M.C., Sun, W., Liu, Y., Jiang, L., 1992. Diamond from the Dabie Shan metamorphic rocks and its implication for tectonic setting. *Science* 256, 80-82.
- Xu, W.L., Hergt, J.M., Gao, S., Pei, F.P., Wang, W., Yang, D.B., 2008b. Interaction of adakitic melt-peridotite: Implications for the high-Mg# signature of Mesozoic adakitic rocks in the eastern North China Craton. *Earth and Planetary Science Letters* 265, 123-137.
- Xu, W.L., Wang, Q.H., Wang, D.Y., Guo, J.H., Pei, F.P., 2006. Mesozoic adakitic rocks from the Xuzhou–Suzhou area, eastern China: Evidence for partial melting of delaminated lower continental crust. *Journal of Asian Earth Sciences* 27, 454-464.
- Yang, J.H., Wu, F.H., Wilde, S.A., Xie, L.W., Yang, Y.H., Liu, X.M., 2007. Tracing magma mixing in granite genesis: in situ U-Pb dating and Hf-isotope analysis of zircons. *Contributions to Mineralogy and Petrology* 153, 177-190.
- Yang, Y.H., Zhang, H.F., Xie, L.W., Liu, Y., Qi, C.S., Tu, X.L., 2006. Petrogenesis of typical Mesozoic and Cenozoic volcanic rocks from the North China Craton: new evidence from Hf isotopic studies. *Acta Petrologica Sinica* 22, 1665-1671 (in Chinese with English abstract).
- Yogodzinski G M and Kelemen P B. 1998. Slab melting in the Aleutians: implications of an ion probe study of clinopyroxene in primitive adakite and basalt. *Earth and Planetary Science Letters*, 158(1-2): 53-65.
- Yogodzinski, G.M., Volynets, O.N., Koloskov, A.V., Seliverstov, N.I., Matvenkov, V.V., 1994. Magnesian andesites and the subduction component in a strongly calc-alkaline series at Piip Volcano, far western Aleutians. *Journal of Petrology* 35, 163-204.
- You, Z., Han, Y., Yang, W., Zhang, Z., Wie, B., Liu, R., 1996. The High-Pressure and Ultra High-Pressure Metamorphic Belt in the East Qinling and Dabie Mountains, China. China University of Geosciences Press, Wuhan. 150 pp (in Chinese with English abstract).
- Yuan, H.L., Gao, S., Liu, X.M., Li, H.M., Gunther, D., Wu, F.Y., 2004. Accurate U-Pb age and trace element determinations of zircon by laser ablation-inductively coupled plasma mass spectrometry. *Geostand Newslett* 28, 353-370.
- Zeck, H.P., Williams, I.S., 2002. Inherited and magmatic zircon from Neogene Hoyazo cordierite dacite, SE Spai - Anatectic source rock provenance and magmatic evolution. *Journal of Petrology* 43, 1089-1104.
- Zhai M G. 2004. Adakite and related granitoids from partial melting of continental lower crust. *Acta Petrologica Sinica*, 20(2): 193-194 (in Chinese with English abstract).
- Zhai, Y.S., Xiong, Y.Y., Yao, S.Z., Liu, X.D., 1996. Metallogeny of copper and iron deposits in the Eastern Yangtze Carton, east-central China. *Ore Geology Review* 11, 229-248.
- Zhang C and Ma C Q. 2008. Large-scale Late Mesozoic magmatism in the Dabie Mountain: Constraints from zircon U-Pb dating and Hf isotopes. *Journal of Mineralogy and Petrology*, 28(4): 71-79 (in Chinese with English abstract).
- Zhang C, Ma C, Holtz F. 2010. Origin of high-Mg adakitic magmatic enclaves from the Meichuan pluton, southern Dabie orogen (central China): Implications for delamination of the lower continental crust and melt-mantle interaction. *Lithos*, 119(3-4): 467-484.
- Zhang C, Ma C, Holtz F. 2011. "Origin of high-Mg adakitic magmatic enclaves from the Meichuan pluton, southern Dabie orogen (central China): Implications for delamination of the lower continental crust and melt-mantle interaction" - Reply. *Lithos*, 125(1-2): 839-844.
- Zhang Q, Qian Q, Wang E, et al. 2001. An east China plateau in mid-late Yanshanian period: Implications from adakites. *Chinese Journal of Geology*, 36(2): 248-255 (in Chinese with English abstract).
- Zhang Q, Wang Y, Liu H, et al. 2003. On the space-time distribution and geodynamic environments of adakites in China. Annex: Controversies over differing opinions for adakites in China. *Earth Science Frontiers*, 10(4): 385-400 (in Chinese with English abstract).
- Zhang Q, Wang Y, Qian Q, et al. 2001. The characteritics and tectonic-metallogenic significances of the adakites in Yanshan period from eastern China. *Acta Petrologica Sinica*, 17(2): 236-244 (in Chinese with English abstract).
- Zhang Q, Xu J, Wang Y, et al. 2004. Diversity of adakite. *Geological Bulletin of China*, 23(9-10): 959-965 (in Chinese with English abstract).
- Zhang Q. 2011. Reappraisal of the origin of C-type adakitic rocks from East China. 30(4): 739-747 (in Chinese with English abstract).
- Zhang, H.F., Gao, S., Zhong, Z.Q., Zhang, B.R., Zhang, L., Hu, S.H., 2002. Geochemical and Sr-Nd-Pb isotopic compositions of Cretaceous granitoids: constrains on tectonic framework and crustal structure of the Dabieshan ultrahigh-pressure metamorphic belt, China. *Chemical Geology* 186, 281-299.
- Zhang, H.F., Sun, M., Zhou, X.H., Zhou, M.F., Fan, W.M., Zheng, J.P., 2003. Secular evolution of the

- lithosphere beneath the eastern North China Craton: Evidence from Mesozoic basalts and high-Mg andesites. *Geochimica et Cosmochimica Acta* 67, 4373-4387.
- Zhang, R.Y., Liou, J.G., Tsai, C.H., 1996. Petrogenesis of a high temperature metamorphic terrane: a new tectonic interpretation for the north Dabieshan, Central China. *Journal of Metamorphic Geology* 14:319-333.
- Zhao Z and Zheng Y. 2009. Remelting of subducted continental lithosphere: Petrogenesis of Mesozoic magmatic rocks in the Dabie-Sulu orogenic belt. *Science in China Series D: Earth Sciences*, 52(9): 1295-1318.
- Zhao Z-F, Zheng Y-F, Wei C-S, et al. 2004. Zircon isotope evidence for recycling of subducted continental crust in post-collisional granitoids from the Dabie terrane in China. *Geophysical Research Letters*, 31(22): L22602.
- Zhao, Z.F., Zheng, Y.F., Wei, C.S., Wu, Y.B., 2005a. Post-collisional granitoids from the Dabie orogen in China: Zircon U-Pb age, element and O isotope evidence for recycling of subducted continental crust. *Lithos* 93, 248-272.
- Zhao, Z.F., Zheng, Y.F., Wei, C.S., Wu, Y.B., Chen, F.K., Jahn, B., 2005b. Zircon U-Pb age, element and C-O isotope geochemistry of post-collisional mafic-ultramafic rocks from the Dabie orogen in east-central China. *Lithos* 83, 1-28.
- Zheng, Y.F., Zhou, J.B., Wu, Y.B., Xie, Z., 2005. Low-grade metamorphic rocks in the Dabie-Sulu orogenic belt: a passive-margin accretionary wedge deformed during continent subduction. *International Geology Review* 47, 851-871.
- Zhong Z, Suo S, Zhang H, et al. 2001. Major constituents and texture of the Tongbai-Dabie collisional orogenic belt. 26(6): 560-567 (in Chinese with English abstract).
- Zhou W G, Xie H S, Liu Y G, et al. 2005. Dehydration melting of solid amphibolite at 2.0 GPa: Effects of time and temperature. *Science in China Series D-Earth Sciences*, 48(8): 1120-1133.

Table II-1 Zircon U-Pb dating results for the Meichuan pluton

| Spot | Element (ppm) | | | | Ratios corrected for common Pb | | | | | | | | Age (Ma) | | | |
|----------------------------|---------------|------|----------|------|--------------------------------------|---------|-------------------------------------|---------|-------------------------------------|---------|--------------------------------------|---------|-------------------------------------|----|-------------------------------------|----|
| | Th | U | Total Pb | Th/U | ²⁰⁷ Pb/ ²⁰⁶ Pb | 1σ | ²⁰⁷ Pb/ ²³⁵ U | 1σ | ²⁰⁶ Pb/ ²³⁸ U | 1σ | ²⁰⁸ Pb/ ²³² Th | 1σ | ²⁰⁷ Pb/ ²³⁵ U | 1σ | ²⁰⁶ Pb/ ²³⁸ U | 1σ |
| <i>MC00-1 felsic host*</i> | | | | | | | | | | | | | | | | |
| 1 | 191 | 218 | 24.71 | 0.88 | 0.04881 | 0.00209 | 0.14587 | 0.00607 | 0.02168 | 0.00021 | 0.00686 | 0.00007 | 138 | 5 | 138 | 1 |
| 2.1 | 407 | 241 | 37.09 | 1.69 | 0.08066 | 0.00242 | 0.29517 | 0.00992 | 0.02627 | 0.00025 | 0.01407 | 0.00027 | 263 | 8 | 167 | 2 |
| 2.2 | 228 | 238 | 53.17 | 0.96 | 0.06854 | 0.00707 | 0.18602 | 0.01905 | 0.01968 | 0.00025 | 0.00599 | 0.00009 | 173 | 16 | 126 | 2 |
| 3.1 | 495 | 386 | 23.27 | 1.28 | 0.05095 | 0.00281 | 0.14663 | 0.00794 | 0.02087 | 0.00021 | 0.00657 | 0.00004 | 139 | 7 | 133 | 1 |
| 3.2 | 176 | 204 | 46.46 | 0.86 | 0.05185 | 0.00243 | 0.14982 | 0.00690 | 0.02095 | 0.00017 | 0.00658 | 0.00003 | 142 | 6 | 134 | 1 |
| 4.1 | 156 | 119 | 24.92 | 1.31 | 0.05446 | 0.00106 | 0.15511 | 0.00314 | 0.02073 | 0.00016 | 0.00701 | 0.00014 | 146 | 3 | 132 | 1 |
| 4.2 | 189 | 223 | 15.10 | 0.85 | 0.09876 | 0.00257 | 0.28332 | 0.00705 | 0.02105 | 0.00022 | 0.00809 | 0.00015 | 253 | 6 | 134 | 1 |
| 5.1 | 218 | 173 | 19.78 | 1.26 | 0.04913 | 0.00203 | 0.14081 | 0.00564 | 0.02079 | 0.00021 | 0.00658 | 0.00006 | 134 | 5 | 133 | 1 |
| 5.2 | 842 | 459 | 53.69 | 1.83 | 0.04955 | 0.00090 | 0.14011 | 0.00265 | 0.02052 | 0.00016 | 0.00617 | 0.00005 | 133 | 2 | 131 | 1 |
| 5.3 | 134 | 178 | 20.70 | 0.75 | 0.05456 | 0.00184 | 0.15610 | 0.00549 | 0.02088 | 0.00024 | 0.00724 | 0.00015 | 147 | 5 | 133 | 2 |
| 6 | 110 | 242 | 25.08 | 0.45 | 0.04688 | 0.00237 | 0.12903 | 0.00633 | 0.01996 | 0.00025 | 0.00635 | 0.00022 | 123 | 6 | 127 | 2 |
| 7 | 107 | 101 | 10.87 | 1.06 | 0.05275 | 0.00171 | 0.14848 | 0.00489 | 0.02058 | 0.00021 | 0.00617 | 0.00009 | 141 | 4 | 131 | 1 |
| 8 | 414 | 318 | 40.14 | 1.30 | 0.05604 | 0.00246 | 0.16018 | 0.00688 | 0.02073 | 0.00019 | 0.00645 | 0.00005 | 151 | 6 | 132 | 1 |
| 9.1 | 176 | 82 | 18.15 | 2.13 | 0.06163 | 0.00892 | 0.17247 | 0.02480 | 0.02030 | 0.00032 | 0.00625 | 0.00010 | 162 | 21 | 130 | 2 |
| 9.2 | 214 | 237 | 25.04 | 0.90 | 0.05451 | 0.00207 | 0.15181 | 0.00558 | 0.02020 | 0.00020 | 0.00631 | 0.00006 | 144 | 5 | 129 | 1 |
| 9.3 | 152 | 146 | 16.92 | 1.04 | 0.05270 | 0.00230 | 0.14912 | 0.00635 | 0.02052 | 0.00020 | 0.00644 | 0.00005 | 141 | 6 | 131 | 1 |
| <i>MC21-3 mafic dike**</i> | | | | | | | | | | | | | | | | |
| 1 | 2094 | 701 | 98.47 | 2.99 | 0.04799 | 0.00096 | 0.13750 | 0.00240 | 0.02078 | 0.00012 | 0.00622 | 0.00003 | 131 | 2 | 133 | 1 |
| 2 | 792 | 558 | 69.17 | 1.42 | 0.05330 | 0.00117 | 0.15459 | 0.00302 | 0.02104 | 0.00013 | 0.00715 | 0.00005 | 146 | 3 | 134 | 1 |
| 3 | 1922 | 850 | 110.52 | 2.26 | 0.04945 | 0.00095 | 0.13952 | 0.00230 | 0.02046 | 0.00011 | 0.00642 | 0.00004 | 133 | 2 | 131 | 1 |
| 4 | 94 | 283 | 29.758 | 0.33 | 0.04970 | 0.00189 | 0.14226 | 0.00515 | 0.02076 | 0.00019 | 0.00692 | 0.00017 | 135 | 5 | 132 | 1 |
| 5 | 3104 | 885 | 130.98 | 3.51 | 0.05387 | 0.00122 | 0.15518 | 0.00315 | 0.02089 | 0.00013 | 0.00626 | 0.00004 | 146 | 3 | 133 | 1 |
| 6 | 2038 | 955 | 120.78 | 2.13 | 0.05051 | 0.00078 | 0.14171 | 0.00173 | 0.02035 | 0.00010 | 0.00624 | 0.00003 | 135 | 2 | 130 | 1 |
| 7 | 1373 | 757 | 94.78 | 1.81 | 0.04719 | 0.00083 | 0.13563 | 0.00200 | 0.02085 | 0.00011 | 0.00652 | 0.00004 | 129 | 2 | 133 | 1 |
| 8 | 1785 | 754 | 98.38 | 2.37 | 0.04874 | 0.00094 | 0.13921 | 0.00232 | 0.02072 | 0.00011 | 0.00616 | 0.00003 | 132 | 2 | 132 | 1 |
| 9 | 1692 | 1057 | 128.4 | 1.60 | 0.04851 | 0.00092 | 0.13922 | 0.00227 | 0.02082 | 0.00011 | 0.00641 | 0.00004 | 132 | 2 | 133 | 1 |
| 10 | 1409 | 594 | 77.25 | 2.37 | 0.04915 | 0.00156 | 0.13966 | 0.00416 | 0.02061 | 0.00016 | 0.00623 | 0.00005 | 133 | 4 | 132 | 1 |
| 11 | 1587 | 743 | 95.49 | 2.14 | 0.04921 | 0.00102 | 0.14090 | 0.00257 | 0.02077 | 0.00012 | 0.00646 | 0.00004 | 134 | 2 | 133 | 1 |
| 12 | 2154 | 670 | 97.85 | 3.21 | 0.05290 | 0.00104 | 0.15389 | 0.00264 | 0.02110 | 0.00012 | 0.00660 | 0.00004 | 145 | 2 | 135 | 1 |
| 13 | 1195 | 658 | 81.41 | 1.82 | 0.04899 | 0.00087 | 0.14078 | 0.00212 | 0.02084 | 0.00011 | 0.00633 | 0.00004 | 134 | 2 | 133 | 1 |

*Spot 1, 2.1, 2.2, 4.2, 6 and 9.1 of sample MC00-1 are not involved in the concordia diagram Fig. II-5a. **Spot 2, 5 and 12 of sample MC21-3 are not involved in the concordia diagram Fig. II-5b.

Table II-2 Zircon Lu-Hf isotopes for the Meichuan pluton*

| Spot | $^{176}\text{Yb}/^{177}\text{Hf}$ | $^{176}\text{Lu}/^{177}\text{Hf}$ | $^{176}\text{Hf}/^{177}\text{Hf}$ | 2σ | Hf_i | $\epsilon_{\text{Hf}}(0)$ | $\epsilon_{\text{Hf}}(t)$ | 2σ | T_{DM1} (Ga) | T_{DM2} (Ga) | $f_{\text{Lu/Hf}}$ |
|---------------------------|-----------------------------------|-----------------------------------|-----------------------------------|-----------|---------------|---------------------------|---------------------------|-----------|--------------------------|--------------------------|--------------------|
| <i>MC00-1 felsic host</i> | | | | | | | | | | | |
| 1 | 0.016615 | 0.000658 | 0.282106 | 0.000014 | 0.282104 | -23.56 | -20.72 | 0.48 | 1.60 | 2.50 | -0.98 |
| 2 | 0.010036 | 0.000396 | 0.282101 | 0.000015 | 0.282100 | -23.74 | -20.88 | 0.52 | 1.60 | 2.51 | -0.99 |
| 3 | 0.020740 | 0.000785 | 0.282149 | 0.000017 | 0.282147 | -22.03 | -19.21 | 0.59 | 1.55 | 2.40 | -0.98 |
| 4 | 0.014055 | 0.000558 | 0.282112 | 0.000015 | 0.282111 | -23.33 | -20.49 | 0.53 | 1.59 | 2.48 | -0.98 |
| 5 | 0.013681 | 0.000524 | 0.282096 | 0.000014 | 0.282095 | -23.90 | -21.06 | 0.51 | 1.61 | 2.52 | -0.98 |
| 6 | 0.008412 | 0.000310 | 0.282227 | 0.000016 | 0.282227 | -19.26 | -16.39 | 0.58 | 1.42 | 2.23 | -0.99 |
| 7 | 0.013069 | 0.000511 | 0.282105 | 0.000018 | 0.282104 | -23.59 | -20.75 | 0.63 | 1.59 | 2.50 | -0.98 |
| 8 | 0.014507 | 0.000573 | 0.282084 | 0.000015 | 0.282082 | -24.34 | -21.50 | 0.53 | 1.63 | 2.55 | -0.98 |
| 9 | 0.014504 | 0.000575 | 0.282088 | 0.000015 | 0.282087 | -24.19 | -21.35 | 0.53 | 1.62 | 2.54 | -0.98 |
| 10 | 0.012480 | 0.000488 | 0.282090 | 0.000016 | 0.282089 | -24.10 | -21.25 | 0.57 | 1.61 | 2.53 | -0.99 |
| 11 | 0.041857 | 0.001398 | 0.282176 | 0.000019 | 0.282172 | -21.08 | -18.31 | 0.69 | 1.53 | 2.35 | -0.96 |
| 12 | 0.021581 | 0.000771 | 0.282110 | 0.000019 | 0.282108 | -23.40 | -20.57 | 0.65 | 1.60 | 2.49 | -0.98 |
| 13 | 0.008745 | 0.000339 | 0.282199 | 0.000016 | 0.282199 | -20.25 | -17.39 | 0.56 | 1.46 | 2.29 | -0.99 |
| 14 | 0.010315 | 0.000411 | 0.282114 | 0.000013 | 0.282113 | -23.27 | -20.41 | 0.48 | 1.58 | 2.48 | -0.99 |
| 15 | 0.009510 | 0.000390 | 0.282084 | 0.000014 | 0.282083 | -24.35 | -21.49 | 0.50 | 1.62 | 2.55 | -0.99 |
| 16 | 0.019081 | 0.000711 | 0.282087 | 0.000017 | 0.282085 | -24.24 | -21.41 | 0.61 | 1.63 | 2.54 | -0.98 |
| 17 | 0.014243 | 0.000548 | 0.282118 | 0.000014 | 0.282116 | -23.14 | -20.30 | 0.51 | 1.58 | 2.47 | -0.98 |
| 18 | 0.011391 | 0.000422 | 0.282140 | 0.000014 | 0.282139 | -22.34 | -19.49 | 0.51 | 1.54 | 2.42 | -0.99 |
| 19 | 0.011029 | 0.000413 | 0.282136 | 0.000014 | 0.282135 | -22.48 | -19.63 | 0.50 | 1.55 | 2.43 | -0.99 |
| 20 | 0.022721 | 0.000884 | 0.282132 | 0.000016 | 0.282130 | -22.64 | -19.82 | 0.55 | 1.57 | 2.44 | -0.97 |
| 21 | 0.027696 | 0.001036 | 0.282122 | 0.000017 | 0.282119 | -23.00 | -20.20 | 0.60 | 1.59 | 2.47 | -0.97 |
| 22 | 0.011318 | 0.000417 | 0.282108 | 0.000015 | 0.282107 | -23.49 | -20.63 | 0.54 | 1.59 | 2.49 | -0.99 |
| 23 | 0.034635 | 0.001215 | 0.282047 | 0.000015 | 0.282044 | -25.65 | -22.87 | 0.53 | 1.71 | 2.63 | -0.96 |
| 24 | 0.015211 | 0.000575 | 0.282144 | 0.000014 | 0.282142 | -22.22 | -19.38 | 0.48 | 1.54 | 2.41 | -0.98 |
| 25 | 0.011393 | 0.000440 | 0.282121 | 0.000014 | 0.282120 | -23.00 | -20.15 | 0.51 | 1.57 | 2.46 | -0.99 |
| 26 | 0.037470 | 0.001421 | 0.282109 | 0.000015 | 0.282106 | -23.44 | -20.67 | 0.54 | 1.63 | 2.50 | -0.96 |
| <i>MC21-3 mafic dike</i> | | | | | | | | | | | |
| 1 | 0.101438 | 0.003459 | 0.282057 | 0.000017 | 0.282048 | -25.30 | -22.71 | 0.62 | 1.80 | 2.62 | -0.90 |
| 2 | 0.104104 | 0.003534 | 0.282066 | 0.000022 | 0.282057 | -24.98 | -22.40 | 0.78 | 1.79 | 2.60 | -0.89 |
| 3 | 0.047442 | 0.001652 | 0.282089 | 0.000020 | 0.282085 | -24.15 | -21.41 | 0.70 | 1.67 | 2.54 | -0.95 |
| 4 | 0.092746 | 0.003351 | 0.282066 | 0.000022 | 0.282057 | -24.98 | -22.38 | 0.79 | 1.78 | 2.60 | -0.90 |
| 5 | 0.107103 | 0.003691 | 0.282069 | 0.000021 | 0.282059 | -24.88 | -22.31 | 0.75 | 1.79 | 2.60 | -0.89 |
| 6 | 0.094554 | 0.003274 | 0.282053 | 0.000021 | 0.282045 | -25.43 | -22.83 | 0.73 | 1.80 | 2.63 | -0.90 |
| 7 | 0.123621 | 0.004441 | 0.282022 | 0.000025 | 0.282011 | -26.54 | -24.04 | 0.88 | 1.90 | 2.70 | -0.87 |
| 8 | 0.073772 | 0.002617 | 0.282077 | 0.000020 | 0.282070 | -24.59 | -21.92 | 0.70 | 1.73 | 2.57 | -0.92 |
| 9 | 0.140211 | 0.004985 | 0.282034 | 0.000023 | 0.282022 | -26.09 | -23.64 | 0.82 | 1.91 | 2.68 | -0.85 |
| 10 | 0.104210 | 0.003350 | 0.282082 | 0.000020 | 0.282074 | -24.39 | -21.79 | 0.72 | 1.76 | 2.56 | -0.90 |
| 11 | 0.092604 | 0.003177 | 0.282039 | 0.000021 | 0.282031 | -25.93 | -23.31 | 0.73 | 1.81 | 2.66 | -0.90 |
| 12 | 0.092802 | 0.003253 | 0.282041 | 0.000022 | 0.282033 | -25.84 | -23.23 | 0.79 | 1.81 | 2.65 | -0.90 |
| 13 | 0.118157 | 0.004084 | 0.282065 | 0.000021 | 0.282055 | -25.01 | -22.47 | 0.73 | 1.82 | 2.61 | -0.88 |
| 14 | 0.097831 | 0.003502 | 0.282022 | 0.000023 | 0.282014 | -26.51 | -23.92 | 0.82 | 1.85 | 2.70 | -0.89 |
| 15 | 0.106656 | 0.003687 | 0.282015 | 0.000024 | 0.282006 | -26.76 | -24.19 | 0.84 | 1.87 | 2.71 | -0.89 |
| 16 | 0.097854 | 0.003391 | 0.282102 | 0.000023 | 0.282094 | -23.68 | -21.09 | 0.82 | 1.73 | 2.52 | -0.90 |
| 17 | 0.091370 | 0.003078 | 0.282037 | 0.000023 | 0.282029 | -26.00 | -23.37 | 0.82 | 1.81 | 2.66 | -0.91 |
| 18 | 0.081013 | 0.002726 | 0.282058 | 0.000023 | 0.282051 | -25.27 | -22.61 | 0.81 | 1.76 | 2.62 | -0.92 |
| 19 | 0.014472 | 0.000577 | 0.282240 | 0.000016 | 0.282238 | -18.82 | -15.98 | 0.55 | 1.41 | 2.20 | -0.98 |
| 20 | 0.071025 | 0.002410 | 0.282041 | 0.000018 | 0.282035 | -25.86 | -23.18 | 0.64 | 1.77 | 2.65 | -0.93 |
| 21 | 0.089644 | 0.002834 | 0.282046 | 0.000020 | 0.282039 | -25.69 | -23.04 | 0.71 | 1.78 | 2.64 | -0.91 |
| 22 | 0.122331 | 0.004193 | 0.282104 | 0.000021 | 0.282094 | -23.61 | -21.08 | 0.76 | 1.76 | 2.52 | -0.87 |
| 23 | 0.103028 | 0.003432 | 0.282040 | 0.000022 | 0.282031 | -25.90 | -23.31 | 0.79 | 1.82 | 2.66 | -0.90 |
| 24 | 0.106776 | 0.003582 | 0.282040 | 0.000023 | 0.282031 | -25.89 | -23.31 | 0.81 | 1.83 | 2.66 | -0.89 |
| 25 | 0.079642 | 0.002562 | 0.281996 | 0.000018 | 0.281989 | -27.46 | -24.79 | 0.62 | 1.84 | 2.75 | -0.92 |

* Initial isotopic ratios are calculated at 132 Ma

Table II-3 Elemental compositions of selected samples from the Meichuan pluton

| Sample Type ^e | MC00-1 | MC01-1 | MC01-2 | MC01-3 | MC02-1 | MC02-2 | MC11-1 | MC12-1 | MC12-2 | MC12-3 | MC13-1 | MC13-2 | MC13-3 | MC14-1 | MC15-1 | MC15-2 | MC17-1 | MC17-2 | MC17-4 | MC21-1 | MC21-2 | MC21-3 | MC21-4 | DB168 ^a | DB171 ^a | DB177 ^a | MC1 ^b | | |
|--------------------------------|--------|--------|--------|--------|--------|--------|--------|--------|--------|--------|--------|--------|--------|--------|--------|--------|--------|--------|--------|--------|--------|-------------------|--------|--------------------|--------------------|--------------------|------------------|--|--|
| <i>Major elements (%)</i> | | | | | | | | | | | | | | | | | | | | | | | | | | | | | |
| SiO ₂ | 64.97 | 69.63 | 57.8 | 61.02 | 65.2 | 55.52 | 64.63 | 60.24 | 59.26 | 64.76 | 58.97 | 67.07 | 58.73 | 50.30 | 64.92 | 75.45 | 59.15 | 60.6 | 63.06 | 64.46 | 64.04 | 63.49 | | | | | | | |
| TiO ₂ | 0.61 | 0.52 | 0.97 | 0.83 | 0.63 | 1.21 | 0.64 | 0.84 | 0.83 | 0.70 | 0.94 | 0.53 | 1.10 | 1.66 | 0.65 | 0.13 | 0.91 | 0.73 | 0.63 | 0.67 | 0.59 | 0.58 | | | | | | | |
| Al ₂ O ₃ | 14.3 | 13.56 | 12.36 | 14.96 | 13.93 | 15.42 | 14.27 | 14.67 | 14.78 | 14.15 | 15.50 | 15.19 | 13.39 | 12.77 | 13.9 | 13.01 | 15.25 | 14.58 | 14.64 | 14.81 | 14.82 | 14.47 | | | | | | | |
| Fe ₂ O ₃ | 1.51 | 1.38 | 2.71 | 1.97 | 1.62 | 3.67 | 1.73 | 2.28 | 3.98 | 1.65 | 2.13 | 0.90 | 2.67 | 4.14 | 1.18 | 0.57 | 2.38 | 1.69 | 1.49 | 1.45 | 1.54 | 1.66 | | | | | | | |
| FeO | 2.40 | 1.85 | 5.60 | 4.25 | 3.00 | 4.15 | 2.5 | 3.55 | 2.55 | 2.75 | 4.45 | 2.12 | 5.45 | 8.25 | 3.10 | 0.27 | 4.25 | 3.75 | 2.85 | 2.57 | 2.85 | 2.94 | | | | | | | |
| MnO | 0.07 | 0.05 | 0.14 | 0.10 | 0.07 | 0.12 | 0.06 | 0.09 | 0.10 | 0.08 | 0.09 | 0.07 | 0.15 | 0.24 | 0.08 | 0.01 | 0.13 | 0.10 | 0.05 | 0.05 | 0.08 | 0.07 | 0.08 | | | | | | |
| MgO | 3.17 | 2.16 | 5.83 | 4.34 | 3.50 | 5.14 | 3.38 | 4.97 | 5.15 | 3.50 | 4.93 | 1.77 | 4.47 | 7.15 | 3.35 | 0.38 | 4.36 | 4.49 | 4.00 | 2.99 | 3.20 | 3.63 | | | | | | | |
| CaO | 3.50 | 2.89 | 3.99 | 4.59 | 3.93 | 6.41 | 3.99 | 5.35 | 5.76 | 4.17 | 3.49 | 2.80 | 4.79 | 6.91 | 3.62 | 0.63 | 4.72 | 5.24 | 4.14 | 3.57 | 4.13 | 3.46 | | | | | | | |
| Na ₂ O | 3.96 | 3.22 | 1.34 | 3.01 | 3.10 | 3.76 | 3.62 | 3.39 | 3.12 | 3.06 | 3.16 | 3.78 | 3.26 | 2.01 | 3.52 | 2.81 | 4.21 | 3.46 | 4.24 | 4.21 | 3.83 | 4.17 | | | | | | | |
| K ₂ O | 3.82 | 3.60 | 6.88 | 3.14 | 3.50 | 2.65 | 3.52 | 2.84 | 2.53 | 3.60 | 4.12 | 3.81 | 3.39 | 2.04 | 3.66 | 5.53 | 2.22 | 3.45 | 3.30 | 3.70 | 3.46 | 3.63 | | | | | | | |
| P ₂ O ₅ | 0.28 | 0.22 | 0.76 | 0.43 | 0.31 | 0.72 | 0.32 | 0.43 | 0.39 | 0.31 | 0.57 | 0.28 | 0.70 | 0.88 | 0.35 | 0.04 | 0.50 | 0.41 | 0.29 | 0.29 | 0.24 | 0.30 | | | | | | | |
| LOI | 1.05 | 0.60 | 1.29 | 1.06 | 0.85 | 0.92 | 0.91 | 0.94 | 1.20 | 0.86 | 1.14 | 1.17 | 1.50 | 3.36 | 1.24 | 0.98 | 1.63 | 1.14 | 0.96 | 0.91 | 0.95 | 1.48 | | | | | | | |
| Total | 99.64 | 99.68 | 99.67 | 99.7 | 99.64 | 99.69 | 99.57 | 99.59 | 99.65 | 99.59 | 99.49 | 99.49 | 99.6 | 99.71 | 99.57 | 99.81 | 99.71 | 99.64 | 99.65 | 99.71 | 99.72 | 99.89 | | | | | | | |
| Mg [#] | 60.1 | 55.5 | 56.4 | 56.2 | 58.3 | 55.2 | 59.8 | 61.3 | 60.0 | 59.6 | 58.0 | 51.9 | 50.4 | 51.6 | 58.9 | 46.4 | 54.9 | 60.3 | 63.0 | 57.9 | 57.4 | 59.3 | | | | | | | |
| <i>Trace elements (ppm)</i> | | | | | | | | | | | | | | | | | | | | | | | | | | | | | |
| Sc | 8.71 | 7.5 | 18.3 | 13.7 | 10.5 | 17.5 | 10.3 | 13.3 | 19. | 11.6 | 17.6 | 7.3 | 17.7 | 28.6 | 10.8 | 0.87 | 14.6 | 14.9 | 12.2 | 2.1 | 2.7 | 8.2 | | | | | | | |
| V | 75.2 | 63.4 | 146 | 120 | 90.4 | 159 | 87.6 | 113 | 130 | 89.1 | 111 | 54.1 | 153 | 210 | 85.7 | 12.6 | 106 | 110 | 99 | 86 | 103 | n.d. ^c | | | | | | | |
| Cr | 144 | 111 | 374 | 238 | 194 | 229 | 171 | 246 | 303 | 167 | 229 | 56 | 134 | 211 | 167 | 5.5 | 155 | 237 | 225.9 | 154.1 | 167.8 | 137 | | | | | | | |
| Co | 15.5 | 10.1 | 27.8 | 21.1 | 16.0 | 26.1 | 15.7 | 21.5 | 24.0 | 16.3 | 21.7 | 9.3 | 25.1 | 37.3 | 15.4 | 1.1 | 19.7 | 18.5 | 24 | 16 | 22 | 18.6 | | | | | | | |
| Ni | 73.0 | 49.3 | 163 | 97.2 | 80.8 | 98.5 | 84.4 | 126 | 126 | 87.3 | 75.4 | 33.9 | 86.5 | 124 | 79.4 | 3.8 | 88.1 | 106 | 99 | 58 | 62 | n.d. | | | | | | | |
| Sr | 813 | 793 | 464 | 790 | 924 | 937 | 1175 | 1259 | 1119 | 1144 | 1405 | 1259 | 907 | 589 | 1058 | 179 | 777 | 967 | 1373 | 1030 | 786 | 904 | | | | | | | |
| Ba | 1737 | 1164 | 1409 | 760 | 1359 | 803 | 1889 | 1495 | 1103 | 1819 | 2584 | 2629 | 1541 | 924 | 2091 | 769 | 770 | 1322 | 1903 | 1471 | 1547 | 1701 | | | | | | | |
| Rb | 83.7 | 92.7 | 245 | 115 | 89.7 | 80.7 | 79.3 | 71.0 | 81.1 | 82.8 | 98.9 | 72.3 | 102 | 54.7 | 66.9 | 76.0 | 68.4 | 63.8 | 88 | 62 | 73 | 70.8 | | | | | | | |
| Ce | 1.45 | 2.2 | 11.9 | 5.8 | 2.3 | 2.3 | 2.6 | 1.5 | 4.4 | 4.3 | 5.6 | 0.50 | 2.2 | 0.48 | 1.1 | 0.09 | 1.7 | 1.7 | 2.7 | 0.31 | 1.07 | n.d. | | | | | | | |
| U | 3.07 | 4.82 | 2.07 | 2.79 | 2.13 | 0.95 | 3.23 | 0.83 | 1.44 | 4.49 | 0.68 | 0.92 | 1.65 | 2.75 | 1.53 | 1.26 | 2.07 | 3.23 | 0.76 | 2.08 | 0.57 | 1.97 | | | | | | | |

| | | | | | | | | | | | | | | | | | | | | | | |
|--------------------|-------|--------|--------|--------|--------|--------|--------|--------|--------|--------|--------|--------|--------|--------|--------|-------|--------|--------|--------|--------|--------|--------|
| Th | 15.4 | 34.4 | 11.8 | 9.5 | 13.6 | 4.6 | 21.5 | 5.8 | 4.9 | 19.2 | 2.8 | 8.9 | 16.8 | 22.5 | 13.1 | 10.9 | 7.5 | 12.7 | 7.08 | 0.97 | 1.98 | 9.0 |
| Ga | 39.6 | 20.2 | 25.6 | 24.7 | 19.6 | 22.8 | 19.9 | 20.4 | 24.9 | 21.7 | 19.8 | 20.2 | 26.6 | 33.6 | 20.9 | 15.8 | 26.5 | 22.0 | 20.8 | 18.7 | 20.8 | nd. |
| Pb | 29.3 | 32.5 | 43.7 | 28.8 | 26.6 | 25.3 | 36.1 | 27.6 | 30.5 | 35.0 | 34.1 | 36.8 | 22.9 | 16.2 | 22.5 | 21.9 | 14.1 | 17.2 | 31.8 | 24.7 | 28.3 | nd. |
| Nb | 11.3 | 11.9 | 10.0 | 13.2 | 9.2 | 12.0 | 10.4 | 7.6 | 9.6 | 12.0 | 6.7 | 12.1 | 24.5 | 38.1 | 11.2 | 3.1 | 16.3 | 12.6 | 8.6 | 8.3 | 9.2 | 10.5 |
| Ta | 0.90 | 1.19 | 0.23 | 0.93 | 0.65 | 0.50 | 1.01 | 0.44 | 0.54 | 1.12 | 0.35 | 0.98 | 1.85 | 2.54 | 0.84 | 0.25 | 1.38 | 0.78 | 0.41 | 0.4 | 0.42 | nd. |
| Y | 11.56 | 7.65 | 9.47 | 12.67 | 7.62 | 14.43 | 9.00 | 8.51 | 11.96 | 11.96 | 12.81 | 10.07 | 21.38 | 32.45 | 9.92 | 3.50 | 20.90 | 15.51 | 10.90 | 3.70 | 8.10 | 12.16 |
| Zr | 166 | 159 | 312 | 204 | 171 | 239 | 166 | 182 | 175 | 172 | 142 | 173 | 364 | 538 | 169 | 85.0 | 236 | 188 | 192 | 150 | 189 | 166 |
| Hf | 6.1 | 5.7 | 9.0 | 7.4 | 6.2 | 7.8 | 6.6 | 7.4 | 7.2 | 6.8 | 5.5 | 7.2 | 11.5 | 14.5 | 6.6 | 2.2 | 8.2 | 6.4 | 4.82 | 6.33 | 4.84 | nd. |
| La | 48.10 | 45.64 | 36.18 | 34.83 | 46.12 | 61.04 | 71.84 | 52.02 | 45.66 | 59.19 | 66.00 | 46.83 | 95.53 | 130.50 | 48.03 | 26.04 | 54.55 | 57.62 | 45.00 | 63.80 | 45.30 | 33.65 |
| Ce | 88.21 | 72.60 | 64.38 | 67.53 | 76.25 | 113.70 | 114.40 | 94.4 | 84.05 | 104.00 | 112.10 | 81.89 | 170.20 | 233.20 | 83.53 | 42.78 | 112.90 | 95.73 | 95.80 | 109.00 | 82.90 | 59.89 |
| Pr | 9.85 | 8.07 | 7.57 | 8.85 | 8.59 | 13.49 | 12.70 | 11.25 | 10.91 | 11.79 | 13.17 | 9.38 | 19.13 | 27.05 | 9.90 | 4.66 | 14.39 | 11.00 | 10.10 | 10.30 | 8.29 | 7.62 |
| Nd | 32.53 | 25.47 | 25.58 | 30.60 | 28.46 | 50.90 | 39.79 | 40.03 | 39.60 | 42.42 | 46.60 | 34.09 | 69.20 | 99.44 | 34.48 | 15.13 | 53.24 | 41.40 | 38.70 | 35.00 | 30.20 | 25.95 |
| Sm | 5.39 | 4.14 | 4.46 | 5.29 | 4.59 | 8.50 | 5.87 | 6.15 | 6.17 | 6.57 | 7.06 | 5.27 | 10.69 | 15.65 | 5.25 | 2.13 | 8.53 | 6.84 | 6.45 | 5.19 | 4.97 | 4.64 |
| Eu | 1.47 | 1.10 | 0.84 | 1.22 | 1.21 | 1.94 | 1.59 | 1.62 | 1.72 | 1.81 | 2.08 | 1.48 | 2.62 | 3.70 | 1.44 | 0.61 | 2.01 | 1.60 | 1.84 | 1.57 | 1.55 | 1.26 |
| Gd | 3.77 | 2.74 | 3.39 | 3.60 | 3.10 | 6.03 | 3.80 | 3.92 | 4.45 | 4.37 | 4.90 | 3.59 | 7.45 | 10.97 | 3.57 | 1.34 | 6.16 | 4.88 | 4.34 | 3.60 | 3.66 | 3.32 |
| Tb | 0.51 | 0.36 | 0.45 | 0.52 | 0.41 | 0.84 | 0.52 | 0.52 | 0.62 | 0.61 | 0.67 | 0.52 | 1.03 | 1.55 | 0.48 | 0.17 | 0.89 | 0.73 | 0.59 | 0.49 | 0.52 | 0.54 |
| Dy | 2.52 | 1.82 | 2.25 | 2.50 | 2.03 | 4.13 | 2.60 | 2.54 | 3.12 | 3.15 | 3.17 | 2.59 | 5.16 | 7.99 | 2.46 | 0.83 | 4.63 | 3.77 | 3.25 | 2.71 | 3.02 | 2.33 |
| Ho | 0.48 | 0.34 | 0.40 | 0.43 | 0.35 | 0.66 | 0.43 | 0.44 | 0.54 | 0.56 | 0.53 | 0.46 | 0.93 | 1.37 | 0.45 | 0.15 | 0.83 | 0.66 | 0.61 | 0.51 | 0.60 | 0.48 |
| Er | 1.26 | 0.81 | 0.99 | 1.02 | 0.83 | 1.51 | 0.95 | 0.96 | 1.28 | 1.31 | 1.16 | 1.06 | 2.33 | 3.52 | 1.08 | 0.4 | 2.27 | 1.72 | 1.51 | 1.24 | 1.55 | 1.27 |
| Tm | 0.18 | 0.11 | 0.14 | 0.14 | 0.11 | 0.20 | 0.13 | 0.12 | 0.19 | 0.18 | 0.15 | 0.15 | 0.35 | 0.51 | 0.15 | 0.06 | 0.35 | 0.25 | 0.18 | 0.15 | 0.20 | 0.21 |
| Yb | 1.12 | 0.70 | 0.91 | 0.82 | 0.64 | 1.17 | 0.75 | 0.63 | 1.08 | 1.10 | 0.86 | 0.94 | 2.05 | 3.11 | 0.86 | 0.33 | 2.10 | 1.54 | 1.07 | 0.87 | 1.21 | 1.21 |
| Lu | 0.17 | 0.11 | 0.15 | 0.12 | 0.10 | 0.17 | 0.11 | 0.09 | 0.15 | 0.16 | 0.13 | 0.13 | 0.31 | 0.45 | 0.13 | 0.06 | 0.33 | 0.24 | 0.15 | 0.12 | 0.17 | 0.18 |
| Total | 207.1 | 171.66 | 157.16 | 170.14 | 180.41 | 278.71 | 264.48 | 223.20 | 211.50 | 248.98 | 271.39 | 198.45 | 408.36 | 571.46 | 201.73 | 98.19 | 284.08 | 243.49 | 209.59 | 234.55 | 184.14 | 142.55 |
| Eu/Eu [#] | 1.00 | 1.00 | 0.66 | 0.85 | 0.98 | 0.83 | 1.03 | 1.01 | 1.00 | 1.05 | 1.08 | 1.04 | 0.89 | 0.86 | 1.01 | 1.10 | 0.85 | 0.84 | 1.06 | 1.11 | 1.11 | 0.98 |
| Sr/Y | 70.3 | 103.7 | 121.3 | 130.6 | 95.7 | 125.0 | 42.4 | 106.7 | 49.0 | 62.4 | 64.9 | 147.9 | 109.7 | 18.2 | 51.1 | 37.2 | 62.3 | 93.6 | 126.0 | 278.4 | 97.0 | 74.3 |
| (La/Th) | 29.2 | 44.3 | 49.0 | 65.1 | 36.6 | 33.8 | 31.7 | 37.9 | 27.0 | 28.9 | 35.4 | 56.1 | 52.1 | 28.5 | 53.6 | 17.6 | 25.4 | 28.7 | 28.6 | 49.8 | 25.4 | 18.9 |

^a Samples are after Zhang et al. (2002a); ^b Sample is after Ma et al. (1998); ^c Type: H=felsic host rock, E=mafic enclave, G=granitic dike, D=mafic dike, M=mixture; ^d Mg[#] = 100×Mg/(Mg + Fe²⁺ + Fe³⁺); ^e n.d. = not detected; ^f Eu/Eu[#]=Eu_N/(Sm_N×Gd_N)^{1/2}, N is the chondrite normalization value, and the chondrite values used for normalization are from McDonough and Sun (1995).

Table II-4 Sm-Nd and Rb-Sr isotopic compositions of selected samples from the Meichuan pluton

| Sample | Rock type | Rb (ppm) | Sr (ppm) | $^{87}\text{Rb}/^{86}\text{Sr}$ | $^{87}\text{Sr}/^{86}\text{Sr}$ | $\pm 2\sigma$ | Sm (ppm) | Nd (ppm) | $^{147}\text{Sm}/^{144}\text{Nd}$ | $^{143}\text{Nd}/^{144}\text{Nd}$ | $\pm 2\sigma$ | $(^{87}\text{Sr}/^{86}\text{Sr})_i^*$ | $(^{143}\text{Nd}/^{144}\text{Nd})_i^*$ | $\epsilon_{\text{Nd}}(t)$ | $T_{\text{DM}}(\text{Ga})$ |
|--------|-----------|----------|----------|---------------------------------|---------------------------------|---------------|----------|----------|-----------------------------------|-----------------------------------|---------------|---------------------------------------|---|---------------------------|----------------------------|
| MC00-1 | H | 82.72 | 812.85 | 0.2926 | 0.706449 | 14 | 4.82 | 29.90 | 0.0975 | 0.511763 | 12 | 0.70590 | 0.51168 | -15.4 | 1.8 |
| MC01-1 | H | 89.22 | 708.43 | 0.3624 | 0.706529 | 13 | 4.00 | 25.74 | 0.0940 | 0.511771 | 12 | 0.70585 | 0.51169 | -15.2 | 1.8 |
| MC01-2 | E | 241.59 | 447.17 | 1.5561 | 0.708536 | 13 | 4.21 | 25.56 | 0.0996 | 0.511788 | 11 | 0.70562 | 0.51170 | -15.0 | 1.8 |
| MC01-3 | E | 110.83 | 673.27 | 0.4717 | 0.706646 | 12 | 5.02 | 29.12 | 0.1041 | 0.511779 | 12 | 0.70576 | 0.51169 | -15.2 | 1.9 |
| MC12-3 | B | 82.95 | 931.11 | 0.2554 | 0.705979 | 10 | 5.97 | 35.70 | 0.1012 | 0.511686 | 15 | 0.70550 | 0.51160 | -17.0 | 2.0 |
| MC21-1 | H | 65.37 | 903.69 | 0.2080 | 0.706201 | 13 | 5.09 | 31.60 | 0.0974 | 0.511730 | 12 | 0.70581 | 0.51165 | -16.1 | 1.9 |
| MC21-2 | G | 81.46 | 158.19 | 1.4791 | 0.708655 | 12 | 1.96 | 14.04 | 0.0846 | 0.511855 | 13 | 0.70588 | 0.51178 | -13.4 | 1.5 |
| MC21-3 | D | 65.47 | 705.11 | 0.2668 | 0.706361 | 13 | 8.34 | 50.02 | 0.1009 | 0.511692 | 11 | 0.70586 | 0.51160 | -16.8 | 2.0 |
| MC21-4 | M | 61.77 | 789.25 | 0.2241 | 0.706386 | 13 | 6.55 | 38.82 | 0.1020 | 0.511766 | 10 | 0.70597 | 0.51168 | -15.4 | 1.9 |
| Mc1** | H | 70.8 | 904 | 0.2663 | 0.70622 | 4 | 4.64 | 25.95 | 0.0966 | 0.511778 | 6 | 0.70572 | 0.51170 | -15.1 | 1.8 |

* Initial isotopic ratios are calculated at 132 Ma; ** sample Mc1 is from Ma et al. (1998)

**Part III Tracing the evolution and distribution
of F and Cl in plutonic systems from volatile-
bearing minerals: A case study from the Liujiawa
pluton (Dabie orogen, China)**

1 Abstract

F and Cl concentrations in amphibole, biotite and apatite from the Liujiawa pluton, eastern Dabie orogen (China), have been determined by electron microprobe to test their potential to trace the evolution of halogen concentrations in melts of plutonic systems. Four lithologies, including gabbro (GN), two-pyroxene diorite (PD), clinopyroxene diorite (CD) and hornblende gabbro (HG), which compose most of the plutonic complex, have been studied. The GN and PD rocks represent mafic magmas without contamination by crustal material, while the CD rocks show clear evidence of mixing between low-F mafic and high-F felsic magmas. The HG rocks contain abundant high-Al amphiboles and may have formed at ~860 °C from water-rich mafic magma. For most amphiboles from GN, PD and CD, $\log(\text{Cl}/\text{OH})$ shows a systematic negative correlation with Mg-number, confirming the effect of Mg-Cl avoidance. Biotites from GN and PD show a rough positive correlation between $\log(\text{Cl}/\text{OH})$ and Mg concentration, whereas the biotites from CD show a reverse trend. Negative correlations between Cl and F contents are observable for all analyzed apatites. Quantitative modeling and comparison indicate that over the course of decompression (magma ascent or crustal uplift and erosion); the apatites have not been re-equilibrated in terms of volatile contents. The absolute concentrations of Cl and F in melts coexisting with amphiboles, biotites and apatites have been estimated based on available models and newly developed calculation procedures. The modeling results indicate that Cl concentration in melt remained nearly constant over the course of crystallization, and decreased dramatically at low temperatures, as a result of fluid exsolution. In contrast, F concentration in melt remained above 1000 ppm and has not been strongly affected by fluid exsolution, because of its preferred incorporation into melt rather than fluid. Our results also indicate that halogen concentrations in early high-temperature amphibole can be preserved and that these minerals have the potential to indicate halogen abundance in melt of an early magmatic stage. Based on the distribution characteristics of F in magmatic systems, the partitioning relation of F between amphibole and melt has been tentatively built by data regression, which is qualitatively consistent with the Fe-F avoidance rule but needs further quantitative experimental calibration.

2 Introduction

Fluorine and chlorine are ubiquitous volatile components in mantle- and crust-derived magmas and continental crystalline rocks with various abundances (Aoki and Kanisawa 1979; Bucher and Stober 2010). F and Cl play important roles

in magmatic differentiation, hydrothermal alteration and related mineralization (e.g., Holland 1972; Yardley 2005), since they can readily affect partitioning behaviors of numerous metal elements between silicate melt and aqueous fluid (Baker and Watson 1988; Webster and Holloway 1988; Webster et al. 1989; Keppler and Wyllie 1991; Keppler 1993; Hu et al. 2009; Botcharnikov et al. 2010), and modify various physicochemical properties of silicate melt (e.g., Dingwell et al. 1985; Holtz et al. 1993; Dingwell and Hess 1998; Antignano and Manning 2008; Filiberto and Treiman 2009a; Bartels et al. 2011). As a result, deciphering the role and variation of F and Cl throughout magmatic-hydrothermal process is crucial for better understanding many petrogenetic and metallogenic key mechanisms. Nevertheless, the contents of halogens determined in bulk igneous rocks are identical to their concentrations in primitive melts at various magmatic stages, owing to pervasive chemical dispersal during late-magmatic processes from igneous bodies to the Earth's surface via gases, hot springs and aerosols for volcanic systems (e.g., Symonds et al. 1988; Symonds et al. 1994; Webster 1997a; Aiuppa et al. 2009; Balcone-Boissard et al. 2010), or to wall rocks via magmatic-hydrothermal volatile-enriched phases for plutonic systems (e.g., Kilinc and Burnham 1972; London 1997; Webster 1997b).

For volcanic systems, glasses and mineral-hosted melt inclusions can work well as monitors of origin and variation of volatiles (mainly H₂O, CO₂, F, Cl, S) in magmatic systems (Harris and Anderson 1984; Lassiter et al. 2002; Straub and Layne 2003; Stroncik and Haase 2004; Webster 2004; Wallace 2005; Sun et al. 2007; Johnson et al. 2009; Balcone-Boissard et al. 2010). For plutonic systems, although melt inclusions have also been identified and successfully analyzed in some cases (Webster 2006), they are generally scarcer and smaller compared to volcanic systems. As a result, volatile-bearing minerals are the only applicable monitors to trace magmatic volatiles in plutonic systems where melt inclusion can hardly be observed and/or analyzed, as it is the case in this study.

Amphibole, biotite and apatite are the main mineral reservoirs of F and Cl in magmatic rocks, which are all common in mafic to felsic systems. The incorporation of F and Cl from liquids into amphibole, biotite and apatite has been thermodynamically and experimentally investigated (Munoz 1984; Edgar and Arima 1985; Volfinger et al. 1985; Zhu and Sverjensky 1991, 1992; Brenan 1993; Oberti et al. 1993; Brenan 1994; Piccoli and Candela 1994; Icenhower and London 1997; Dong 2005; Mathez and Webster 2005; Sato et al. 2005; Chevychelov et al. 2008; Webster et al. 2009b; Hovis and Harlov 2010; Konzett et al. 2011), which enables hydrous minerals to be monitors reflecting environmental volatile properties based

on the assumption of mineral-melt (or mineral-fluid) equilibria. However, as demonstrated by these experimental studies, which are numerous but insufficient, the partitioning behaviors of F and Cl between hydrous minerals, silicate melts and aqueous fluids (low-density vapor and/or high-density brine) remain partly controversial because they are difficult to predict for a variety of magmatic systems and over the large field of magmatic conditions.

Many case studies using hydrous minerals to decipher halogen evolutions during magmatic or fluid-rock processes have been addressed for the Earth system (e.g., Finch et al. 1995; Markl and Piazzolo 1998; Piccoli et al. 1999; O'Reilly and Griffin 2000; Selby and Nesbitt 2000; Coulson et al. 2001; Harlov and Förster 2002; Rubenach 2005; Boyce and Hervig 2009; Humphreys et al. 2009; Patiño Douce et al. 2011), as well as for other terrestrial planets (e.g., the Moon and the Mars, Patiño Douce and Roden 2006; Filiberto and Treiman 2009b; Boyce et al. 2010; McCubbin et al. 2010a; McCubbin et al. 2010b; Ustunisik et al. 2011), which extended our understanding of the fate of volatile components corresponding to various processes of planetary evolution. Although hydrothermal alteration in late magmatic stages might largely change halogen concentration of apatite in a geologically short time (Brenan 1994), practical observations have demonstrated that magmatic apatites, amphiboles and biotites can sustain their original halogen abundances (Piccoli and Candela 1994; Sato et al. 1997; Selby and Nesbitt 2000). Therefore, for mafic or felsic intrusive systems, F and Cl concentrations of amphiboles, biotites and apatites, which may crystallize at different magmatic stages, are essentially capable of tracing volatile properties of the mantle- or crust-originated magmas for various magmatic stages correspondingly. Some early studies have offered qualitative conceptual models in which hydrous minerals were used as volatile probes to reflect volatile concentrations in the magmas roughly (Nash 1976; Fuge 1977). Recently, quantitative modeling on natural magmatic systems applying newly developed halogen partitioning (thermodynamic or empirical) models become more feasible (e.g., Coulson et al. 2001; Yang and Lentz 2005; Humphreys et al. 2009). However, our current knowledge of the partition and distribution of volatiles in magmatic systems is still insufficient for accurate quantitative modeling over wide ranges of temperature and pressure.

In this paper, we report mineral compositions of pyroxene, plagioclase, amphibole, biotite and apatite from distinct lithological units of the Liujiawa pluton (Dabie orogen, China), and focus on F and Cl abundances of the hydrous minerals. Conditions of formation of hydrous minerals are estimated based on mineral

assemblages and compositions by applying available thermometers and barometers. We then apply available halogen partitioning models involving amphibole, biotite and apatite to estimate the F and Cl concentrations in the coexisting melts. Provided that conditions (e.g. P, T) prevailing at magmatic stages have been properly estimated, the volatile evolution over the course of magma evolution is traced quantitatively. In addition, calculation procedures of melt halogen concentrations from mineral compositions have been combined and developed, and applicability and deficiency of different partitioning models are discussed based on this case study.

3 Geological background

The Liujiawa pluton is located at the eastern boundary of the Dabie orogen, which is part of the Qinling-Tongbai-Dabie-Sulu orogenic belt lying west-eastward in central China and regarded as the world's largest ultra high-pressure (UHP) metamorphic terrane. Geochronological and tectonic studies have indicated a Triassic northward subduction/collision of the Yangtze Block beneath the North China Block (Zhang et al. 2009 and reference therein). Five fault-bounded petrotectonic units which constitute the Dabie orogen are outlined according to their metamorphic grades (Fig. III-1): (1) the North Huaiyang low-grade unit (NHU), (2) the North Dabie metamorphic core complex unit (NDU), (3) the central Dabie medium-T/UHP metamorphic unit (CDU), (4) the southern Dabie lower-T/UHP metamorphic unit (SDU) and (5) the Su-Song low-T/high-P metamorphic unit (SSU), and they have been widely intruded by massive Early Cretaceous granitoids (Zhang and Ma 2008; Zhang et al. 2010). Mafic-ultramafic intrusions are scattered as small stocks in the northeast of NDU, which infer a magmatic source of enriched sublithospheric mantle (Jahn et al. 1999; Wang et al. 2005). The Liujiawa pluton is located tectonically inside the SDU, adjacent to the Tan-Lu fault (Fig. III-1). To the east of the Tan-Lu fault lies the Yangtze Rive fault zone, along which spreads the Yangtze River metallogenic belt consisting of seven mining districts (Pan and Dong 1999).

Geochronological and geochemical investigations on the mafic-ultramafic intrusive rocks from the northern Dabie orogen (e.g., Li et al. 1989; Jahn et al. 1999; Li et al. 2002; Wang et al. 2005; Huang et al. 2007) have suggested partial melting of a sublithospheric mantle with a highly crustal-enriched affinity. However, detailed petrographic and mineralogical studies on them are extremely inadequate (Tsai et al. 2000), which handicapped more essential knowledge about their petrogenesis and geological significance. Synchronously to the intrusion of the mantle-originated

magmas in the northern Dabie orogen, the Liujiawa plutonic complex formed also at the Early Cretaceous (Ma et al. 2004) and is composed of different lithological units likely including both mantle- and crust-derived magmas (Zhang et al. 2011).

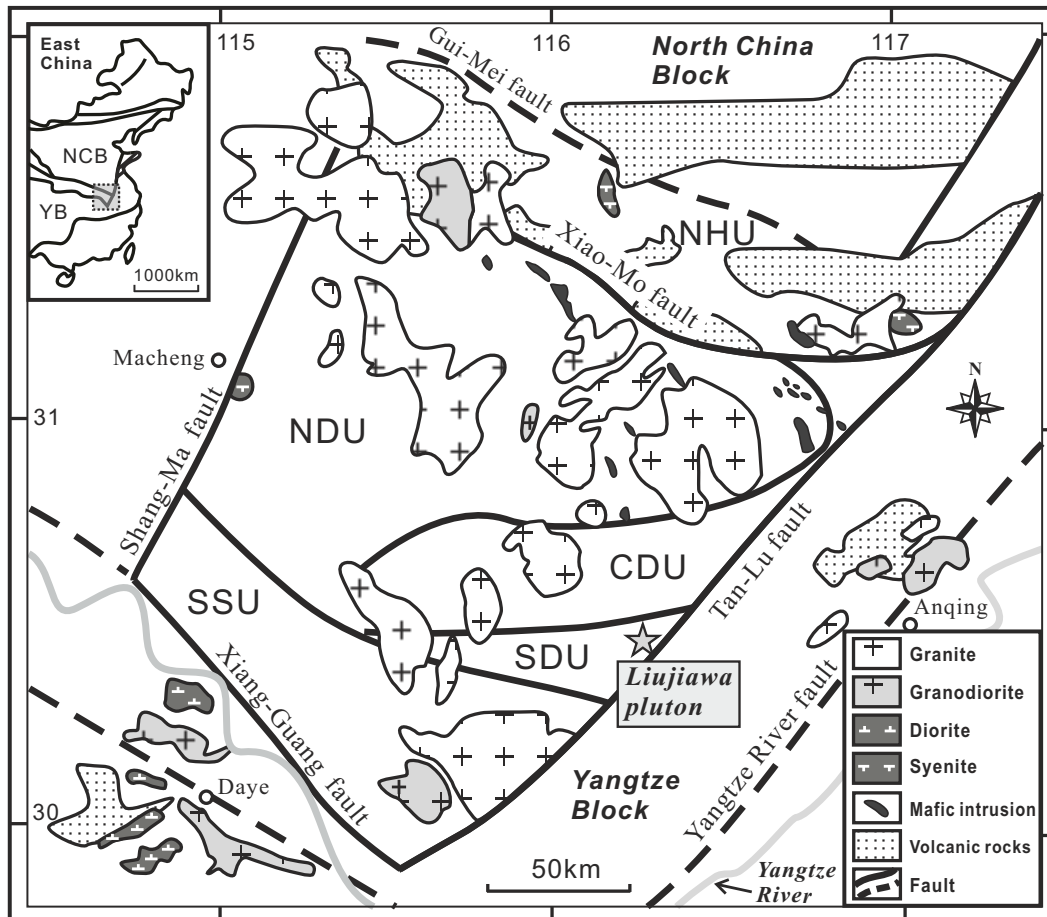


Fig. III-1 Geological overview map of the Dabie orogen, showing position of the Liujiawa pluton (signed as star)

4 Sample descriptions

Several lithological units composing the Liujiawa pluton are identified according to different mineral assemblage, i.e. gabbro (GN), two-pyroxene diorite (PD), clinopyroxene diorite (CD), non-pyroxene diorite (ND), diorite porphyry (DP), hornblende gabbro (HG) and granite (GR). The dioritic components (ND and DP) (Huang et al. 2008) often contain mafic enclaves (similar to PD and CD in composition) (Zhang et al. 2011), implying that magma mixing should be important accounting for the geochemical characteristics of the plutonic complex (Zhang et al. in preparation). In this study, four rock types, i.e. GN, PD, CD and HG, are investigated for their mineral composition and petrogenesis, and their mineral

proportions estimated by point-counting are listed in Supplementary Table 1.

4.1 Gabbronorite (GN)

The GN rocks are characterized by near-euhedral orthopyroxene and clinopyroxene grains. The orthopyroxene has often narrow rims composed of amphibole and usually forms aggregate-like cumulate (Fig. III-2a). Clinopyroxene occurs as individual grains which are directly in contact with anhedral amphibole and biotite (Fig. III-2b~c). Some large biotite grains contain tiny relics of rounded orthopyroxene and surface-curved amphibole coexisting with interstitial quartz (Fig. III-2d~e), indicating that the biotite may have formed by a hydration reaction of orthopyroxene (also indicated by Fig. III-2c, in which previous orthopyroxene could have been completely replaced by biotite) and transformation of earlier amphibole. In Fig. III-2f, amphibole and biotite are found successively forming the rim of clinopyroxene, which demonstrates that biotite formed later than amphibole even though the amphibole (~1 wt%) is much less abundant than biotite (16 wt%).

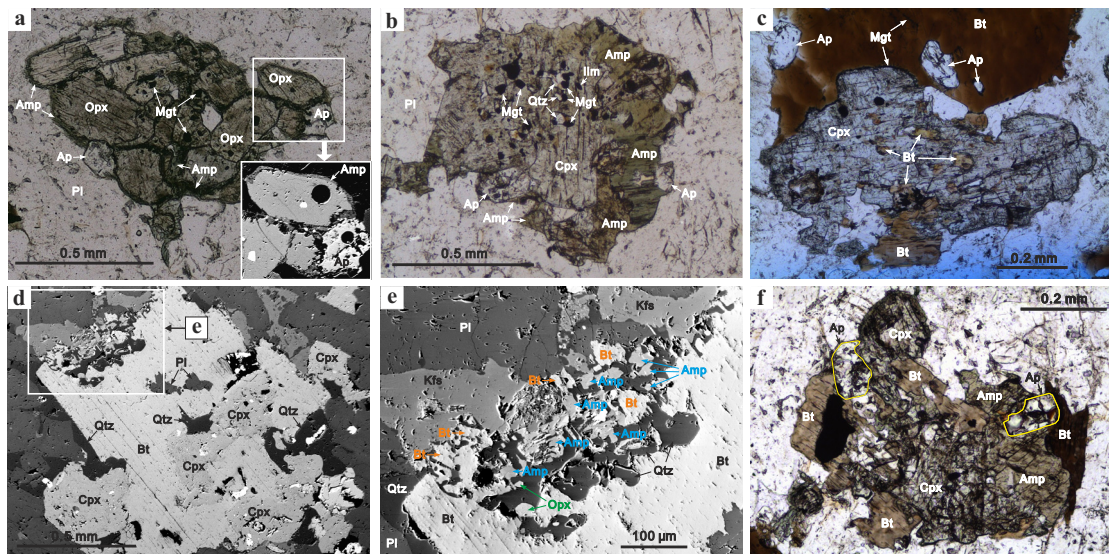


Fig.III-2 Mineral textures of the gabbronorite (GN). (a) aggregation of euhedral or subhedral grains of apatite and orthopyroxene which suffered amphibolization indicated by widespread rims of amphibole; (b) amphibole occurs as mantle attached to clinopyroxene; primary apatite grains coexist with clinopyroxene; inclusions of quartz and magnetite indicate decomposition of clinopyroxene; (c) biotite as inclusion and individual grain coexists with clinopyroxene; boundary-rounded apatite grains are enclosed in or adjacent to biotite; (d) biotite intersecting with clinopyroxene, together with enclosed or surrounding quartz; e amplified reaction zone in d, showing rounded relics of orthopyroxene and amphibole embraced by

myrmekitic quartz; f clinopyroxene partly mantled amphibole and outer biotite; primary apatite grains contact directly to biotite or amphibole; mineral abbreviations: Amp, amphibole; Ap, apatite; Bt, biotite; Chl, chlorite; Cpx, clinopyroxene; Ep, epidote; Ilm, ilmenite; Kfs, K-feldspar; Mgt, magnetite; Opx, orthopyroxene; Pl, plagioclase; Qtz, quartz; Ttn, titanite

Prismatic grains of apatite with a small length/width ratio (<3/1) occur adjacent to orthopyroxene (Fig. III-2a) or clinopyroxene (Fig. III-2b, central left), indicating their simultaneous crystallization with pyroxene. In contrast, apatites which are directly in contact with biotite or amphibole show clear rounded boundaries (Fig. III-2b~c, f), and it is believed that they may have been equilibrated with the later biotite or amphibole. Fe-Ti-oxides are frequently present as inclusions in both orthopyroxene and clinopyroxene. No obvious zoning of plagioclase is observed. Quartz and K-feldspar occur interstitially between all the other minerals, indicating that they are both last magmatic stage phases.

4.2 Two-pyroxene diorite (PD)

Compared to the GN, the PD rocks have similar amounts of plagioclase, amphibole and biotite, but less orthopyroxene and clinopyroxene, more K-feldspar and quartz. Both orthopyroxene and clinopyroxene are anhedral grains with irregular boundaries. Plagioclase phenocrysts with a normal zoning (from core to rim: An₆₀ to An₃₀, Fig. III-3a) are common among the majority of tabular subhedral ones. Biotite (~18 wt%) is present as small individual grains isolated by plagioclases, or relatively large grains surrounding relics of clinopyroxene (Fig. III-3b). The minor amphibole (~2 wt%) is present as narrow rims surrounding orthopyroxene (similar to that in Fig. III-2a). In the PD, no apatite phenocryst is present, but only a few acicular and prismatic microcrystals within the plagioclase matrix could be found (Fig. III-3c).

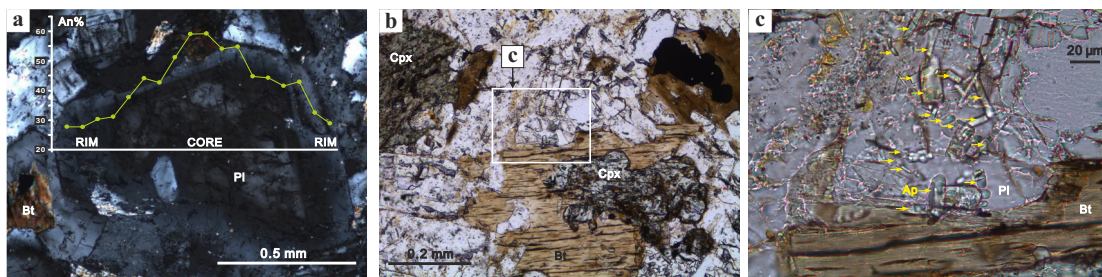


Fig. III-3 Mineral textures of the two-pyroxene diorite (PD). (a) plagioclase phenocryst with normal zoning (core = An₆₀, rim = An₃₀); (b) biotite partly surrounds clinopyroxene; (c) apatite microcrystals (indicated by arrows) occur

within the matrix of low-Ca plagioclase. See mineral abbreviations in the caption of Fig. III-2

4.3 Clinopyroxene diorite (CD)

The CD rocks have no orthopyroxene but minor anhedral relics of clinopyroxene enclosed in amphiboles which usually accompany rounded minerals of quartz, apatite and Fe-Ti oxide (Fig. III-4a). Similar to the PD, the CD rocks also have zoning-featured plagioclase phenocrysts (from core to rim: An₅₅ to An₂₅, Fig. III-4b). Apart from those enclosed in amphiboles, some other apatites (prismatic, length/width ratio >3/1) are partly enclosed in or directly in contact with biotite (Fig. III-4c). Very few acicular apatite microcrysts are found within plagioclase matrix (similar to that in Fig. III-3c), but they are too small to be analyzed.

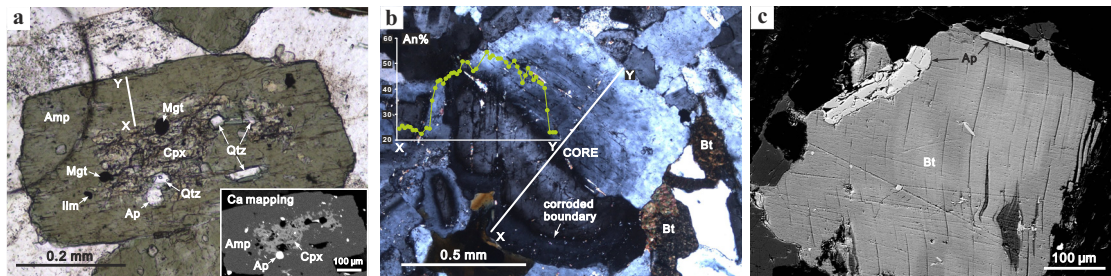


Fig. III-4 Mineral textures of the clinopyroxene diorite (CD). (a) euhedral amphibole grain with clinopyroxene relics and rounded apatite, quartz and magnetite (the inset shows Ca X-ray mapping); the profile along the white-line section (X-Y) (shown in Supplementary Fig. III-5) indicates no systematic compositional variation; (b) plagioclase with segmental normal zoning (core = An₅₂, mantle = An₄₂, rim = An₂₅); (c) apatite grains contacts directly to biotite. See mineral abbreviations in the caption of Fig. III-2

4.4 Hornblende gabbro (HG)

The HG rocks are characterized by aggregated amphibole grains, as well as by the absence of orthopyroxene, clinopyroxene and biotite. Tabular subhedral plagioclases and amphiboles form the typical gabbroic texture (Fig. III-5a), with minor interstitial quartz in between. Chlorite and titanite are present as late phases along the cleavage of some amphiboles (Fig. III-5a). Among the amphibole phenocrysts, three types (HG-I, HG-II and HG-III) can be identified primarily on the compositional basis (explained in detail later, also see Fig. III-6). The HG-I grains are dark yellow green in color and have no late alteration. The HG-II grains grow

adjacently with the HG-I grains, with weak alteration along the cleavage (indicated by later chlorite and titanite). Comparatively, the HG-III grains seem to have lighter color and stronger alteration along the cleavage (Fig. III-5a). Between tabular high-An plagioclase (An_{80}) and amphiboles, interstitial plagioclase with zoning compositions (from inner to outer: An_{60} to An_{30}) and a fourth type of amphibole (HG-IV) occurring as narrow rim (darker than the primary body in a BSE image) are present (Fig. III-5b). Granular apatites are usually found enclosed in or in contact with amphiboles or magnetite (Fig. III-5c).

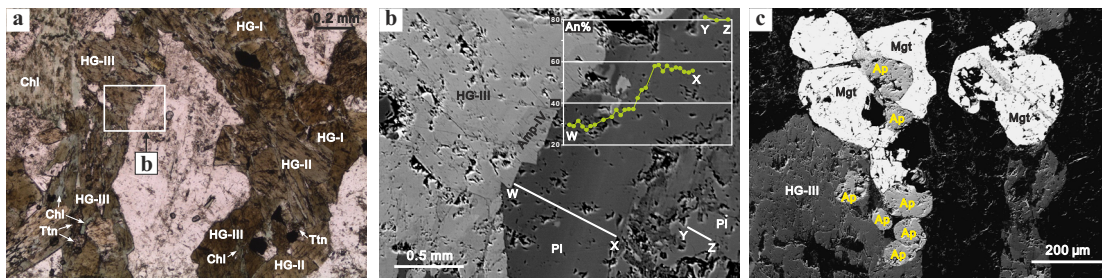


Fig. III-5 Mineral textures of the hornblende gabbro (HG). (a) accumulative subhedral amphibole and interstitial plagioclase, as well as lateral chlorite and titanite; (b) lateral rim of amphibole phenocryst contacts interstitial plagioclase which has compositional zoning (core = An_{80} , mantle = An_{60} ; rim = An_{30}); (c) amphibole and magnetite enclose or contacts directly rounded apatites. The four groups of amphibole (HG-I, HG-II, HG-III and HG-IV) are explained in detail in the text (also see Fig. III-6). See mineral abbreviations in the caption of Fig. III-2

5 Analytical methods

All mineral analyses were performed using a Cameca SX100 electron microprobe at the Institute of Mineralogy, Leibniz University of Hannover, Germany. The standard materials include wollastonite (Si and Ca), albite (Na), orthoclase (K), apatite (P), halite (Cl), strontium fluoride (F) and synthetic Al_2O_3 , TiO_2 , Fe_2O_3 , MgO , Mn_3O_4 and Cr_2O_3 . A 15 kV acceleration voltage was used for all the analyses. Raw data were corrected using the standard PAP procedures (Pouchou and Pichoir 1991).

For amphibole and biotite, a 2 μm -diameter defocused beam was used, and the operating conditions were 40 nA for Cl but 15 nA for all the other elements. TAP was used as the diffracting crystal for Na, Mg, Si and Al, PET for Ca, P and Cr, LIF for Fe and Mn, LPET for K, Ti and Cl, and PC1 for F. Counting times were 10 s for Na, K, Fe, Mg, Si, Al and Ca, 30 s for Mn, Cr and F, and 60 s for Cl. The detection

limits for F and Cl are ca. 750 ppm and ca. 60 ppm utilizing above analytical settings, respectively. Relative uncertainties (1σ) are estimated to be 10-15% for F at the 0.2-1.0 wt% level, and ~10% for Cl at the 0.01-0.10 wt% level, respectively, for both amphibole and biotite analytical results. Using the same setting (5 μm -diameter defocused beam), we measured the Juan de Fuca Ridge basaltic glass USNM 111240/52 VG-2 (recommended value of 0.030 wt% Cl, Sun et al. 2007), and a concentration of 0.030 ± 0.003 (1σ) wt% Cl and 0.149 ± 0.010 (1σ) wt% F was obtained. Additionally, we also measured the halogen concentrations of Kakanui (New Zealand) hornblende (USNM 143965) and the results were 0.018 ± 0.001 (1σ) wt% Cl and 0.346 ± 0.005 (1σ) wt% F.

For apatite, quantitative analysis of halogen concentrations by electron microprobe can be problematic due to the X-ray sensitivities for F and Cl (especially F) and crystallographic orientation effects (Stormer et al. 1993; Pyle et al. 2002; Henderson 2011). As demonstrated by Stormer et al. (1993) and Henderson (2011), a protocol with a defocused beam or rastered beam of ≥ 5 μm and a crystallographic orientation of c-axis perpendicular to the electron beam is recommended to determine accurately F concentrations in apatite. In this study, using morphological criteria from thin section observations, we excluded the apatite crystals with c-axis parallel or nearly parallel to the electron beam. During analyzing selected apatite crystals with large angle between c-axis and the beam, 5 and 10 μm -diameter defocused beams were used, with a current of 10 nA for F, Cl and S, but 15 nA for all the other elements. TAP was used as the diffracting crystal for Na, Mg, Si and Al, PET for Ca, LIF for Fe and Mn, LPET for P, K, Cl and S, and PC1 for F. Counting times were 40 s for F, and 60 s for Cl and S. F and Cl were analyzed firstly. The detection limits are ca. 1200 ppm for F, 160 ppm for Cl and 150 ppm for S, respectively. Relative uncertainties (1σ) are estimated to be ~5% for F, ~10% for Cl, and ~25% for S, respectively, at the concentration levels reported in this work. In order to test the reliability and accuracy, we measured several fragments of the Durango apatite USNM 104021 (recommended value of 0.41 wt% Cl, 3.53 wt% F, 0.085 wt% H_2O ; Young et al. 1969; Wang et al. 2011), and the results (15 analyses) were 0.406 ± 0.012 (1σ) wt% Cl and 4.138 ± 0.227 (1σ) wt% F. The Cl analyses are in excellent agreement with the recommended value, but the F analyses deviate significantly. We then performed time scans on some Durango apatite crystals, and the results show that X-ray count rates for F varied largely as a function of beam exposure time (Supplementary Fig. 1), which likely indicates that these crystal fragments are far away from the optimal orientation of c-axis normal to the electron beam (Stormer et al. 1993; Henderson 2011). As a result, the large deviation of F

analyses for the Durango apatite is most likely due to their unsuitable crystallographic orientations, rather than due to the analytical setting. Considering that the electron beam utilized to measure apatites from the Liujiawa pluton were orientated nearly perpendicular to the c-axis, we conclude that Cl and F analyses of natural apatites are valid within the uncertainty ranges given above.

6 Results

6.1 Pyroxene

The compositions of the pyroxenes from the Liujiawa pluton vary systematically in different lithologies (Supplementary Fig. III-2a). The clinopyroxene in the CD has the highest Ca content ($X_{W_0} = 0.44-0.49$), whereas clinopyroxene in the GN and PD has relatively lower Ca content with X_{W_0} of 0.42-0.45 and 0.40-0.46, respectively. The Mg# values (molar $Mg/(Mg + Fe)$) of orthopyroxene in the GN are within 0.50-0.60, which are lower than that of the minor orthopyroxene in the PD. The Mg# values of clinopyroxene in the GN are within 0.65-0.70, whereas Mg# values of the clinopyroxene in the PD and CD rocks are in the range of 0.70-0.75 (Supplementary Fig. III-2b).

Cpx-Opx pairs are used to estimate crystallization temperatures applying the QUILF program (Andersen et al. 1993). Data obtained for the GN are between 800 and 910°C, whereas those for the PD are between 940 and 970°C, implying that pyroxenes in the PD crystallized at a relatively higher temperature and might not have been affected by re-equilibration (Supplementary Fig. III-2a).

6.2 Feldspar

The plagioclase compositions in the various lithologies are shown in Supplementary Fig. III-3 as An-content (mole%) histograms. The plagioclase in the GN is characterized by a unimodal distribution within $An_{30}-An_{45}$, whereas the plagioclase in the PD has a relatively larger compositional range within $An_{26}-An_{62}$. The plagioclases of the CD rocks, in which clinopyroxene is present but orthopyroxene is absent, are characterized by a bimodal-distribution of the An content, i.e. $An_{18}-An_{26}$ and $An_{40}-An_{58}$. The HG rocks have a small proportion of high-An plagioclase ($\sim An_{80}$) and a large proportion of low-An plagioclase ($An_{26}-An_{60}$), and the peak of the latter population is in the range of $An_{54}-An_{58}$.

K-feldspar is present in the GN, PD and CD but absent in the HG rocks. Their

compositions are similar for the three rock types, within the range of Or₈₀-Or₁₀₀.

6.3 Amphibole

The amphibole compositions of the four lithological units are fully listed in Supplementary Table III-2 and shown in nomenclature diagrams (after Leake et al. 1997) in Supplementary Fig. III-4.

6.3.1 Cation distribution

As shown in the ^[4]Al versus ΣA diagram (Fig. III-6a), the variations in cations of all amphiboles from the Liujiawa pluton are mainly controlled by pargasite substitution as indicated by the slope of ~ 2.0 , as well as minor additional tschermakite substitutions indicated by the deviation of plots from the pargasite line (Spear 1981).

The amphiboles in the GN, present as rims or mantles surrounding pyroxenes, are of calcic type (magnesiohornblende and minor actinolite) and have relatively large variations in the values of Si (6.8-7.7 pfu, pfu = per formula unit), ΣA (0.05-0.40 pfu), ^[4]Al (0.2-1.2 pfu) and Mg# (0.58-0.70). The minor amphiboles (~ 2 wt%) in the PD, with similar textural features than those in the GN, are relatively Ca-poor and Mg- and Fe-rich (anthophyllite). They are distinctively low in the values of ΣA (0.01-0.05 pfu), ^[4]Al (0.1-0.3 pfu), but high in Mg# (0.69-0.72). The amphiboles in the CD, which are usually euhedral and contain clinopyroxene relics, are of calcic type (magnesiohornblende) and have small ranges of values of Si (7.0-7.3 pfu), ΣA (0.25-0.40 pfu), ^[4]Al (0.7-1.0 pfu) and Mg# (0.61-0.66), even though they are of a large proportion in the rock (~ 18 wt%, Supplementary Table III-1).

The amphiboles in the HG are of calcic type and have large variations in their cation constituents. The four groups mentioned above have systematically different cation contents especially for Al, Na, K and Mg (HG-I: Si = 6.0-6.5 pfu, ^[4]Al = 1.6-1.9 pfu, ΣA = 0.6-0.7 pfu, Mg# = 0.62-0.66; HG-II: Si = 6.0-6.5 pfu, ^[4]Al = 1.6-1.9 pfu, ΣA = 0.6-0.7 pfu, Mg# = 0.56-0.60; HG-III: Si = 6.5-7.0 pfu, ^[4]Al = 1.0-1.5 pfu, ΣA = 0.6-0.7 pfu, ΣA = 0.3-0.6 pfu, Mg# = 0.55-0.65; and HG-IV: Si = 7.0-7.5 pfu, ^[4]Al = 0.6-1.0 pfu, ΣA = 0.2-0.3 pfu, Mg# = 0.62-0.68). HG-I and HG-II have different Mg# values but similar values of ^[4]Al and ΣA , which are higher than those of HG-III and HG-IV (Fig. III-6a-b). Based on the composition of the four amphiboles groups in the HG, their formation order is suggested to be identical to the number of groups, i.e. the HG-I amphibole phenocrysts formed initially, immediately

followed by the HG-II, and then by the HG-III, and at a late stage by the rim-forming HG-IV amphiboles (Fig. III-6b).

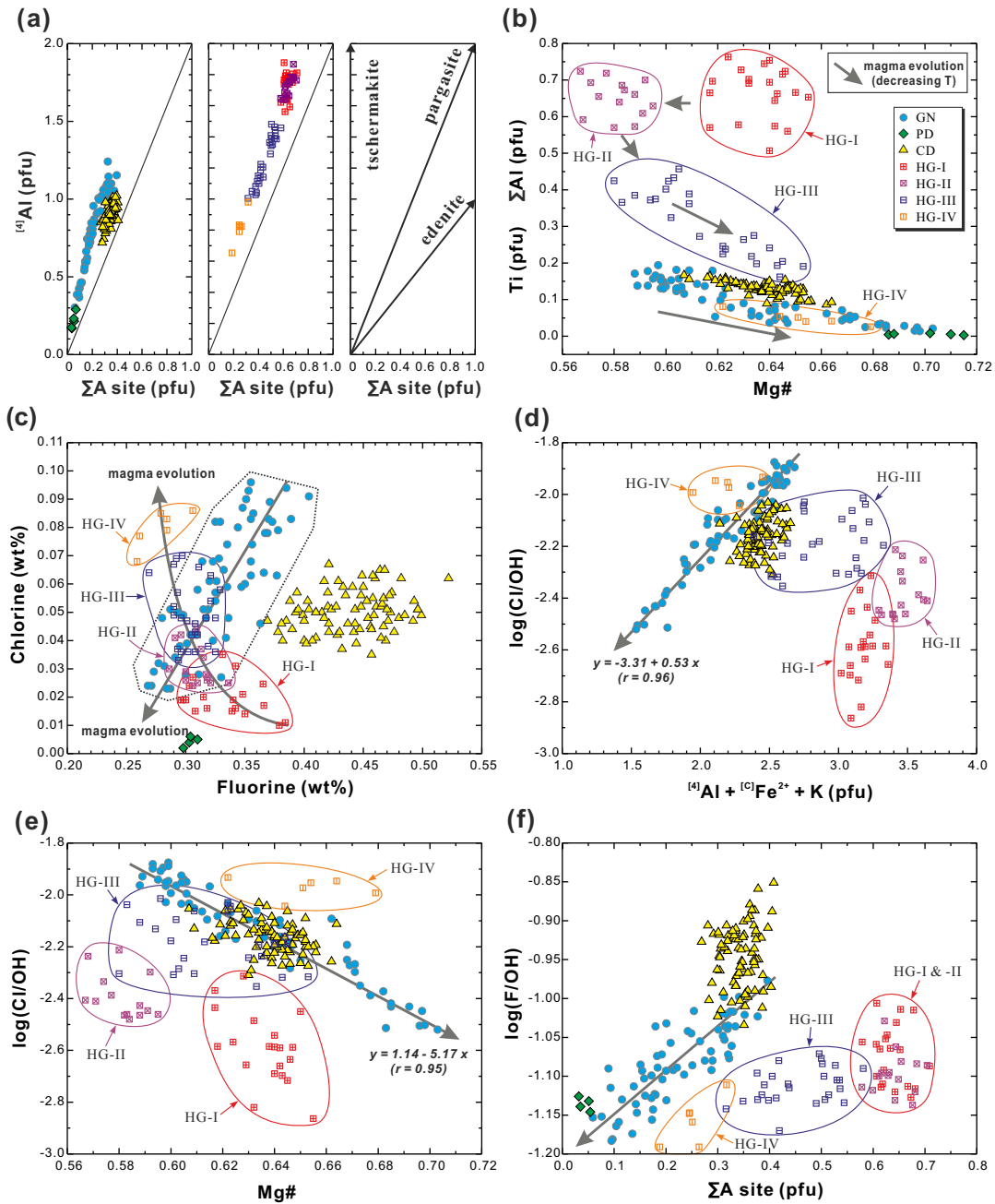


Fig. III-6 Amphibole compositions. (a) $^{[4]}Al$ versus ΣA site diagram, showing cationic substitution, after Spear (1981); (b) $Ti \times \Sigma Al$ versus $Mg\#$ diagram; (c) Cl versus F diagram; (d) $\log(Cl/OH)$ versus $^{[4]}Al + ^{[C]}Fe^{2+} + K$ diagram; (e) $\log(Cl/OH)$ versus $Mg\#$ diagram; (f) $\log(F/OH)$ versus ΣA site diagram; corresponding to the chronological order of formation, the four types of HG amphiboles (HG-I, HG-II, HG-III and HG-IV) are systematically different in the values of $^{[4]}Al$ (pfu), ΣA site (pfu), $Mg\#$, and Cl and F contents (see text for more explanation)

As the total Al and Ti contents in amphibole are both potential indicators of formation temperature (Spear 1981; Ernst and Liu 1998), $Ti \times Al_{total}$ versus Mg# for amphiboles from different rock types are plotted (Fig. III-6b) in order to illustrate the temperature variation. It can be noted that from HG-I to HG-II, Mg# values of amphibole decrease within nearly the same temperature range. In contrast, from HG-II to HG-III and HG-IV, as well as for the amphiboles in the GN, PD and CD, Mg# values increase with decreasing temperature. Detailed estimations of temperature and pressure of formation of amphiboles are given below.

6.3.2 Halogen distribution

The Cl content of the GN amphiboles varies in the range of 0.02-0.10 wt%, with an approximately positive correlation with F content (0.25-0.40 wt%) (Fig. III-6c). The minor amphiboles in the PD have distinctively low Cl content (<0.01 wt%). The CD amphiboles are characteristically rich in F (>0.35 wt%) with moderate Cl content (0.03-0.07 wt%), without clear covariation between F and Cl contents. For the four types of HG amphiboles, Cl becomes gradually enriched from HG-I (0.01-0.03 wt%), through HG-II and HG-III, to HG-IV (0.07-0.09 wt%). The F content decreases slightly from HG-I to HG-IV (Fig. III-6c).

Structural refinements of Cl-rich amphiboles (Volfinger et al. 1985; Morrison 1991; Enami et al. 1992; Makino et al. 1993; Oberti et al. 1993; Sato et al. 1997) have demonstrated that, for a given Cl content in the equilibrated liquid, the fixation of the large Cl anion (radius of 0.181 nm) at the O(3) site causes expansion of octahedral sheet. This can be accommodated by (1) $^{[4]}Al$ substitution for Si, (2) Fe^{2+} substitution at M1 and M3 sites for Mg, and (3) occupation in the A site, preferably by K. As shown in Fig. 6d, a clear positive correlation exists between $\log(Cl/OH)$ and $^{[4]}Al + ^{[Cl]}Fe^{2+} + K$ values for the GN amphiboles, to a less extent for the CD amphiboles, but not for the HG amphiboles which show complex relationships for the different groups.

As demonstrated by Morrison (1991) and Sato et al. (2005), the Mg-Cl avoidance might be the dominant mechanism which controls Cl incorporation into amphibole for a given Cl abundance in the coexisting silicate melt. In this study, the $\log(Cl/OH)$ and Mg# values show good negative correlations for the GN amphiboles, and to a less extent for the CD amphiboles (Fig. III-6e). However, no similar relationship exists for the HG amphiboles, which possibly implies complex variation

of Cl abundance in the melt that ever coexisted with the amphibole.

Because the F anion has nearly the same ionic radius (0.133 nm) as that of the OH anion (0.132-0.137 nm), the partitioning behavior of F between a hydrous mineral and fluid or melt might be similar to that of OH. Hence, incorporation of F into amphiboles should be much easier than Cl, and F contents in amphiboles might be to a great extent constrained by the F/H₂O ratio in the coexisting melt. As shown in Fig. 6f, the variations of log(F/OH) and ΣA values of the GN and HG amphiboles suggest similarly rough positive relations; such a relation is however not valid for the CD amphiboles which have distinctively higher log(F/OH) values and extremely restricted ΣA values.

6.4 Biotite

The biotite compositions are fully listed in Supplementary Table III-3 and are illustrated in Fig. III-7.

6.4.1 Cation distribution

All the biotites from the GN, PD and CD rocks have similar values of Mg/(Mg+Fe) (0.5-0.6 mostly), total Al (2.3-2.5 pfu mostly) and Ti (0.4-0.6 pfu), and their composition plots are near the center in the quadrilateral nomenclature diagram (Fig. III-7a, after Rieder et al. 1998). The octahedral Al in biotite formula is nearly zero for all samples. The PD biotites show a rough negative correlation between Mg/(Mg+Fe) and ΣA values, whereas for the other rock types no such correlation exists. The MnO content of the GN biotite (0.05-0.2 wt%) is slightly lower than that of the PD biotite (0.25-0.4 wt%) and CD biotite (0.2-0.3 wt%).

6.4.2 Halogen distribution

Generally, all the biotites from the three rock types (GN, PD and CD) have systematically higher F and Cl contents than their coexisting amphiboles. The CD biotites are characterized by distinctive high F content (0.55-0.70 wt%) compared to the GN and PD biotites (Fig. III-7b), consistent with the higher F content of the CD amphiboles when compared to the amphiboles from other rocks types (Fig. III-6c).

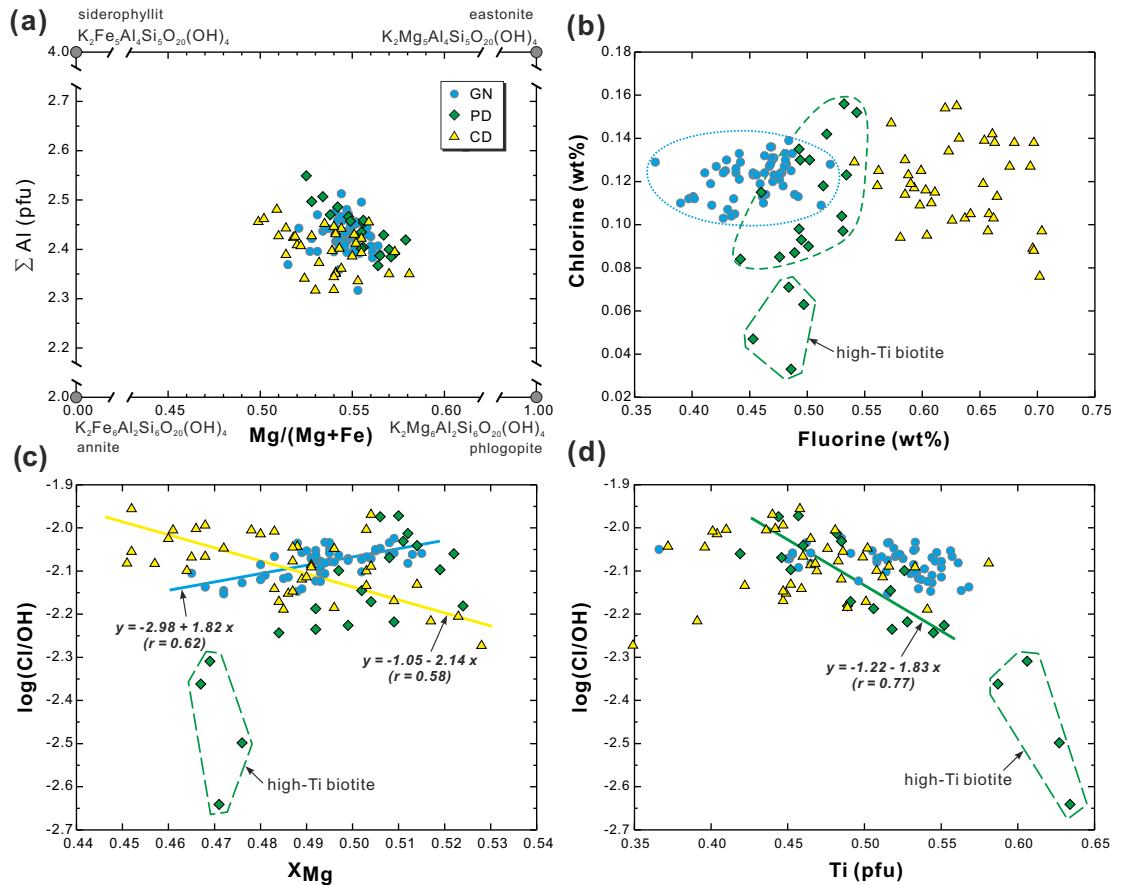


Fig. III-7 Biotite compositions. (a) ΣAl versus $\text{Mg}/(\text{Mg}+\text{Fe})$ diagram, endmembers are after Rieder et al. (1998); (b) Cl versus F diagram; (c) $\log(\text{Cl}/\text{OH})$ versus X_{Mg} diagram, linear regression lines for the biotites from GN and CD have respectively positive and negative slopes; (d) $\log(\text{Cl}/\text{OH})$ versus Ti (pfu) diagram

The mechanism of Mg-Cl avoidance (vice versa, Fe-F avoidance) for biotites (Munoz 1984; Mason 1992; Leger et al. 1996) promotes Cl (and suppresses F) incorporation effectively with substitution of Mg by Fe and some other cations (Al, Ti and Mn). Here we assess the effect of Mg-Cl avoidance by plotting $\log(\text{Cl}/\text{OH})$ versus X_{Mg} , where $X_{\text{Mg}} = \text{Mg}/(\text{Mg} + \text{Fe} + [{}^6]\text{Al} + \text{Ti} + \text{Mn})$. As shown in Fig. 7c, a weak negative correlation between $\log(\text{Cl}/\text{OH})$ and X_{Mg} for the CD biotites could be observed, which is consistent with the Mg-Cl avoidance. On the contrary, a rough positive correlation between $\log(\text{Cl}/\text{OH})$ and X_{Mg} for the GN biotites exists, which precludes cation substitution for Mg as the major controlling factor for the modest variation of Cl content. In fact, the GN biotites have nearly constant Cl content (Fig. III-7b) compared to the relatively large variation in the Cl content of the GN amphiboles (Fig. III-6c). The extremely low $\log(\text{Cl}/\text{OH})$ values of some PD biotites can not be attributed to the Mg-Cl avoidance, but might be related to the strong Ti substitution (Leger et al. 1996) (see Fig. III-7d).

It is notable that for both GN and CD rocks, Cl in amphibole can not be correlated with Cl in biotite using the relation of $X_{\text{Cl}}^{\text{Bt}} \approx 0.33 \times X_{\text{Cl}}^{\text{Amp}}$ derived from an intrusive syenite by Markl and Piazzolo (1998), which implies either that this relationship might not be valid for non-syenite magmatic systems or that the halogen concentrations in amphibole and biotite in GN or CD rocks does not reflect an equilibrium distribution.

6.5 Apatite

The compositions of apatite for the four rock types are listed in Supplementary Table III-4, and their variations are illustrated in Fig. III-8. According to the various occurrences of apatites (see the previous sample description and Fig. III-2-5), three groups can be identified: (I) phenocryst between anhydrous minerals, (II) phenocryst enclosed in or in contact with hydrous minerals, and (III) microcrystal in matrix plagioclase.

6.5.1 Cation distribution

Generally for all the apatites, substitutions of Na and Fe for Ca are conspicuous whereas Mn substitution can be neglected in barren mafic rocks (Piccoli and Candela 2002). The molar Fe/Na ratios of group-I apatites (only observed in GN) are primarily in the range 3/2~1/4, while the ratios of group-II apatites (observed in GN, CD and HG) have a relatively large range (Fig. III-8a).

6.5.2 Halogen distribution

For different rock types, the F contents of apatite increase from GN (2.6-3.2 wt%), through HG (2.8-3.5 wt%) and PD (3.2-3.3 wt%), and finally to CD (3.5-3.9 wt%); the variation of Cl content shows a reverse trend within the total range of 0-0.8 wt% (Fig. III-8b). Calculated based on the assumption that $F + Cl + OH = 1$ for the apatite formula (25 oxygen atoms), as shown in the F-Cl-OH ternary diagram (Fig. III-8c), all the apatites are extremely rich in fluorapatite (FAp) relative to hydroxylapatite (HAp) and chlorapatite (ClAp), while the CD apatites have the highest mole fraction of FAp (>0.93). All the apatites have Cl/OH mole ratios higher than 1/2, and the GN apatites have approximately a constant mole fraction of ClAp of ~0.1. It should be noted that 15 analyses out of a total 17 analyses of CD apatites have a sum of mole fractions of FAp and ClAp exceeding 1 by 0.01-0.07 (Supplementary Table 4), which can be ascribed to the uncertainty of F analysis (~5% at 1σ) if it is assumed that the actual mole fraction of HAp for these analytical

points is zero. The plot of these 15 analyses in Fig. III-8c is recalibrated upon the assumption that the HAp mole fractions are zero.

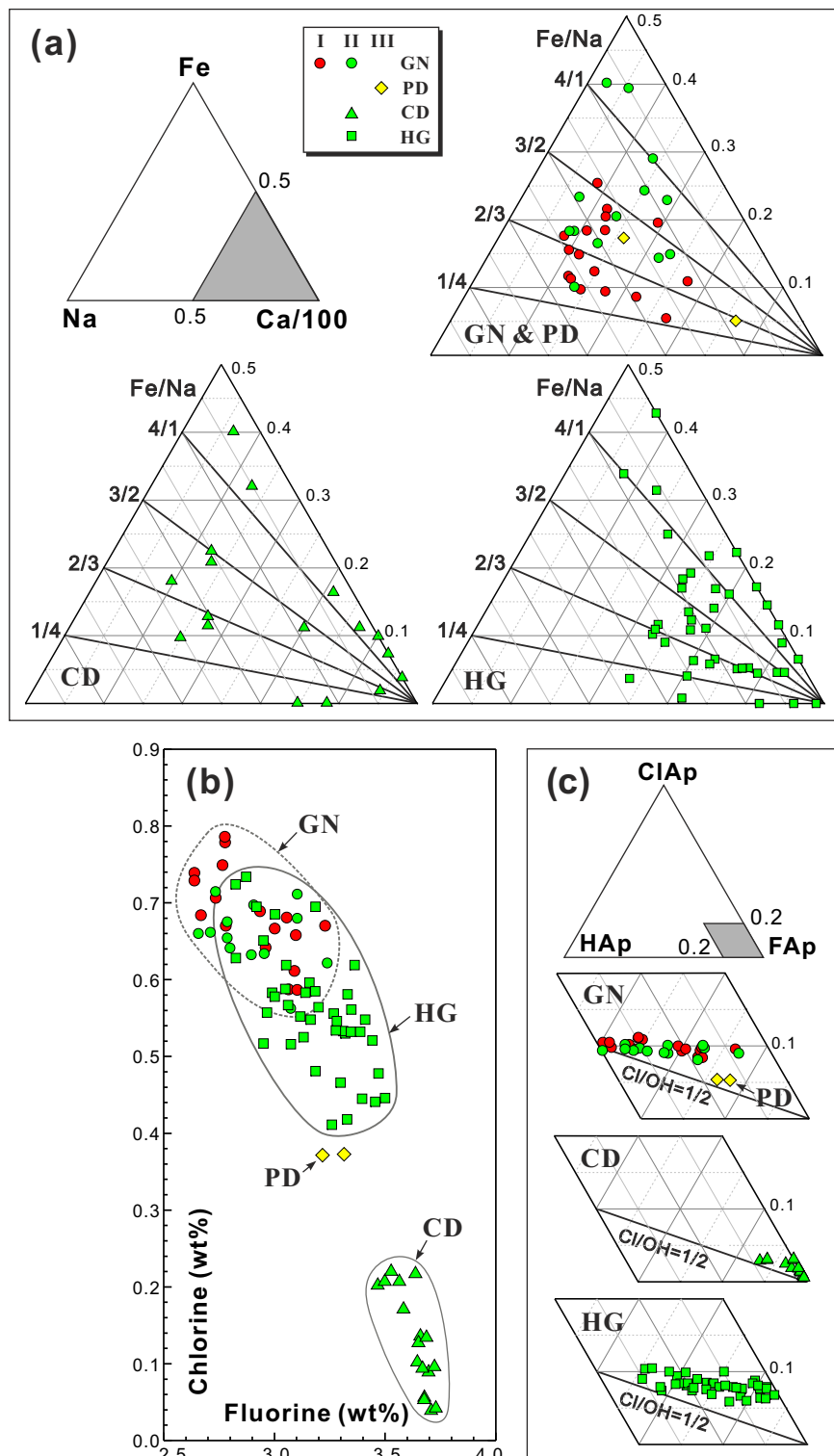


Fig. III-8 Apatite compositions. (a) Ca/100-Fe-Na ternary diagram; (b) Cl versus F diagram; (c) FAp-ClAp-HAp ternary diagram

7 Estimation of crystallization conditions

7.1 Amphibole

The application of available geothermobarometers based on amphibole compositions is quite dependent on pressure, temperature and composition. Al-in-hornblende barometers proposed by Hammarstrom and Zen (1986), Hollister et al. (1987), Johnson and Rutherford (1989) and Schmidt (1992) are principally based on tschermakite substitution which is pressure sensitive. One important assumption of these Al-in hornblende barometers is that the composition of magmatic amphiboles has been equilibrated at near-solidus temperatures (Hollister et al. 1987; Blundy and Holland 1992). However, if a small magma body, such as the Liujiawa pluton (~2 km² area, Ma et al. 1998), cooled to the solidus in a relatively short time compared to large plutons, supersolidus amphiboles might record high-temperature compositions. For the overall dataset of the Liujiawa pluton, Σ Al and TiO₂ contents in amphibole vary largely within 0.2-2.2 pfu and 0.1-3.0 wt%, respectively, which reflect distinct temperatures of amphibole formation for various rock types (Spear 1981; Ernst and Liu 1998). The formation temperatures of amphibole are estimated using the amphibole-plagioclase thermometer of Holland and Blundy (1994), while the pressures are estimated using barometers of Anderson and Smith (1995) or Schmidt (1992) according to their application limits. Because the barometer of Anderson and Smith (1995) is highly dependent on oxygen fugacity, it is only applicable for amphibole compositions with $Fe^{3+}/(Fe^{2+}+Fe^{3+})$ higher than 0.25. The results of P-T estimation for various types of amphibole are listed in Table III-1.

Compared to the Cpx-Opx pair temperatures (Supplementary Fig. III-2), the formation of amphibole in the GN rocks was much later than pyroxene (910-800 °C) and proceeded probably during a moderate cooling duration (685-615 °C) associated with magma ascent (from ~3.5 to ~1.0 kbar). With decreasing temperature and pressure the GN amphiboles, present as rims around clinopyroxenes or orthopyroxenes, are continuously enriched in Mg relative to Fe (increasing Mg#, Fig. III-6b), but depleted in both F and Cl (Fig. III-6c~f). The amphiboles in the PD are compositionally similar to the low-Al (high Mg#) end-member of GN amphiboles (Fig. III-6a~b) and also indicate equilibration at a very low pressure (assumed to be ca. 1.0 kbar) and temperature (<500 °C), which indicates that they might have formed at subsolidus conditions. The amphibole compositions for the CD rocks indicate similar temperature (ca. 700 °C) but lower pressure (from ~2.6 to ~1.3 kbar), inferring a process similar to adiabatic ascent. Their distinctive high F concentrations (Fig. III-6c) and texture features (with enclosed relics of clinopyroxene, Fig. III-4a)

suggest a contribution from F-rich crust-derived felsic melts, which might have been involved by magma mixing (see discussion below).

The four types of amphiboles in the HG rocks exhibit moderate temperature and large pressure variations. In estimating the P-T conditions, the plagioclases in equilibrium with the respective amphibole types are supposed to have compositions between An₅₅ and An₃₀, which is inferred from plagioclase composition statistics (Supplementary Fig. III-3) and related mineral textures (e.g. Fig. III-5b). Although the HG-I and HG-II amphiboles differ from each other in Mg#, they might have formed at similar temperatures (ca. 850 °C) and pressures (ca. 6.5 kbar). These high-T amphiboles have similar formation conditions than that of the GN pyroxenes (Supplementary Fig. III-2), which suggests that the initial pyroxenes (if ever existed) in the early HG magmas reacted totally to form these high temperature amphiboles. High water concentrations (e.g. nearly H₂O-saturated) might be the major cause. The HG-III amphiboles are estimated to be formed at ~ 3.9 kbar and ~750 °C, and the HG-IV amphiboles (as rims of other types) at ~1.7 kbar and ~690 °C. Along the cooling and crystallization trend, amphiboles of various types tend to systematically have higher Cl but lower F concentrations (Fig. III-6c).

In summary, as indicated by P-T estimation of amphiboles, the Liujiawa pluton-forming magmas have ascent from ca. 22 km (~6.8 kbar) to near ca. 4.3 km (~1.3 kbar), and the pluton could have been uplifted to even shallower levels in a short time after solidification probably due to extensional unroofing of the orogen. By comparing the variation of Cl concentration with the formation temperature of amphiboles, it can be noted that the Cl concentration generally increases from ca. 860 °C to ca. 700 °C (from HG-I to HG-IV) but decreases again from ca. 690 °C to ca. 520 °C (from GN-1 to GN-2 and PD).

7.2 Biotite

In this case study, the formation P-T conditions of biotites can only be estimated based on petrographical determination of the crystallization sequence together with the formation temperatures of pyroxenes and amphiboles.

For the GN rocks, textural observations show that biotites crystallized after clinopyroxene (Fig. III-2d), and the biotite probably has replaced former orthopyroxene. In the reaction zone shown in Fig. III-2e, tiny relics of orthopyroxene can be observed enclosed in quartz, and the quartz occurs as myrmekitic grains

together with biotite indicating synchronous formation of them. Considering a reaction of $\text{Opx} + \text{Kfs} + \text{H}_2\text{O} = \text{Bt} + \text{Q}$, we propose that biotite has been formed by reaction of orthopyroxene with late magmatic K-rich melt. Amphibole also occurs as relics surrounded by quartz (Fig. III-2e), suggesting that some amphiboles formed prior to biotite. For the clusters of orthopyroxene (Fig. III-2a), amphiboles exclusively form the rims of orthopyroxenes, which also implies that high-temperature amphiboles formed prior to biotites. This estimation is consistent with crystallization experiments of mafic magmas, in which biotite generally started to form later than amphibole (e.g. Yoder and Tilley 1962). For the CD rocks, all biotites are anhedral and directly in contact with low-Ca plagioclase ($\sim\text{An}_{25}$, Fig. III-4b) and K-feldspar, indicating their crystallization temperature and pressure were much lower than those of amphibole and high-Ca plagioclase.

Since the igneous amphiboles in the GN rocks are estimated to have crystallized until ~ 615 °C and ~ 1.3 kbar (Table III-2), we propose that most biotites in the GN could have crystallized at this condition. This P-T estimation for biotites is assumed to be also valid for the biotites in the PD and CD rocks.

7.3 Apatite

Temperature strongly influences halogen distribution in apatite/melt equilibria, which makes the estimation of apatite saturation temperature (AST) a prerequisite before determining halogen fugacity of melt from apatite halogen concentrations (Piccoli and Candela 1994). As all of the types of lithologies treated in this paper are metaluminous, it is possible to determine the AST using the equation calibrated experimentally by Harrison and Watson (1984).

The apatites in the GN rocks are mostly euhedral to subhedral, contacting directly with orthopyroxene clusters (Fig. III-2a) or clinopyroxene (Fig. III-2b), implying that apatites crystallized close to pyroxenes in the crystallization sequence. These apatites are noted as type-I (Fig. III-8a). Piccoli and Candela (1994) suggested that the P_2O_5 content of melt is better to be estimated by using mode proportion of apatite in the igneous rock. However, for a case in which the apatite should have started to crystallize at a high temperature earlier than most other silicate minerals (similar to the case in this study), the whole rock P_2O_5 content is more close to the real content in melt than that estimated from mode of apatite tanking into account that some phosphorus has been incorporated by other minerals later as a minor element. The GN rocks have 54.75 wt% SiO_2 and 0.39 wt% P_2O_5 (bulk composition

on a volatile-free basis, unpublished data of C. Zhang). Assuming that 5-10% of both orthopyroxene and clinopyroxene crystallized prior to that of apatite, the melt composition at the AST can be estimated by mass balance calculation, i.e. 55.06-55.46 wt% SiO₂ and 0.43-0.49 wt% P₂O₅. The estimated AST for apatites in the GN is 900-923 °C, which is close to the upper limit of the equilibrium temperature of Cpx-Opx pairs (800-910 °C, Supplementary Fig. III-2a) and consistent with their nearly contemporary crystallization indicated by petrographical features. For simplicity, 900 °C is used as the AST for the type-I apatites from GN.

In the CD and HG rocks, most apatites are generally rounded and enclosed in amphiboles or biotites (Fig. III-4a, Fig. III-4c and Fig. III-5c). They are similar to rounded apatites in the GN rocks which are enclosed or in contact with biotites or amphiboles, and they are denoted as type-II apatites (Fig. III-8). Because magma mixing between felsic and mafic members could have contributed to the bulk composition of the CD rocks, the AST calculated from the analyzed bulk SiO₂ and P₂O₅ contents may not be representative for the apatite crystallization temperatures. We suggest that most of the apatites in the CD and HG rocks have been inherited from the mafic magmas (represented by GN) in equilibrium with high-Mg clinopyroxene and that they may have a similar AST (~900 °C). Their rounded morphology implies that they might have experienced late magmatic re-equilibrium and redistribution of halogens between apatite and biotite (Zhu and Sverjensky 1992) and/or between apatite and amphibole, or between apatite and magmatic fluid (e.g. Dilles 1987). As a result, the equilibrium conditions of type-II apatites in GN, CD and HG apatites are supposed to be identical to those of biotite or amphibole (Table III-3). Apatites in the PD rocks only exist as microcrystals in matrix plagioclase, i.e. type-III apatite (Fig. III-8) and thus are proposed to have formed at a late magmatic stage (ca. 550 °C).

8 Calculation procedure to determine partitioning of Cl and F in melt-fluid systems

Many experimental and theoretical modeling studies have been performed to constrain partitioning behaviors of halogen in melt-fluid systems for a variety of temperature, pressure and composition (Holland 1972; Kilinc and Burnham 1972; Foley et al. 1986; Webster and Holloway 1988; Shinohara et al. 1989; Webster and Holloway 1990; Webster 1990; Schaller et al. 1992; Webster 1992a; Webster 1992b; Shinohara 1994; Shinohara and Fujimoto 1994; London 1997; Webster 1997a; Webster 1997b; Webster and Rebbert 1998; Student and Bodnar 1999; Villemant and

Boudon 1999; Webster et al. 1999; Signorelli and Carroll 2000; Frank et al. 2003; Shinohara 2009; Webster et al. 2009a). However, to reach the initial goal of this study (halogen contents of melts derived from mineral compositions), the fugacities of Cl and F in the fluids coexisting with melts and minerals need to be known. In the following part, the procedure adopted to determine the halogen fugacities and the partitioning of Cl and F between fluids and melts is described, in which *fluid* is used to denote any magmatic volatile phase, such as low density aqueous phase, high density saline phase, or vapor (after Webster et al. 2009a).

Crystallization experiments on hydrous basaltic magmas have demonstrated that amphiboles are only stable with high water contents in melts, mostly water-saturated conditions (e.g. Yoder and Tilley 1962; Sisson and Grove 1993; Berndt et al. 2005; Feig et al. 2006). Under water-saturated conditions, biotites generally form later than amphiboles in hydrous basaltic magmas (Yoder and Tilley 1962). For apatites, they usually occur enclosed in or in contact with amphiboles or biotites, and thus could have been equilibrated with fluid in terms of volatile components. As a result, when considering partition and distribution of volatile components in the magmatic system, we assume a free fluid (vapor) phase coexisting with the silicate melt and minerals provided that the hydrous minerals are stable, i.e. a fluid-saturated system. In this case, the fluid phase is supposed to consist exclusively of H₂O and Cl- and F-associated species.

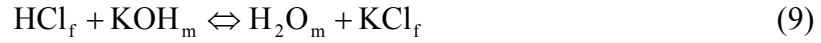
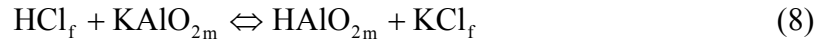
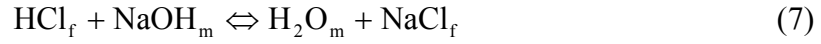
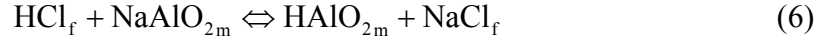
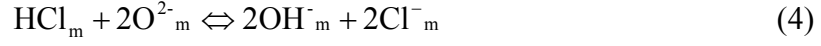
8.1 Chlorine

In a magmatic system where H₂O, fluorine and chlorine are present but sulfur and CO₂ are absent (supposed to be the case in this study), the fluid exsolved from silicate melt consists of H₂O, fluorides and chlorides. According to Stolper (1982), the speciation of H₂O in coexisting melt and fluid is controlled by



where H₂O_m is molecular water in melt, H₂O_f is molecular water in fluid, O²⁻_m is non-bridging oxygen in silicate melt and OH⁻_m is hydroxyl in melt. More discussion on the calculation of H₂O species, especially on estimation of mole fraction of OH in melt from total water content, could be found in Appendix A.

Following the works of Frank et al. (2003) and Shinohara (2009) and references therein, the speciation of Cl is controlled by



in which the components with subscript f are in the fluid phase, and those with subscript m are in the melt phase. In both fluid and melt phases, Cl ion prefers to bond with the alkali metals relative to H^+ or alkaline earth cations (Webster and Holloway 1988). It is worth noting that KOH might be only present in K-bearing but Na-free hydrated silicate melts (Mysen and Acton 1999), and thus Eq (9) can be neglected for normal Na-bearing magmatic systems (Frank et al. 2003). Additionally, mass balance constrains these relations

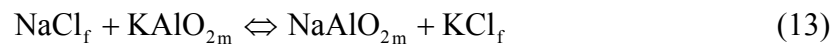
$$\sum \text{Cl}_m = \text{HCl}_m + \text{Cl}^-_m \quad (10)$$

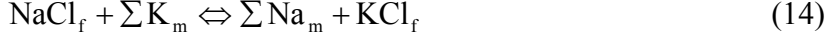
$$\sum \text{Cl}_f = \text{HCl}_f + \text{NaCl}_f + \text{KCl}_f \quad (11)$$

$$\sum \text{Cl}_{\text{tot}} = \sum \text{Cl}_m + \sum \text{Cl}_f \quad (12)$$

in which $\sum \text{Cl}_m$, $\sum \text{Cl}_f$ and $\sum \text{Cl}_{\text{tot}}$ are sums of Cl species in melt, fluid and whole melt-fluid system, respectively.

The Cl species in fluid consists of NaCl, KCl and HCl, and HCl are much less than the other two components at pressures above 1~2 kbar (Frank et al. 2003; Shinohara 2009). The relation between NaCl and KCl in fluid could be expressed as





and these equilibria are respectively controlled by

$$K'_{\text{ex}} = (C_{\text{NaAlO}_2}^m \times C_{\text{KCl}}^f) / (C_{\text{NaCl}}^f \times C_{\text{KAlO}_2}^m) \quad (15)$$

$$K_{\text{meas}} = (C_{\text{Na}}^m \times C_{\text{KCl}}^f) / (C_{\text{NaCl}}^f \times C_{\text{K}}^m) \quad (16)$$

where C is molality (mol/kg), and C_{Na}^m , for example, can be calculated as

$$C_{\text{Na}}^m = W_{\text{Na}_2\text{O}}^m \times 2 \times 10 / mW_{\text{Na}_2\text{O}} \quad (17)$$

in which $W_{\text{Na}_2\text{O}}^m$ is the weight percent (wt%) of Na_2O in melt and $mW_{\text{Na}_2\text{O}}$ is the molecular weight of Na_2O . Comparing Eqs (15) and (16), the measured constant K_{meas} differs from the apparent equilibrium constant K'_{ex} by using the sum molality of Na in melt (C_{Na}^m) to replace the molality of NaAlO_2 in melt ($C_{\text{NaAlO}_2}^m$), and using the sum molality of K in melt (C_{K}^m) to replace the molality of KAlO_2 in melt ($C_{\text{KAlO}_2}^m$). At the condition of 800 °C and 1 kbar, Frank et al. (2003) experimentally determined

$$K'_{\text{ex}} = 0.40 \pm 0.03(1\sigma) \quad (18)$$

$$K_{\text{meas}} = K'_{\text{ex}} + a / W_{\text{HCl}}^f \quad (19)$$

in which $a = 0.03$ and W_{HCl}^f is weight percent of HCl (in wt%) in fluid. Rearranging Eq (16), we can obtain

$$C_{\text{KCl}}^f / C_{\text{NaCl}}^f = K_{\text{meas}} \times C_{\text{K}}^m / C_{\text{Na}}^m \quad (20)$$

where $C_{\text{K}}^m / C_{\text{Na}}^m$ can be estimated by subtracting mineral phases from a bulk composition for plutonic systems. The relation of C_{NaCl}^f and C_{HCl}^f has been demonstrated to be mainly pressure-dependent (see Fig. 6 of Shinohara 2009), and the following equation can be derived accordingly

$$C_{\text{HCl}}^f / C_{\text{NaCl}}^f = 0.269 \times P^{-5.01} \quad (21)$$

($r^2 = 0.87$, $N = 8$), in which P is pressure in kbar. Rearranging Eqs (11), (20) and (21), we can obtain the relation of molalities of total Cl (C_{Cl}^f) and HCl (C_{HCl}^f) in fluid as

$$C_{\text{Cl}}^{\text{f}} = C_{\text{HCl}}^{\text{f}} + C_{\text{HCl}}^{\text{f}} \times \frac{P^{5.01}}{0.269} \times \left[1 + \left(K'_{\text{ex}} + \frac{1}{C_{\text{HCl}}^{\text{f}} \times 121.67} \right) \times \frac{C_{\text{K}}^{\text{m}}}{C_{\text{Na}}^{\text{m}}} \right] \quad (22)$$

in which P is pressure in kbar.

The partitioning coefficient of Cl between fluid and melt can be written as (Kilinc and Burnham 1972; Shinohara et al. 1989; Shinohara 2009):

$$D_{\text{Cl}}^{\text{f/m}} = C_{\text{Cl}}^{\text{f}} / C_{\text{Cl}}^{\text{m}} \quad (23)$$

and numerous experiments (e.g. Webster and Holloway 1988; Shinohara et al. 1989; Webster 1992a; Webster 1992b; Signorelli and Carroll 2000) demonstrated that $D_{\text{Cl}}^{\text{f/m}}$ is a complex function of a variety of intensive and extensive properties, e.g. it increases strongly with increasing pressure, decreasing temperature and increasing concentration of Cl in the system. It is worth noting that $D_{\text{Cl}}^{\text{f/m}}$ is defined as ratio of molalities of Cl⁻ in fluid and Cl⁻ in melt, and this is essentially different from the definition in the studies of Webster and Holloway (1988) and Webster (1992a) in which the partitioning coefficients were defined as ratio of mass concentrations of Cl⁻ in fluid and Cl⁻ in melt.

According to Shinohara (2009), at conditions of low Cl concentration in the system (e.g. $C_{\text{Cl}}^{\text{f}} < 1$ mol/kg), as supposed for this case (the Liujiawa plutonic system), $D_{\text{Cl}}^{\text{f/m}}$ tends to be independent of Cl concentration. In addition, as our above theoretical considerations are intended to determine the Cl partitioning in biotite-melt-fluid system and since the biotites in the Liujiawa pluton are estimated to have formed within a small temperature range (600-650 °C), thus we ignore the temperature effect on $D_{\text{Cl}}^{\text{f/m}}$ for simplicity. Piccoli and Candela (1994) have also calibrated an expression of $D_{\text{Cl}}^{\text{f/m}}$ based on the work of Shinohara (1987) data as

$$D_{\text{Cl}}^{\text{f/m}} = 19.8 \times P + 3.75 \quad (24)$$

We reprocessed the data of Shinohara (2009) (see his Fig. 3, data compiled from Shinohara et al. 1989; Signorelli and Carroll 2000; Simon et al. 2004) with fitting regression and obtained

$$D_{\text{Cl}}^{\text{f/m}} = 4.51 \times P^{2.16} \quad (25)$$

($r^2 = 0.72$, $N = 16$), in which P is pressure in kbar. Eqs (24) and (25) are plotted in Fig. III-9a for comparison, and it is notable that Eq (25) gives lower values of $D_{\text{Cl}}^{\text{f/m}}$

than Eq (24) at pressures below ~3.7 kbar. As we cannot access the data of Shinohara (1987) which is an unpublished thesis, it is not possible for us to assess the validity of Eq (24). Additionally, because decreasing Cl concentration in system tends to decrease $D^{f/m}_{Cl}$, we apply Eq (25) to approximate Cl partitioning coefficient for the Liujiawa plutonic system in which the Cl concentration is supposed to be much lower than most experimental conditions.

Assuming that fugacity coefficients of H₂O, HF and HCl in fluid are similar to each other, the relation of fugacity ratio and molality ratio of components in fluid phase can be written as

$$f_{HCl}^f / f_{H_2O}^f = C_{HCl}^f / C_{H_2O}^f \quad (26)$$

and thus we yield

$$C_{HCl}^f = C_{H_2O}^f \times f_{HCl}^f / f_{H_2O}^f \quad (27)$$

The definition of molality and mass balance constrain that

$$C_{H_2O}^f \text{ (mol/kg)} = 1000 / 18.02 = 55.49 \quad (28)$$

Introducing Eq (27) and (28) into Eq (22), we obtain the sum of molality of total chlorine in fluid as

$$C_{Cl}^f = 55.49 \times \frac{f_{HCl}^f}{f_{H_2O}^f} \times \left\{ 1 + \frac{P^{5.01}}{0.269} \times \left[1 + \left(K'_{ex} + \frac{1}{6751.94} \times \frac{f_{H_2O}^f}{f_{HCl}^f} \right) \times \frac{C_K^m}{C_{Na}^m} \right] \right\} \quad (29)$$

Furthermore, by introducing Eq (29) into Eq (25),

$$C_{Cl}^m = \frac{12.30}{P^{2.16}} \times \frac{f_{HCl}^f}{f_{H_2O}^f} \times \left\{ 1 + \frac{P^{5.01}}{0.269} \times \left[1 + \left(K'_{ex} + \frac{1}{6751.94} \times \frac{f_{H_2O}^f}{f_{HCl}^f} \right) \times \frac{C_K^m}{C_{Na}^m} \right] \right\} \quad (30)$$

Thus, given that f_{HCl}/f_{H_2O} of fluid, C_K/C_{Na} of melt and pressure (kbar) are known or estimated, molality of total Cl (mol/kg) in melt could be calculated according to Eq (30).

8.2 Fluorine

The partitioning behavior of fluorine in melt-fluid systems is different from that of chlorine. In the fluid (vapor) phase, nearly all F is present as HF at conditions

similar to natural igneous environments (Zhu and Sverjensky 1991). Thus, we assume that molality of HF (C_{HF}^f) in fluid is equal to that of total F species (C_F^f):

$$f_{HF}^f / f_{H_2O}^f = C_{HF}^f / C_{H_2O}^f = C_F^f / C_{H_2O}^f \quad (31)$$

The partitioning of F between aqueous fluid and silicate melt is mainly dependent on F concentration in the system, temperature, but independent on pressure for water-saturated systems (Webster and Holloway 1990; Webster 1990). Using Webster (1990)'s experimental data of water-saturated runs with $\leq 10,000$ ppm F in melt, we regressed an equation of $D_F^{f/m}$ as

$$D_F^{f/m} = W_F^f / W_F^m = 0.000943 \times T - 0.574 \quad (32)$$

($r^2 = 0.92$, $N = 9$), in which W_F^f and W_F^m are concentrations (mass fraction) of F in fluid and melt respectively, and T is temperature in °C. Eq (32) is slightly different from the regression of Piccoli and Candela (1994)

$$D_F^{f/m} = W_F^f / W_F^m = 0.00093 \times T - 0.56 \quad (33)$$

($r^2 = 0.92$, $N = 7$), which was derived from Webster (1990)'s experimental data of 2 kbar only (water-saturated runs with $< 10,000$ ppm F in melt). As demonstrated by experimental data of water-saturated runs with $> 10,000$ ppm F in melt, the effect of F concentration on $D_F^{f/m}$ is remarkable whereas temperature seems to exert little effect, and we regressed the following equation for melts containing $> 10,000$ ppm F

$$D_F^{f/m} = W_F^f / W_F^m = 0.0000107 \times W_F^m + 0.120 \quad (34)$$

($r^2 = 0.75$, $N = 19$), in which W_F^m is F concentration in melt in ppm. Eqs (32) and (34) are plotted in Fig. III-9b for comparison. We propose that Eq (32) is valid approximately true for water-saturated natural plutonic systems in which F concentration of melt is relatively low (≤ 1.0 wt%); a condition which is fulfilled for the Lijiawa pluton.

Assuming that fluid is exclusively composed of H₂O and HF (all F species as HF), the following relation is valid

$$W_F^f = \frac{1}{1 + f_{H_2O}^f / f_{HF}^f} \times \frac{19}{18.02} \times 10^6 \quad (35)$$

By introducing Eq (35) into Eq (34), we obtain

$$W_F^m = \frac{1}{1 + f_{H_2O}^f / f_{HF}^f} \times \frac{19}{18.02} \times \frac{10^6}{0.000943 \times T - 0.574} \quad (36)$$

Thus, given that $f_{HF}^f / f_{H_2O}^f$ of fluid and temperature ($^{\circ}C$) are known or estimated, the concentration of F (ppm) in melt could be calculated according to Eq (36).

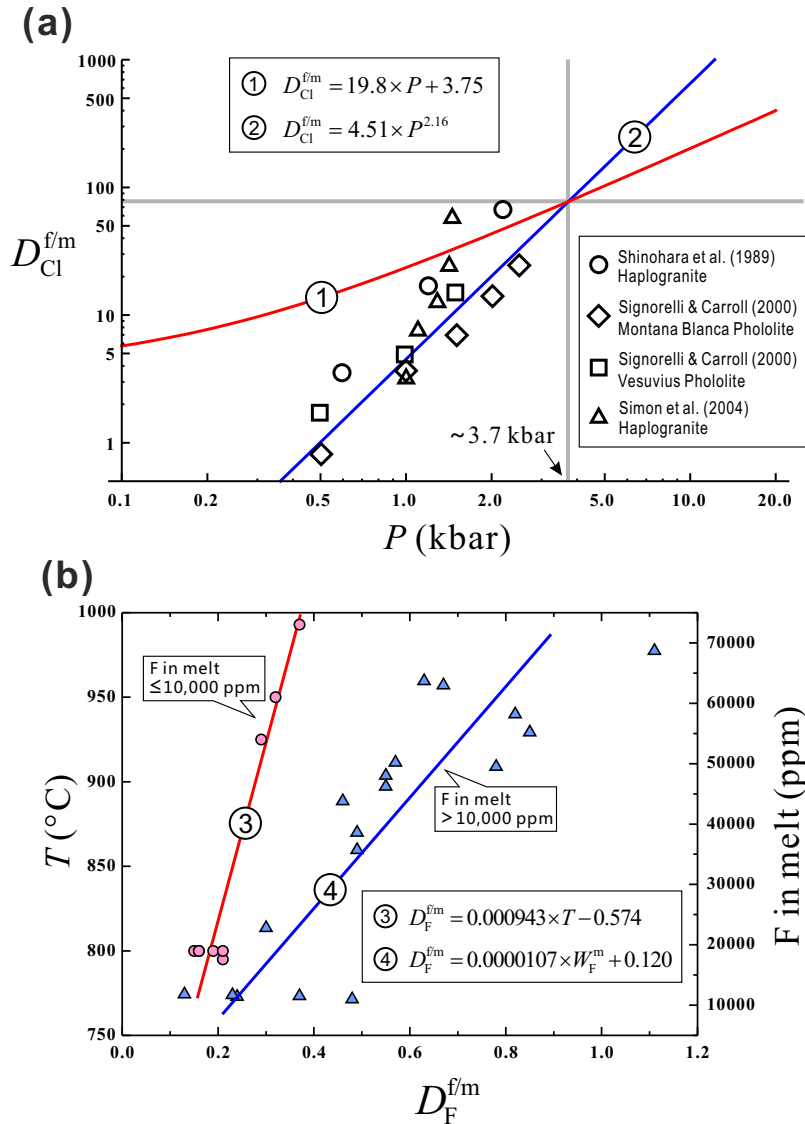


Fig. III-9 Fitting regressions of fluid-melt partitioning coefficients of Cl and F. (a) $D_{Cl}^{f/m}$ versus pressure; curve ① is according to Eq (24) and line ② is according to Eq (25); experimental data used to fit Eq (25) are indicated (see Shinohara 2009); (b) $D_F^{f/m}$ versus temperature and F concentration in melt; line ③ is according to Eq (32) and line ④ is according to Eq (34); experimental data are from Webster (1990)

9 Estimation of Cl and F in melts from hydrous minerals

9.1 Amphibole-melt-fluid system

Numerous studies have revealed that the partitioning of F-Cl-OH between amphiboles and liquids (melts or fluid) depends on the volatile properties of liquids, the crystallographic structure of amphibole and temperature (e.g., Volfinger et al. 1985; Vanko 1986; Morrison 1991; Makino et al. 1993; Oberti et al. 1993; Sato et al. 1997; Sato et al. 2005; Xiao et al. 2005). However, except for one study (Sato et al. 2005) there is no model to relate the Cl concentration in amphibole with that in melt. Currently, no thermodynamic or experimental calibration of F-OH partition between amphibole and silicate melt has been performed.

Sato et al. (2005) performed Cl-OH partitioning experiments (2-3 kbar, 800-850 °C, the nickel-nickel oxide buffer) between amphibole and melt in a dacitic composition, and calibrated an equation to fit the partition coefficient of Cl-OH as a function of the magnesium number of amphiboles, and we rewrite it as

$$\log(\text{Cl/OH})_{\text{melt}} = \log(\text{Cl/OH})_{\text{Amp}} - 3.74 + 1.5 \times \text{Mg\#} + 0.0027 \times T \quad (37)$$

in which $(\text{Cl/OH})_{\text{melt}}$ and $(\text{Cl/OH})_{\text{Amp}}$ are molar ratios of Cl/OH in melt and amphiboles, respectively, Mg# is molar ratio of Mg/(Mg + Fe) and T is temperature in Kelvin. Comparing this equation with the fitted relationship between $\log(\text{Cl/OH})_{\text{Amp}}$ and Mg# for the GN amphiboles (Fig. III-6e), one can observe that the effect of Mg# (indicated by absolute values of slopes) on the partitioning of Cl-OH is larger than that in the Sato et al. (2005)'s equation. We explain this phenomena tentatively by a concomitant variation of $(\text{Cl/OH})_{\text{melt}}$ and Mg# during magma evolution.

In the experiments of Sato et al. (2005), vapor-saturated conditions were maintained, but the composition of vapor was not determined and thus not involved in the calibration model for Cl. In order to apply the model of Sato et al. (2005) to calculate Cl concentration in the melt, water content of the melt coexisting with amphibole needs to be estimated firstly. On the assumption that all the amphiboles have formed at vapor (mainly H₂O)-saturated conditions, we estimated the water content by applying the pressure-dependent water solubility model of Holtz et al. (2001). Based on the calculation of H₂O species in silicate melt (see Appendix A), we obtained the values of molar fraction of OH in silicate melt which is supposed to have been in equilibrium with the different types of amphiboles. The data are then

used to calculate $\log(\text{Cl}/\text{OH})_{\text{melt}}$ according to the model of Sato et al. (2005) (Eq 37) and the results are summarized in Table III-1 and illustrated in Fig. III-10. It is notable that $\log(\text{Cl}/\text{OH})_{\text{melt}}$ is approximately constant above ~ 700 °C (at -2.3) as well as the calculated Cl concentration in the melt (~ 1000 ppm). However, between ~ 700 and ~ 500 °C, the values of $\log(\text{Cl}/\text{OH})_{\text{melt}}$ and Cl concentration in melt decrease dramatically to -4.0 and 10 ppm, respectively.

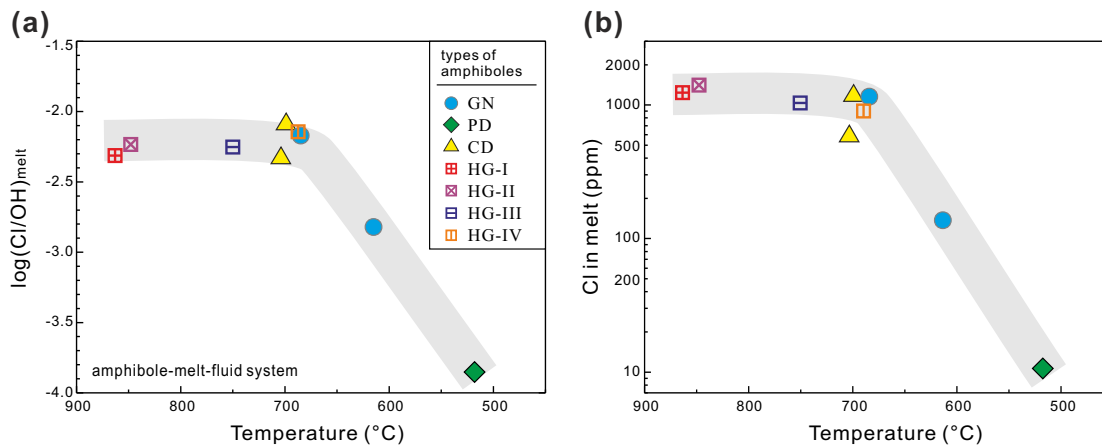
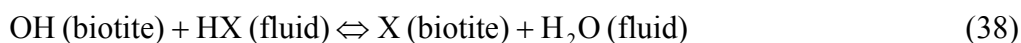


Fig. III-10 Modeling of Cl in melt calculated from amphibole compositions. (a) $\log(\text{Cl}/\text{OH})_{\text{melt}}$ versus temperature; (b) Cl concentration versus temperature; calculated according to the model of Sato et al. (2005); see Table 1 for detailed calculation results

9.2 Biotite-melt-vapor system

Compared to amphibole, quantitative calibration of halogen partitioning in the biotite-melt-vapor system has been addressed more, and consequently biotite has been more typically employed as a monitor for investigating volatile properties (e.g., Munoz 1984; Zhu and Sverjensky 1991; Munoz 1992; Zhu and Sverjensky 1992; Finch et al. 1995; Icenhower and London 1997; Coulson et al. 2001; Harlov and Förster 2002). Munoz (1984) firstly calibrated quantitative F-Cl-OH partitioning models between biotite and aqueous fluid for the halogen-hydroxyl exchange reaction



in which X denotes either F or Cl. Applying the partitioning coefficients of halogens between biotite and fluid determined by Zhu and Sverjensky (1991, 1992), Munoz (1992) re-calibrated the model, leading to the following formulations

$$\log(f_{\text{H}_2\text{O}}/f_{\text{HF}}) = (1000/T) \times (2.37 + 1.1 \times X_{\text{Mg}}) + 0.43 - \log(\text{F/OH})_{\text{Bt}} \quad (39)$$

$$\log(f_{\text{H}_2\text{O}}/f_{\text{HCl}}) = (1000/T) \times (1.15 - 0.55 \times X_{\text{Mg}}) + 0.68 - \log(\text{Cl/OH})_{\text{Bt}} \quad (40)$$

$$\log(f_{\text{HF}}/f_{\text{HCl}}) = (1000/T) \times (-1.22 - 1.65 \times X_{\text{Mg}}) + 0.25 + \log(\text{F/Cl})_{\text{Bt}} \quad (41)$$

In the above equations, $f_{\text{H}_2\text{O}}$, f_{HF} and f_{HCl} are fugacities of H_2O , HF and HCl in the fluid phase, T is temperature in Kelvin, $X_{\text{Mg}} = \text{Mg}/([\text{Al}^{6+}] + \text{Ti} + \text{Mn} + \text{Mg} + \text{Fe})$ in biotite, and $(\text{F/OH})_{\text{Bt}}$ and $(\text{Cl/OH})_{\text{Bt}}$ are molar ratios in biotite. By introducing Eq (39) into Eq (36) we can calculate the concentration of F (ppm) in melt, and by introducing Eq (40) into Eq (30) we can calculate the molality of Cl (mol/kg) in melt. Before performing the calculation, $C_{\text{K}}/C_{\text{Na}}$ of melt (molar ratio) was estimated on the basis of bulk composition, petrographical features and crystallization order (see Appendix B).

As indicate by the calculation results summarized in Table III-2, the melts which are in equilibrium with biotites from the GN, PD and CD rocks have nearly identical Cl concentrations within 1100-1300 ppm, whereas the melts for the CD rocks have higher F concentration (~3000 ppm) than the others (~1000 ppm).

Icenhower and London (1997) experimentally determined that the partition coefficient of F between biotite and rhyolitic melt at 200 MPa H_2O and oxygen fugacity ~NNO (nickel-nickel oxide) could be a function of Mg# of biotite (London 1997):

$$D_{\text{F}}^{\text{Bt/m}} = W_{\text{F}}^{\text{Bt}} / W_{\text{F}}^{\text{m}} = 10.08 \times \text{Mg\#} - 1.08 \quad (42)$$

in which W_{F}^{Bt} and W_{F}^{m} are respectively the F concentrations in biotite and melt. The melt F concentrations calculated according to Eq (42) are also indicated in Table III-2, and they are lower by a factor of 2 approximately when compared to the concentrations calculated according to the models of Webster (1990) and Munoz (1992).

The reason of the discrepancy might be from a variety of sources, including estimated crystallization temperature of biotite, and the applicability of the partitioning models of Webster (1990) (Eq 32), Munoz (1992) (Eq 39) and Icenhower and London (1997) (Eq 42) for the natural magmatic system in this case. The two sets of calculated F concentrations in melt versus temperature are compared

in Fig. III-11a, and it is notable that the calculate values for F according to Webster (1990) and Munoz (1992) are strongly dependent on temperature especially for low temperatures. At about 620 °C, the values derived from the two modeling procedures are nearly consistent with each other. In this perspective, F content and Mg# of igneous biotite could be potentially used as a geothermometer in the future.

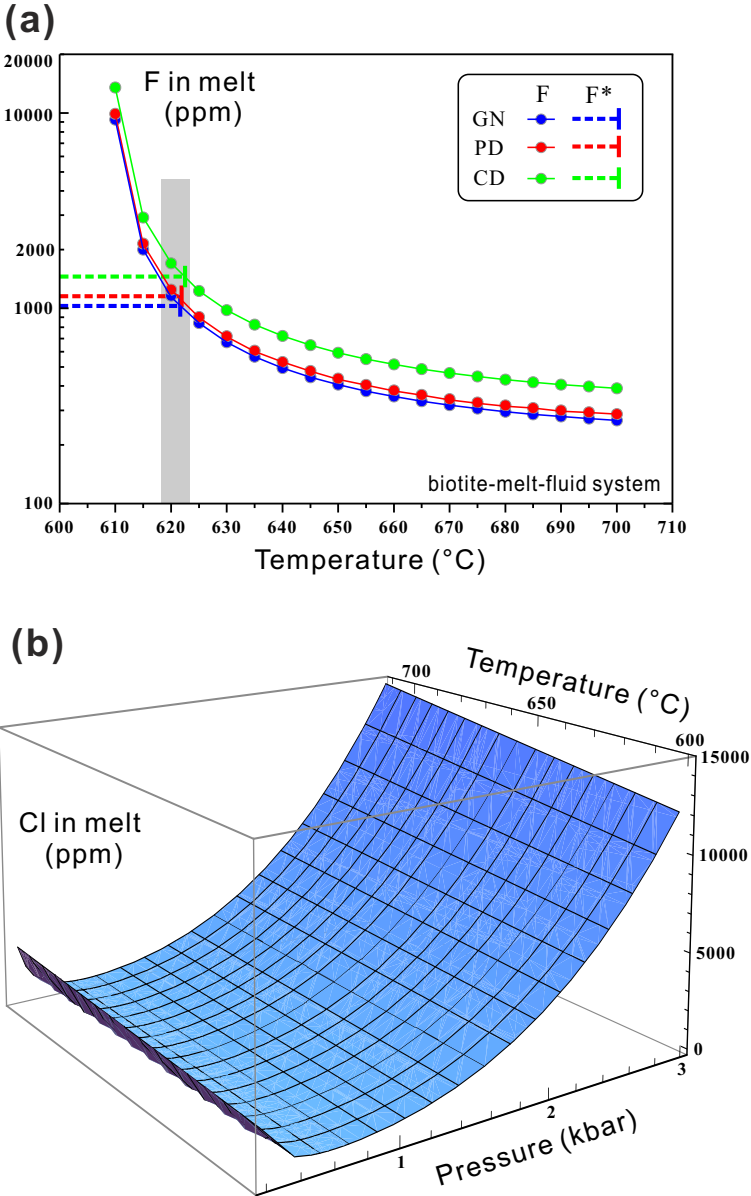


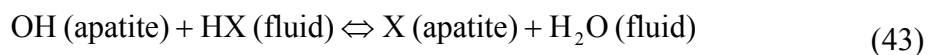
Fig. III-11 Modeling of F and Cl in melt calculated from biotite compositions. (a) F (circle) denotes F concentrations in melt calculated according to the models of Webster (1990) and Munoz (1992); F* denotes F concentrations in melt (error not shown) calculated according to the T-independent model of Icenhower and London (1997); (b) 3D plot of calculated Cl concentration in melt versus temperature and pressure (made with Mathematica©), average composition of CD biotites is used for this example modeling (see Table III-2)

In the same study, Icenhower and London (1997) also determined the partition coefficients of Cl between biotite and the rhyolitic melt ($D^{\text{Bt/m}}_{\text{Cl}}$), which seem also dependent on Mg# values of biotite. The $D^{\text{Bt/m}}_{\text{Cl}}$ determined at Run SM-12 (Icenhower and London 1997) for biotite with Mg# = 0.57 ± 0.02 was 1.22 ± 0.34 , which is applied in this case because the similar Mg# of biotites in GN, PD and CD rocks than the experimental biotite. The results are slightly lower (by <20% relative) than the values calculated according to the models of Webster (1990) and Munoz (1992) (Table III-2), showing good consistency between the two modeling procedures. Additionally, we used the average composition of CD biotites (Table III-2) to examine the concomitant effects of temperature and pressure and the modeling is illustrated as the 3D plot in Fig. III-11b. Accordingly, it is clear that temperature cannot exert an effect on calculated Cl concentration in melt as strong as that on calculated F concentration. However, variation in pressure would strongly change the calculation results with an exponentially growing effect, and the resulted Cl concentration in melt would reach a lowest value at ~ 0.6 kbar (Fig. III-11b). As a result, deviation in the estimation of crystallization pressure of biotite would potentially cause a huge error in the calculated Cl concentration in melt, whereas effect of temperature is negligible.

In summary, if the three types of biotites are assumed to have crystallized at nearly identical temperature and pressure conditions, the silicate melts in equilibrium with them are estimated to have similar Cl concentrations and $\log(\text{Cl}/\text{OH})$. The CD biotites have crystallized in melts with higher F abundance relative to GN and PD biotites, likely indicating input of F-rich melts into the magmatic system (magma mixing) which might derive from biotite-rich crustal rocks (Aoki and Kanisawa 1979).

9.3 Apatite-melt-fluid system

Numerous theoretical and experimental studies have been addressed to investigate the partitioning of F and Cl in apatite-melt-fluid systems (Zhu and Sverjensky 1991, 1992; Piccoli and Candela 1994; Piccoli et al. 1999; Mathez and Webster 2005; Patiño Douce and Roden 2006; Webster et al. 2009b). Assuming that apatite is equilibrated with aqueous fluid in magmatic system, the halogen-hydroxyl exchange reaction is



Because activity coefficients of the three end-members of apatites are nearly 1 at above 500 °C (Tacker and Stormer 1989), the corresponding equilibrium constant for F and Cl can be calculated as

$$K_F = (f_{H_2O}^f / f_{HF}^f) \times (X_{FAp}^{Ap} / X_{HAp}^{Ap}) \quad (44)$$

$$K_{Cl} = (f_{H_2O}^f / f_{HCl}^f) \times (X_{ClAp}^{Ap} / X_{HAp}^{Ap}) \quad (45)$$

in which f_{H_2O} , f_{HF} and f_{HCl} is fugacity of H₂O, HF and HCl in the fluid phase, and X_{FAp}^{Ap} , X_{ClAp}^{Ap} and X_{HAp}^{Ap} is mole fraction of fluorapatite, chlorapatite and hydroxylapatite in apatite (Piccoli and Candela 1994), respectively. Based on the calculation method of Perkins et al. (1987) and the thermodynamic data from Stull and Prophet (1971), Robie et al. (1979) and Zhu and Sverjensky (1991), Piccoli and Candela (1994) calibrated quantitative relations of temperature- and pressure-dependent equilibrium constants and further applied the relations to calculated F and Cl concentrations in melt of apatite-melt-fluid systems. However, as demonstrated by the halogen partitioning experiments of Mathez and Webster (2005) and Webster et al. (2009), the partitioning behavior of F and Cl in apatite-melt-fluid systems varies strongly with different melt composition such as basicity, and thus the equilibrium constants in Eqs (44) and (45) should be also dependent on melt-composition. As a result, the calculation procedure provided by Piccoli and Candela (1994), which is independent of any compositional variable of melt, might not be valid for all circumstances and is thus not utilized in this case study.

Mathez and Webster (2005) experimentally determined the partition coefficients (mass ratios) of F and Cl between apatite and basaltic melt (51.1 wt% SiO₂) as the following empirical relations

$$D_F^{Ap/m} = W_F^{Ap} / W_F^m \approx 3.4 \quad (46)$$

$$D_{Cl}^{Ap/m} = W_{Cl}^{Ap} / W_{Cl}^m \approx 0.8 \quad (47)$$

in which W_F^{Ap} and W_F^m are concentrations (mass fraction) of F in apatite and melt, and W_{Cl}^{Ap} and W_{Cl}^m are concentrations (mass fraction) of Cl in apatite and melt, respectively. These partition coefficients were proposed to be valid for basaltic melts with low Cl concentration (<3.8 wt%) and wide F concentration ranges (Mathez and Webster 2005). Using rhyodacitic melts (70.4 wt% SiO₂), Webster et al. (2009b) experimentally determined the partitioning relations of F and Cl for apatite-melt-

fluid system as follows

$$X_{\text{FAp}}^{\text{Ap}} = 3.02 \times W_{\text{F}}^{\text{m}} + 0.12 \quad (48)$$

$$X_{\text{ClAp}}^{\text{Ap}} = 0.011 \times W_{\text{Cl}}^{\text{f}} \quad (49)$$

where W_{F}^{m} is F concentration (wt%) in melt and W_{Cl}^{f} is Cl concentration (wt%) in fluid, respectively. We can further obtain the corresponding Cl concentration in melt by using Eq (25). It is worthy of noting that the partition coefficient of F in the model of Webster et al. (2009b) is physically unrealistic at very low F concentrations (e.g. $X_{\text{FAp}}^{\text{Ap}} = 0.12$ in F-free melt), but it should be valid for apatite-melt systems with F concentration in melt >300 ppm (Webster et al. 2009b).

Comparing the partitioning models of Mathez and Webster (2005) and Webster et al. (2009b), it is notable that the partitioning behavior of F in apatite-basic melt system is apparently different from that in apatite-acid melt system for a wide range of F concentration in melt (see Fig. 6 of Webster et al. 2009b). Simple mass balance calculation on F indicates that crystallization of small proportions of apatite, amphibole and biotite cannot modify F concentration in melt efficiently, and thus W_{F}^{m} should stay approximately constant within one order of magnitude. Therefore, as the estimated results based on the model of Webster et al. (2009b) correspond well to those calculated from biotite compositions using the model of Munoz (1992) (2000-3000 ppm, Tables III-2~3), these data are supposed to be qualitatively valid to infer F concentration in melt.

The partition coefficient of Cl between apatite and melt tend to be similar with each other assuming that Cl concentration in melt is below 10,000 ppm (Webster et al. 2009b). Consequently, calculated Cl concentrations in melt using these two models should be similar if they are not very high. As shown in Fig. III-12, the resultant estimations of Cl in melt based on the two models do agree well if it is assumed that all types of apatites have been equilibrated or re-equilibrated at ~1.5 kbar in the apatite-melt-fluid system. The value of pressure (1.5 kbar) is slightly different from the experimental pressure (2.0 kbar), and one possible reason is the actual difference in $D_{\text{Cl}}^{\text{Ap/m}}$ for melts of different compositions (see Fig. 4b of Webster et al. 2009b).

Although the differences in molar volume of fluorapatite, chlorapatite and hydroxylapatite are very small and negligible, the partitioning behavior of Cl in the

melt-fluid system is strongly dependent on pressure (Fig. III-11b), thus the Cl partitioning model of Mathez and Webster (2005) calibrated at ~2.0 kbar might cause large errors if it is applied for natural apatite-melt-fluid systems at pressure other than 2.0 kbar. However, when applying Eq (49), the pressure effect of Cl partitioning behavior in melt-fluid system has been involved, and the corresponding estimated Cl concentrations in melt are believed to be valid provided that pressure estimation is reasonable. The estimation results from apatite compositions are summarized in Table III-3, and it is notable that low pressures (1.3 kbar) lead to much higher values of W_{Cl}^m than other estimations assuming high pressures (2.7 and 3.9 kbar). Evaluation on the quality of these estimation results can only be made by accurately determining equilibrium pressures of various apatites, or by comparing these estimations to corresponding values made from amphibole and biotite compositions; the former method is not possible for this case study and the latter method is performed as follows.

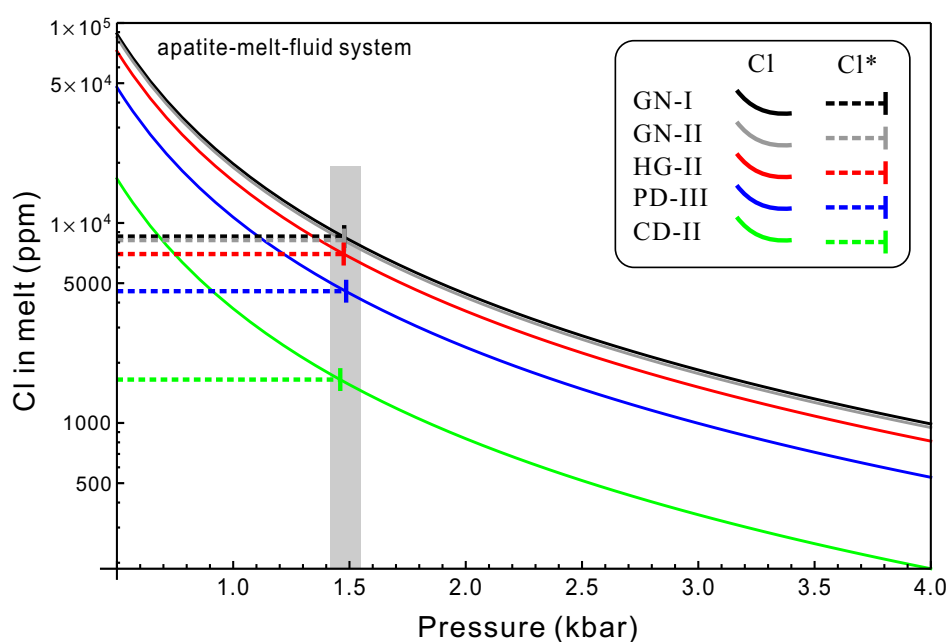


Fig. III-12 Modeling of F and Cl in melt calculated from apatite compositions. Cl (curves) denotes Cl concentration in melt calculated according to the model of Webster et al. (2009) and Shinohara (2009); Cl^* denotes Cl concentrations in melt calculated according to the model of Mathez and Webster (2005)

Estimated Cl concentration in melt from amphiboles, apatites and biotites (Tables 1-3) are illustrated together in Fig. III-13, from which it is notable that the Cl concentrations in melt calculated from GN type-I apatites and HG and CD type-II apatites are in good agreement with those calculated from amphibole and biotite compositions. However, the respective values of W_{Cl}^m calculated from GN type-II

and PD type-III apatites are much higher, which is apparently due to underestimated pressures. We thus propose that, over the course of decompression (crustal uplift and erosion or magma ascent), the apatites in the various types of magmas of the Liujiawa pluton have not been re-equilibrated in terms of volatile contents.

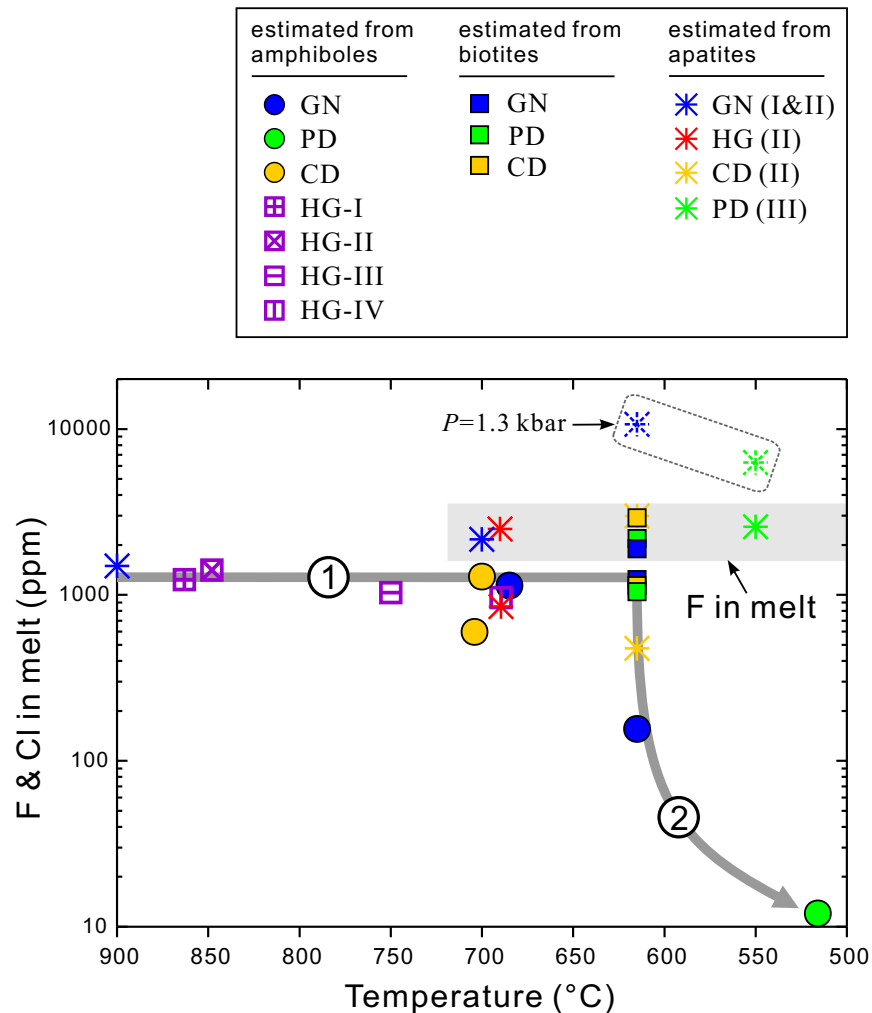


Fig. III-13 Estimated F and Cl concentration in melt versus temperature. Calculation data are summarized in Tables 1-3; note that estimated F concentration in melt from biotites and apatites are concordantly within 2000-3000 ppm (gray zone); type-I apatites of GN are not included because of their unclear equilibrium P-T conditions (see Fig. III-12 and related explanation in text); the upper right dotted asterisks represent data corresponding to low pressure (1.3 kbar) which are supposed to be false due to incorrect pressure estimation; the two processes referring to the variation of Cl concentration in melt refer respectively to: ① closed-system crystallization, and ② fluid exsolution

10 Discussion

10.1 Evolution of F and Cl in melt over the course of crystallization

Based on the above description of distribution and partition relations of F and Cl in magmatic systems involving volatile-containing phases of silicate melt, aqueous fluid and hydrous minerals (amphibole, biotite and apatite), halogen abundance in melts corresponding to different magmatic stages (denoted as temperature) can be quantitatively estimated from compositions of hydrous minerals which have been equilibrated with melt at respective magmatic stages. Combining the calculation results summarized in Tables 1-3, the estimated concentration of F and Cl in melt is illustrated versus temperature in Fig. 13 from which several lines of qualitative features could be observed.

Firstly, the estimated values of W_F^m from GN and PD and HG biotites and/or apatites are concordant with each other within the range of 2000-2500 ppm; the estimated values of W_F^m from CD biotites and apatites are concordant with each other at ~3000 ppm. This could be explained by the fact that silicate melt accommodates F more readily than aqueous fluid at conditions with low F abundance in the system (Fig. III-9b), i.e. $D_F^{f/m} < 1$ (Webster 1990), and thus depression and possible exsolution of aqueous fluid cannot strongly change F concentration in melt.

Second, Cl concentration in melt remains approximately constant at 1000 ppm until crystallization of biotite (at ~615 °C) (process 1 in Fig. III-13), but decreases dramatically to lower temperatures (process 2 in Fig. III-13). Mass balance calculation on Cl in melt-mineral systems indicates that crystallization of apatites, amphiboles and biotites cannot extensively enrich or deplete Cl in the melt, which might explain the constant W_{Cl}^m within a large temperature range. Therefore, process 1 refers to mineral crystallization in closed system (no extraction of fluid). In addition, because the partition coefficient of Cl between aqueous fluid and silicate melt is always larger than 1 (see Eq (25) and related statements), process 2 is thus supposed to refer to exsolution of aqueous fluid which is essentially identical to a shallow volcanic degassing process (Villemant and Boudon 1999; Villemant et al. 2003; Shinohara 2009).

10.2 Partitioning of F in amphibole-melt-fluid system

As described previously, because the partition coefficient of F between fluid and melt is much lower than one for low-F systems and $D_F^{f/m}$ does not increase with

decreasing temperature or pressure, F concentration in melt over the crystallization of apatites and biotites seems to be constant (Fig. III-13). Since amphiboles from the GN, CD and HG rocks could have formed later than apatites and prior to biotites for a given rock type, we suggest that the melts in equilibrium with amphiboles should also contain F with a similar concentration for each rock type. After the pattern of Eq (37), we construct a similar equation to ascribe the partitioning of F between melt and amphibole as

$$\log(\text{F/OH})_{\text{melt}} = \log(\text{F/OH})_{\text{Amp}} + a + b \times \text{Mg\#} \quad (50)$$

in which the effect of temperature is neglected (in fact, the effect of temperature on Cl partitioning might be also negligible, see Sato et al. 2005). Assuming that the average F concentration in melt in equilibrium with GN amphiboles is 2000 ppm, and the averaged F concentration in melt in equilibrium with CD amphiboles is 3000 ppm, the constants in Eq (50) can be calculated, i.e. $a = 0.19$ and $b = -1.00$. The negative value of b is consistent with the proved promoting effect of Mg on F incorporation in amphibole (i.e. Fe-F avoidance). Detailed evaluation on the validity and uncertainty of this apparent F partitioning relation between melt and amphibole cannot be made in this case study, which calls for future experimental investigations. Based on Eq (50), F concentrations in melt corresponding to PD and HG amphiboles are calculated and summarized in Table 1, and the variation exhibits slight decrease of F in melt with decreasing temperature which can be explained by continuous incorporation of F in apatites, amphiboles and biotites over the course of crystallization.

Volatile (H_2O , F and Cl) abundances of melts corresponding to different magmatic stages (indicated by temperature) can be reflected by volatile abundances in hydrous minerals which have been equilibrated with melt at respective magmatic stages. Here, by combining the above estimations based on amphibole, biotite and apatite compositions, we attempted to trace the variations in volatile abundances and ratios over the course of magma crystallization for the Liujiawa pluton. Fig. 10 shows the Cl and F concentrations of melt monitored by amphiboles, biotites and apatites with various formation temperatures decrease systematically with temperature.

10.3 Mixing of high-F and low-F magmas

The clinopyroxene diorites (CD) are suggested to be products of magma

mixing for several petrographical and geochemical evidences. Mafic enclaves compositionally similar to CD have been found in the Liujiawa pluton, which can be explained by mixing of mantle-derived mafic magmas and crust-derived felsic magmas (Zhang et al. 2010, 2011; Zhang et al. in preparation). Clinopyroxenes are present as corroded residues enclosed by amphiboles, indicating strong disequilibrium between clinopyroxene and surrounding silicate melt before the amphiboles formed. As a result, the halogen concentrations of amphiboles and biotites should record this mixing event, which is confirmed by relatively higher F concentrations in amphiboles and biotites compared to other rock types. Our above estimation of W_F^m indicates that these mixed melts originally contain ~3000-4000 ppm F, which is higher than F concentrations of the other melts which originally contain ~2000 ppm F (Tables III-1~3). These high-F magmas might have derived by dehydration melting of biotite-rich crustal rocks (Aoki and Kanisawa 1979).

11 Concluding remarks

Integrating and applying available partitioning models of F and Cl in the system involving silicate melt, aqueous fluid, amphibole, biotite and apatite, halogen concentrations in melt have been reasonably estimated from amphibole, biotite and apatite compositions. Two endmember magmas might have been involved in the formation of the Liujiawa plutonic complex, i.e. low-F mantle-derived and high-F crust-derived magmas respectively. The modeling results indicate that Cl concentration in melt remained nearly constant over the course of crystallization, and decreased dramatically at low temperatures corresponding to fluid exsolution. In contrast, F concentration in melt was not affected by fluid exsolution at late magmatic stages because of the different partitioning behaviors of Cl and F between fluid and melt. Based on the characteristics of F in magmatic systems, the partitioning relation of F between amphibole and melt has been tentatively built, which is qualitatively consistent with Fe-F avoidance but needs further quantitative experimental calibration.

12 Appendix A: Calculation of H₂O species

In this case study, a vapor phase, composed of main H₂O and minor F- and Cl-associated species, is assumed to be present over the courses of crystallization of amphiboles, biotites and apatites, i.e. water-saturated conditions. Thus, the water content in melt is estimated according to the calibration model of water solubility of Holtz et al. (2001):

$$S_{\text{H}_2\text{O}} = 2.859 \times 10^{-2} \times P - 1.495 \times 10^{-3} \times P^{1.5} + 2.702 \times 10^{-5} \times P^2 + 0.257 \times P^{0.5}$$

In this equation, $S_{\text{H}_2\text{O}}$ is water solubility of silicate melt in wt%, and P is pressure in MPa. Although this equation was calibrated upon data of rhyolitic melts at 800 °C (Holtz et al. 2001), it can also provide reasonable estimation for this case because of the following reasons: (1) most amphiboles, biotites and apatites from the Liujiawa pluton have formed later than pyroxene and magnetite, and thus have been in equilibrium with highly evolved melts of silica-rich (andesitic, dacitic or even rhyolitic) compositions; (2) the difference between water solubility values of rhyolitic and andesitic melts are very small at low pressures (Hamilton et al. 1964; Burnham 1979) and (3) the dependence of temperature on water solubility is generally very small and negligible for approximate estimation (Holtz et al. 1995; Holtz et al. 2001). Consequently, we believe that the total H₂O content in melt is equal to $S_{\text{H}_2\text{O}}$ within a relative error of $\pm 10\%$.

Following the works of Stolper (1982) and Zhang (1999), the relation of different species of water in silicate melt is as follows:

$$[\text{H}_2\text{O}_t] = (C/18)/(C/18 + (1-C)/W)$$

$$[\text{H}_2\text{O}_t] = [\text{H}_2\text{O}_m] + [\text{OH}]/2$$

$$[\text{O}] + [\text{H}_2\text{O}_m] + [\text{OH}] = 1$$

$$K = [\text{OH}]^2/([\text{H}_2\text{O}_m] \times [\text{O}])$$

In the above equations, $[\text{H}_2\text{O}_t]$, $[\text{H}_2\text{O}_m]$, $[\text{OH}]$ and $[\text{O}]$ are the mole fractions of total H₂O, molecular H₂O, OH group (not bonded with H) and bridging O atom, C is the mass fraction of total H₂O, and W is the molar mass of dry silicate melt. Here a unique value of W (32.5 g/mol) is used for simplicity. Nowak and Behrens (2001) experimental determined K as

$$K = 27.98 \times e^{-4210/T}$$

By solving these equations, we obtain

$$[\text{OH}] = 2a + \left(8a + K - 2aK + \sqrt{K} \times \sqrt{16a - 16a^2 + K - 4aK + 4a^2K}\right)/(K - 4)$$

in which a denotes $[H_2O]$. As a result, $[OH]$ can be calculated from mass fraction of total water in silicate melt.

13 Appendix B: Estimation of C_K/C_{Na} in melt

The molar ratios of K/Na (C_K/C_{Na}) of the melts which are supposed to have been equilibrated with biotites, are estimated by subtracting the minerals phases which crystallized prior to them from the bulk rock composition. As stated previously concerning estimation of crystallization conditions, biotites in the GN, PD and CD rocks crystallized later than most pyroxene and amphibole and part of plagioclase. Accordingly, respective bulk rock composition subtracting these mineral phases is supposed to approximate the melt composition, i.e. C_K/C_{Na} . K-feldspars are proposed to have crystallized simultaneously with, or later than biotites. In addition, accessory minerals, such as magnetite, titanite and apatite, do not contain notable K or Na, and thus the effects of their crystallization on melt compositions are neglected. The calculation is summarized in Supplementary Table 5, and the values of C_K/C_{Na} are estimated to be ~ 0.8 , ~ 0.65 and ~ 0.65 for melts which have been equilibrated with biotites in GN, PD and CD rocks, respectively.

14 References

- Aiuppa A, Baker DR, Webster JD (2009) Halogens in volcanic systems. *Chem Geol* 263:1-18
- Andersen D, Lindsley D, Davidson P (1993) QUILF: A pascal program to assess equilibria among Fe-Mg-Mn-Ti oxides, pyroxenes, olivine, and quartz. *Comp Geosci* 19:1333-1350
- Anderson JL, Smith DR (1995) The effects of temperature and fO_2 on the Al-in-hornblende barometer. *Am Mineral* 80:549-559
- Antignano A, Manning CE (2008) Fluorapatite solubility in H_2O and H_2O -NaCl at 700 to 900 °C and 0.7 to 2.0 GPa. *Chem Geol* 251:112-119
- Aoki K-I, Kanisawa S (1979) Fluorine contents of some hydrous minerals derived from upper mantle and lower crust. *Lithos* 12:167-171
- Baker DR, Watson EB (1988) Diffusion of major and trace elements in compositionally complex Cl- and F-bearing silicate melts. *Journal of Non-Crystalline Solids* 102:62-70
- Balcone-Boissard H, Villemant B, Boudon G (2010) Behavior of halogens during the degassing of felsic magmas. *Geochem Geophys Geosyst* 11:Q09005
- Bartels A, Vetere F, Holtz F, Behrens H, Linnen R (2011) Viscosity of flux-rich pegmatitic melts. *Contrib Mineral Petrol* 162:51-60
- Berndt J, Koepke J, Holtz F (2005) An Experimental Investigation of the Influence of Water and Oxygen Fugacity on Differentiation of MORB at 200 MPa. *J Petrol* 46:135-167
- Blundy JD, Holland TJB (1992) "Calcic amphibole equilibria and a new amphibole-plagioclase geothermometer": Reply to the comments of Hammarstrom and Zen, and Rutherford and Johnson. *Contrib Mineral Petrol* 111:269-272
- Botcharnikov RE, Linnen RL, Holtz F (2010) Solubility of Au in Cl- and S-bearing hydrous silicate melts. *Geochim Cosmochim Acta* 74:2396-2411
- Boyce J, Hervig R (2009) Apatite as a monitor of late-stage magmatic processes at Volcán Irazú, Costa Rica. *Contrib Mineral Petrol* 157:135-145
- Boyce JW, Liu Y, Rossman GR, Guan Y, Eiler JM, Stolper EM, Taylor LA (2010) Lunar apatite with terrestrial volatile abundances. *Nature* 466:466-469
- Brenan J (1994) Kinetics of fluorine, chlorine and hydroxyl exchange in fluorapatite. *Chem Geol* 110:195-210

- Brenan JM (1993) Partitioning of fluorine and chlorine between apatite and aqueous fluids at high pressure and temperature: implications for the F and Cl content of highP-T fluids. *Earth Planet Sci Lett* 117:251-263
- Bucher K, Stober I (2010) Fluids in the upper continental crust. *Geofluids* 10:241-253
- Burnham CW (1979) The importance of volatile constituents. In: Yoder HS (ed) *The evolution of the igneous rocks*, Princeton University Press, Princeton, pp 439-482
- Chevychelov V, Botcharnikov R, Holtz F (2008) Experimental study of fluorine and chlorine contents in mica (biotite) and their partitioning between mica, phonolite melt, and fluid. *Geochemistry International* 46:1081-1089
- Coulson I, Dipple G, Raudsepp M (2001) Evolution of HF and HCl activity in magmatic volatiles of the gold-mineralized Emerald Lake pluton, Yukon Territory, Canada. *Miner Deposita* 36:594-606
- Dilles JH (1987) Petrology of the Yerington Batholith, Nevada; evidence for evolution of porphyry copper ore fluids. *Econ Geol* 82:1750-1789
- Dingwell DB, Hess KU (1998) Melt viscosities in the system Na-Fe-Si-O-F-Cl; contrasting effects of F and Cl in alkaline melts. *Am Mineral* 83:1016-1021
- Dingwell DB, Scarfe CM, Cronin DJ (1985) The effect of fluorine on viscosities in the system Na₂O-Al₂O₃-SiO₂; implications for phonolites, trachytes and rhyolites. *Am Mineral* 70:80-87
- Dong P (2005) Halogen-element (F, Cl, and Br) behaviour in apatites, scapolite, and sodalite: an experimental investigation with field applications. Ph.D. thesis, University of Saskatchewan, pp 234, Saskatoon
- Edgar AD, Arima M (1985) Fluorine and chlorine contents of phlogopites crystallized from ultrapotassic rock compositions in high pressure experiments; implication for halogen reservoirs in source regions. *Am Mineral* 70:529
- Enami M, Liou JG, Bird DK (1992) Cl-bearing amphibole in the Salton Sea geothermal system, California. *Can Mineral* 30:1077-1092
- Ernst WG, Liu J (1998) Experimental phase-equilibrium study of Al- and Ti-contents of calcic amphibole in MORB—a semiquantitative thermobarometer. *Am Mineral* 83:952-969
- Feig S, Koepke J, Snow J (2006) Effect of water on tholeiitic basalt phase equilibria: an experimental study under oxidizing conditions. *Contrib Mineral Petrol* 152:611-638
- Filiberto J, Treiman AH (2009a) The effect of chlorine on the liquidus of basalt: First results and implications for basalt genesis on Mars and Earth. *Chem Geol* 263:60-68
- Filiberto J, Treiman AH (2009b) Martian magmas contained abundant chlorine, but little water. *Geology* 37:1087-1090
- Finch AA, Parsons I, Mingard SC (1995) Biotites as indicators of fluorine fugacities in late-stage magmatic fluids: The Gardar Province of South Greenland. *J Petrol* 36:1701-1728
- Foley SF, Taylor WR, Green DH (1986) The effect of fluorine on phase relationships in the system KAlSiO₄-Mg₂SiO₄-SiO₂ at 28 kbar and the solution mechanism of fluorine in silicate melts. *Contrib Mineral Petrol* 93:46-55
- Frank MR, Candela PA, Piccoli PM (2003) Alkali exchange equilibria between a silicate melt and coexisting magmatic volatile phase: an experimental study at 800°C and 100 MPa. *Geochim Cosmochim Acta* 67:1415-1427
- Fuge R (1977) On the behaviour of fluorine and chlorine during magmatic differentiation. *Contrib Mineral Petrol* 61:245-249
- Hamilton D, Burnham CW, Osborn E (1964) The solubility of water and effects of oxygen fugacity and water content on crystallization in mafic magmas. *J Petrol* 5:21
- Hammarstrom JM, Zen E-a (1986) Aluminum in hornblende; an empirical igneous geobarometer. *Am Mineral* 71:1297-1313
- Harlov DE, Förster HJ (2002) High-grade fluid metasomatism on both a local and a regional scale: the Seward peninsula, Alaska, and the Val Strona di Omegna, Ivrea-Verbano Zone, Northern Italy. Part I: Petrography and silicate mineral chemistry. *J Petrol* 43:769-799
- Harris D, Anderson A (1984) Volatiles H₂O, CO₂, and Cl in a subduction related basalt. *Contrib Mineral Petrol* 87:120-128
- Harrison TM, Watson EB (1984) The behavior of apatite during crustal anatexis: Equilibrium and kinetic considerations. *Geochim Cosmochim Acta* 48:1467-1477
- Henderson CE (2011) *Protocols and Pitfalls of Electron Microprobe Analysis of Apatite*. Master Thesis, University of Michigan, pp 68, Michigan
- Holland HD (1972) Granites, Solutions, and Base Metal Deposits. *Econ Geol* 67:281-301
- Holland T, Blundy J (1994) Non-ideal interactions in calcic amphiboles and their bearing on amphibole-plagioclase thermometry. *Contrib Mineral Petrol* 116:433-447
- Hollister LS, Grissom GC, Peters EK, Stowell HH, Sisson VB (1987) Confirmation of the empirical

- correlation of Al in hornblende with pressure of solidification of calc-alkaline plutons. *Am Mineral* 72:231-239
- Holtz F, Behrens H, Dingwell DB, Johannes W (1995) H₂O solubility in haplogranitic melts: Compositional, pressure, and temperature dependence. *Am Mineral* 80:94-108
- Holtz F, Dingwell DB, Behrens H (1993) Effects of F, B₂O₃ and P₂O₅ on the solubility of water in haplogranite melts compared to natural silicate melts. *Contrib Mineral Petrol* 113:492-501
- Holtz F, Johannes W, Tamic N, Behrens H (2001) Maximum and minimum water contents of granitic melts generated in the crust: A reevaluation and implications. *Lithos* 56:1-14
- Hovis GL, Harlov DE (2010) Solution calorimetric investigation of fluor-chlorapatite crystalline solutions. *Am Mineral* 95:946-952
- Hu X, Bi X, Shang L, Hu R, Cai G, Chen Y (2009) An experimental study of tin partition between melt and aqueous fluid in F/Cl-coexisting magma. *Chin Sci Bull* 54:1087-1097
- Huang F, Li SG, Dong F, He YS, Chen FK (2008) High-Mg adakitic rocks in the Dabie orogen, central China: Implications for foundering mechanism of lower continental crust. *Chem Geol* 255:1-13
- Huang F, Li SG, Dong F, Li QL, Chen FK, Wang Y, Yang W (2007) Recycling of deeply subducted continental crust in the Dabie Mountains, central China. *Lithos* 96:151-169
- Humphreys MCS, Edmonds M, Christopher T, Hards V (2009) Chlorine variations in the magma of Soufrière Hills Volcano, Montserrat: Insights from Cl in hornblende and melt inclusions. *Geochim Cosmochim Acta* 73:5693-5708
- Icenhower JP, London D (1997) Partitioning of fluorine and chlorine between biotite and granitic melt: experimental calibration at 200 MPa H₂O. *Contrib Mineral Petrol* 127:17-29
- Jahn BM, Wu FY, Lo CH, Tsai CH (1999) Crust-mantle interaction induced by deep subduction of the continental crust: Geochemical and Sr-Nd isotopic evidence from post-collisional mafic-ultramafic intrusions of the northern Dabie complex, central China. *Chem Geol* 157:119-146
- Johnson ER, Wallace PJ, Delgado Granados H, Manea VC, Kent AJR, Bindeman IN, Donegan CS (2009) Subduction-related volatile recycling and magma generation beneath central Mexico: Insights from melt inclusions, oxygen isotopes and geodynamic models. *J Petrol* 50:1729
- Johnson MC, Rutherford MJ (1989) Experimental calibration of the aluminum-in-hornblende geobarometer with application to Long Valley caldera (California) volcanic rocks. *Geology* 17:837-841
- Keppeler H (1993) Influence of fluorine on the enrichment of high field strength trace elements in granitic rocks. *Contrib Mineral Petrol* 114:479-488
- Keppeler H, Wyllie PJ (1991) Partitioning of Cu, Sn, Mo, W, U, and Th between melt and aqueous fluid in the systems haplogranite-H₂O-HCl and haplogranite-H₂O-HF. *Contrib Mineral Petrol* 109:139-150
- Kilinc IA, Burnham CW (1972) Partitioning of Chloride Between a Silicate Melt and Coexisting Aqueous Phase from 2 to 8 Kilobars. *Econ Geol* 67:231-235
- Konzett J, Rhede D, Frost D (2011) The high PT stability of apatite and Cl partitioning between apatite and hydrous potassic phases in peridotite: an experimental study to 19 GPa with implications for the transport of P, Cl and K in the upper mantle. *Contrib Mineral Petrol*:1-20
- Lassiter JC, Hauri EH, Nikogosian IK, Barszczus HG (2002) Chlorine-potassium variations in melt inclusions from Raivavae and Rapa, Austral Islands: constraints on chlorine recycling in the mantle and evidence for brine-induced melting of oceanic crust. *Earth Planet Sci Lett* 202:525-540
- Leake BE, Woolley AR, Arps CES et al. (1997) Nomenclature of amphiboles: Report of the Subcommittee on Amphiboles of the International Mineralogical Association, Commission on New Minerals and Mineral Names. *Am Mineral* 82:1019-1037
- Leger A, Rebbert C, Webster J (1996) Cl-rich biotite and amphibole from Black Rock forest, Cornwall, New York. *Am Mineral* 81:495-504
- Li S, Hart S, Zheng S, Liu D, Zhang G, Guo A (1989) Timing of collision between the north and south China blocks-The Sm-Nd isotopic age evidence. *Sci China Ser B* 32:1393-1400
- Li SG, Huang F, Li H (2002) Post-collisional lithosphere delamination of the Dabie-Sulu orogen. *Chin Sci Bull* 47:259-263
- London D (1997) Estimating Abundances of Volatile and Other Mobile Components in Evolved Silicic Melts Through Mineral-Melt Equilibria. *J Petrol* 38:1691-1706
- Ma CQ, Li ZC, Ehlers C, Yang KG, Wang RJ (1998) A post-collisional magmatic plumbing system: Mesozoic granitoid plutons from the Dabieshan high-pressure and ultrahigh-pressure metamorphic zone, east-central China. *Lithos* 45:431-456
- Ma CQ, Yang KG, Ming HL, Lin GC (2004) The timing of tectonic transition from compression to extension in Dabieshan: Evidence from Mesozoic granites. *Sci China Ser D* 47:453-462

- Makino K, Tomita K, Suwa K (1993) Effect of chlorine on the crystal structure of a chlorine-rich hastingsite. *Mineral Mag* 57:677-685
- Markl G, Piazzolo S (1998) Halogen-bearing minerals in syenites and high-grade marbles of Dronning Maud Land, Antarctica: monitors of fluid compositional changes during late-magmatic fluid-rock interaction processes. *Contrib Mineral Petrol* 132:246-268
- Mason RA (1992) Models of order and iron-fluorine avoidance in biotite. *Can Mineral* 30:343-354
- Mathez EA, Webster JD (2005) Partitioning behavior of chlorine and fluorine in the system apatite-silicate melt-fluid. *Geochim Cosmochim Acta* 69:1275-1286
- McCubbin FM, Steele A, Hauri EH, Nekvasil H, Yamashita S, Hemley RJ (2010a) Nominally hydrous magmatism on the Moon. *Proc Natl Acad Sci* 107:11223-11228
- McCubbin FM, Steele A, Nekvasil H, Schnieders A, Rose T, Fries M, Carpenter PK, Jolliff BL (2010b) Detection of structurally bound hydroxyl in fluorapatite from Apollo Mare basalt 15058,128 using TOF-SIMS. *Am Mineral* 95:1141-1150
- Morrison J (1991) Compositional constraints on the incorporation of Cl into amphiboles. *Am Mineral* 76:1920-1930
- Munoz J (1992) Calculation of HF and HCl fugacities from biotite compositions: revised equations. In, vol 26. Geological Society of America, Abstracts with Programs, p A221
- Munoz JL (1984) F-OH and Cl-OH exchange in micas with applications to hydrothermal ore deposits. *Rev Mineral* 13:469-493
- Mysen BO, Acton M (1999) Water in H₂O-saturated magma–fluid systems: solubility behavior in K₂O–Al₂O₃–SiO₂–H₂O to 2.0 GPa and 1300°C. *Geochim Cosmochim Acta* 63:3799-3815
- Nash WP (1976) Fluorine, chlorine, and OH-bearing minerals in the Skaergaard Intrusion. *Am J Sci* 276:546-556
- Nowak M, Behrens H (2001) Water in rhyolitic magmas: getting a grip on a slippery problem. *Earth Planet Sci Lett* 184:515-522
- O'Reilly SY, Griffin WL (2000) Apatite in the mantle: implications for metasomatic processes and high heat production in Phanerozoic mantle. *Lithos* 53:217-232
- Oberti R, Ungaretti L, Cannillo E, Hawthorne FC (1993) The mechanism of Cl incorporation in amphibole. *Am Mineral* 78:746-752
- Pan Y, Dong P (1999) The Lower Changjiang (Yangzi/Yangtze River) metallogenic belt, east central China: intrusion-and wall rock-hosted Cu-Fe-Au, Mo, Zn, Pb, Ag deposits. *Ore Geol Rev* 15:177-242
- Patiño Douce AE, Roden M (2006) Apatite as a probe of halogen and water fugacities in the terrestrial planets. *Geochim Cosmochim Acta* 70:3173-3196
- Patiño Douce AE, Roden MF, Chaumba J, Fleisher C, Yogodzinski G (2011) Compositional variability of terrestrial mantle apatites, thermodynamic modeling of apatite volatile contents, and the halogen and water budgets of planetary mantles. *Chem Geol* 288:14-31
- Perkins D, Essene EJ, Wall VJ (1987) THERMO: a computer program for calculation of mixed-volatile equilibria. *Am Mineral* 72:446-447
- Piccoli P, Candela P (1994) Apatite in felsic rocks: A model for the estimation of initial halogen concentrations in the Bishop Tuff (Long Valley) and Tuolumne Intrusive Suite (Sierra Nevada Batholith) magmas. *Am J Sci* 294:92-135
- Piccoli P, Candela P, Williams T (1999) Estimation of aqueous HCl and Cl concentrations in felsic systems. *Lithos* 46:591-604
- Piccoli PM, Candela PA (2002) Apatite in Igneous Systems. *Rev Mineral Geochem* 48:255-292
- Pouchou JL, Pichoir F (1991) Quantitative analysis of homogeneous or stratified microvolumes applying the model "PAP". In: Heinrich, Newbury (eds) *Electron probe quantitation*, Plenum Press, New York, pp 31-75
- Pyle JM, Spear FS, Wark DA (2002) Electron Microprobe Analysis of REE in Apatite, Monazite and Xenotime: Protocols and Pitfalls. *Rev Mineral Geochem* 48:337-362
- Rieder M, Cavazzini G, D'yakonov YS et al. (1998) Nomenclature of the micas. *Clays and Clay Minerals* 46:586-595
- Robie RA, Hemingway BS, Fisher JR (1979) Thermodynamic properties of minerals and related substances at 298.15 K and 1 bar (10⁵ pascals) pressure and at higher temperatures. *US Geological Survey Bulletin* 1452:456
- Rubenach MJ (2005) Relative timing of albitization and chlorine enrichment in biotite in proterozoic schists, snake creek anticline, Mount Isa Inlier, Northeastern Australia. *Can Mineral* 43:349-366
- Sato H, Holtz F, Behrens H, Botcharnikov R, Nakada S (2005) Experimental Petrology of the 1991–1995 Unzen Dacite, Japan. Part II: Cl/OH Partitioning between Hornblende and Melt and its Implications for the Origin of Oscillatory Zoning of Hornblende Phenocrysts. *J Petrol* 46:339-

- Sato H, Yamaguchi Y, Makino K (1997) Cl incorporation into successively zoned amphiboles from the Ramnes cauldron, Norway. *Am Mineral* 82:316-324
- Schaller T, Dingwell DB, Keppler H, Knoller W, Merwin L, Sebald A (1992) Fluorine in silicate glasses: A multinuclear nuclear magnetic resonance study. *Geochim Cosmochim Acta* 56:701-707
- Schmidt MW (1992) Amphibole composition in tonalite as a function of pressure: an experimental calibration of the Al-in-hornblende barometer. *Contrib Mineral Petrol* 110:304-310
- Selby D, Nesbitt BE (2000) Chemical composition of biotite from the Casino porphyry Cu-Au-Mo mineralization, Yukon, Canada: evaluation of magmatic and hydrothermal fluid chemistry. *Chem Geol* 171:77-93
- Shinohara H (1987) Partition of chlorine compounds in the system silicate melt and hydrothermal solutions. PhD thesis, Tokyo Institute of Technology, pp 192, Tokyo
- Shinohara H (1994) Exsolution of immiscible vapor and liquid phases from a crystallizing silicate melt: Implications for chlorine and metal transport. *Geochim Cosmochim Acta* 58:5215-5221
- Shinohara H (2009) A missing link between volcanic degassing and experimental studies on chloride partitioning. *Chem Geol* 263:51-59
- Shinohara H, Fujimoto K (1994) Experimental study in the system albite-andalusite-quartz-NaCl-HCl-H₂O at 600°C and 400 to 2000 bars. *Geochim Cosmochim Acta* 58:4857-4866
- Shinohara H, Iiyama JT, Matsuo S (1989) Partition of chlorine compounds between silicate melt and hydrothermal solutions: I. Partition of NaCl-KCl. *Geochim Cosmochim Acta* 53:2617-2630
- Signorelli S, Carroll MR (2000) Solubility and fluid-melt partitioning of Cl in hydrous phonolitic melts. *Geochim Cosmochim Acta* 64:2851-2862
- Simon AC, Pettke T, Candela PA, Piccoli PM, Heinrich CA (2004) Magnetite solubility and iron transport in magmatic-hydrothermal environments. *Geochim Cosmochim Acta* 68:4905-4914
- Sisson TW, Grove TL (1993) Experimental investigations of the role of H₂O in calc-alkaline differentiation and subduction zone magmatism. *Contrib Mineral Petrol* 113:143-166
- Spear FS (1981) An experimental study of hornblende stability and compositional variability in amphibolite. *Am J Sci* 281:697-734
- Stolper E (1982) The speciation of water in silicate melts. *Geochim Cosmochim Acta* 46:2609-2620
- Stormer JC, Pierson ML, Tacker RC (1993) Variation of F and Cl X-ray intensity due to anisotropic diffusion in apatite during electron microprobe analysis. *Am Mineral* 78:641-648
- Straub SM, Layne GD (2003) The systematics of chlorine, fluorine, and water in Izu arc front volcanic rocks: Implications for volatile recycling in subduction zones. *Geochim Cosmochim Acta* 67:4179-4203
- Stroncik NA, Haase KM (2004) Chlorine in oceanic intraplate basalts: Constraints on mantle sources and recycling processes. *Geology* 32:945-948
- Student JJ, Bodnar RJ (1999) Synthetic Fluid Inclusions XIV: Coexisting Silicate Melt and Aqueous Fluid Inclusions in the Haplogranite-H₂O-NaCl-KCl System. *J Petrol* 40:1509-1525
- Stull DR, Prophet H (1971) JANAF Thermochemical Tables. National standard Reference Data Service, US National Bureau of Standards 37:220
- Sun W, Binns R, Fan A, Kamenetsky V, Wysoczanski R, Wei G, Hu Y, Arculus R (2007) Chlorine in submarine volcanic glasses from the eastern Manus basin. *Geochim Cosmochim Acta* 71:1542-1552
- Symonds RB, Rose WI, Bluth GJS, Gerlach TM (1994) Volcanic-gas studies; methods, results, and applications. *Rev Mineral Geochem* 30:1-66
- Symonds RB, Rose WI, Reed MH (1988) Contributions of Cl- and F-bearing gases to the atmosphere by volcanoes. *Nature* 334:415-418
- Tacker RC, Stormer JC (1989) A thermodynamic model for apatite solid solutions, applicable to high-temperature geologic problems. *Am Mineral* 74:877-888
- Tsai CH, Lo CH, Liou JG, Jahn BM (2000) Evidence against subduction-related magmatism for the Jiaoziyuan Gabbro, northern Dabie Shan, China. *Geology* 28:943-946
- Ustunisik G, Nekvasil H, Lindsley D (2011) Differential degassing of H₂O, Cl, F, and S: Potential effects on lunar apatite. *Am Mineral* 96:1650-1653
- Vanko DA (1986) High-chlorine amphiboles from oceanic rocks: product of highly-saline hydrothermal fluids? *Am Mineral* 71:51-59
- Villemant B, Boudon G, Nougirgat S, Poteaux S, Michel A (2003) Water and halogens in volcanic clasts: tracers of degassing processes during Plinian and dome-building eruptions. Geological Society, London, Special Publications 213:63-79
- Villemant Bt, Boudon G (1999) H₂O and halogen (F, Cl, Br) behaviour during shallow magma

- degassing processes. *Earth Planet Sci Lett* 168:271-286
- Volfinger M, Robert JL, Vielzeuf D, Neiva AMR (1985) Structural control of the chlorine content of OH-bearing silicates (micas and amphiboles). *Geochim Cosmochim Acta* 49:37-48
- Wallace PJ (2005) Volatiles in subduction zone magmas: concentrations and fluxes based on melt inclusion and volcanic gas data. *J Volcan Geotherm Res* 140:217-240
- Wang KL, Zhang Y, Naab FU (2011) Calibration for IR measurements of OH in apatite. *Am Mineral* 96:1392-1397
- Wang YJ, Fan WM, Peng TP, Zhang HF, Guo F (2005) Nature of the Mesozoic lithospheric mantle and tectonic decoupling beneath the Dabie Orogen, Central China: Evidence from Ar-40/Ar-39 geochronology, elemental and Sr-Nd-Pb isotopic compositions of early Cretaceous mafic igneous rocks. *Chem Geol* 220:165-189
- Webster J, Holloway JR (1990) Partitioning of F and Cl between magmatic hydrothermal fluids and highly evolved granitic magmas. In: Stein HJ, Hannah JL (eds) *Ore-bearing Granitic Systems: Petrogenesis and mineralizing processes*, Geological Society of America Special Paper, pp 21-34
- Webster JD (1990) Partitioning of F between H₂O and CO₂ fluids and topaz rhyolite melt. *Contrib Mineral Petrol* 104:424-438
- Webster JD (1992a) Fluid-melt interactions involving Cl-rich granites: Experimental study from 2 to 8 kbar. *Geochim Cosmochim Acta* 56:659-678
- Webster JD (1992b) Water solubility and chlorine partitioning in Cl-rich granitic systems: Effects of melt composition at 2 kbar and 800°C. *Geochim Cosmochim Acta* 56:679-687
- Webster JD (1997a) Chloride solubility in felsic melts and the role of chloride in magmatic degassing. *J Petrol* 38:1793-1807
- Webster JD (1997b) Exsolution of magmatic volatile phases from Cl-enriched mineralizing granitic magmas and implications for ore metal transport. *Geochim Cosmochim Acta* 61:1017-1029
- Webster JD (2004) The exsolution of magmatic hydrosaline chloride liquids. *Chem Geol* 210:33-48
- Webster JD (2006) *Melt Inclusions in Plutonic Rocks*. The Mineralogical Association of Canada, Québec
- Webster JD, Holloway JR (1988) Experimental constraints on the partitioning of Cl between topaz rhyolite melt and H₂O and H₂O + CO₂ fluids: New implications for granitic differentiation and ore deposition. *Geochim Cosmochim Acta* 52:2091-2105
- Webster JD, Holloway JR, Hervig RL (1989) Partitioning of lithophile trace elements between H₂O and H₂O + CO₂ fluids and topaz rhyolite melt. *Econ Geol* 84:116-134
- Webster JD, Kinzler RJ, Mathez EA (1999) Chloride and water solubility in basalt and andesite melts and implications for magmatic degassing. *Geochim Cosmochim Acta* 63:729-738
- Webster JD, Rebbert CR (1998) Experimental investigation of H₂O and Cl- solubilities in F-enriched silicate liquids; implications for volatile saturation of topaz rhyolite magmas. *Contrib Mineral Petrol* 132:198-207
- Webster JD, Sintoni MF, De Vivo B (2009a) The partitioning behavior of Cl, S, and H₂O in aqueous vapor- ±saline-liquid saturated phonolitic and trachytic melts at 200 MPa. *Chem Geol* 263:19-36
- Webster JD, Tappen CM, Mandeville CW (2009b) Partitioning behavior of chlorine and fluorine in the system apatite-melt-fluid. II: Felsic silicate systems at 200 MPa. *Geochim Cosmochim Acta* 73:559-581
- Xiao Y, Hoefs J, Kronz A (2005) Compositionally zoned Cl-rich amphiboles from North Dabie Shan, China: monitor of high-pressure metamorphic fluid/rock interaction processes. *Lithos* 81:279-295
- Yang X-M, Lentz D (2005) Chemical composition of rock-forming minerals in gold-related granitoid intrusions, southwestern New Brunswick, Canada: implications for crystallization conditions, volatile exsolution, and fluorine-chlorine activity. *Contrib Mineral Petrol* 150:287-305
- Yardley BWD (2005) Metal Concentrations in Crustal Fluids and Their Relationship to Ore Formation. *Econ Geol* 100:613-632
- Yoder HS, Tilley CE (1962) Origin of Basalt Magmas: An Experimental Study of Natural and Synthetic Rock Systems. *J Petrol* 3:342-532
- Young EJ, Myers AT, Munson EL, Conklin NM (1969) Mineralogy and geochemistry of fluorapatite from Cerro de Mercado, Durango, Mexico. US Geological Survey of Professional Paper 650-D:D84-D93
- Zhang C, Ma C, Holtz F (2010) Origin of high-Mg adakitic magmatic enclaves from the Meichuan pluton, southern Dabie orogen (central China): Implications for delamination of the lower continental crust and melt-mantle interaction. *Lithos* 119:467-484
- Zhang C, Ma C, Holtz F (2011) "Origin of high-Mg adakitic magmatic enclaves from the Meichuan pluton, southern Dabie orogen (central China): Implications for delamination of the lower continental crust and melt-mantle interaction" - Reply. *Lithos* 125:839-844

- Zhang C, Ma CQ (2008) Large-scale late Mesozoic magmatism in the Dabie Mountain: Constraints from zircon U-Pb dating and Hf isotopes. *J Mineral Petrol* 28:71-79
- Zhang RY, Liou JG, Ernst WG (2009) The Dabie-Sulu continental collision zone: A comprehensive review. *Gond Res* 16:1-26
- Zhang Y (1999) H₂O in rhyolitic glasses and melts: Measurement, speciation, solubility, and diffusion. *Rev Geophys* 37:493-516
- Zhu C, Sverjensky DA (1991) Partitioning of F-Cl-OH between minerals and hydrothermal fluids. *Geochim Cosmochim Acta* 55:1837-1858
- Zhu C, Sverjensky DA (1992) F-Cl-OH partitioning between biotite and apatite. *Geochim Cosmochim Acta* 56:3435-3467

Table III-1 Estimation of crystallization conditions of amphibole and volatile contents of coexisting melt

| Type* | Amphibole | | | | | | Plagioclase** | | Melt | | | | | | | | | |
|--------|----------------------|-------------|---------------------|------|---|------------|---------------|-----------|------------|--------|--------|------------------|----------------------------|----------------|------------------------|--------------|-------------|-----------------------|
| | Σ Al (gfu) | Ti (gfu) | Σ A (gfu) | Mg# | Fe ³⁺ / (Fe ²⁺ +Fe ³⁺) | F (ppm) | Cl (ppm) | log(F/OH) | log(Cl/OH) | An (%) | T(°C)† | P (kbar)‡ | H ₂ O§ (wt%) | OH (mol%) | log(Cl/OH)// (mol%) | Cl (mol%) | Cl (ppm) | F \diamond (ppm) |
| GN-1 | 1.46 | 0.11 | 0.32 | 0.60 | 0.31 | 3710 | 890 | -1.02 | -1.91 | 30 | 685 | 3.9 ^a | 8.8 | 14.5 | -2.17 | 0.097 | 1141 | 2000 ^a |
| GN-2 | 0.45 | 0.05 | 0.06 | 0.70 | 0.05 | 2870 | 230 | -1.15 | -2.52 | 30 | 615 | 1.3 ^c | 4.9 | 9.1 | -2.82 | 0.014 | 156 | 2000 ^a |
| PD | 0.21 | 0.02 | 0.05 | 0.71 | 0.06 | 3040 | 40 | -1.14 | -3.29 | 30 | 516 | 1.3 ^c | 4.9 | 7.6 | -3.86 | 0.001 | 12 | 1030 ^b |
| CD-1 | 1.17 | 0.14 | 0.37 | 0.62 | 0.16 | 4590 | 490 | -0.92 | -2.17 | 25 | 700 | 2.6 ^b | 7.1 | 12.9 | -2.10 | 0.104 | 1195 | 3000 ^a |
| CD-2 | 0.91 | 0.10 | 0.32 | 0.66 | 0.16 | 4430 | 460 | -0.94 | -2.19 | 25 | 704 | 1.3 ^b | 4.9 | 10.8 | -2.31 | 0.053 | 599 | 3000 ^a |
| HG-I | 2.07 | 0.32 | 0.64 | 0.64 | 0.17 | 3330 | 200 | -1.07 | -2.59 | 55 | 863 | 6.8 ^b | 12.2 | 21.2 | -2.31 | 0.103 | 1236 | 4110 ^b |
| HG-II | 2.00 | 0.32 | 0.64 | 0.59 | 0.14 | 3120 | 310 | -1.10 | -2.38 | 45 | 848 | 6.5 ^b | 11.8 | 20.2 | -2.23 | 0.118 | 1411 | 4180 ^b |
| HG-III | 1.46 | 0.21 | 0.46 | 0.64 | 0.15 | 3040 | 490 | -1.11 | -2.18 | 35 | 750 | 3.9 ^b | 8.9 | 15.8 | -2.25 | 0.088 | 1034 | 2920 ^b |
| HG-IV | 0.98 | 0.05 | 0.25 | 0.67 | 0.21 | 2790 | 800 | -1.16 | -1.97 | 30 | 690 | 1.7 ^b | 5.6 | 11.3 | -2.14 | 0.081 | 926 | 1660 ^b |

* For the amphiboles from gabbro (GN) and clinopyroxene diorite (CD), the two types represent respective compositions with highest and lowest Al₂O₃ contents (indicating the highest and lowest temperature); for the amphiboles from two-pyroxene diorite (PD) and the four types of hornblende gabbro (HG), respective average values are used; see text and Fig. III-6 for explanation of the amphibole types;

** Plagioclase with different An content (Supplementary Fig. III-3) is proposed to correspond to a respective amphibole type; † Temperature calculated applying the thermometer of Holland and Blundy (1994) and the correspondingly pressure values;

‡ Pressure estimated according to *a*) Anderson and Smith (1995), *b*) Schmidt (1992), *c*) assumed to identical to that of CD-2 (lower than barometer limit);

§ Mass fraction of total H₂O in melt, calculated according to Holtz et al. (2001); see text for detailed explanation; || Mole fraction of OH in melt, calculated according to Zhang (1999) and Nowak and Behrens (2001); see text for detailed explanation; // Log(Cl/OH) values of melt calculated according to Sato et al. (2005);

◇ F concentration in melt estimated by *a*) assuming identical to the values calculated from biotite and apatite, *b*) according to Eq (50)

Table III-2 Estimation of crystallization conditions of biotite and coexisting melt composition *

| Type*** | Biotite | | | | | | | Melt† | | | | Melt‡ | | | | | |
|---------|---------------------|------------|------|-----------------|------------|-------------|------------|------------|-----------------------------------|------------|------------|---------------|----------------|------------|-------------|------------|-------------|
| | Σ Al (ph) | Ti (ph) | Mg# | X _{Mg} | F (ppm) | Cl (ppm) | log(F/OH) | log(Cl/OH) | C _K /C _{Na} † | log(F/OH) | log(Cl/OH) | F (mol/kg) | Cl (mol/kg) | F (ppm) | Cl (ppm) | F (ppm) | Cl (ppm) |
| GN | 2.43 | 0.51 | 0.55 | 0.49 | 0.45±0.03 | 0.12±0.01 | -1.24±0.03 | -2.08±0.03 | 0.80 | -1.43±0.03 | -1.90±0.02 | 0.11±0.01 | 0.04±0.00 | 1998±147 | 1256±70 | 1025±70 | 999±74 |
| PD | 2.42 | 0.49 | 0.56 | 0.51 | 0.50±0.03 | 0.11±0.02 | -1.19±0.03 | -2.12±0.09 | 0.65 | -1.40±0.02 | -1.96±0.07 | 0.11±0.01 | 0.03±0.00 | 2145±122 | 1110±171 | 1097±58 | 935±195 |
| CD | 2.40 | 0.46 | 0.54 | 0.49 | 0.63±0.04 | 0.12±0.02 | -1.08±0.03 | -2.09±0.07 | 0.65 | -1.26±0.03 | -1.95±0.05 | 0.15±0.01 | 0.03±0.00 | 2920±212 | 1128±123 | 1450±93 | 969±156 |

* All calculated results are average values; uncertainty is 1 standard deviation;

** For types of rocks, see detailed explanation in text; high-Ti biotites (see Fig. III-7) are excluded from PD biotite dataset for calculation;

† Calculated according to the model of Munoz (1992) and partitioning relations of Cl and F in melt-fluid systems; crystallization conditions of 615 °C and 1.3 kbar are used for all biotites in the calculation;

‡ Molar ratio of K/Na in silicate melts (see Appendix B);

§ Calculated according to the model of Icenhower and London (1997)

Table III-3 Estimation of crystallization conditions of apatite and coexisting melt composition*

| Type** | Apatite | | | | T† (°C) | P† (kbar) | Melt‡ | | Melt§ | |
|----------|-----------|-----------|-----------|-----------|---------|-----------|-----------|----------|----------|-----------|
| | F (ppm) | Cl (ppm) | X(FAp) | X(ClAp) | | | F (ppm) | Cl (ppm) | F (ppm) | Cl (ppm) |
| GN (I) | 2.90±0.19 | 0.68±0.06 | 0.78±0.05 | 0.10±0.01 | 900 | 3.9 | 8532±556 | 8555±743 | 2180±168 | 1049±90 |
| GN (II) | 2.90±0.18 | 0.66±0.04 | 0.78±0.05 | 0.09±0.01 | 615 | 1.3 | 8540±529 | 8218±515 | 2180±158 | 10804±648 |
| PD (III) | 3.27±0.07 | 0.37±0.01 | 0.87±0.01 | 0.05±0.01 | 550 | 1.3 | 9605±203 | 4651±12 | 2494±38 | 6099±34 |
| CD (II) | 3.74±0.15 | 0.13±0.07 | 0.97±0.02 | 0.02±0.01 | 615 | 2.7 | 10993±431 | 1649±815 | 2920±132 | 447±221 |
| HG (II) | 3.18±0.18 | 0.56±0.08 | 0.85±0.05 | 0.08±0.01 | 690 | 3.9 | 9351±541 | 6997±984 | 2424±164 | 857±120 |

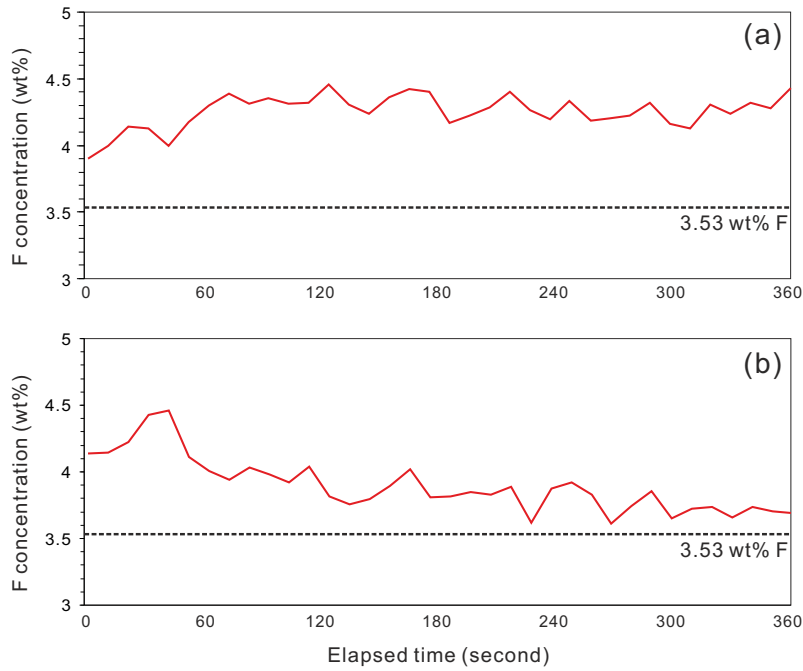
* All calculated results are averaged values; uncertainty is 1 standard deviation;

** For types of rocks and apatites, see detailed explanation in text;

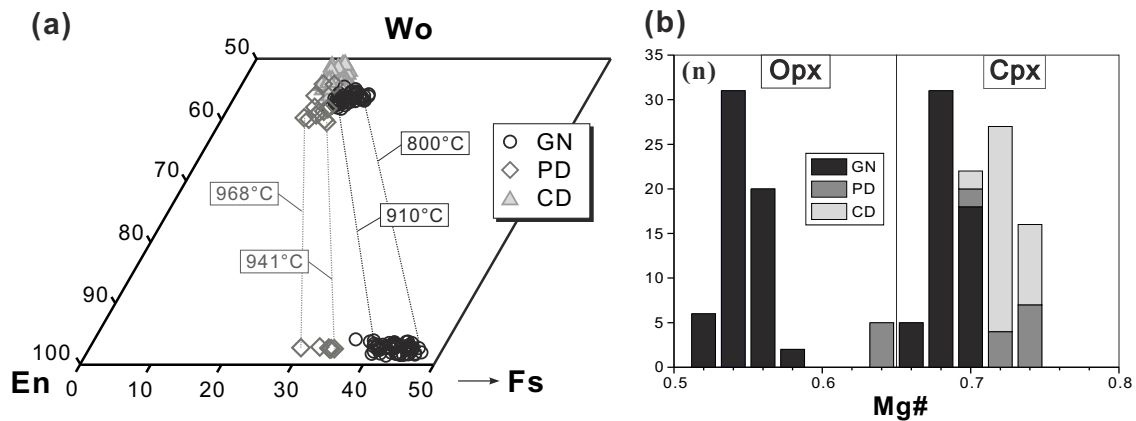
† Temperature and pressure estimated to be identical to associated biotites and amphiboles (Tables III-1~2) except for type-I apatite;

‡ Calculated according to the model of Mathez and Webster (2005);

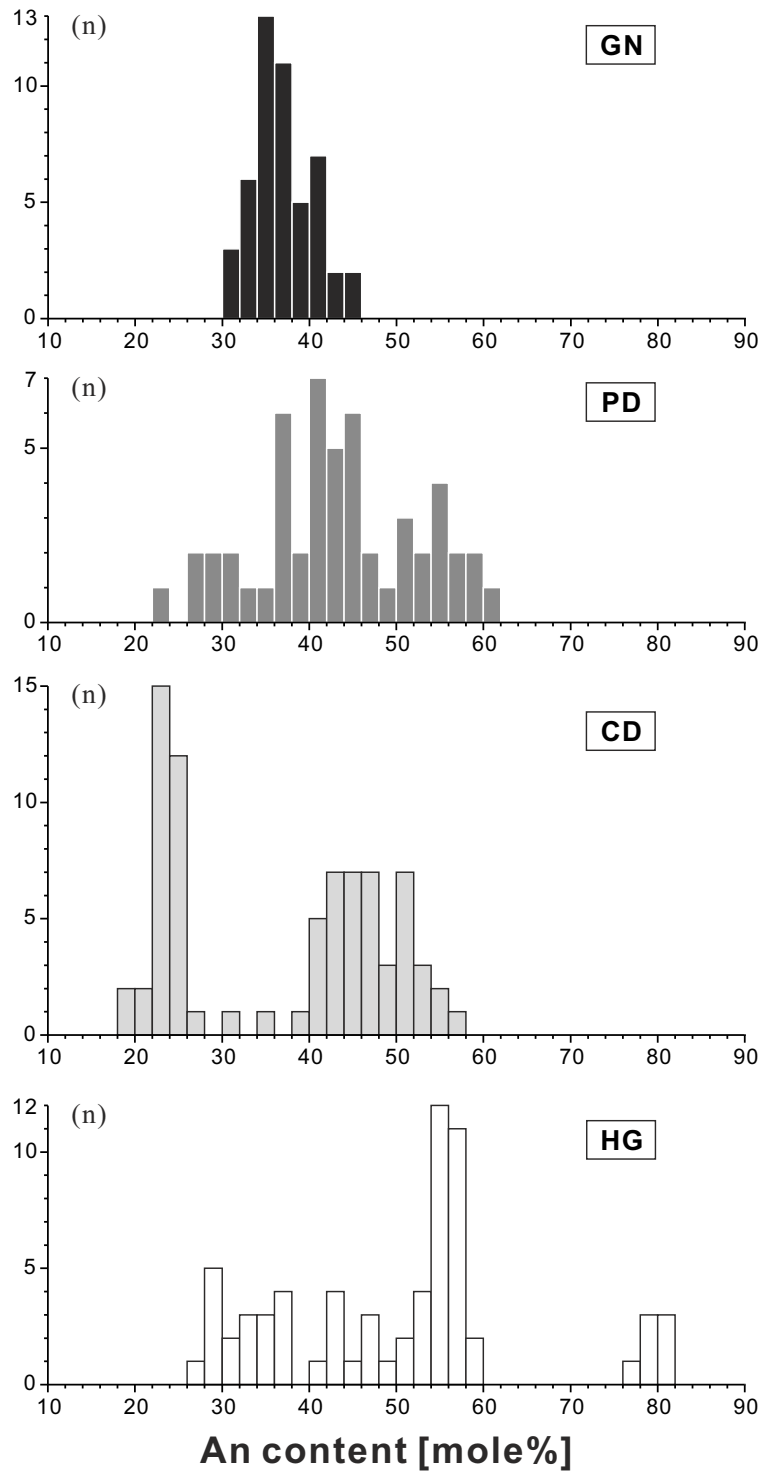
§ Calculated according to the model of Webster et al. (2009)



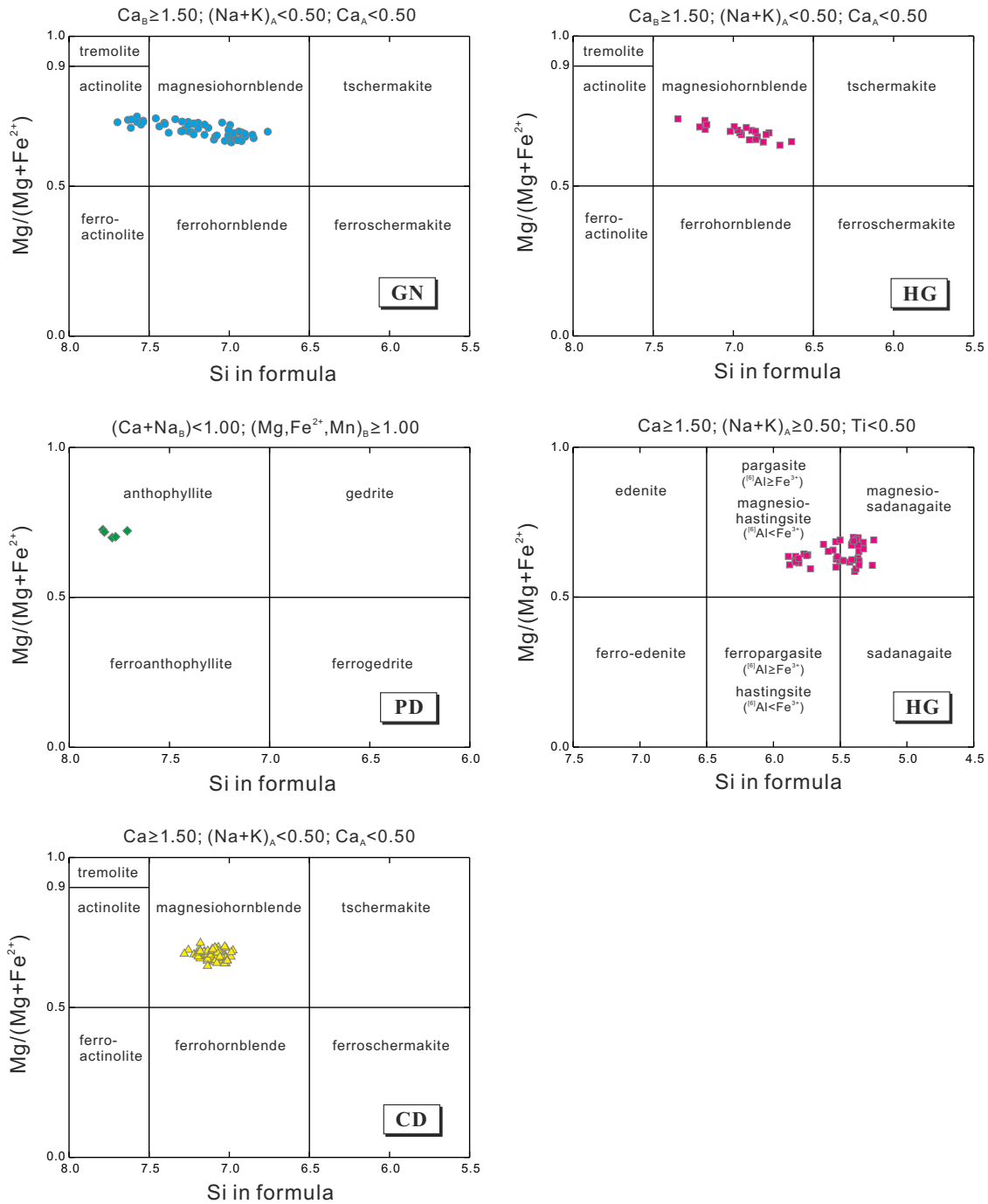
Supplementary Fig. III-1 F concentration with time measured on two Durango apatite crystals (equipped with the Cameca SX100 electron microprobe at the Institute of Mineralogy, Leibniz University of Hannover). Analysis setting: 15 kV, 10 nA, 10 μ m-diameter defocused beam.



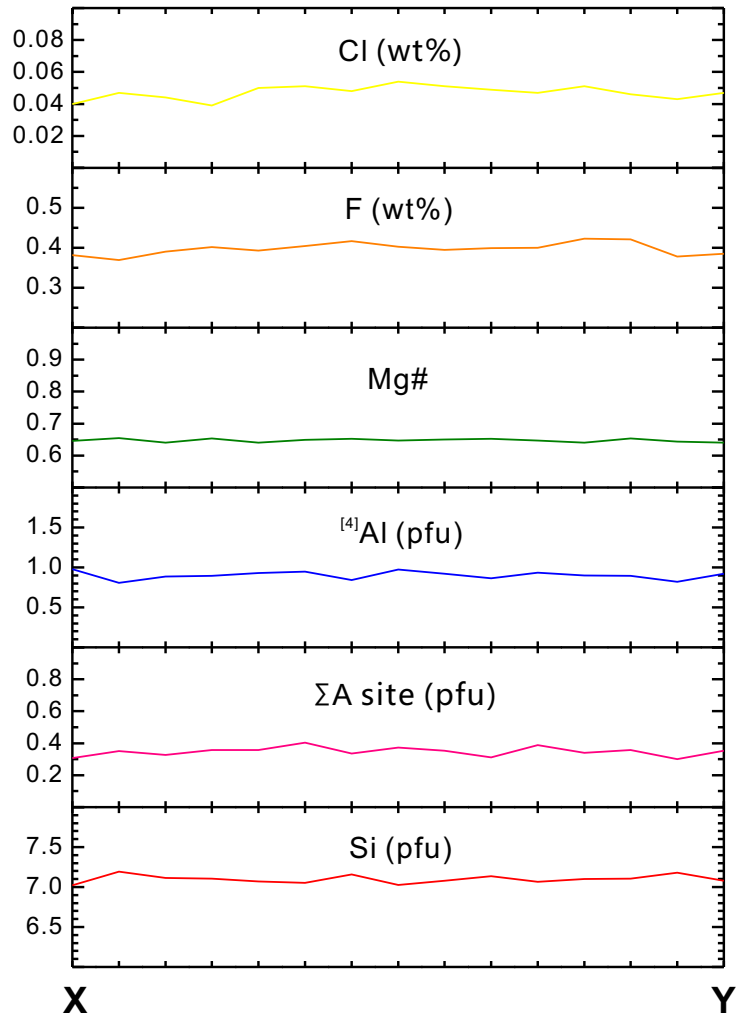
Supplementary Fig. III-2 Compositions of pyroxene in the GN, PD and CD rocks from the Liujiawa pluton. a normative compositions of Cpx and Opx; temperatures of Cpx-Opx pairs (linked by dotted line) are calculated using the QUILF program (Andersen et al. 1993); b histogram of Mg# values; n is the number of analyses. See text for rock type abbreviations and explanation.



Supplementary Fig. III-3 An contents of plagioclase in the GN, PD, CD and HG rocks from the Liujiawa pluton; n is the number of analyses. See text for rock type abbreviations and explanation.



Supplementary Fig. III-4 Nomenclature of amphiboles in the GN, PD, CD and HG rocks from the Liujiawa pluton (after Leake et al. 1997); note that two sets of amphiboles, with $(Na+K)_A < 0.5$ and ≥ 0.5 respectively, are shown in separated diagrams.



Supplementary Fig. III-5 Composition profile of the X-Y section the for the CD amphibole (see Fig. III-2j for position), the data are listed in Supplementary Table III-2 (points a76/1~a76/15 of the CD amphibole); from inner to outer, no systematic variation exists.

Supplementary Table III-1 Mineral assemblages of studies rocks types from the Liujiawa pluton (wt%)

| Rock type | GN | PD | CD | HG |
|-----------|-----|------|-----|-----|
| Opx | 12 | 10 | - | - |
| Cpx | 14 | 6 | 4 | - |
| Pl | 50 | 50 | 40 | 38 |
| Kfs | 2 | 2 | 15 | - |
| Amp | 1 | 2 | 18 | 48 |
| Bt | 16 | 18 | 8 | - |
| Ep | - | - | - | 3 |
| Qtz | 2 | 10 | 12 | 4 |
| Mgt | 1 | 1 | 1.5 | 4.5 |
| Ilm | 0.5 | 1 | 0.5 | 1 |
| Ttn | 0.5 | - | 0.5 | 0.5 |
| Ap | 1 | <0.1 | 0.5 | 1 |

Note: Mineral proportions acquired by point-counting (>3000 points per sample) and then adjusted according to common values of mineral densities. Uncertainty for major phases (>5 wt%) and minor phases (<5 wt%) are believed to be ~1 wt% and ~0.5 wt%, respectively. Minus means not observed. Rock types: GN, gabbro; PD, two-pyroxene diorite; CD, clinopyroxene diorite; HG, hornblende gabbro; Mineral abbreviations: Amp, amphibole; Ap, apatite; Bt, biotite; Cpx, clinopyroxene; Ep, epidote; Ilm, ilmenite; Kfs, K-feldspar; Mgt, magnetite; Opx, orthopyroxene; Pl, plagioclase; Qtz, quartz; Ttn, titanite.

Supplementary Table III-2 Composition of amphiboles from the Liujiawa pluton, Dabie orogen (China)

| Rock type ^a | GN | GN | GN | GN | GN | GN | GN | GN | GN | GN |
|-----------------------------------|-------|-------|-------|-------|-------|-------|--------|-------|--------|-------|
| Spot | 38 | 39 | 40 | 41 | 42 | 43 | 45 | 46 | 47 | 48 |
| Group ^b | | | | | | | | | | |
| Chemical composition (oxides wt%) | | | | | | | | | | |
| SiO ₂ | 46.35 | 46.87 | 46.53 | 46.09 | 47.14 | 47.10 | 48.68 | 47.90 | 48.29 | 45.73 |
| Al ₂ O ₃ | 7.43 | 7.14 | 6.83 | 7.00 | 7.10 | 6.71 | 6.29 | 6.58 | 6.42 | 8.41 |
| TiO ₂ | 1.32 | 1.12 | 1.09 | 1.21 | 1.13 | 1.03 | 0.75 | 0.88 | 1.07 | 0.99 |
| FeO ^c | 15.66 | 15.90 | 15.62 | 16.21 | 15.56 | 15.87 | 15.04 | 15.08 | 15.12 | 15.53 |
| MnO | 0.26 | 0.27 | 0.24 | 0.27 | 0.21 | 0.25 | 0.20 | 0.24 | 0.23 | 0.21 |
| MgO | 13.03 | 13.13 | 13.11 | 12.96 | 13.38 | 13.34 | 14.37 | 13.91 | 14.01 | 12.85 |
| CaO | 10.97 | 10.87 | 10.98 | 10.71 | 10.94 | 11.03 | 11.30 | 11.13 | 11.38 | 11.13 |
| Na ₂ O | 1.36 | 1.29 | 1.15 | 1.23 | 1.18 | 1.13 | 0.76 | 0.99 | 1.10 | 1.05 |
| K ₂ O | 0.78 | 0.72 | 0.65 | 0.67 | 0.67 | 0.62 | 0.55 | 0.57 | 0.65 | 0.79 |
| F | 0.404 | 0.370 | 0.325 | 0.369 | 0.389 | 0.356 | 0.350 | 0.355 | 0.377 | 0.371 |
| Cl | 0.091 | 0.083 | 0.082 | 0.078 | 0.083 | 0.074 | 0.060 | 0.068 | 0.063 | 0.089 |
| -O=F+Cl | 0.191 | 0.175 | 0.155 | 0.173 | 0.183 | 0.167 | 0.161 | 0.165 | 0.173 | 0.176 |
| Total | 97.46 | 97.59 | 96.45 | 96.62 | 97.60 | 97.34 | 98.19 | 97.54 | 98.54 | 96.97 |
| H ₂ O ^d | 1.81 | 1.84 | 1.84 | 1.82 | 1.84 | 1.85 | 1.89 | 1.87 | 1.87 | 1.83 |
| Total _{calc} | 99.28 | 99.43 | 98.29 | 98.44 | 99.44 | 99.19 | 100.08 | 99.40 | 100.41 | 98.80 |
| Mg# ^e | 0.597 | 0.595 | 0.599 | 0.588 | 0.605 | 0.600 | 0.630 | 0.622 | 0.623 | 0.596 |
| Cations based on 23 oxygen atoms | | | | | | | | | | |
| Si | 6.85 | 6.90 | 6.92 | 6.86 | 6.92 | 6.93 | 7.04 | 6.99 | 7.00 | 6.76 |
| [^{IV}]Al | 1.15 | 1.10 | 1.08 | 1.15 | 1.08 | 1.07 | 0.96 | 1.01 | 1.00 | 1.24 |
| ∑ T | 8.00 | 8.00 | 8.00 | 8.00 | 8.00 | 8.00 | 8.00 | 8.00 | 8.00 | 8.00 |
| [^{VI}]Al | 0.14 | 0.14 | 0.12 | 0.08 | 0.15 | 0.10 | 0.12 | 0.13 | 0.10 | 0.22 |
| Ti | 0.15 | 0.12 | 0.12 | 0.14 | 0.13 | 0.11 | 0.08 | 0.10 | 0.12 | 0.11 |
| Fe ^{3+f} | 0.46 | 0.52 | 0.53 | 0.61 | 0.53 | 0.58 | 0.57 | 0.58 | 0.48 | 0.60 |
| Mg | 2.87 | 2.88 | 2.91 | 2.87 | 2.93 | 2.93 | 3.10 | 3.03 | 3.03 | 2.83 |
| [^C]Fe ²⁺ | 1.38 | 1.34 | 1.32 | 1.30 | 1.28 | 1.28 | 1.13 | 1.17 | 1.27 | 1.24 |
| ∑ M1,2,3 | 5.00 | 5.00 | 5.00 | 5.00 | 5.00 | 5.00 | 5.00 | 5.00 | 5.00 | 5.00 |
| [^B]Fe ²⁺ | 0.09 | 0.10 | 0.09 | 0.11 | 0.11 | 0.09 | 0.12 | 0.09 | 0.08 | 0.09 |
| Mn | 0.03 | 0.03 | 0.03 | 0.03 | 0.03 | 0.03 | 0.03 | 0.03 | 0.03 | 0.03 |
| Ca | 1.74 | 1.71 | 1.75 | 1.71 | 1.72 | 1.74 | 1.75 | 1.74 | 1.77 | 1.76 |
| [^B]Na | 0.14 | 0.15 | 0.13 | 0.15 | 0.15 | 0.14 | 0.11 | 0.14 | 0.12 | 0.13 |
| ∑ M4 | 2.00 | 2.00 | 2.00 | 2.00 | 2.00 | 2.00 | 2.00 | 2.00 | 2.00 | 2.00 |
| [^A]Na | 0.25 | 0.22 | 0.20 | 0.20 | 0.19 | 0.18 | 0.11 | 0.14 | 0.19 | 0.18 |
| K | 0.15 | 0.14 | 0.12 | 0.13 | 0.13 | 0.12 | 0.10 | 0.11 | 0.12 | 0.15 |
| ∑ A | 0.40 | 0.35 | 0.32 | 0.33 | 0.31 | 0.30 | 0.21 | 0.25 | 0.31 | 0.32 |
| sum cations | 15.40 | 15.35 | 15.32 | 15.33 | 15.31 | 15.30 | 15.21 | 15.25 | 15.31 | 15.32 |
| F | 0.189 | 0.172 | 0.153 | 0.174 | 0.181 | 0.166 | 0.160 | 0.164 | 0.173 | 0.173 |
| Cl | 0.023 | 0.021 | 0.021 | 0.020 | 0.021 | 0.018 | 0.015 | 0.017 | 0.015 | 0.022 |
| OH | 1.788 | 1.807 | 1.826 | 1.807 | 1.799 | 1.816 | 1.825 | 1.819 | 1.812 | 1.804 |
| log(F/OH) | -0.98 | -1.02 | -1.08 | -1.02 | -1.00 | -1.04 | -1.06 | -1.05 | -1.02 | -1.02 |
| log(Cl/OH) | -1.89 | -1.94 | -1.95 | -1.96 | -1.94 | -1.99 | -2.09 | -2.03 | -2.07 | -1.91 |

^a Rock type: GN = gabbro; PD = two-pyroxene diorite; CD = clinopyroxene diorite; HG = hornblende gabbro;

^b Group: four groups (i.e., I, II, III and IV) of amphibole from HG are identified according to different composition;

^c Total iron reported as FeO.

^d H₂O calculated assuming F+Cl+OH=2 in the structural formula based on 23 oxygen atoms;

^e Mg# = molar Mg/(Mg+Fe);

^f Fe³⁺ calculated as the mean value using 13eCNK and 15eNK methods (Robinson et al. 1982).

Supplementary Table III-2 continued

| Rock type ^a | GN | GN | GN | GN | GN | GN | GN | GN | GN | GN |
|-----------------------------------|-------|-------|-------|-------|-------|-------|-------|-------|-------|-------|
| Spot | 58 | 59 | 61 | 62 | 71 | 72 | 73 | 74 | 77 | 78 |
| Group ^b | | | | | | | | | | |
| Chemical composition (oxides wt%) | | | | | | | | | | |
| SiO ₂ | 50.09 | 52.66 | 48.36 | 49.97 | 50.10 | 48.94 | 47.55 | 52.65 | 49.43 | 48.88 |
| Al ₂ O ₃ | 5.02 | 2.90 | 5.83 | 5.42 | 4.79 | 5.62 | 6.76 | 2.78 | 5.55 | 5.74 |
| TiO ₂ | 0.38 | 0.27 | 0.46 | 0.50 | 0.40 | 0.51 | 0.93 | 0.26 | 0.42 | 0.74 |
| FeO ^c | 14.58 | 12.91 | 15.17 | 14.30 | 14.09 | 14.40 | 15.51 | 12.54 | 14.45 | 14.34 |
| MnO | 0.25 | 0.28 | 0.29 | 0.26 | 0.26 | 0.19 | 0.22 | 0.24 | 0.21 | 0.18 |
| MgO | 14.96 | 16.61 | 13.82 | 14.43 | 14.07 | 13.95 | 13.27 | 16.23 | 14.56 | 14.41 |
| CaO | 11.15 | 10.99 | 11.01 | 11.04 | 11.27 | 11.02 | 11.13 | 11.24 | 11.30 | 11.21 |
| Na ₂ O | 0.62 | 0.42 | 0.87 | 0.78 | 0.71 | 0.71 | 0.90 | 0.42 | 0.72 | 0.69 |
| K ₂ O | 0.38 | 0.21 | 0.47 | 0.39 | 0.37 | 0.48 | 0.65 | 0.21 | 0.44 | 0.50 |
| F | 0.317 | 0.271 | 0.319 | 0.336 | 0.298 | 0.310 | 0.323 | 0.268 | 0.325 | 0.335 |
| Cl | 0.048 | 0.024 | 0.051 | 0.048 | 0.049 | 0.058 | 0.068 | 0.024 | 0.057 | 0.059 |
| -O=F+Cl | 0.144 | 0.120 | 0.146 | 0.152 | 0.137 | 0.144 | 0.151 | 0.118 | 0.150 | 0.154 |
| Total | 97.65 | 97.43 | 96.50 | 97.32 | 96.27 | 96.04 | 97.16 | 96.74 | 97.31 | 96.93 |
| H ₂ O ^d | 1.91 | 1.95 | 1.87 | 1.89 | 1.88 | 1.86 | 1.87 | 1.93 | 1.89 | 1.87 |
| Total _{calc} | 99.56 | 99.37 | 98.37 | 99.21 | 98.15 | 97.91 | 99.03 | 98.68 | 99.20 | 98.80 |
| Mg ^{#e} | 0.647 | 0.696 | 0.619 | 0.643 | 0.640 | 0.633 | 0.604 | 0.698 | 0.642 | 0.642 |
| Cations based on 23 oxygen atoms | | | | | | | | | | |
| Si | 7.26 | 7.58 | 7.13 | 7.28 | 7.38 | 7.24 | 7.00 | 7.63 | 7.20 | 7.15 |
| [⁴]Al | 0.74 | 0.42 | 0.87 | 0.72 | 0.62 | 0.76 | 1.00 | 0.37 | 0.81 | 0.85 |
| ∑ T | 8.00 | 8.00 | 8.00 | 8.00 | 8.00 | 8.00 | 8.00 | 8.00 | 8.00 | 8.00 |
| [⁶]Al | 0.11 | 0.07 | 0.14 | 0.21 | 0.21 | 0.22 | 0.17 | 0.11 | 0.15 | 0.14 |
| Ti | 0.04 | 0.03 | 0.05 | 0.06 | 0.04 | 0.06 | 0.10 | 0.03 | 0.05 | 0.08 |
| Fe ^{3+f} | 0.48 | 0.26 | 0.54 | 0.33 | 0.28 | 0.34 | 0.51 | 0.17 | 0.48 | 0.45 |
| Mg | 3.23 | 3.56 | 3.04 | 3.13 | 3.09 | 3.08 | 2.91 | 3.51 | 3.16 | 3.14 |
| [^C]Fe ²⁺ | 1.14 | 1.08 | 1.23 | 1.27 | 1.38 | 1.31 | 1.31 | 1.19 | 1.16 | 1.19 |
| ∑ M1,2,3 | 5.00 | 5.00 | 5.00 | 5.00 | 5.00 | 5.00 | 5.00 | 5.00 | 5.00 | 5.00 |
| [^B]Fe ²⁺ | 0.15 | 0.21 | 0.10 | 0.14 | 0.08 | 0.13 | 0.09 | 0.16 | 0.11 | 0.12 |
| Mn | 0.03 | 0.03 | 0.04 | 0.03 | 0.03 | 0.02 | 0.03 | 0.03 | 0.03 | 0.02 |
| Ca | 1.73 | 1.69 | 1.74 | 1.72 | 1.78 | 1.75 | 1.76 | 1.75 | 1.76 | 1.76 |
| [^B]Na | 0.09 | 0.06 | 0.12 | 0.11 | 0.11 | 0.10 | 0.13 | 0.06 | 0.10 | 0.10 |
| ∑ M4 | 2.00 | 2.00 | 2.00 | 2.00 | 2.00 | 2.00 | 2.00 | 2.00 | 2.00 | 2.00 |
| [^A]Na | 0.09 | 0.06 | 0.13 | 0.11 | 0.09 | 0.10 | 0.13 | 0.06 | 0.10 | 0.10 |
| K | 0.07 | 0.04 | 0.09 | 0.07 | 0.07 | 0.09 | 0.12 | 0.04 | 0.08 | 0.09 |
| ∑ A | 0.16 | 0.10 | 0.21 | 0.18 | 0.16 | 0.19 | 0.25 | 0.10 | 0.18 | 0.19 |
| sum cations | 15.16 | 15.10 | 15.21 | 15.18 | 15.16 | 15.19 | 15.25 | 15.10 | 15.18 | 15.19 |
| F | 0.145 | 0.123 | 0.149 | 0.155 | 0.139 | 0.145 | 0.150 | 0.123 | 0.150 | 0.155 |
| Cl | 0.012 | 0.006 | 0.013 | 0.012 | 0.012 | 0.015 | 0.017 | 0.006 | 0.014 | 0.015 |
| OH | 1.843 | 1.871 | 1.839 | 1.833 | 1.849 | 1.840 | 1.833 | 1.871 | 1.836 | 1.830 |
| log(F/OH) | -1.10 | -1.18 | -1.09 | -1.07 | -1.12 | -1.10 | -1.09 | -1.18 | -1.09 | -1.07 |
| log(Cl/OH) | -2.19 | -2.50 | -2.16 | -2.19 | -2.18 | -2.10 | -2.03 | -2.50 | -2.12 | -2.10 |

Supplementary Table III-2 continued

| Rock type ^a | GN | GN | GN | GN | GN | GN | GN | GN | GN | GN |
|----------------------------------|-----------------------------------|-------|-------|-------|-------|-------|-------|-------|-------|-------|
| Spot | 79 | 80-1 | 80-2 | 81-1 | 81-2 | 82 | 83 | 88 | 89 | 90 |
| Group ^b | | | | | | | | | | |
| | Chemical composition (oxides wt%) | | | | | | | | | |
| SiO ₂ | 49.40 | 53.28 | 53.01 | 46.79 | 47.25 | 52.03 | 51.49 | 51.37 | 49.77 | 49.83 |
| Al ₂ O ₃ | 5.55 | 2.62 | 2.72 | 7.08 | 7.07 | 3.29 | 3.84 | 4.47 | 4.94 | 5.22 |
| TiO ₂ | 0.64 | 0.43 | 0.48 | 1.29 | 1.30 | 0.38 | 0.40 | 0.64 | 0.74 | 0.80 |
| FeO ^c | 14.88 | 12.35 | 12.77 | 15.17 | 14.88 | 13.11 | 12.98 | 13.22 | 13.22 | 14.05 |
| MnO | 0.24 | 0.21 | 0.26 | 0.24 | 0.23 | 0.30 | 0.22 | 0.25 | 0.18 | 0.26 |
| MgO | 14.40 | 16.43 | 16.46 | 13.27 | 13.49 | 15.98 | 15.84 | 15.27 | 14.94 | 14.64 |
| CaO | 10.95 | 10.89 | 11.29 | 11.38 | 11.08 | 11.05 | 11.21 | 11.27 | 11.24 | 11.52 |
| Na ₂ O | 0.77 | 0.33 | 0.39 | 1.04 | 1.06 | 0.50 | 0.60 | 0.75 | 0.71 | 0.72 |
| K ₂ O | 0.49 | 0.19 | 0.19 | 0.69 | 0.65 | 0.24 | 0.27 | 0.30 | 0.38 | 0.41 |
| F | 0.366 | 0.287 | 0.330 | 0.332 | 0.320 | 0.300 | 0.273 | 0.291 | 0.280 | 0.304 |
| Cl | 0.064 | 0.023 | 0.027 | 0.065 | 0.061 | 0.028 | 0.029 | 0.034 | 0.048 | 0.042 |
| -O=F+Cl | 0.169 | 0.126 | 0.145 | 0.154 | 0.149 | 0.133 | 0.121 | 0.130 | 0.129 | 0.137 |
| Total | 97.58 | 96.91 | 97.78 | 97.19 | 97.24 | 97.08 | 97.03 | 97.73 | 96.32 | 97.66 |
| H ₂ O ^d | 1.87 | 1.93 | 1.92 | 1.86 | 1.87 | 1.92 | 1.93 | 1.93 | 1.90 | 1.91 |
| Total _{calc} | 99.45 | 98.85 | 99.71 | 99.05 | 99.11 | 98.99 | 98.96 | 99.67 | 98.22 | 99.57 |
| Mg ^{#e} | 0.633 | 0.703 | 0.697 | 0.609 | 0.618 | 0.685 | 0.685 | 0.673 | 0.668 | 0.650 |
| | Cations based on 23 oxygen atoms | | | | | | | | | |
| Si | 7.19 | 7.70 | 7.61 | 6.90 | 6.94 | 7.54 | 7.46 | 7.41 | 7.29 | 7.23 |
| [⁴]Al | 0.81 | 0.30 | 0.39 | 1.10 | 1.06 | 0.46 | 0.54 | 0.60 | 0.71 | 0.77 |
| ∑ T | 8.00 | 8.00 | 8.00 | 8.00 | 8.00 | 8.00 | 8.00 | 8.00 | 8.00 | 8.00 |
| [⁶]Al | 0.15 | 0.14 | 0.07 | 0.13 | 0.17 | 0.10 | 0.11 | 0.16 | 0.15 | 0.12 |
| Ti | 0.07 | 0.05 | 0.05 | 0.14 | 0.14 | 0.04 | 0.04 | 0.07 | 0.08 | 0.09 |
| Fe ^{3+f} | 0.43 | 0.08 | 0.18 | 0.47 | 0.45 | 0.24 | 0.29 | 0.27 | 0.32 | 0.40 |
| Mg | 3.13 | 3.54 | 3.52 | 2.92 | 2.95 | 3.45 | 3.42 | 3.28 | 3.26 | 3.17 |
| [^C]Fe ²⁺ | 1.23 | 1.20 | 1.17 | 1.34 | 1.28 | 1.17 | 1.13 | 1.22 | 1.18 | 1.23 |
| ∑ M1,2,3 | 5.00 | 5.00 | 5.00 | 5.00 | 5.00 | 5.00 | 5.00 | 5.00 | 5.00 | 5.00 |
| [^B]Fe ²⁺ | 0.15 | 0.22 | 0.18 | 0.06 | 0.09 | 0.18 | 0.15 | 0.11 | 0.11 | 0.08 |
| Mn | 0.03 | 0.03 | 0.03 | 0.03 | 0.03 | 0.04 | 0.03 | 0.03 | 0.02 | 0.03 |
| Ca | 1.71 | 1.69 | 1.74 | 1.80 | 1.74 | 1.72 | 1.74 | 1.74 | 1.77 | 1.79 |
| [^B]Na | 0.11 | 0.07 | 0.05 | 0.11 | 0.14 | 0.07 | 0.08 | 0.12 | 0.10 | 0.10 |
| ∑ M4 | 2.00 | 2.00 | 2.00 | 2.00 | 2.00 | 2.00 | 2.00 | 2.00 | 2.00 | 2.00 |
| [^A]Na | 0.11 | 0.02 | 0.05 | 0.19 | 0.17 | 0.07 | 0.09 | 0.09 | 0.10 | 0.10 |
| K | 0.09 | 0.04 | 0.04 | 0.13 | 0.12 | 0.04 | 0.05 | 0.06 | 0.07 | 0.08 |
| ∑ A | 0.20 | 0.06 | 0.32 | 0.11 | 0.13 | 0.14 | 0.17 | 0.18 | 0.23 | 0.29 |
| sum cations | 15.20 | 15.06 | 15.09 | 15.32 | 15.29 | 15.12 | 15.14 | 15.14 | 15.17 | 15.18 |
| F | 0.169 | 0.131 | 0.150 | 0.155 | 0.149 | 0.137 | 0.125 | 0.133 | 0.130 | 0.139 |
| Cl | 0.016 | 0.006 | 0.007 | 0.016 | 0.015 | 0.007 | 0.007 | 0.008 | 0.012 | 0.010 |
| OH | 1.816 | 1.863 | 1.844 | 1.829 | 1.836 | 1.856 | 1.868 | 1.859 | 1.858 | 1.850 |
| log(F/OH) | -1.03 | -1.15 | -1.09 | -1.07 | -1.09 | -1.13 | -1.17 | -1.15 | -1.16 | -1.12 |
| log(Cl/OH) | -2.06 | -2.52 | -2.45 | -2.05 | -2.08 | -2.43 | -2.42 | -2.35 | -2.19 | -2.25 |

Supplementary Table III-2 continued

| Rock type ^a | GN | GN | GN | GN | GN | GN | GN | GN | GN | GN |
|-----------------------------------|-------|-------|-------|-------|-------|-------|-------|-------|-------|-------|
| Spot | 123 | 124 | 125 | 126 | 127 | 128 | 129 | 135-1 | 135-2 | 136-1 |
| Group ^b | | | | | | | | | | |
| Chemical composition (oxides wt%) | | | | | | | | | | |
| SiO ₂ | 48.09 | 49.36 | 47.53 | 47.57 | 46.73 | 48.19 | 47.26 | 47.14 | 47.21 | 47.15 |
| Al ₂ O ₃ | 6.57 | 5.51 | 6.80 | 6.71 | 7.03 | 6.20 | 6.74 | 6.87 | 6.70 | 6.79 |
| TiO ₂ | 0.90 | 0.51 | 0.99 | 0.97 | 1.28 | 1.18 | 1.14 | 0.99 | 1.04 | 0.96 |
| FeO ^c | 15.19 | 14.35 | 15.74 | 15.40 | 15.74 | 15.13 | 15.17 | 15.52 | 16.03 | 15.49 |
| MnO | 0.25 | 0.25 | 0.20 | 0.20 | 0.20 | 0.25 | 0.22 | 0.26 | 0.21 | 0.21 |
| MgO | 13.14 | 14.07 | 13.16 | 13.31 | 12.88 | 13.39 | 12.88 | 13.00 | 12.87 | 12.99 |
| CaO | 11.04 | 11.18 | 11.33 | 11.01 | 11.08 | 11.02 | 10.86 | 10.92 | 10.82 | 11.07 |
| Na ₂ O | 0.84 | 0.67 | 1.01 | 1.08 | 1.16 | 0.96 | 1.25 | 1.15 | 1.21 | 1.11 |
| K ₂ O | 0.62 | 0.42 | 0.63 | 0.63 | 0.72 | 0.60 | 0.64 | 0.66 | 0.67 | 0.67 |
| F | 0.314 | 0.287 | 0.328 | 0.335 | 0.385 | 0.355 | 0.367 | 0.355 | 0.357 | 0.353 |
| Cl | 0.068 | 0.051 | 0.069 | 0.074 | 0.094 | 0.063 | 0.078 | 0.096 | 0.085 | 0.093 |
| -O=F+Cl | 0.148 | 0.132 | 0.154 | 0.158 | 0.183 | 0.164 | 0.172 | 0.171 | 0.169 | 0.170 |
| Total | 96.87 | 96.53 | 97.63 | 97.13 | 97.12 | 97.17 | 96.43 | 96.79 | 97.03 | 96.72 |
| H ₂ O ^d | 1.86 | 1.89 | 1.87 | 1.86 | 1.82 | 1.85 | 1.82 | 1.83 | 1.83 | 1.83 |
| Total _{calc} | 98.74 | 98.41 | 99.50 | 98.99 | 98.93 | 99.03 | 98.25 | 98.62 | 98.86 | 98.54 |
| Mg ^{#e} | 0.607 | 0.636 | 0.598 | 0.606 | 0.593 | 0.612 | 0.602 | 0.599 | 0.589 | 0.599 |
| Cations based on 23 oxygen atoms | | | | | | | | | | |
| Si | 7.10 | 7.26 | 6.98 | 7.01 | 6.92 | 7.09 | 7.03 | 6.99 | 6.99 | 7.00 |
| [⁴]Al | 0.91 | 0.75 | 1.02 | 0.99 | 1.08 | 0.91 | 0.97 | 1.01 | 1.01 | 1.00 |
| ∑ T | 8.00 | 8.00 | 8.00 | 8.00 | 8.00 | 8.00 | 8.00 | 8.00 | 8.00 | 8.00 |
| [⁶]Al | 0.24 | 0.21 | 0.16 | 0.17 | 0.15 | 0.16 | 0.21 | 0.19 | 0.16 | 0.18 |
| Ti | 0.10 | 0.06 | 0.11 | 0.11 | 0.14 | 0.13 | 0.13 | 0.11 | 0.12 | 0.11 |
| Fe ^{3+f} | 0.36 | 0.34 | 0.47 | 0.46 | 0.43 | 0.39 | 0.36 | 0.43 | 0.45 | 0.42 |
| Mg | 2.89 | 3.08 | 2.88 | 2.92 | 2.85 | 2.94 | 2.86 | 2.87 | 2.84 | 2.87 |
| [^C]Fe ²⁺ | 1.42 | 1.31 | 1.38 | 1.34 | 1.43 | 1.38 | 1.45 | 1.40 | 1.43 | 1.42 |
| ∑ M1,2,3 | 5.00 | 5.00 | 5.00 | 5.00 | 5.00 | 5.00 | 5.00 | 5.00 | 5.00 | 5.00 |
| [^B]Fe ²⁺ | 0.10 | 0.11 | 0.08 | 0.10 | 0.09 | 0.09 | 0.08 | 0.09 | 0.10 | 0.09 |
| Mn | 0.03 | 0.03 | 0.03 | 0.03 | 0.03 | 0.03 | 0.03 | 0.03 | 0.03 | 0.03 |
| Ca | 1.75 | 1.76 | 1.78 | 1.74 | 1.76 | 1.74 | 1.73 | 1.73 | 1.72 | 1.76 |
| [^B]Na | 0.12 | 0.10 | 0.12 | 0.14 | 0.13 | 0.14 | 0.17 | 0.14 | 0.15 | 0.13 |
| ∑ M4 | 2.00 | 2.00 | 2.00 | 2.00 | 2.00 | 2.00 | 2.00 | 2.00 | 2.00 | 2.00 |
| [^A]Na | 0.12 | 0.10 | 0.17 | 0.17 | 0.21 | 0.13 | 0.19 | 0.19 | 0.19 | 0.19 |
| K | 0.12 | 0.08 | 0.12 | 0.12 | 0.14 | 0.11 | 0.12 | 0.13 | 0.13 | 0.13 |
| ∑ A | 0.17 | 0.29 | 0.34 | 0.24 | 0.32 | 0.31 | 0.32 | 0.32 | 0.33 | 0.20 |
| sum cations | 15.24 | 15.18 | 15.29 | 15.29 | 15.34 | 15.24 | 15.32 | 15.31 | 15.32 | 15.32 |
| F | 0.147 | 0.133 | 0.152 | 0.156 | 0.180 | 0.165 | 0.173 | 0.166 | 0.167 | 0.166 |
| Cl | 0.017 | 0.013 | 0.017 | 0.018 | 0.024 | 0.016 | 0.020 | 0.024 | 0.021 | 0.023 |
| OH | 1.836 | 1.854 | 1.831 | 1.825 | 1.796 | 1.819 | 1.808 | 1.809 | 1.811 | 1.811 |
| log(F/OH) | -1.10 | -1.14 | -1.08 | -1.07 | -1.00 | -1.04 | -1.02 | -1.04 | -1.03 | -1.04 |
| log(Cl/OH) | -2.03 | -2.16 | -2.03 | -1.99 | -1.88 | -2.06 | -1.96 | -1.88 | -1.93 | -1.89 |

Supplementary Table III-2 continued

| Rock type ^a | GN | GN | GN | GN | GN | GN | GN | GN | GN | GN |
|-----------------------------------|-------|-------|-------|-------|-------|-------|-------|-------|-------|-------|
| Spot | 136-2 | 141 | 142 | 144 | 146 | 170 | 171 | 172 | 176 | 186 |
| Group ^b | | | | | | | | | | |
| Chemical composition (oxides wt%) | | | | | | | | | | |
| SiO ₂ | 46.52 | 48.91 | 49.77 | 51.02 | 49.69 | 52.41 | 52.09 | 50.88 | 51.75 | 50.85 |
| Al ₂ O ₃ | 6.77 | 5.55 | 5.35 | 4.31 | 5.26 | 3.30 | 3.29 | 4.24 | 3.39 | 4.24 |
| TiO ₂ | 1.00 | 0.72 | 0.67 | 0.52 | 0.45 | 0.46 | 0.54 | 0.69 | 0.50 | 0.60 |
| FeO ^c | 15.51 | 14.65 | 14.47 | 13.41 | 14.33 | 12.68 | 12.70 | 13.28 | 12.94 | 13.36 |
| MnO | 0.23 | 0.27 | 0.25 | 0.28 | 0.18 | 0.32 | 0.22 | 0.30 | 0.29 | 0.23 |
| MgO | 12.68 | 13.67 | 14.41 | 15.11 | 14.70 | 15.99 | 15.33 | 15.20 | 15.55 | 15.14 |
| CaO | 10.94 | 11.15 | 10.99 | 11.01 | 10.94 | 11.14 | 11.24 | 11.34 | 11.17 | 11.34 |
| Na ₂ O | 1.15 | 0.80 | 0.70 | 0.60 | 0.74 | 0.43 | 0.38 | 0.58 | 0.44 | 0.65 |
| K ₂ O | 0.66 | 0.46 | 0.43 | 0.34 | 0.40 | 0.22 | 0.25 | 0.32 | 0.26 | 0.34 |
| F | 0.351 | 0.293 | 0.363 | 0.309 | 0.301 | 0.311 | 0.284 | 0.295 | 0.277 | 0.323 |
| Cl | 0.090 | 0.050 | 0.046 | 0.042 | 0.039 | 0.028 | 0.023 | 0.038 | 0.032 | 0.040 |
| -O=F+Cl | 0.168 | 0.135 | 0.163 | 0.140 | 0.136 | 0.137 | 0.125 | 0.133 | 0.124 | 0.145 |
| Total | 95.73 | 96.39 | 97.29 | 96.81 | 96.89 | 97.15 | 96.22 | 97.03 | 96.48 | 96.97 |
| H ₂ O ^d | 1.81 | 1.88 | 1.87 | 1.90 | 1.90 | 1.92 | 1.91 | 1.91 | 1.91 | 1.89 |
| Total _{calc} | 97.54 | 98.27 | 99.16 | 98.71 | 98.79 | 99.07 | 98.13 | 98.94 | 98.39 | 98.86 |
| Mg# ^e | 0.593 | 0.625 | 0.640 | 0.668 | 0.646 | 0.692 | 0.683 | 0.671 | 0.682 | 0.669 |
| Cations based on 23 oxygen atoms | | | | | | | | | | |
| Si | 6.99 | 7.22 | 7.26 | 7.44 | 7.26 | 7.58 | 7.61 | 7.40 | 7.55 | 7.40 |
| [⁴]Al | 1.01 | 0.78 | 0.74 | 0.56 | 0.74 | 0.42 | 0.39 | 0.60 | 0.45 | 0.60 |
| ∑ T | 8.00 | 8.00 | 8.00 | 8.00 | 8.00 | 8.00 | 8.00 | 8.00 | 8.00 | 8.00 |
| [⁶]Al | 0.18 | 0.19 | 0.18 | 0.18 | 0.16 | 0.14 | 0.18 | 0.13 | 0.13 | 0.13 |
| Ti | 0.11 | 0.08 | 0.07 | 0.06 | 0.05 | 0.05 | 0.06 | 0.08 | 0.06 | 0.07 |
| Fe ^{3+f} | 0.40 | 0.34 | 0.33 | 0.23 | 0.41 | 0.16 | 0.09 | 0.26 | 0.17 | 0.27 |
| Mg | 2.84 | 3.01 | 3.13 | 3.28 | 3.20 | 3.45 | 3.34 | 3.30 | 3.38 | 3.29 |
| [^C]Fe ²⁺ | 1.47 | 1.38 | 1.28 | 1.25 | 1.18 | 1.21 | 1.33 | 1.24 | 1.26 | 1.24 |
| ∑ M1,2,3 | 5.00 | 5.00 | 5.00 | 5.00 | 5.00 | 5.00 | 5.00 | 5.00 | 5.00 | 5.00 |
| [^B]Fe ²⁺ | 0.08 | 0.09 | 0.15 | 0.15 | 0.16 | 0.17 | 0.13 | 0.11 | 0.15 | 0.11 |
| Mn | 0.03 | 0.03 | 0.03 | 0.04 | 0.02 | 0.04 | 0.03 | 0.04 | 0.04 | 0.03 |
| Ca | 1.76 | 1.76 | 1.72 | 1.72 | 1.71 | 1.73 | 1.76 | 1.77 | 1.75 | 1.77 |
| [^B]Na | 0.13 | 0.12 | 0.10 | 0.09 | 0.10 | 0.07 | 0.08 | 0.08 | 0.07 | 0.09 |
| ∑ M4 | 2.00 | 2.00 | 2.00 | 2.00 | 2.00 | 2.00 | 2.00 | 2.00 | 2.00 | 2.00 |
| [^A]Na | 0.21 | 0.11 | 0.10 | 0.08 | 0.11 | 0.05 | 0.03 | 0.08 | 0.06 | 0.09 |
| K | 0.13 | 0.09 | 0.08 | 0.06 | 0.08 | 0.04 | 0.05 | 0.06 | 0.05 | 0.06 |
| ∑ A | 0.18 | 0.14 | 0.18 | 0.09 | 0.08 | 0.14 | 0.10 | 0.09 | 0.29 | 0.15 |
| sum cations | 15.33 | 15.20 | 15.18 | 15.14 | 15.18 | 15.09 | 15.08 | 15.14 | 15.10 | 15.15 |
| F | 0.167 | 0.137 | 0.167 | 0.142 | 0.139 | 0.142 | 0.131 | 0.136 | 0.128 | 0.149 |
| Cl | 0.023 | 0.013 | 0.011 | 0.010 | 0.010 | 0.007 | 0.006 | 0.009 | 0.008 | 0.010 |
| OH | 1.810 | 1.851 | 1.821 | 1.847 | 1.851 | 1.851 | 1.863 | 1.855 | 1.864 | 1.841 |
| log(F/OH) | -1.04 | -1.13 | -1.04 | -1.11 | -1.12 | -1.11 | -1.15 | -1.14 | -1.16 | -1.09 |
| log(Cl/OH) | -1.90 | -2.17 | -2.20 | -2.25 | -2.28 | -2.43 | -2.51 | -2.30 | -2.37 | -2.27 |

Supplementary Table III-2 continued

| Rock type ^a | GN | GN | GN | GN | GN | GN | GN | GN | GN | GN |
|-----------------------------------|-------|-------|-------|-------|-------|-------|-------|-------|-------|-------|
| Spot | 187 | 188 | 191 | a15 | a18 | a19 | a31 | a46 | a47 | a52 |
| Group ^b | | | | | | | | | | |
| Chemical composition (oxides wt%) | | | | | | | | | | |
| SiO ₂ | 49.61 | 49.73 | 51.98 | 47.65 | 48.06 | 47.73 | 48.12 | 51.23 | 50.26 | 48.30 |
| Al ₂ O ₃ | 5.20 | 5.13 | 3.09 | 6.92 | 6.67 | 6.78 | 6.66 | 4.65 | 6.06 | 6.48 |
| TiO ₂ | 0.70 | 0.87 | 0.43 | 1.35 | 1.06 | 1.00 | 1.07 | 0.54 | 0.55 | 0.79 |
| FeO ^c | 13.93 | 13.97 | 13.32 | 15.47 | 15.79 | 15.68 | 15.28 | 13.51 | 13.54 | 15.06 |
| MnO | 0.29 | 0.23 | 0.26 | 0.22 | 0.25 | 0.20 | 0.24 | 0.21 | 0.21 | 0.24 |
| MgO | 14.01 | 14.30 | 15.68 | 13.22 | 13.63 | 13.40 | 13.72 | 15.45 | 14.88 | 13.45 |
| CaO | 11.27 | 11.15 | 11.51 | 11.00 | 11.26 | 11.14 | 11.11 | 11.69 | 11.32 | 11.42 |
| Na ₂ O | 0.76 | 0.69 | 0.47 | 1.20 | 1.14 | 1.04 | 1.00 | 0.62 | 0.78 | 0.93 |
| K ₂ O | 0.40 | 0.44 | 0.23 | 0.70 | 0.66 | 0.62 | 0.60 | 0.35 | 0.51 | 0.60 |
| F | 0.315 | 0.297 | 0.282 | 0.348 | 0.355 | 0.329 | 0.378 | 0.334 | 0.326 | 0.347 |
| Cl | 0.051 | 0.049 | 0.031 | 0.087 | 0.083 | 0.082 | 0.079 | 0.041 | 0.061 | 0.059 |
| -O=F+Cl | 0.144 | 0.136 | 0.126 | 0.115 | 0.115 | 0.109 | 0.119 | 0.093 | 0.099 | 0.103 |
| Total | 96.39 | 96.72 | 97.16 | 98.05 | 98.84 | 97.89 | 98.14 | 98.53 | 98.40 | 97.57 |
| H ₂ O ^d | 1.87 | 1.89 | 1.92 | 0.47 | 0.44 | 0.47 | 0.39 | 0.24 | 0.36 | 0.32 |
| Total _{calc} | 98.27 | 98.61 | 99.08 | 98.51 | 99.28 | 98.36 | 98.53 | 98.77 | 98.76 | 97.89 |
| Mg# ^e | 0.642 | 0.646 | 0.677 | 0.604 | 0.606 | 0.604 | 0.615 | 0.671 | 0.662 | 0.614 |
| Cations based on 23 oxygen atoms | | | | | | | | | | |
| Si | 7.30 | 7.29 | 7.54 | 6.97 | 6.97 | 6.98 | 7.00 | 7.34 | 7.22 | 7.08 |
| [⁴]Al | 0.70 | 0.71 | 0.46 | 1.03 | 1.03 | 1.02 | 1.00 | 0.66 | 0.78 | 0.92 |
| ∑ T | 8.00 | 8.00 | 8.00 | 8.00 | 8.00 | 8.00 | 8.00 | 8.00 | 8.00 | 8.00 |
| [⁶]Al | 0.20 | 0.18 | 0.06 | 0.17 | 0.11 | 0.15 | 0.15 | 0.12 | 0.25 | 0.20 |
| Ti | 0.08 | 0.10 | 0.05 | 0.15 | 0.12 | 0.11 | 0.12 | 0.06 | 0.06 | 0.09 |
| Fe ^{3+f} | 0.29 | 0.27 | 0.26 | 0.41 | 0.51 | 0.52 | 0.50 | 0.36 | 0.32 | 0.40 |
| Mg | 3.07 | 3.13 | 3.39 | 2.88 | 2.95 | 2.92 | 2.98 | 3.30 | 3.19 | 2.94 |
| [^C]Fe ²⁺ | 1.36 | 1.33 | 1.24 | 1.39 | 1.32 | 1.31 | 1.26 | 1.16 | 1.18 | 1.38 |
| ∑ M1,2,3 | 5.00 | 5.00 | 5.00 | 5.00 | 5.00 | 5.00 | 5.00 | 5.00 | 5.00 | 5.00 |
| [^B]Fe ²⁺ | 0.07 | 0.11 | 0.11 | 0.09 | 0.09 | 0.10 | 0.10 | 0.10 | 0.12 | 0.07 |
| Mn | 0.04 | 0.03 | 0.03 | 0.03 | 0.03 | 0.03 | 0.03 | 0.03 | 0.03 | 0.03 |
| Ca | 1.78 | 1.75 | 1.79 | 1.72 | 1.75 | 1.75 | 1.73 | 1.79 | 1.74 | 1.79 |
| [^B]Na | 0.12 | 0.11 | 0.07 | 0.16 | 0.13 | 0.14 | 0.14 | 0.09 | 0.11 | 0.11 |
| ∑ M4 | 2.00 | 2.00 | 2.00 | 2.00 | 2.00 | 2.00 | 2.00 | 2.00 | 2.00 | 2.00 |
| [^A]Na | 0.10 | 0.09 | 0.07 | 0.18 | 0.19 | 0.16 | 0.14 | 0.09 | 0.11 | 0.15 |
| K | 0.08 | 0.08 | 0.04 | 0.13 | 0.12 | 0.12 | 0.11 | 0.06 | 0.09 | 0.11 |
| ∑ A | 0.17 | 0.17 | 0.11 | 0.31 | 0.31 | 0.28 | 0.25 | 0.15 | 0.20 | 0.27 |
| sum cations | 15.17 | 15.17 | 15.11 | 15.31 | 15.31 | 15.28 | 15.25 | 15.15 | 15.20 | 15.27 |
| F | 0.147 | 0.138 | 0.129 | 0.161 | 0.163 | 0.152 | 0.174 | 0.151 | 0.148 | 0.161 |
| Cl | 0.013 | 0.012 | 0.008 | 0.022 | 0.020 | 0.020 | 0.019 | 0.010 | 0.015 | 0.015 |
| OH | 1.841 | 1.850 | 1.863 | 1.817 | 1.817 | 1.828 | 1.807 | 1.839 | 1.837 | 1.825 |
| log(F/OH) | -1.10 | -1.13 | -1.16 | -1.05 | -1.05 | -1.08 | -1.02 | -1.08 | -1.09 | -1.05 |
| log(Cl/OH) | -2.16 | -2.18 | -2.39 | -1.93 | -1.95 | -1.95 | -1.97 | -2.27 | -2.09 | -2.10 |

Supplementary Table III-2 continued

| Rock type ^a | GN | GN | GN | PD | PD | PD | PD | PD | CD | CD |
|-----------------------------------|-------|-------|-------|--------|--------|-------|-------|-------|--------|-------|
| Spot | a53 | a62 | a63 | 47 | 48 | 51 | 52 | 53 | 2 | 3 |
| Group ^b | | | | | | | | | | |
| Chemical composition (oxides wt%) | | | | | | | | | | |
| SiO ₂ | 49.15 | 47.77 | 47.76 | 55.46 | 55.04 | 55.15 | 54.42 | 54.38 | 49.55 | 48.85 |
| Al ₂ O ₃ | 6.07 | 6.98 | 6.91 | 1.27 | 1.31 | 1.35 | 1.77 | 1.43 | 5.94 | 5.90 |
| TiO ₂ | 0.85 | 1.20 | 1.16 | 0.12 | 0.19 | 0.21 | 0.24 | 0.23 | 1.04 | 1.04 |
| FeO ^c | 15.00 | 15.83 | 15.92 | 15.09 | 17.59 | 15.94 | 16.41 | 16.99 | 14.03 | 13.84 |
| MnO | 0.28 | 0.24 | 0.26 | 1.21 | 1.14 | 1.33 | 0.91 | 1.21 | 0.43 | 0.45 |
| MgO | 13.81 | 13.21 | 13.29 | 21.27 | 21.59 | 21.89 | 21.71 | 20.97 | 14.19 | 13.99 |
| CaO | 11.13 | 11.33 | 11.33 | 3.41 | 1.31 | 1.43 | 2.10 | 2.00 | 11.68 | 11.61 |
| Na ₂ O | 0.85 | 1.13 | 1.33 | 0.18 | 0.21 | 0.18 | 0.28 | 0.22 | 1.11 | 1.25 |
| K ₂ O | 0.54 | 0.71 | 0.68 | 0.06 | 0.02 | 0.05 | 0.01 | 0.04 | 0.59 | 0.59 |
| F | 0.325 | 0.344 | 0.373 | 0.303 | 0.298 | 0.310 | | 0.304 | 0.444 | 0.480 |
| Cl | 0.054 | 0.080 | 0.082 | 0.004 | 0.002 | 0.005 | | 0.006 | 0.039 | 0.048 |
| -O=F+Cl | 0.096 | 0.111 | 0.119 | 0.128 | 0.126 | 0.132 | 0.000 | 0.129 | 0.196 | 0.213 |
| Total | 97.96 | 98.71 | 98.98 | 98.25 | 98.57 | 97.71 | 97.85 | 97.65 | 98.85 | 97.84 |
| H ₂ O ^d | 0.31 | 0.44 | 0.41 | 1.98 | 1.98 | 1.96 | | 1.95 | 1.85 | 1.81 |
| Total _{calc} | 98.28 | 99.15 | 99.39 | 100.23 | 100.55 | 99.68 | | 99.60 | 100.70 | 99.64 |
| Mg ^{#e} | 0.621 | 0.598 | 0.598 | 0.715 | 0.686 | 0.710 | 0.702 | 0.688 | 0.643 | 0.643 |
| Cations based on 23 oxygen atoms | | | | | | | | | | |
| Si | 7.15 | 6.96 | 6.95 | 7.82 | 7.78 | 7.81 | 7.70 | 7.76 | 7.15 | 7.14 |
| [⁴]Al | 0.85 | 1.05 | 1.05 | 0.18 | 0.22 | 0.19 | 0.30 | 0.24 | 0.85 | 0.86 |
| ∑ T | 8.00 | 8.00 | 8.00 | 8.00 | 8.00 | 8.00 | 8.00 | 8.00 | 8.00 | 8.00 |
| [⁶]Al | 0.20 | 0.15 | 0.13 | 0.03 | 0.00 | 0.04 | 0.00 | 0.00 | 0.16 | 0.16 |
| Ti | 0.09 | 0.13 | 0.13 | 0.01 | 0.02 | 0.02 | 0.03 | 0.02 | 0.11 | 0.11 |
| Fe ^{3+f} | 0.36 | 0.43 | 0.41 | 0.17 | 0.15 | 0.14 | 0.21 | 0.19 | 0.27 | 0.24 |
| Mg | 3.00 | 2.87 | 2.88 | 4.47 | 4.55 | 4.62 | 4.58 | 4.46 | 3.05 | 3.05 |
| [^C]Fe ²⁺ | 1.35 | 1.42 | 1.45 | 0.32 | 0.28 | 0.17 | 0.18 | 0.32 | 1.40 | 1.44 |
| ∑ M1,2,3 | 5.00 | 5.00 | 5.00 | 5.00 | 5.00 | 5.00 | 5.00 | 5.00 | 5.00 | 5.00 |
| [^B]Fe ²⁺ | 0.11 | 0.08 | 0.08 | 1.29 | 1.65 | 1.57 | 1.55 | 1.51 | 0.02 | 0.01 |
| Mn | 0.04 | 0.03 | 0.03 | 0.14 | 0.14 | 0.16 | 0.11 | 0.15 | 0.05 | 0.06 |
| Ca | 1.74 | 1.77 | 1.77 | 0.52 | 0.20 | 0.22 | 0.32 | 0.31 | 1.81 | 1.82 |
| [^B]Na | 0.12 | 0.12 | 0.12 | 0.05 | 0.01 | 0.05 | 0.02 | 0.04 | 0.12 | 0.11 |
| ∑ M4 | 2.00 | 2.00 | 2.00 | 2.00 | 2.00 | 2.00 | 2.00 | 2.00 | 2.00 | 2.00 |
| [^A]Na | 0.12 | 0.20 | 0.25 | 0.00 | 0.04 | 0.00 | 0.06 | 0.03 | 0.19 | 0.24 |
| K | 0.10 | 0.13 | 0.13 | 0.01 | 0.00 | 0.01 | 0.00 | 0.01 | 0.11 | 0.11 |
| ∑ A | 0.22 | 0.33 | 0.38 | 0.01 | 0.05 | 0.01 | 0.06 | 0.03 | 0.30 | 0.35 |
| sum cations | 15.22 | 15.33 | 15.38 | 15.01 | 15.05 | 15.01 | 15.06 | 15.03 | 15.30 | 15.35 |
| F | 0.150 | 0.158 | 0.172 | 0.135 | 0.133 | 0.139 | | 0.137 | 0.203 | 0.222 |
| Cl | 0.013 | 0.020 | 0.020 | 0.001 | 0.000 | 0.001 | | 0.001 | 0.010 | 0.012 |
| OH | 1.837 | 1.822 | 1.808 | 1.86 | 1.87 | 1.86 | | 1.86 | 1.79 | 1.77 |
| log(F/OH) | -1.09 | -1.06 | -1.02 | -1.14 | -1.15 | -1.13 | | -1.13 | -0.95 | -0.90 |
| log(Cl/OH) | -2.14 | -1.97 | -1.95 | -3.29 | -3.59 | -3.19 | | -3.11 | -2.27 | -2.17 |

Supplementary Table III-2 continued

| Rock type ^a | CD | CD | CD | CD | CD | CD | CD | CD | CD | CD |
|-----------------------------------|-------|--------|--------|-------|-------|-------|-------|-------|-------|-------|
| Spot | 4 | 5 | 6 | 7 | 8 | 9 | 10 | 11 | 12 | 13 |
| Group ^b | | | | | | | | | | |
| Chemical composition (oxides wt%) | | | | | | | | | | |
| SiO ₂ | 48.48 | 50.08 | 49.98 | 48.58 | 48.52 | 48.18 | 48.88 | 48.30 | 47.93 | 48.43 |
| Al ₂ O ₃ | 6.58 | 5.36 | 5.74 | 6.05 | 6.26 | 6.35 | 6.32 | 6.40 | 6.61 | 6.16 |
| TiO ₂ | 1.13 | 0.85 | 0.89 | 1.05 | 1.09 | 1.18 | 1.08 | 1.11 | 1.22 | 1.08 |
| FeO ^c | 14.23 | 13.26 | 13.62 | 14.05 | 13.85 | 14.16 | 13.73 | 14.00 | 14.44 | 13.94 |
| MnO | 0.39 | 0.41 | 0.36 | 0.43 | 0.37 | 0.42 | 0.40 | 0.46 | 0.39 | 0.43 |
| MgO | 13.50 | 14.54 | 14.25 | 13.81 | 13.54 | 13.29 | 13.63 | 13.35 | 13.28 | 14.08 |
| CaO | 11.45 | 11.75 | 11.96 | 11.49 | 11.65 | 11.64 | 11.99 | 11.61 | 11.57 | 11.35 |
| Na ₂ O | 1.17 | 1.15 | 1.09 | 1.16 | 1.18 | 1.21 | 1.24 | 1.15 | 1.22 | 1.23 |
| K ₂ O | 0.63 | 0.46 | 0.52 | 0.57 | 0.59 | 0.67 | 0.60 | 0.61 | 0.66 | 0.61 |
| F | 0.474 | 0.469 | 0.442 | 0.461 | 0.465 | 0.482 | 0.465 | 0.457 | 0.499 | 0.471 |
| Cl | 0.057 | 0.040 | 0.043 | 0.052 | 0.052 | 0.062 | 0.041 | 0.035 | 0.049 | 0.047 |
| -O=F+Cl | 0.212 | 0.207 | 0.196 | 0.206 | 0.208 | 0.217 | 0.205 | 0.200 | 0.221 | 0.209 |
| Total | 97.88 | 98.16 | 98.70 | 97.50 | 97.36 | 97.43 | 98.17 | 97.28 | 97.65 | 97.62 |
| H ₂ O ^d | 1.81 | 1.84 | 1.85 | 1.81 | 1.80 | 1.79 | 1.82 | 1.81 | 1.79 | 1.81 |
| Total _{calc} | 99.69 | 100.00 | 100.55 | 99.31 | 99.16 | 99.22 | 99.99 | 99.09 | 99.43 | 99.43 |
| Mg ^{#e} | 0.628 | 0.662 | 0.651 | 0.637 | 0.635 | 0.626 | 0.639 | 0.630 | 0.621 | 0.643 |
| Cations based on 23 oxygen atoms | | | | | | | | | | |
| Si | 7.09 | 7.26 | 7.22 | 7.12 | 7.13 | 7.10 | 7.14 | 7.11 | 7.05 | 7.08 |
| [⁴]Al | 0.91 | 0.74 | 0.78 | 0.88 | 0.87 | 0.90 | 0.86 | 0.89 | 0.95 | 0.92 |
| ∑ T | 8.00 | 8.00 | 8.00 | 8.00 | 8.00 | 8.00 | 8.00 | 8.00 | 8.00 | 8.00 |
| [⁶]Al | 0.22 | 0.17 | 0.20 | 0.17 | 0.22 | 0.20 | 0.22 | 0.22 | 0.20 | 0.15 |
| Ti | 0.12 | 0.09 | 0.10 | 0.12 | 0.12 | 0.13 | 0.12 | 0.12 | 0.13 | 0.12 |
| Fe ^{3+f} | 0.26 | 0.21 | 0.18 | 0.27 | 0.19 | 0.18 | 0.12 | 0.20 | 0.23 | 0.33 |
| Mg | 2.94 | 3.14 | 3.07 | 3.02 | 2.97 | 2.92 | 2.97 | 2.93 | 2.91 | 3.07 |
| [^C]Fe ²⁺ | 1.45 | 1.38 | 1.46 | 1.42 | 1.51 | 1.56 | 1.56 | 1.52 | 1.52 | 1.34 |
| ∑ M1,2,3 | 5.00 | 5.00 | 5.00 | 5.00 | 5.00 | 5.00 | 5.00 | 5.00 | 5.00 | 5.00 |
| [^B]Fe ²⁺ | 0.03 | 0.01 | 0.01 | 0.03 | 0.01 | 0.00 | 0.00 | 0.00 | 0.02 | 0.04 |
| Mn | 0.05 | 0.05 | 0.04 | 0.05 | 0.05 | 0.05 | 0.03 | 0.06 | 0.05 | 0.05 |
| Ca | 1.79 | 1.82 | 1.85 | 1.80 | 1.83 | 1.84 | 1.88 | 1.83 | 1.82 | 1.78 |
| [^B]Na | 0.13 | 0.12 | 0.10 | 0.12 | 0.11 | 0.11 | 0.09 | 0.11 | 0.11 | 0.13 |
| ∑ M4 | 2.00 | 2.00 | 2.00 | 2.00 | 2.00 | 2.00 | 2.00 | 2.00 | 2.00 | 2.00 |
| [^A]Na | 0.20 | 0.21 | 0.21 | 0.21 | 0.22 | 0.24 | 0.26 | 0.22 | 0.24 | 0.22 |
| K | 0.12 | 0.09 | 0.10 | 0.11 | 0.11 | 0.13 | 0.11 | 0.11 | 0.12 | 0.11 |
| ∑ A | 0.32 | 0.29 | 0.30 | 0.32 | 0.34 | 0.36 | 0.37 | 0.33 | 0.36 | 0.33 |
| sum cations | 15.32 | 15.29 | 15.30 | 15.32 | 15.34 | 15.36 | 15.37 | 15.33 | 15.36 | 15.33 |
| F | 0.219 | 0.215 | 0.202 | 0.214 | 0.216 | 0.225 | 0.215 | 0.213 | 0.232 | 0.218 |
| Cl | 0.014 | 0.010 | 0.011 | 0.013 | 0.013 | 0.015 | 0.010 | 0.009 | 0.012 | 0.012 |
| OH | 1.77 | 1.78 | 1.79 | 1.77 | 1.77 | 1.76 | 1.78 | 1.78 | 1.76 | 1.77 |
| log(F/OH) | -0.91 | -0.92 | -0.95 | -0.92 | -0.91 | -0.89 | -0.92 | -0.92 | -0.88 | -0.91 |
| log(Cl/OH) | -2.10 | -2.26 | -2.23 | -2.14 | -2.14 | -2.06 | -2.24 | -2.31 | -2.16 | -2.18 |

Supplementary Table III-2 continued

| Rock type ^a | CD | CD | CD | CD | CD | CD | CD | CD | CD | CD |
|-----------------------------------|--------|-------|-------|-------|-------|-------|-------|-------|-------|-------|
| Spot | 14 | 15 | 16 | 17 | 18 | 19 | 33 | 34 | 35 | 39 |
| Group ^b | | | | | | | | | | |
| Chemical composition (oxides wt%) | | | | | | | | | | |
| SiO ₂ | 47.86 | 47.93 | 49.03 | 48.69 | 48.10 | 48.09 | 48.26 | 48.01 | 47.88 | 47.53 |
| Al ₂ O ₃ | 6.69 | 6.39 | 5.29 | 6.01 | 6.44 | 6.51 | 6.23 | 6.17 | 6.50 | 6.61 |
| TiO ₂ | 1.23 | 1.22 | 0.92 | 1.09 | 1.08 | 1.14 | 1.05 | 1.05 | 1.14 | 1.12 |
| FeO ^c | 14.70 | 14.37 | 13.51 | 13.81 | 14.03 | 14.24 | 14.29 | 14.16 | 14.32 | 14.16 |
| MnO | 0.38 | 0.45 | 0.41 | 0.35 | 0.38 | 0.45 | 0.42 | 0.39 | 0.39 | 0.33 |
| MgO | 13.62 | 13.43 | 14.45 | 14.18 | 13.94 | 13.67 | 13.98 | 13.77 | 13.66 | 14.02 |
| CaO | 11.65 | 11.34 | 11.87 | 11.46 | 11.66 | 11.53 | 11.73 | 11.71 | 11.79 | 11.47 |
| Na ₂ O | 1.19 | 1.22 | 1.03 | 1.23 | 1.21 | 1.15 | 1.21 | 1.11 | 1.14 | 1.34 |
| K ₂ O | 0.65 | 0.64 | 0.53 | 0.59 | 0.61 | 0.67 | 0.63 | 0.63 | 0.66 | 0.64 |
| F | 0.420 | 0.415 | 0.443 | 0.458 | 0.441 | 0.432 | 0.428 | 0.443 | 0.473 | 0.470 |
| Cl | 0.057 | 0.050 | 0.046 | 0.055 | 0.059 | 0.037 | 0.042 | 0.051 | 0.050 | 0.051 |
| -O=F+Cl | 0.190 | 0.186 | 0.197 | 0.205 | 0.199 | 0.190 | 0.190 | 0.198 | 0.210 | 0.209 |
| Total | 98.26 | 97.27 | 97.33 | 97.72 | 97.75 | 97.73 | 98.08 | 97.30 | 97.79 | 97.53 |
| H ₂ O ^d | 1.84 | 1.82 | 1.82 | 1.82 | 1.82 | 1.83 | 1.84 | 1.81 | 1.81 | 1.81 |
| Total _{calc} | 100.10 | 99.09 | 99.15 | 99.54 | 99.57 | 99.56 | 99.92 | 99.11 | 99.60 | 99.34 |
| Mg# ^e | 0.623 | 0.625 | 0.656 | 0.647 | 0.639 | 0.631 | 0.636 | 0.634 | 0.630 | 0.638 |
| Cations based on 23 oxygen atoms | | | | | | | | | | |
| Si | 6.99 | 7.06 | 7.19 | 7.11 | 7.04 | 7.05 | 7.05 | 7.07 | 7.03 | 6.98 |
| [⁴]Al | 1.01 | 0.94 | 0.81 | 0.89 | 0.96 | 0.95 | 0.95 | 0.93 | 0.97 | 1.02 |
| ∑ T | 8.00 | 8.00 | 8.00 | 8.00 | 8.00 | 8.00 | 8.00 | 8.00 | 8.00 | 8.00 |
| [⁶]Al | 0.14 | 0.17 | 0.10 | 0.15 | 0.15 | 0.17 | 0.12 | 0.14 | 0.15 | 0.12 |
| Ti | 0.14 | 0.14 | 0.10 | 0.12 | 0.12 | 0.13 | 0.12 | 0.12 | 0.13 | 0.12 |
| Fe ^{3+/f} | 0.33 | 0.29 | 0.27 | 0.29 | 0.29 | 0.29 | 0.32 | 0.29 | 0.28 | 0.36 |
| Mg | 2.97 | 2.95 | 3.16 | 3.09 | 3.04 | 2.99 | 3.04 | 3.02 | 2.99 | 3.07 |
| [^c]Fe ²⁺ | 1.43 | 1.46 | 1.38 | 1.36 | 1.39 | 1.43 | 1.40 | 1.44 | 1.45 | 1.33 |
| ∑ M1,2,3 | 5.00 | 5.00 | 5.00 | 5.00 | 5.00 | 5.00 | 5.00 | 5.00 | 5.00 | 5.00 |
| [^B]Fe ²⁺ | 0.04 | 0.03 | 0.01 | 0.04 | 0.03 | 0.03 | 0.02 | 0.02 | 0.02 | 0.05 |
| Mn | 0.05 | 0.06 | 0.05 | 0.04 | 0.05 | 0.06 | 0.05 | 0.05 | 0.05 | 0.04 |
| Ca | 1.82 | 1.79 | 1.86 | 1.79 | 1.83 | 1.81 | 1.84 | 1.85 | 1.85 | 1.80 |
| [^B]Na | 0.09 | 0.13 | 0.07 | 0.12 | 0.09 | 0.11 | 0.09 | 0.08 | 0.08 | 0.10 |
| ∑ M4 | 2.00 | 2.00 | 2.00 | 2.00 | 2.00 | 2.00 | 2.00 | 2.00 | 2.00 | 2.00 |
| [^A]Na | 0.24 | 0.22 | 0.22 | 0.23 | 0.25 | 0.22 | 0.25 | 0.24 | 0.25 | 0.28 |
| K | 0.12 | 0.12 | 0.10 | 0.11 | 0.11 | 0.13 | 0.12 | 0.12 | 0.12 | 0.12 |
| ∑ A | 0.36 | 0.34 | 0.32 | 0.34 | 0.37 | 0.35 | 0.37 | 0.35 | 0.37 | 0.40 |
| sum cations | 15.36 | 15.34 | 15.32 | 15.34 | 15.37 | 15.35 | 15.37 | 15.35 | 15.37 | 15.40 |
| F | 0.194 | 0.193 | 0.205 | 0.212 | 0.204 | 0.200 | 0.198 | 0.206 | 0.219 | 0.218 |
| Cl | 0.014 | 0.012 | 0.011 | 0.014 | 0.015 | 0.009 | 0.010 | 0.013 | 0.012 | 0.013 |
| OH | 1.79 | 1.79 | 1.78 | 1.77 | 1.78 | 1.79 | 1.79 | 1.78 | 1.77 | 1.77 |
| log(F/OH) | -0.97 | -0.97 | -0.94 | -0.92 | -0.94 | -0.95 | -0.96 | -0.94 | -0.91 | -0.91 |
| log(Cl/OH) | -2.10 | -2.16 | -2.19 | -2.12 | -2.09 | -2.29 | -2.24 | -2.15 | -2.15 | -2.14 |

Supplementary Table III-2 continued

| Rock type ^a | CD | CD | CD | CD | CD | CD | CD | CD | CD | CD |
|-----------------------------------|-------|-------|--------|-------|-------|-------|--------|--------|-------|-------|
| Spot | 40 | 41 | 70 | 71 | 72 | 73 | 74 | 75 | 76 | 77 |
| Group ^b | | | | | | | | | | |
| Chemical composition (oxides wt%) | | | | | | | | | | |
| SiO ₂ | 47.76 | 48.11 | 48.80 | 48.82 | 47.92 | 48.96 | 49.00 | 48.99 | 49.22 | 49.86 |
| Al ₂ O ₃ | 6.11 | 6.00 | 5.88 | 5.52 | 6.15 | 6.12 | 5.91 | 6.14 | 5.87 | 5.34 |
| TiO ₂ | 1.10 | 1.02 | 1.11 | 0.83 | 1.19 | 1.05 | 1.10 | 1.13 | 1.06 | 0.95 |
| FeO ^c | 13.76 | 13.62 | 13.91 | 14.12 | 14.33 | 13.88 | 13.85 | 14.03 | 13.67 | 13.20 |
| MnO | 0.40 | 0.35 | 0.44 | 0.38 | 0.36 | 0.35 | 0.38 | 0.36 | 0.44 | 0.40 |
| MgO | 14.08 | 14.30 | 14.17 | 14.04 | 13.61 | 13.86 | 14.17 | 13.82 | 13.93 | 14.15 |
| CaO | 11.71 | 11.80 | 11.57 | 11.91 | 11.44 | 11.63 | 11.73 | 11.50 | 11.66 | 11.73 |
| Na ₂ O | 1.21 | 1.08 | 1.38 | 0.96 | 1.30 | 1.25 | 1.31 | 1.35 | 1.18 | 1.12 |
| K ₂ O | 0.60 | 0.58 | 0.61 | 0.53 | 0.63 | 0.58 | 0.59 | 0.60 | 0.57 | 0.46 |
| F | 0.430 | 0.456 | 0.460 | 0.420 | 0.429 | 0.448 | 0.496 | 0.464 | 0.457 | 0.476 |
| Cl | 0.043 | 0.045 | 0.062 | 0.052 | 0.061 | 0.056 | 0.051 | 0.065 | 0.044 | 0.043 |
| -O=F+Cl | 0.191 | 0.202 | 0.208 | 0.189 | 0.194 | 0.201 | 0.220 | 0.210 | 0.202 | 0.210 |
| Total | 97.01 | 97.16 | 98.18 | 97.39 | 97.23 | 97.98 | 98.37 | 98.24 | 97.90 | 97.52 |
| H ₂ O ^d | 1.82 | 1.81 | 1.82 | 1.83 | 1.81 | 1.83 | 1.81 | 1.82 | 1.83 | 1.82 |
| Total _{calc} | 98.83 | 98.97 | 100.01 | 99.22 | 99.04 | 99.81 | 100.18 | 100.06 | 99.72 | 99.33 |
| Mg# ^e | 0.646 | 0.652 | 0.645 | 0.639 | 0.629 | 0.640 | 0.646 | 0.637 | 0.645 | 0.656 |
| Cations based on 23 oxygen atoms | | | | | | | | | | |
| Si | 7.04 | 7.07 | 7.11 | 7.16 | 7.07 | 7.14 | 7.13 | 7.13 | 7.18 | 7.28 |
| [⁴]Al | 0.96 | 0.93 | 0.89 | 0.84 | 0.93 | 0.86 | 0.87 | 0.87 | 0.82 | 0.72 |
| ∑ T | 8.00 | 8.00 | 8.00 | 8.00 | 8.00 | 8.00 | 8.00 | 8.00 | 8.00 | 8.00 |
| [⁶]Al | 0.11 | 0.11 | 0.12 | 0.12 | 0.14 | 0.19 | 0.14 | 0.19 | 0.19 | 0.20 |
| Ti | 0.12 | 0.11 | 0.12 | 0.09 | 0.13 | 0.12 | 0.12 | 0.12 | 0.12 | 0.10 |
| Fe ^{3+f} | 0.31 | 0.34 | 0.26 | 0.30 | 0.27 | 0.21 | 0.23 | 0.22 | 0.20 | 0.15 |
| Mg | 3.10 | 3.13 | 3.08 | 3.07 | 2.99 | 3.01 | 3.07 | 3.00 | 3.03 | 3.08 |
| [^C]Fe ²⁺ | 1.37 | 1.31 | 1.42 | 1.42 | 1.47 | 1.46 | 1.44 | 1.47 | 1.47 | 1.46 |
| ∑ M1,2,3 | 5.00 | 5.00 | 5.00 | 5.00 | 5.00 | 5.00 | 5.00 | 5.00 | 5.00 | 5.00 |
| [^B]Fe ²⁺ | 0.02 | 0.02 | 0.02 | 0.01 | 0.03 | 0.02 | 0.02 | 0.02 | 0.00 | 0.00 |
| Mn | 0.05 | 0.04 | 0.05 | 0.05 | 0.04 | 0.04 | 0.05 | 0.04 | 0.05 | 0.04 |
| Ca | 1.85 | 1.86 | 1.81 | 1.87 | 1.81 | 1.82 | 1.83 | 1.79 | 1.82 | 1.83 |
| [^B]Na | 0.08 | 0.08 | 0.12 | 0.07 | 0.12 | 0.12 | 0.11 | 0.14 | 0.12 | 0.12 |
| ∑ M4 | 2.00 | 2.00 | 2.00 | 2.00 | 2.00 | 2.00 | 2.00 | 2.00 | 2.00 | 2.00 |
| [^A]Na | 0.27 | 0.23 | 0.27 | 0.20 | 0.26 | 0.23 | 0.26 | 0.24 | 0.21 | 0.20 |
| K | 0.11 | 0.11 | 0.11 | 0.10 | 0.12 | 0.11 | 0.11 | 0.11 | 0.11 | 0.09 |
| ∑ A | 0.38 | 0.34 | 0.38 | 0.30 | 0.38 | 0.34 | 0.37 | 0.35 | 0.32 | 0.28 |
| sum cations | 15.38 | 15.34 | 15.38 | 15.30 | 15.38 | 15.34 | 15.37 | 15.35 | 15.32 | 15.28 |
| F | 0.201 | 0.212 | 0.212 | 0.195 | 0.200 | 0.207 | 0.228 | 0.214 | 0.211 | 0.220 |
| Cl | 0.011 | 0.011 | 0.015 | 0.013 | 0.015 | 0.014 | 0.013 | 0.016 | 0.011 | 0.011 |
| OH | 1.79 | 1.78 | 1.77 | 1.79 | 1.78 | 1.78 | 1.76 | 1.77 | 1.78 | 1.77 |
| log(F/OH) | -0.95 | -0.92 | -0.92 | -0.96 | -0.95 | -0.93 | -0.89 | -0.92 | -0.93 | -0.91 |
| log(Cl/OH) | -2.22 | -2.20 | -2.06 | -2.14 | -2.07 | -2.11 | -2.15 | -2.04 | -2.21 | -2.22 |

Supplementary Table III-2 continued

| Rock type ^e | CD | CD | CD | CD | CD | CD | CD | CD | CD | CD |
|-----------------------------------|--------|--------|--------|--------|-------|--------|--------|-------|--------|-------|
| Spot | 106 | 107 | 108 | 109 | 110 | 126 | 127 | 133 | 134 | 137 |
| Group ^b | | | | | | | | | | |
| Chemical composition (oxides wt%) | | | | | | | | | | |
| SiO ₂ | 48.87 | 49.68 | 48.11 | 48.38 | 48.78 | 48.50 | 49.12 | 48.04 | 49.40 | 49.05 |
| Al ₂ O ₃ | 6.22 | 5.50 | 6.78 | 6.42 | 6.06 | 6.46 | 6.15 | 6.69 | 5.88 | 6.10 |
| TiO ₂ | 1.10 | 0.97 | 1.23 | 1.18 | 1.13 | 1.20 | 1.11 | 1.20 | 1.12 | 0.96 |
| FeO ^c | 13.86 | 13.78 | 14.48 | 14.07 | 14.10 | 14.31 | 14.39 | 14.62 | 13.95 | 14.39 |
| MnO | 0.32 | 0.38 | 0.42 | 0.42 | 0.38 | 0.39 | 0.37 | 0.34 | 0.38 | 0.35 |
| MgO | 14.09 | 14.51 | 13.44 | 13.97 | 13.69 | 13.50 | 13.88 | 13.55 | 14.21 | 13.89 |
| CaO | 11.58 | 11.64 | 11.56 | 11.46 | 11.28 | 11.49 | 11.58 | 11.11 | 11.42 | 11.46 |
| Na ₂ O | 1.35 | 1.16 | 1.41 | 1.34 | 1.07 | 1.39 | 1.22 | 1.44 | 1.21 | 1.09 |
| K ₂ O | 0.55 | 0.52 | 0.70 | 0.64 | 0.60 | 0.64 | 0.62 | 0.73 | 0.59 | 0.57 |
| F | 0.485 | 0.450 | 0.493 | 0.448 | 0.454 | 0.468 | 0.466 | 0.522 | 0.467 | 0.410 |
| Cl | 0.049 | 0.059 | 0.054 | 0.052 | 0.048 | 0.065 | 0.053 | 0.062 | 0.055 | 0.041 |
| -O=F+Cl | 0.215 | 0.203 | 0.220 | 0.200 | 0.202 | 0.212 | 0.208 | 0.234 | 0.209 | 0.182 |
| Total | 98.26 | 98.45 | 98.46 | 98.18 | 97.39 | 98.20 | 98.75 | 98.07 | 98.47 | 98.13 |
| H ₂ O ^d | 1.82 | 1.84 | 1.81 | 1.83 | 1.82 | 1.81 | 1.83 | 1.79 | 1.83 | 1.86 |
| Total _{calc} | 100.08 | 100.29 | 100.26 | 100.01 | 99.21 | 100.01 | 100.58 | 99.86 | 100.31 | 99.98 |
| Mg# ^e | 0.644 | 0.652 | 0.623 | 0.639 | 0.634 | 0.627 | 0.632 | 0.623 | 0.645 | 0.632 |
| Cations based on 23 oxygen atoms | | | | | | | | | | |
| Si | 7.11 | 7.19 | 7.02 | 7.05 | 7.15 | 7.08 | 7.12 | 7.02 | 7.15 | 7.13 |
| [⁴]Al | 0.89 | 0.81 | 0.98 | 0.95 | 0.85 | 0.92 | 0.88 | 0.98 | 0.85 | 0.87 |
| ∑ T | 8.00 | 8.00 | 8.00 | 8.00 | 8.00 | 8.00 | 8.00 | 8.00 | 8.00 | 8.00 |
| [⁶]Al | 0.17 | 0.13 | 0.19 | 0.15 | 0.19 | 0.20 | 0.17 | 0.18 | 0.16 | 0.18 |
| Ti | 0.12 | 0.11 | 0.14 | 0.13 | 0.12 | 0.13 | 0.12 | 0.13 | 0.12 | 0.11 |
| Fe ^{3+f} | 0.25 | 0.28 | 0.24 | 0.29 | 0.29 | 0.22 | 0.27 | 0.32 | 0.29 | 0.31 |
| Mg | 3.05 | 3.13 | 2.92 | 3.03 | 2.99 | 2.94 | 3.00 | 2.95 | 3.07 | 3.01 |
| [^C]Fe ²⁺ | 1.40 | 1.36 | 1.51 | 1.39 | 1.40 | 1.51 | 1.45 | 1.41 | 1.37 | 1.39 |
| ∑ M1,2,3 | 5.00 | 5.00 | 5.00 | 5.00 | 5.00 | 5.00 | 5.00 | 5.00 | 5.00 | 5.00 |
| [^B]Fe ²⁺ | 0.03 | 0.03 | 0.02 | 0.03 | 0.04 | 0.01 | 0.03 | 0.05 | 0.04 | 0.05 |
| Mn | 0.04 | 0.05 | 0.05 | 0.05 | 0.05 | 0.05 | 0.05 | 0.04 | 0.05 | 0.04 |
| Ca | 1.80 | 1.81 | 1.81 | 1.79 | 1.77 | 1.80 | 1.80 | 1.74 | 1.77 | 1.79 |
| [^B]Na | 0.12 | 0.12 | 0.12 | 0.13 | 0.15 | 0.14 | 0.13 | 0.17 | 0.15 | 0.12 |
| ∑ M4 | 2.00 | 2.00 | 2.00 | 2.00 | 2.00 | 2.00 | 2.00 | 2.00 | 2.00 | 2.00 |
| [^A]Na | 0.26 | 0.21 | 0.27 | 0.25 | 0.16 | 0.25 | 0.22 | 0.24 | 0.19 | 0.18 |
| K | 0.10 | 0.10 | 0.13 | 0.12 | 0.11 | 0.12 | 0.11 | 0.14 | 0.11 | 0.11 |
| ∑ A | 0.36 | 0.31 | 0.41 | 0.37 | 0.27 | 0.37 | 0.33 | 0.38 | 0.30 | 0.29 |
| sum cations | 15.36 | 15.31 | 15.41 | 15.37 | 15.27 | 15.37 | 15.33 | 15.38 | 15.30 | 15.29 |
| F | 0.223 | 0.206 | 0.228 | 0.206 | 0.210 | 0.216 | 0.214 | 0.241 | 0.214 | 0.189 |
| Cl | 0.012 | 0.014 | 0.013 | 0.013 | 0.012 | 0.016 | 0.013 | 0.015 | 0.013 | 0.010 |
| OH | 1.76 | 1.78 | 1.76 | 1.78 | 1.78 | 1.77 | 1.77 | 1.74 | 1.77 | 1.80 |
| log(F/OH) | -0.90 | -0.94 | -0.89 | -0.94 | -0.93 | -0.91 | -0.92 | -0.86 | -0.92 | -0.98 |
| log(Cl/OH) | -2.16 | -2.09 | -2.12 | -2.14 | -2.17 | -2.04 | -2.13 | -2.05 | -2.12 | -2.25 |

Supplementary Table III-2 continued

| Rock type ^a | CD | CD | CD | CD | CD | CD | CD | CD | CD | CD |
|-----------------------------------|-------|-------|-------|-------|--------|--------|--------|-------|--------|--------|
| Spot | 138 | 139 | 140 | 141 | 172 | 174 | 175 | 181 | 193 | 194 |
| Group ^b | | | | | | | | | | |
| Chemical composition (oxides wt%) | | | | | | | | | | |
| SiO ₂ | 49.14 | 47.71 | 47.81 | 48.92 | 48.07 | 48.89 | 48.11 | 48.66 | 48.66 | 48.85 |
| Al ₂ O ₃ | 5.50 | 6.70 | 6.76 | 6.01 | 6.79 | 6.40 | 6.81 | 6.15 | 6.56 | 6.15 |
| TiO ₂ | 0.96 | 1.26 | 1.28 | 1.04 | 1.20 | 1.19 | 1.23 | 1.17 | 1.08 | 1.08 |
| FeO ^c | 13.85 | 14.70 | 15.05 | 13.82 | 14.98 | 14.78 | 14.84 | 13.97 | 14.42 | 14.25 |
| MnO | 0.37 | 0.41 | 0.36 | 0.36 | 0.45 | 0.40 | 0.39 | 0.40 | 0.38 | 0.35 |
| MgO | 14.01 | 13.29 | 13.06 | 13.59 | 13.10 | 13.56 | 13.37 | 13.58 | 14.05 | 14.02 |
| CaO | 11.60 | 11.37 | 11.36 | 11.66 | 11.53 | 11.50 | 11.50 | 11.50 | 11.31 | 11.56 |
| Na ₂ O | 1.16 | 1.29 | 1.25 | 1.09 | 1.18 | 1.29 | 1.31 | 1.29 | 1.27 | 1.10 |
| K ₂ O | 0.51 | 0.66 | 0.66 | 0.55 | 0.66 | 0.65 | 0.68 | 0.63 | 0.61 | 0.58 |
| F | 0.447 | 0.492 | 0.458 | 0.421 | 0.388 | 0.449 | 0.459 | 0.421 | 0.472 | 0.453 |
| Cl | 0.044 | 0.047 | 0.063 | 0.043 | 0.054 | 0.063 | 0.049 | 0.067 | 0.056 | 0.054 |
| -O=F+Cl | 0.198 | 0.218 | 0.207 | 0.187 | 0.176 | 0.203 | 0.204 | 0.192 | 0.211 | 0.203 |
| Total | 97.39 | 97.71 | 97.90 | 97.32 | 98.23 | 98.97 | 98.54 | 97.65 | 98.66 | 98.24 |
| H ₂ O ^d | 1.82 | 1.79 | 1.81 | 1.83 | 1.85 | 1.84 | 1.83 | 1.83 | 1.83 | 1.83 |
| Total _{calc} | 99.21 | 99.50 | 99.71 | 99.15 | 100.08 | 100.81 | 100.37 | 99.47 | 100.49 | 100.08 |
| Mg ^{#e} | 0.643 | 0.617 | 0.607 | 0.637 | 0.609 | 0.621 | 0.616 | 0.634 | 0.635 | 0.637 |
| Cations based on 23 oxygen atoms | | | | | | | | | | |
| Si | 7.20 | 7.01 | 7.02 | 7.18 | 7.03 | 7.08 | 7.01 | 7.13 | 7.04 | 7.10 |
| [⁴]Al | 0.80 | 0.99 | 0.98 | 0.82 | 0.97 | 0.92 | 0.99 | 0.87 | 0.96 | 0.90 |
| ∑ T | 8.00 | 8.00 | 8.00 | 8.00 | 8.00 | 8.00 | 8.00 | 8.00 | 8.00 | 8.00 |
| [⁶]Al | 0.15 | 0.17 | 0.19 | 0.22 | 0.20 | 0.18 | 0.18 | 0.20 | 0.16 | 0.16 |
| Ti | 0.11 | 0.14 | 0.14 | 0.11 | 0.13 | 0.13 | 0.13 | 0.13 | 0.12 | 0.12 |
| Fe ^{3+f} | 0.23 | 0.29 | 0.29 | 0.18 | 0.27 | 0.27 | 0.28 | 0.20 | 0.37 | 0.31 |
| Mg | 3.06 | 2.91 | 2.86 | 2.97 | 2.86 | 2.93 | 2.91 | 2.97 | 3.03 | 3.04 |
| [^c]Fe ²⁺ | 1.45 | 1.48 | 1.52 | 1.51 | 1.54 | 1.49 | 1.49 | 1.51 | 1.32 | 1.38 |
| ∑ M1,2,3 | 5.00 | 5.00 | 5.00 | 5.00 | 5.00 | 5.00 | 5.00 | 5.00 | 5.00 | 5.00 |
| [^B]Fe ²⁺ | 0.02 | 0.03 | 0.04 | 0.01 | 0.02 | 0.03 | 0.03 | 0.01 | 0.06 | 0.05 |
| Mn | 0.05 | 0.05 | 0.04 | 0.04 | 0.06 | 0.05 | 0.05 | 0.05 | 0.05 | 0.04 |
| Ca | 1.82 | 1.79 | 1.79 | 1.83 | 1.81 | 1.79 | 1.80 | 1.81 | 1.75 | 1.80 |
| [^B]Na | 0.11 | 0.13 | 0.13 | 0.11 | 0.11 | 0.14 | 0.12 | 0.14 | 0.14 | 0.11 |
| ∑ M4 | 2.00 | 2.00 | 2.00 | 2.00 | 2.00 | 2.00 | 2.00 | 2.00 | 2.00 | 2.00 |
| [^A]Na | 0.22 | 0.24 | 0.23 | 0.20 | 0.22 | 0.23 | 0.25 | 0.23 | 0.22 | 0.20 |
| K | 0.10 | 0.12 | 0.12 | 0.10 | 0.12 | 0.12 | 0.13 | 0.12 | 0.11 | 0.11 |
| ∑ A | 0.31 | 0.37 | 0.35 | 0.30 | 0.34 | 0.35 | 0.37 | 0.35 | 0.33 | 0.31 |
| sum cations | 15.31 | 15.37 | 15.35 | 15.30 | 15.34 | 15.35 | 15.37 | 15.35 | 15.33 | 15.31 |
| F | 0.207 | 0.229 | 0.213 | 0.195 | 0.179 | 0.206 | 0.212 | 0.195 | 0.216 | 0.208 |
| Cl | 0.011 | 0.012 | 0.016 | 0.011 | 0.013 | 0.015 | 0.012 | 0.017 | 0.014 | 0.013 |
| OH | 1.78 | 1.76 | 1.77 | 1.79 | 1.81 | 1.78 | 1.78 | 1.79 | 1.77 | 1.78 |
| log(F/OH) | -0.93 | -0.89 | -0.92 | -0.96 | -1.00 | -0.94 | -0.92 | -0.96 | -0.91 | -0.93 |
| log(Cl/OH) | -2.21 | -2.18 | -2.05 | -2.22 | -2.13 | -2.06 | -2.17 | -2.03 | -2.11 | -2.13 |

Supplementary Table III-2 continued

| Rock type ^a | CD | CD | CD | CD | CD | CD | CD | CD | CD | CD |
|-----------------------------------|--------|--------|-------|--------|--------|--------|--------|--------|--------|--------|
| Spot | 197 | 198 | 201 | 202 | a69 | a70 | a76/1 | a76/2 | a76/3 | a76/4 |
| Group ^b | | | | | | | | | | |
| Chemical composition (oxides wt%) | | | | | | | | | | |
| SiO ₂ | 48.61 | 48.86 | 49.30 | 48.54 | 48.79 | 49.06 | 48.34 | 49.82 | 48.97 | 48.87 |
| Al ₂ O ₃ | 6.18 | 6.80 | 6.00 | 6.58 | 6.15 | 6.30 | 6.53 | 5.48 | 5.99 | 5.92 |
| TiO ₂ | 1.04 | 1.20 | 0.98 | 1.10 | 1.16 | 1.15 | 1.24 | 0.93 | 1.11 | 1.15 |
| FeO ^c | 14.37 | 14.62 | 13.77 | 14.22 | 14.23 | 13.89 | 13.89 | 13.70 | 14.08 | 13.64 |
| MnO | 0.44 | 0.40 | 0.34 | 0.38 | 0.31 | 0.37 | 0.38 | 0.32 | 0.39 | 0.34 |
| MgO | 14.17 | 13.30 | 13.80 | 13.88 | 14.10 | 14.33 | 14.19 | 14.59 | 14.06 | 14.40 |
| CaO | 11.78 | 11.64 | 11.57 | 11.63 | 11.86 | 11.56 | 11.78 | 12.16 | 12.02 | 11.92 |
| Na ₂ O | 1.23 | 1.28 | 1.15 | 1.31 | 1.14 | 1.23 | 1.00 | 1.10 | 1.04 | 1.14 |
| K ₂ O | 0.62 | 0.66 | 0.59 | 0.61 | 0.63 | 0.63 | 0.61 | 0.58 | 0.56 | 0.61 |
| F | 0.437 | 0.435 | 0.467 | 0.433 | 0.40 | 0.41 | 0.382 | 0.369 | 0.390 | 0.402 |
| Cl | 0.046 | 0.056 | 0.045 | 0.059 | 0.04 | 0.05 | 0.040 | 0.047 | 0.044 | 0.039 |
| -O=F+Cl | 0.194 | 0.196 | 0.207 | 0.196 | 0.177 | 0.184 | 0.170 | 0.166 | 0.174 | 0.178 |
| Total | 98.73 | 99.06 | 97.81 | 98.55 | 98.63 | 98.80 | 98.21 | 98.93 | 98.48 | 98.25 |
| H ₂ O ^d | 1.85 | 1.85 | 1.82 | 1.84 | 1.86 | 1.87 | 1.87 | 1.89 | 1.87 | 1.86 |
| Total _{calc} | 100.58 | 100.90 | 99.63 | 100.39 | 100.50 | 100.66 | 100.08 | 100.82 | 100.35 | 100.11 |
| Mg# ^e | 0.637 | 0.619 | 0.641 | 0.635 | 0.639 | 0.648 | 0.646 | 0.655 | 0.640 | 0.653 |
| Cations based on 23 oxygen atoms | | | | | | | | | | |
| Si | 7.05 | 7.08 | 7.19 | 7.05 | 7.08 | 7.08 | 7.02 | 7.19 | 7.11 | 7.11 |
| [⁴]Al | 0.95 | 0.92 | 0.81 | 0.95 | 0.92 | 0.92 | 0.98 | 0.81 | 0.89 | 0.89 |
| ∑ T | 8.00 | 8.00 | 8.00 | 8.00 | 8.00 | 8.00 | 8.00 | 8.00 | 8.00 | 8.00 |
| [⁶]Al | 0.11 | 0.24 | 0.23 | 0.18 | 0.13 | 0.16 | 0.14 | 0.12 | 0.14 | 0.12 |
| Ti | 0.11 | 0.13 | 0.11 | 0.12 | 0.13 | 0.12 | 0.14 | 0.10 | 0.12 | 0.13 |
| Fe ^{3+/f} | 0.34 | 0.21 | 0.20 | 0.27 | 0.26 | 0.30 | 0.36 | 0.20 | 0.25 | 0.24 |
| Mg | 3.06 | 2.87 | 3.00 | 3.01 | 3.05 | 3.08 | 3.07 | 3.14 | 3.04 | 3.12 |
| [^C]Fe ²⁺ | 1.38 | 1.55 | 1.47 | 1.42 | 1.43 | 1.33 | 1.30 | 1.44 | 1.45 | 1.39 |
| ∑ M1,2,3 | 5.00 | 5.00 | 5.00 | 5.00 | 5.00 | 5.00 | 5.00 | 5.00 | 5.00 | 5.00 |
| [^B]Fe ²⁺ | 0.03 | 0.01 | 0.01 | 0.03 | 0.03 | 0.04 | 0.03 | 0.02 | 0.01 | 0.02 |
| Mn | 0.05 | 0.05 | 0.04 | 0.05 | 0.04 | 0.05 | 0.05 | 0.04 | 0.05 | 0.04 |
| Ca | 1.83 | 1.81 | 1.81 | 1.81 | 1.84 | 1.79 | 1.83 | 1.88 | 1.87 | 1.86 |
| [^B]Na | 0.09 | 0.13 | 0.13 | 0.11 | 0.08 | 0.13 | 0.09 | 0.06 | 0.07 | 0.08 |
| ∑ M4 | 2.00 | 2.00 | 2.00 | 2.00 | 2.00 | 2.00 | 2.00 | 2.00 | 2.00 | 2.00 |
| [^A]Na | 0.26 | 0.23 | 0.19 | 0.26 | 0.24 | 0.22 | 0.19 | 0.24 | 0.22 | 0.25 |
| K | 0.11 | 0.12 | 0.11 | 0.11 | 0.12 | 0.12 | 0.11 | 0.11 | 0.10 | 0.11 |
| ∑ A | 0.37 | 0.35 | 0.30 | 0.37 | 0.35 | 0.34 | 0.31 | 0.35 | 0.33 | 0.36 |
| sum cations | 15.37 | 15.35 | 15.30 | 15.37 | 15.35 | 15.34 | 15.31 | 15.35 | 15.33 | 15.36 |
| F | 0.200 | 0.199 | 0.216 | 0.199 | 0.184 | 0.187 | 0.175 | 0.168 | 0.179 | 0.185 |
| Cl | 0.011 | 0.014 | 0.011 | 0.015 | 0.010 | 0.012 | 0.010 | 0.011 | 0.011 | 0.010 |
| OH | 1.79 | 1.79 | 1.77 | 1.79 | 1.81 | 1.80 | 1.81 | 1.82 | 1.81 | 1.81 |
| log(F/OH) | -0.95 | -0.95 | -0.92 | -0.95 | -0.99 | -0.98 | -1.01 | -1.03 | -1.00 | -0.99 |
| log(Cl/OH) | -2.20 | -2.11 | -2.20 | -2.09 | -2.26 | -2.17 | -2.27 | -2.20 | -2.22 | -2.27 |

Supplementary Table III-2 continued

| Rock type ^a | CD | CD | CD | CD | CD | CD | CD | CD | CD | CD |
|-----------------------------------|-------|--------|-------|--------|-------|--------|--------|--------|--------|--------|
| Spot | a76/5 | a76/6 | a76/7 | a76/8 | a76/9 | a76/10 | a76/11 | a76/12 | a76/13 | a76/14 |
| Group ^b | | | | | | | | | | |
| Chemical composition (oxides wt%) | | | | | | | | | | |
| SiO ₂ | 48.43 | 48.38 | 49.22 | 48.56 | 48.50 | 49.01 | 48.57 | 49.05 | 48.91 | 49.85 |
| Al ₂ O ₃ | 6.45 | 6.14 | 5.77 | 6.03 | 5.95 | 6.00 | 6.13 | 5.95 | 6.04 | 5.67 |
| TiO ₂ | 1.23 | 1.19 | 1.11 | 1.19 | 1.15 | 1.15 | 1.12 | 1.08 | 1.05 | 1.02 |
| FeO ^c | 13.87 | 13.75 | 13.57 | 14.15 | 13.81 | 13.55 | 13.91 | 14.29 | 13.64 | 14.14 |
| MnO | 0.38 | 0.40 | 0.37 | 0.36 | 0.37 | 0.35 | 0.38 | 0.41 | 0.37 | 0.39 |
| MgO | 13.83 | 14.26 | 14.29 | 14.57 | 14.37 | 14.24 | 14.31 | 14.28 | 14.41 | 14.35 |
| CaO | 11.62 | 11.90 | 11.68 | 11.70 | 11.51 | 11.63 | 11.69 | 11.43 | 11.57 | 11.43 |
| Na ₂ O | 1.23 | 1.27 | 1.23 | 1.27 | 1.25 | 1.11 | 1.33 | 1.29 | 1.28 | 1.24 |
| K ₂ O | 0.67 | 0.64 | 0.56 | 0.62 | 0.58 | 0.60 | 0.59 | 0.59 | 0.62 | 0.56 |
| F | 0.393 | 0.404 | 0.417 | 0.403 | 0.395 | 0.399 | 0.400 | 0.423 | 0.421 | 0.378 |
| Cl | 0.050 | 0.051 | 0.048 | 0.054 | 0.051 | 0.049 | 0.047 | 0.051 | 0.046 | 0.043 |
| -O=F+Cl | 0.177 | 0.182 | 0.186 | 0.182 | 0.178 | 0.179 | 0.179 | 0.190 | 0.188 | 0.169 |
| Total | 97.98 | 98.20 | 98.08 | 98.73 | 97.76 | 97.91 | 98.30 | 98.65 | 98.17 | 98.90 |
| H ₂ O ^d | 1.85 | 1.85 | 1.85 | 1.87 | 1.85 | 1.86 | 1.86 | 1.86 | 1.85 | 1.89 |
| Total _{calc} | 99.83 | 100.05 | 99.93 | 100.59 | 99.61 | 99.77 | 100.16 | 100.51 | 100.02 | 100.79 |
| Mg# ^e | 0.640 | 0.649 | 0.652 | 0.647 | 0.650 | 0.652 | 0.647 | 0.640 | 0.653 | 0.644 |
| Cations based on 23 oxygen atoms | | | | | | | | | | |
| Si | 7.07 | 7.05 | 7.16 | 7.03 | 7.08 | 7.13 | 7.07 | 7.10 | 7.11 | 7.18 |
| [^H]Al | 0.93 | 0.95 | 0.84 | 0.97 | 0.92 | 0.87 | 0.93 | 0.90 | 0.89 | 0.82 |
| ∑ T | 8.00 | 8.00 | 8.00 | 8.00 | 8.00 | 8.00 | 8.00 | 8.00 | 8.00 | 8.00 |
| [^G]Al | 0.18 | 0.11 | 0.15 | 0.06 | 0.10 | 0.16 | 0.12 | 0.12 | 0.14 | 0.14 |
| Ti | 0.14 | 0.13 | 0.12 | 0.13 | 0.13 | 0.13 | 0.12 | 0.12 | 0.11 | 0.11 |
| Fe ^{3+f} | 0.23 | 0.25 | 0.23 | 0.38 | 0.32 | 0.25 | 0.28 | 0.34 | 0.28 | 0.30 |
| Mg | 3.01 | 3.10 | 3.10 | 3.14 | 3.13 | 3.09 | 3.10 | 3.08 | 3.12 | 3.08 |
| [^C]Fe ²⁺ | 1.44 | 1.41 | 1.40 | 1.29 | 1.32 | 1.37 | 1.38 | 1.35 | 1.34 | 1.36 |
| ∑ M1,2,3 | 5.00 | 5.00 | 5.00 | 5.00 | 5.00 | 5.00 | 5.00 | 5.00 | 5.00 | 5.00 |
| [^B]Fe ²⁺ | 0.02 | 0.02 | 0.02 | 0.04 | 0.05 | 0.03 | 0.03 | 0.05 | 0.04 | 0.04 |
| Mn | 0.05 | 0.05 | 0.05 | 0.04 | 0.05 | 0.04 | 0.05 | 0.05 | 0.05 | 0.05 |
| Ca | 1.82 | 1.86 | 1.82 | 1.81 | 1.80 | 1.81 | 1.82 | 1.77 | 1.80 | 1.76 |
| [^B]Na | 0.12 | 0.08 | 0.11 | 0.10 | 0.11 | 0.11 | 0.10 | 0.13 | 0.12 | 0.15 |
| ∑ M4 | 2.00 | 2.00 | 2.00 | 2.00 | 2.00 | 2.00 | 2.00 | 2.00 | 2.00 | 2.00 |
| [^A]Na | 0.23 | 0.28 | 0.23 | 0.26 | 0.25 | 0.20 | 0.28 | 0.23 | 0.24 | 0.20 |
| K | 0.12 | 0.12 | 0.10 | 0.11 | 0.11 | 0.11 | 0.11 | 0.11 | 0.11 | 0.10 |
| ∑ A | 0.36 | 0.40 | 0.34 | 0.37 | 0.35 | 0.31 | 0.39 | 0.34 | 0.36 | 0.30 |
| sum cations | 15.36 | 15.40 | 15.34 | 15.37 | 15.35 | 15.31 | 15.39 | 15.34 | 15.36 | 15.30 |
| F | 0.181 | 0.186 | 0.192 | 0.184 | 0.182 | 0.184 | 0.184 | 0.194 | 0.193 | 0.172 |
| Cl | 0.012 | 0.013 | 0.012 | 0.013 | 0.013 | 0.012 | 0.012 | 0.013 | 0.011 | 0.010 |
| OH | 1.81 | 1.80 | 1.80 | 1.80 | 1.80 | 1.80 | 1.80 | 1.79 | 1.80 | 1.82 |
| log(F/OH) | -1.00 | -0.99 | -0.97 | -0.99 | -1.00 | -0.99 | -0.99 | -0.97 | -0.97 | -1.02 |
| log(Cl/OH) | -2.16 | -2.16 | -2.18 | -2.13 | -2.16 | -2.17 | -2.19 | -2.16 | -2.20 | -2.24 |

Supplementary Table III-2 continued

| Rock type ^a | CD | CD | CD | CD | CD | CD | CD | HG | HG | HG |
|-----------------------------------|--------|-------|--------|--------|--------|-------|-------|--------|-------|-------|
| Spot | a76/15 | a82 | a86 | a87 | a100 | a101 | a107 | 19 | 20 | 22 |
| Group ^b | | | | | | | | II | I | I |
| Chemical composition (oxides wt%) | | | | | | | | | | |
| SiO ₂ | 48.71 | 48.58 | 49.71 | 48.00 | 48.83 | 48.27 | 48.77 | 43.01 | 42.45 | 42.17 |
| Al ₂ O ₃ | 6.01 | 6.39 | 5.48 | 6.46 | 6.00 | 6.35 | 6.07 | 11.12 | 12.02 | 12.58 |
| TiO ₂ | 1.14 | 1.16 | 0.90 | 1.10 | 1.02 | 1.12 | 1.10 | 2.63 | 2.79 | 3.06 |
| FeO ^c | 14.17 | 13.97 | 13.47 | 14.62 | 13.89 | 14.27 | 13.68 | 14.89 | 12.33 | 12.78 |
| MnO | 0.42 | 0.37 | 0.39 | 0.36 | 0.34 | 0.37 | 0.40 | 0.26 | 0.23 | 0.24 |
| MgO | 14.15 | 14.01 | 14.93 | 13.99 | 14.49 | 13.80 | 14.31 | 11.9 | 13.15 | 12.61 |
| CaO | 11.84 | 11.52 | 11.51 | 11.78 | 11.58 | 11.66 | 11.45 | 11.23 | 11.31 | 11.15 |
| Na ₂ O | 1.16 | 1.18 | 1.10 | 1.27 | 1.17 | 1.28 | 1.24 | 2.11 | 2.23 | 2.41 |
| K ₂ O | 0.59 | 0.63 | 0.51 | 0.62 | 0.60 | 0.66 | 0.65 | 0.84 | 0.81 | 0.88 |
| F | 0.385 | 0.410 | 0.394 | 0.417 | 0.407 | 0.381 | 0.427 | 0.365 | 0.379 | 0.378 |
| Cl | 0.047 | 0.050 | 0.057 | 0.061 | 0.040 | 0.046 | 0.052 | 0.025 | 0.010 | 0.019 |
| -O=F+Cl | 0.173 | 0.184 | 0.179 | 0.189 | 0.180 | 0.171 | 0.192 | 0.159 | 0.162 | 0.163 |
| Total | 98.45 | 98.09 | 98.27 | 98.49 | 98.19 | 98.04 | 97.96 | 98.22 | 97.55 | 98.11 |
| H ₂ O ^d | 1.87 | 1.85 | 1.87 | 1.85 | 1.86 | 1.86 | 1.84 | 1.85 | 1.85 | 1.86 |
| Total _{calc} | 100.32 | 99.94 | 100.15 | 100.33 | 100.05 | 99.89 | 99.80 | 100.07 | 99.40 | 99.97 |
| Mg ^{#e} | 0.640 | 0.641 | 0.664 | 0.630 | 0.650 | 0.633 | 0.651 | 0.588 | 0.655 | 0.638 |
| Cations based on 23 oxygen atoms | | | | | | | | | | |
| Si | 7.08 | 7.07 | 7.18 | 6.99 | 7.09 | 7.06 | 7.10 | 6.36 | 6.25 | 6.19 |
| ^[4] Al | 0.92 | 0.93 | 0.82 | 1.01 | 0.91 | 0.94 | 0.90 | 1.64 | 1.75 | 1.81 |
| ∑ T | 8.00 | 8.00 | 8.00 | 8.00 | 8.00 | 8.00 | 8.00 | 8.00 | 8.00 | 8.00 |
| ^[6] Al | 0.11 | 0.17 | 0.11 | 0.10 | 0.12 | 0.15 | 0.14 | 0.29 | 0.34 | 0.37 |
| Ti | 0.12 | 0.13 | 0.10 | 0.12 | 0.11 | 0.12 | 0.12 | 0.29 | 0.31 | 0.34 |
| Fe ^{3+f} | 0.29 | 0.29 | 0.35 | 0.38 | 0.34 | 0.26 | 0.30 | 0.28 | 0.28 | 0.25 |
| Mg | 3.07 | 3.04 | 3.21 | 3.04 | 3.14 | 3.01 | 3.11 | 2.62 | 2.89 | 2.76 |
| ^[C] Fe ²⁺ | 1.41 | 1.37 | 1.23 | 1.37 | 1.29 | 1.46 | 1.33 | 1.51 | 1.19 | 1.28 |
| ∑ M1,2,3 | 5.00 | 5.00 | 5.00 | 5.00 | 5.00 | 5.00 | 5.00 | 5.00 | 5.00 | 5.00 |
| ^[B] Fe ²⁺ | 0.02 | 0.04 | 0.05 | 0.03 | 0.05 | 0.03 | 0.04 | 0.05 | 0.05 | 0.04 |
| Mn | 0.05 | 0.05 | 0.05 | 0.04 | 0.04 | 0.05 | 0.05 | 0.03 | 0.03 | 0.03 |
| Ca | 1.84 | 1.80 | 1.78 | 1.84 | 1.80 | 1.83 | 1.79 | 1.78 | 1.78 | 1.75 |
| ^[B] Na | 0.08 | 0.12 | 0.12 | 0.09 | 0.11 | 0.10 | 0.13 | 0.14 | 0.14 | 0.17 |
| ∑ M4 | 2.00 | 2.00 | 2.00 | 2.00 | 2.00 | 2.00 | 2.00 | 2.00 | 2.00 | 2.00 |
| ^[A] Na | 0.24 | 0.21 | 0.19 | 0.27 | 0.22 | 0.26 | 0.22 | 0.46 | 0.50 | 0.51 |
| K | 0.11 | 0.12 | 0.09 | 0.12 | 0.11 | 0.12 | 0.12 | 0.16 | 0.15 | 0.16 |
| ∑ A | 0.35 | 0.33 | 0.28 | 0.39 | 0.33 | 0.39 | 0.34 | 0.62 | 0.65 | 0.68 |
| sum cations | 15.35 | 15.33 | 15.28 | 15.39 | 15.33 | 15.39 | 15.34 | 15.62 | 15.65 | 15.68 |
| F | 0.177 | 0.189 | 0.180 | 0.192 | 0.187 | 0.176 | 0.197 | 0.171 | 0.176 | 0.176 |
| Cl | 0.012 | 0.012 | 0.014 | 0.015 | 0.010 | 0.011 | 0.013 | 0.006 | 0.002 | 0.005 |
| OH | 1.81 | 1.80 | 1.81 | 1.79 | 1.80 | 1.81 | 1.79 | 1.82 | 1.82 | 1.82 |
| log(F/OH) | -1.01 | -0.98 | -1.00 | -0.97 | -0.98 | -1.01 | -0.96 | -0.95 | -0.90 | -0.91 |
| log(Cl/OH) | -2.19 | -2.16 | -2.11 | -2.08 | -2.26 | -2.20 | -2.14 | -2.27 | -2.17 | -2.10 |

Supplementary Table III-2 continued

| Rock type ^a | HG | HG | HG | HG | HG | HG | HG | HG | HG | HG |
|-----------------------------------|-------|-------|-------|--------|-------|-------|-------|-------|-------|-------|
| Spot | 23 | 26 | 27 | 209 | 210 | 211 | 212 | 214 | 215 | 225 |
| Group ^b | I | I | I | III | III | II | III | IV | IV | IV |
| Chemical composition (oxides wt%) | | | | | | | | | | |
| SiO ₂ | 42.42 | 42.83 | 42.51 | 45.22 | 44.24 | 42.32 | 47.24 | 50.57 | 49.24 | 49.32 |
| Al ₂ O ₃ | 12.14 | 11.11 | 12.25 | 9.27 | 9.94 | 11.29 | 7.19 | 4.73 | 5.9 | 5.83 |
| TiO ₂ | 2.91 | 2.58 | 3.06 | 2.17 | 2.35 | 2.78 | 1.56 | 0.29 | 0.35 | 0.37 |
| FeO ^c | 12.98 | 13.6 | 12.49 | 14.54 | 14.38 | 14.17 | 13.92 | 12.75 | 13.4 | 13.27 |
| MnO | 0.24 | 0.28 | 0.17 | 0.3 | 0.32 | 0.25 | 0.31 | 0.28 | 0.28 | 0.27 |
| MgO | 12.51 | 12.3 | 12.79 | 12.69 | 12.38 | 11.68 | 13.47 | 15.12 | 14.21 | 14.68 |
| CaO | 11.06 | 11.26 | 11.38 | 11.44 | 11.52 | 11.33 | 11.55 | 12.22 | 12.15 | 12.1 |
| Na ₂ O | 2.17 | 1.94 | 2.23 | 1.62 | 1.64 | 2.08 | 1.13 | 0.67 | 0.81 | 0.88 |
| K ₂ O | 0.83 | 0.77 | 0.84 | 0.81 | 0.88 | 0.88 | 0.7 | 0.28 | 0.35 | 0.34 |
| F | 0.384 | 0.342 | 0.366 | 0.293 | 0.310 | 0.336 | 0.294 | 0.261 | 0.284 | 0.279 |
| Cl | 0.011 | 0.031 | 0.017 | 0.037 | 0.042 | 0.025 | 0.033 | 0.077 | 0.083 | 0.085 |
| -O=F+Cl | 0.164 | 0.151 | 0.158 | 0.132 | 0.140 | 0.147 | 0.131 | 0.127 | 0.138 | 0.137 |
| Total | 97.49 | 96.89 | 97.95 | 98.26 | 97.86 | 96.99 | 97.27 | 97.12 | 96.92 | 97.29 |
| H ₂ O ^d | 1.85 | 1.84 | 1.86 | 1.89 | 1.87 | 1.84 | 1.89 | 1.92 | 1.89 | 1.90 |
| Total _{calc} | 99.34 | 98.73 | 99.81 | 100.15 | 99.73 | 98.83 | 99.15 | 99.04 | 98.81 | 99.19 |
| Mg ^{##} ^e | 0.632 | 0.617 | 0.646 | 0.609 | 0.605 | 0.595 | 0.633 | 0.679 | 0.654 | 0.664 |
| Cations based on 23 oxygen atoms | | | | | | | | | | |
| Si | 6.26 | 6.38 | 6.25 | 6.64 | 6.54 | 6.34 | 6.95 | 7.35 | 7.21 | 7.18 |
| [⁴]Al | 1.74 | 1.62 | 1.75 | 1.36 | 1.46 | 1.66 | 1.05 | 0.65 | 0.79 | 0.82 |
| ∑ T | 8.00 | 8.00 | 8.00 | 8.00 | 8.00 | 8.00 | 8.00 | 8.00 | 8.00 | 8.00 |
| [⁶]Al | 0.37 | 0.33 | 0.37 | 0.24 | 0.27 | 0.33 | 0.20 | 0.16 | 0.23 | 0.18 |
| Ti | 0.32 | 0.29 | 0.34 | 0.24 | 0.26 | 0.31 | 0.17 | 0.03 | 0.04 | 0.04 |
| Fe ^{3+f} | 0.28 | 0.27 | 0.21 | 0.28 | 0.25 | 0.19 | 0.26 | 0.30 | 0.29 | 0.37 |
| Mg | 2.75 | 2.73 | 2.80 | 2.78 | 2.73 | 2.61 | 2.95 | 3.27 | 3.10 | 3.19 |
| [^C]Fe ²⁺ | 1.27 | 1.39 | 1.28 | 1.47 | 1.50 | 1.56 | 1.41 | 1.24 | 1.34 | 1.22 |
| ∑ M1,2,3 | 5.00 | 5.00 | 5.00 | 5.00 | 5.00 | 5.00 | 5.00 | 5.00 | 5.00 | 5.00 |
| [^B]Fe ²⁺ | 0.05 | 0.04 | 0.04 | 0.04 | 0.03 | 0.02 | 0.04 | 0.01 | 0.01 | 0.02 |
| Mn | 0.03 | 0.04 | 0.02 | 0.04 | 0.04 | 0.03 | 0.04 | 0.03 | 0.03 | 0.03 |
| Ca | 1.75 | 1.80 | 1.79 | 1.80 | 1.82 | 1.82 | 1.82 | 1.90 | 1.91 | 1.89 |
| [^B]Na | 0.17 | 0.13 | 0.15 | 0.12 | 0.11 | 0.13 | 0.10 | 0.05 | 0.05 | 0.06 |
| ∑ M4 | 2.00 | 2.00 | 2.00 | 2.00 | 2.00 | 2.00 | 2.00 | 2.00 | 2.00 | 2.00 |
| [^A]Na | 0.45 | 0.43 | 0.49 | 0.34 | 0.36 | 0.48 | 0.22 | 0.14 | 0.18 | 0.19 |
| K | 0.16 | 0.15 | 0.16 | 0.15 | 0.17 | 0.17 | 0.13 | 0.05 | 0.07 | 0.06 |
| ∑ A | 0.61 | 0.58 | 0.65 | 0.49 | 0.53 | 0.64 | 0.35 | 0.19 | 0.25 | 0.25 |
| sum cations | 15.61 | 15.58 | 15.65 | 15.49 | 15.53 | 15.64 | 15.35 | 15.19 | 15.25 | 15.25 |
| F | 0.179 | 0.161 | 0.170 | 0.136 | 0.145 | 0.159 | 0.137 | 0.120 | 0.132 | 0.128 |
| Cl | 0.003 | 0.008 | 0.004 | 0.009 | 0.011 | 0.006 | 0.008 | 0.019 | 0.021 | 0.021 |
| OH | 1.82 | 1.83 | 1.83 | 1.85 | 1.84 | 1.83 | 1.85 | 1.86 | 1.85 | 1.85 |
| log(F/OH) | -0.92 | -0.95 | -0.92 | -0.91 | -0.89 | -0.92 | -0.92 | -0.88 | -0.91 | -0.97 |
| log(Cl/OH) | -2.26 | -2.23 | -2.14 | -2.14 | -2.06 | -2.24 | -2.31 | -2.16 | -2.18 | -2.10 |

Supplementary Table III-2 continued

| Rock type ^d | HG | HG | HG | HG | HG | HG | HG | HG | HG | HG |
|-----------------------------------|-------|-------|-------|-------|-------|-------|-------|-------|-------|-------|
| Spot | 227 | 228 | 231 | 232 | 233 | 237 | 238 | 239 | 258 | 259 |
| Group ^b | III | III | I | I | I | III | III | III | I | I |
| Chemical composition (oxides wt%) | | | | | | | | | | |
| SiO ₂ | 47.74 | 46.89 | 42.47 | 43.19 | 41.83 | 47.48 | 44.37 | 46.64 | 41.56 | 41.9 |
| Al ₂ O ₃ | 7.14 | 7.3 | 12.17 | 11.3 | 11.93 | 7.08 | 9.28 | 7.48 | 12.63 | 12.67 |
| TiO ₂ | 1.42 | 1.4 | 2.82 | 2.55 | 2.81 | 1.4 | 2.07 | 1.66 | 3.08 | 3.04 |
| FeO ^c | 13.71 | 14.05 | 12.95 | 12.69 | 13.79 | 13.21 | 14.76 | 13.78 | 13.51 | 12.57 |
| MnO | 0.31 | 0.23 | 0.25 | 0.23 | 0.26 | 0.31 | 0.26 | 0.24 | 0.28 | 0.26 |
| MgO | 13.87 | 13.74 | 13.06 | 13.07 | 12.44 | 13.93 | 11.81 | 13.74 | 12.6 | 12.53 |
| CaO | 11.79 | 11.8 | 11.24 | 11.45 | 11.16 | 11.79 | 11.76 | 11.58 | 10.89 | 11.16 |
| Na ₂ O | 1.24 | 1.17 | 2.13 | 2.11 | 2.05 | 1.22 | 1.38 | 1.28 | 2.13 | 2.1 |
| K ₂ O | 0.66 | 0.71 | 0.77 | 0.82 | 0.78 | 0.59 | 0.95 | 0.75 | 0.83 | 0.95 |
| F | 0.302 | 0.308 | 0.308 | 0.340 | 0.306 | 0.296 | 0.293 | 0.296 | 0.315 | 0.348 |
| Cl | 0.036 | 0.043 | 0.015 | 0.019 | 0.027 | 0.036 | 0.057 | 0.048 | 0.020 | 0.021 |
| -O=F+Cl | 0.135 | 0.139 | 0.133 | 0.147 | 0.135 | 0.133 | 0.136 | 0.135 | 0.137 | 0.151 |
| Total | 98.08 | 97.50 | 98.05 | 97.62 | 97.25 | 97.21 | 96.85 | 97.36 | 97.71 | 97.40 |
| H ₂ O ^d | 1.90 | 1.88 | 1.90 | 1.87 | 1.87 | 1.89 | 1.85 | 1.88 | 1.88 | 1.86 |
| Total _{calc} | 99.99 | 99.38 | 99.95 | 99.49 | 99.11 | 99.10 | 98.70 | 99.24 | 99.59 | 99.26 |
| Mg# ^e | 0.643 | 0.635 | 0.643 | 0.647 | 0.617 | 0.653 | 0.588 | 0.640 | 0.624 | 0.640 |
| Cations based on 23 oxygen atoms | | | | | | | | | | |
| Si | 6.96 | 6.89 | 6.22 | 6.36 | 6.21 | 6.97 | 6.65 | 6.86 | 6.12 | 6.19 |
| [⁴]Al | 1.04 | 1.11 | 1.78 | 1.64 | 1.79 | 1.03 | 1.35 | 1.14 | 1.88 | 1.81 |
| ∑ T | 8.00 | 8.00 | 8.00 | 8.00 | 8.00 | 8.00 | 8.00 | 8.00 | 8.00 | 8.00 |
| [⁶]Al | 0.19 | 0.15 | 0.32 | 0.32 | 0.30 | 0.20 | 0.29 | 0.16 | 0.32 | 0.40 |
| Ti | 0.16 | 0.15 | 0.31 | 0.28 | 0.31 | 0.15 | 0.23 | 0.18 | 0.34 | 0.34 |
| Fe ^{3+f} | 0.24 | 0.34 | 0.35 | 0.24 | 0.37 | 0.22 | 0.15 | 0.29 | 0.43 | 0.27 |
| Mg | 3.02 | 3.01 | 2.85 | 2.87 | 2.75 | 3.05 | 2.64 | 3.01 | 2.77 | 2.76 |
| [^C]Fe ²⁺ | 1.40 | 1.35 | 1.16 | 1.28 | 1.27 | 1.37 | 1.69 | 1.35 | 1.15 | 1.24 |
| ∑ M1,2,3 | 5.00 | 5.00 | 5.00 | 5.00 | 5.00 | 5.00 | 5.00 | 5.00 | 5.00 | 5.00 |
| [^B]Fe ²⁺ | 0.03 | 0.04 | 0.07 | 0.04 | 0.07 | 0.03 | 0.01 | 0.05 | 0.09 | 0.05 |
| Mn | 0.04 | 0.03 | 0.03 | 0.03 | 0.03 | 0.04 | 0.03 | 0.03 | 0.03 | 0.03 |
| Ca | 1.84 | 1.86 | 1.76 | 1.81 | 1.77 | 1.86 | 1.89 | 1.83 | 1.72 | 1.77 |
| [^B]Na | 0.09 | 0.08 | 0.13 | 0.12 | 0.12 | 0.08 | 0.07 | 0.09 | 0.16 | 0.16 |
| ∑ M4 | 2.00 | 2.00 | 2.00 | 2.00 | 2.00 | 2.00 | 2.00 | 2.00 | 2.00 | 2.00 |
| [^A]Na | 0.26 | 0.26 | 0.47 | 0.48 | 0.47 | 0.27 | 0.33 | 0.27 | 0.45 | 0.45 |
| K | 0.12 | 0.13 | 0.14 | 0.15 | 0.15 | 0.11 | 0.18 | 0.14 | 0.16 | 0.18 |
| ∑ A | 0.38 | 0.39 | 0.61 | 0.63 | 0.62 | 0.38 | 0.51 | 0.41 | 0.61 | 0.62 |
| sum cations | 15.38 | 15.39 | 15.61 | 15.63 | 15.62 | 15.38 | 15.51 | 15.41 | 15.61 | 15.62 |
| F | 0.139 | 0.143 | 0.143 | 0.158 | 0.144 | 0.137 | 0.139 | 0.138 | 0.147 | 0.163 |
| Cl | 0.009 | 0.011 | 0.004 | 0.005 | 0.007 | 0.009 | 0.014 | 0.012 | 0.005 | 0.005 |
| OH | 1.85 | 1.85 | 1.85 | 1.84 | 1.85 | 1.85 | 1.85 | 1.85 | 1.85 | 1.83 |
| log(F/OH) | -0.97 | -0.94 | -0.92 | -0.94 | -0.95 | -0.96 | -0.94 | -0.91 | -0.91 | -0.95 |
| log(Cl/OH) | -2.16 | -2.19 | -2.12 | -2.09 | -2.29 | -2.24 | -2.15 | -2.15 | -2.14 | -2.22 |

Supplementary Table III-2 continued

| Rock type ^d | HG | HG | HG | HG | HG | HG | HG | HG | HG | HG |
|-----------------------------------|-------|-------|-------|-------|-------|-------|-------|-------|-------|-------|
| Spot | 260 | 261 | 263 | 264 | 266 | 267 | 271 | 274 | 275 | a2 |
| Group ^b | I | I | I | III | III | III | I | I | I | III |
| Chemical composition (oxides wt%) | | | | | | | | | | |
| SiO ₂ | 42.1 | 42.65 | 42.59 | 43.36 | 48.03 | 44.08 | 41.97 | 43.62 | 42.08 | 44.09 |
| Al ₂ O ₃ | 12.15 | 11.12 | 10.48 | 9.99 | 6.79 | 9.51 | 12.09 | 10.88 | 12.7 | 9.26 |
| TiO ₂ | 2.98 | 3.03 | 2.73 | 2.15 | 1.25 | 2.23 | 2.88 | 2.39 | 2.29 | 2.3 |
| FeO ^c | 12.34 | 12.47 | 13.12 | 15.94 | 13.94 | 15.17 | 12.49 | 12.94 | 12.6 | 14.78 |
| MnO | 0.19 | 0.2 | 0.23 | 0.26 | 0.28 | 0.28 | 0.2 | 0.22 | 0.21 | 0.27 |
| MgO | 12.6 | 13.01 | 12.45 | 11.2 | 14.15 | 11.76 | 12.43 | 12.93 | 12.66 | 12.51 |
| CaO | 11.08 | 11.09 | 11.45 | 11.36 | 11.43 | 11.33 | 11.17 | 11.31 | 11.26 | 11.37 |
| Na ₂ O | 2.26 | 2.11 | 2.01 | 1.43 | 1.1 | 1.6 | 2.25 | 2.19 | 2.04 | 1.66 |
| K ₂ O | 0.76 | 0.93 | 0.9 | 0.93 | 0.65 | 0.78 | 0.76 | 0.7 | 0.75 | 0.82 |
| F | 0.350 | 0.318 | 0.331 | 0.308 | 0.290 | 0.325 | 0.298 | 0.339 | 0.342 | 0.308 |
| Cl | 0.014 | 0.026 | 0.035 | 0.046 | 0.052 | 0.036 | 0.019 | 0.015 | 0.016 | 0.036 |
| -O=F+Cl | 0.151 | 0.140 | 0.147 | 0.140 | 0.134 | 0.145 | 0.130 | 0.146 | 0.148 | 0.138 |
| Total | 96.67 | 96.81 | 96.18 | 96.83 | 97.83 | 96.96 | 96.43 | 97.39 | 96.80 | 97.27 |
| H ₂ O ^d | 1.85 | 1.86 | 1.83 | 1.84 | 1.91 | 1.84 | 1.86 | 1.87 | 1.86 | 1.86 |
| Total _{calc} | 98.52 | 98.67 | 98.00 | 98.67 | 99.73 | 98.80 | 98.29 | 99.25 | 98.66 | 99.12 |
| Mg# ^e | 0.645 | 0.650 | 0.628 | 0.556 | 0.644 | 0.580 | 0.640 | 0.640 | 0.642 | 0.601 |
| Cations based on 23 oxygen atoms | | | | | | | | | | |
| Si | 6.26 | 6.33 | 6.41 | 6.52 | 6.99 | 6.59 | 6.26 | 6.44 | 6.23 | 6.56 |
| [⁴]Al | 1.74 | 1.67 | 1.59 | 1.48 | 1.01 | 1.41 | 1.74 | 1.56 | 1.77 | 1.44 |
| ∑ T | 8.00 | 8.00 | 8.00 | 8.00 | 8.00 | 8.00 | 8.00 | 8.00 | 8.00 | 8.00 |
| [⁶]Al | 0.38 | 0.28 | 0.27 | 0.29 | 0.16 | 0.27 | 0.39 | 0.33 | 0.45 | 0.18 |
| Ti | 0.33 | 0.34 | 0.31 | 0.24 | 0.14 | 0.25 | 0.32 | 0.27 | 0.26 | 0.26 |
| Fe ^{3+f} | 0.23 | 0.25 | 0.16 | 0.29 | 0.37 | 0.25 | 0.21 | 0.23 | 0.32 | 0.31 |
| Mg | 2.79 | 2.88 | 2.79 | 2.51 | 3.07 | 2.62 | 2.76 | 2.85 | 2.80 | 2.77 |
| [^C]Fe ²⁺ | 1.26 | 1.25 | 1.47 | 1.67 | 1.26 | 1.61 | 1.31 | 1.33 | 1.18 | 1.48 |
| ∑ M1,2,3 | 5.00 | 5.00 | 5.00 | 5.00 | 5.00 | 5.00 | 5.00 | 5.00 | 5.00 | 5.00 |
| [^B]Fe ²⁺ | 0.04 | 0.05 | 0.02 | 0.05 | 0.07 | 0.04 | 0.04 | 0.04 | 0.06 | 0.05 |
| Mn | 0.02 | 0.03 | 0.03 | 0.03 | 0.03 | 0.04 | 0.03 | 0.03 | 0.03 | 0.03 |
| Ca | 1.76 | 1.76 | 1.85 | 1.83 | 1.78 | 1.82 | 1.79 | 1.79 | 1.79 | 1.81 |
| [^B]Na | 0.17 | 0.16 | 0.11 | 0.09 | 0.12 | 0.11 | 0.15 | 0.15 | 0.12 | 0.10 |
| ∑ M4 | 2.00 | 2.00 | 2.00 | 2.00 | 2.00 | 2.00 | 2.00 | 2.00 | 2.00 | 2.00 |
| [^A]Na | 0.48 | 0.44 | 0.48 | 0.33 | 0.20 | 0.35 | 0.50 | 0.48 | 0.46 | 0.38 |
| K | 0.14 | 0.18 | 0.17 | 0.18 | 0.12 | 0.15 | 0.14 | 0.13 | 0.14 | 0.16 |
| ∑ A | 0.63 | 0.62 | 0.65 | 0.50 | 0.32 | 0.50 | 0.64 | 0.61 | 0.61 | 0.53 |
| sum cations | 15.63 | 15.62 | 15.65 | 15.50 | 15.32 | 15.50 | 15.64 | 15.61 | 15.61 | 15.53 |
| F | 0.165 | 0.149 | 0.157 | 0.146 | 0.134 | 0.154 | 0.141 | 0.158 | 0.160 | 0.145 |
| Cl | 0.004 | 0.007 | 0.009 | 0.012 | 0.013 | 0.009 | 0.005 | 0.004 | 0.004 | 0.009 |
| OH | 1.83 | 1.84 | 1.83 | 1.84 | 1.85 | 1.84 | 1.85 | 1.84 | 1.84 | 1.85 |
| log(F/OH) | -0.92 | -0.92 | -0.96 | -0.95 | -0.93 | -0.89 | -0.92 | -0.93 | -0.91 | -0.90 |
| log(Cl/OH) | -2.20 | -2.06 | -2.14 | -2.07 | -2.11 | -2.15 | -2.04 | -2.21 | -2.22 | -2.16 |

Supplementary Table III-2 continued

| Rock type ^a | HG | HG | HG | HG | HG | HG | HG | HG | HG | HG |
|-----------------------------------|-------|-------|--------|-------|-------|-------|-------|-------|-------|-------|
| Spot | a47 | a48 | a49 | a50 | a51 | a59 | a60 | a75 | a76 | a88 |
| Group ^b | III | III | II | II | III | III | I | III | II | II |
| Chemical composition (oxides wt%) | | | | | | | | | | |
| SiO ₂ | 46.51 | 44.91 | 41.46 | 41.89 | 45.85 | 47.05 | 42.21 | 44.55 | 41.55 | 41.34 |
| Al ₂ O ₃ | 7.41 | 8.49 | 12.58 | 11.88 | 7.72 | 7.07 | 11.52 | 8.88 | 11.54 | 11.44 |
| TiO ₂ | 1.63 | 1.91 | 2.93 | 2.98 | 1.62 | 1.48 | 2.84 | 2.12 | 2.87 | 2.98 |
| FeO ^c | 14.16 | 14.71 | 15.33 | 15.51 | 14.46 | 13.72 | 12.96 | 15.15 | 14.63 | 14.96 |
| MnO | 0.26 | 0.27 | 0.24 | 0.25 | 0.26 | 0.26 | 0.2 | 0.28 | 0.28 | 0.29 |
| MgO | 13.1 | 12.48 | 11.26 | 10.95 | 13.32 | 14 | 13.04 | 12.45 | 11.53 | 11.18 |
| CaO | 11.62 | 11.5 | 11.77 | 11.53 | 11.85 | 11.37 | 11.41 | 11.63 | 11.1 | 11.75 |
| Na ₂ O | 1.21 | 1.39 | 2.05 | 1.98 | 1.16 | 1.24 | 2.17 | 1.5 | 2.17 | 2.02 |
| K ₂ O | 0.77 | 0.95 | 0.87 | 0.88 | 0.81 | 0.71 | 0.83 | 0.93 | 0.76 | 0.87 |
| F | 0.311 | 0.329 | 0.300 | 0.291 | 0.269 | 0.317 | 0.296 | 0.321 | 0.306 | 0.317 |
| Cl | 0.066 | 0.058 | 0.029 | 0.041 | 0.064 | 0.048 | 0.019 | 0.054 | 0.024 | 0.028 |
| -O=F+Cl | 0.146 | 0.152 | 0.133 | 0.132 | 0.128 | 0.144 | 0.129 | 0.147 | 0.134 | 0.140 |
| Total | 96.90 | 96.85 | 98.69 | 98.05 | 97.26 | 97.12 | 97.37 | 97.72 | 96.63 | 97.04 |
| H ₂ O ^d | 1.86 | 1.83 | 1.88 | 1.86 | 1.88 | 1.87 | 1.88 | 1.85 | 1.84 | 1.83 |
| Total _{calc} | 98.76 | 98.68 | 100.56 | 99.91 | 99.14 | 99.00 | 99.24 | 99.57 | 98.47 | 98.86 |
| Mg ^{#e} | 0.623 | 0.602 | 0.567 | 0.557 | 0.622 | 0.645 | 0.642 | 0.594 | 0.584 | 0.571 |
| Cations based on 23 oxygen atoms | | | | | | | | | | |
| Si | 6.90 | 6.71 | 6.13 | 6.24 | 6.78 | 6.92 | 6.25 | 6.61 | 6.25 | 6.24 |
| [⁴]Al | 1.10 | 1.29 | 1.87 | 1.76 | 1.22 | 1.08 | 1.75 | 1.39 | 1.75 | 1.76 |
| ∑ T | 8.00 | 8.00 | 8.00 | 8.00 | 8.00 | 8.00 | 8.00 | 8.00 | 8.00 | 8.00 |
| [⁶]Al | 0.20 | 0.20 | 0.33 | 0.33 | 0.12 | 0.14 | 0.26 | 0.16 | 0.30 | 0.27 |
| Ti | 0.18 | 0.21 | 0.33 | 0.33 | 0.18 | 0.16 | 0.32 | 0.24 | 0.32 | 0.34 |
| Fe ^{3+f} | 0.22 | 0.25 | 0.28 | 0.21 | 0.39 | 0.34 | 0.29 | 0.30 | 0.29 | 0.17 |
| Mg | 2.90 | 2.78 | 2.48 | 2.43 | 2.94 | 3.07 | 2.88 | 2.75 | 2.59 | 2.51 |
| [^C]Fe ²⁺ | 1.50 | 1.55 | 1.59 | 1.69 | 1.38 | 1.28 | 1.25 | 1.54 | 1.51 | 1.71 |
| ∑ M1,2,3 | 5.00 | 5.00 | 5.00 | 5.00 | 5.00 | 5.00 | 5.00 | 5.00 | 5.00 | 5.00 |
| [^B]Fe ²⁺ | 0.03 | 0.04 | 0.03 | 0.03 | 0.02 | 0.07 | 0.06 | 0.04 | 0.05 | 0.01 |
| Mn | 0.03 | 0.03 | 0.03 | 0.03 | 0.03 | 0.03 | 0.03 | 0.04 | 0.04 | 0.04 |
| Ca | 1.85 | 1.84 | 1.87 | 1.84 | 1.88 | 1.79 | 1.81 | 1.85 | 1.79 | 1.90 |
| [^B]Na | 0.09 | 0.09 | 0.07 | 0.10 | 0.07 | 0.11 | 0.11 | 0.08 | 0.13 | 0.05 |
| ∑ M4 | 2.00 | 2.00 | 2.00 | 2.00 | 2.00 | 2.00 | 2.00 | 2.00 | 2.00 | 2.00 |
| [^A]Na | 0.26 | 0.31 | 0.52 | 0.47 | 0.27 | 0.24 | 0.52 | 0.35 | 0.50 | 0.54 |
| K | 0.15 | 0.18 | 0.16 | 0.17 | 0.15 | 0.13 | 0.16 | 0.18 | 0.15 | 0.17 |
| ∑ A | 0.40 | 0.50 | 0.68 | 0.64 | 0.42 | 0.38 | 0.67 | 0.53 | 0.65 | 0.70 |
| sum cations | 15.40 | 15.50 | 15.68 | 15.64 | 15.42 | 15.38 | 15.67 | 15.53 | 15.65 | 15.70 |
| F | 0.146 | 0.155 | 0.140 | 0.137 | 0.126 | 0.147 | 0.139 | 0.151 | 0.146 | 0.151 |
| Cl | 0.017 | 0.015 | 0.007 | 0.010 | 0.016 | 0.012 | 0.005 | 0.014 | 0.006 | 0.007 |
| OH | 1.84 | 1.83 | 1.85 | 1.85 | 1.86 | 1.84 | 1.86 | 1.84 | 1.85 | 1.84 |
| log(F/OH) | -0.94 | -0.89 | -0.94 | -0.93 | -0.91 | -0.92 | -0.86 | -0.92 | -0.98 | -0.93 |
| log(Cl/OH) | -2.09 | -2.12 | -2.14 | -2.17 | -2.04 | -2.13 | -2.05 | -2.12 | -2.25 | -2.21 |

Supplementary Table III-2 continued

| Rock type ^a | HG | HG | HG | HG | HG | HG | HG | HG | HG | HG |
|-----------------------------------|-------|-------|-------|-------|-------|-------|-------|-------|-------|-------|
| Spot | a89 | a95 | a96 | a98 | a112 | a123 | a124 | a125 | a126 | a127 |
| Group ^b | II | II | II | III | III | IV | IV | IV | III | III |
| Chemical composition (oxides wt%) | | | | | | | | | | |
| SiO ₂ | 42.16 | 41.52 | 42.26 | 44.62 | 44.34 | 49 | 47.74 | 48.81 | 45.84 | 46.36 |
| Al ₂ O ₃ | 10.96 | 11.64 | 11.67 | 9.36 | 9.41 | 5.71 | 6.37 | 5.7 | 7.87 | 7.65 |
| TiO ₂ | 2.9 | 3.08 | 3.05 | 2.19 | 1.95 | 0.49 | 0.65 | 0.46 | 1.75 | 1.5 |
| FeO ^c | 14.92 | 14.88 | 14.44 | 14.54 | 15.17 | 13.88 | 14.74 | 13.63 | 14.44 | 14.29 |
| MnO | 0.28 | 0.31 | 0.31 | 0.31 | 0.29 | 0.28 | 0.3 | 0.25 | 0.27 | 0.27 |
| MgO | 11.66 | 11.4 | 11.77 | 12.26 | 11.92 | 14.06 | 13.59 | 14.27 | 12.81 | 13.18 |
| CaO | 11.24 | 11.64 | 11.56 | 11.97 | 11.71 | 12.47 | 12.36 | 12.28 | 11.81 | 11.91 |
| Na ₂ O | 1.89 | 1.98 | 1.91 | 1.53 | 1.34 | 0.76 | 0.92 | 0.75 | 1.15 | 1.07 |
| K ₂ O | 0.92 | 0.9 | 0.95 | 0.84 | 0.99 | 0.38 | 0.44 | 0.37 | 0.79 | 0.81 |
| F | 0.310 | 0.286 | 0.313 | 0.290 | 0.290 | 0.259 | 0.306 | 0.284 | 0.325 | 0.292 |
| Cl | 0.025 | 0.030 | 0.037 | 0.049 | 0.067 | 0.068 | 0.086 | 0.079 | 0.048 | 0.069 |
| -O=F+Cl | 0.136 | 0.127 | 0.140 | 0.133 | 0.137 | 0.124 | 0.148 | 0.137 | 0.148 | 0.139 |
| Total | 97.13 | 97.54 | 98.13 | 97.83 | 97.34 | 97.23 | 97.35 | 96.75 | 96.96 | 97.26 |
| H ₂ O ^d | 1.85 | 1.86 | 1.86 | 1.87 | 1.85 | 1.91 | 1.87 | 1.89 | 1.85 | 1.87 |
| Total _{calc} | 98.98 | 99.40 | 99.99 | 99.70 | 99.19 | 99.14 | 99.22 | 98.63 | 98.80 | 99.13 |
| Mg ^{#e} | 0.582 | 0.577 | 0.592 | 0.600 | 0.583 | 0.644 | 0.622 | 0.651 | 0.613 | 0.622 |
| Cations based on 23 oxygen atoms | | | | | | | | | | |
| Si | 6.31 | 6.22 | 6.26 | 6.61 | 6.61 | 7.18 | 7.02 | 7.17 | 6.81 | 6.85 |
| [⁴]Al | 1.69 | 1.78 | 1.74 | 1.39 | 1.39 | 0.82 | 0.98 | 0.83 | 1.19 | 1.15 |
| ∑ T | 8.00 | 8.00 | 8.00 | 8.00 | 8.00 | 8.00 | 8.00 | 8.00 | 8.00 | 8.00 |
| [⁶]Al | 0.25 | 0.27 | 0.30 | 0.25 | 0.26 | 0.16 | 0.12 | 0.15 | 0.19 | 0.18 |
| Ti | 0.33 | 0.35 | 0.34 | 0.24 | 0.22 | 0.05 | 0.07 | 0.05 | 0.20 | 0.17 |
| Fe ^{3+^f} | 0.29 | 0.22 | 0.23 | 0.16 | 0.25 | 0.31 | 0.42 | 0.37 | 0.25 | 0.30 |
| Mg | 2.60 | 2.54 | 2.60 | 2.71 | 2.65 | 3.07 | 2.98 | 3.12 | 2.84 | 2.90 |
| [^C]Fe ²⁺ | 1.53 | 1.62 | 1.53 | 1.64 | 1.62 | 1.39 | 1.39 | 1.30 | 1.52 | 1.45 |
| ∑ M1,2,3 | 5.00 | 5.00 | 5.00 | 5.00 | 5.00 | 5.00 | 5.00 | 5.00 | 5.00 | 5.00 |
| [^B]Fe ²⁺ | 0.05 | 0.02 | 0.03 | 0.01 | 0.02 | 0.00 | 0.00 | 0.00 | 0.02 | 0.02 |
| Mn | 0.04 | 0.04 | 0.04 | 0.04 | 0.04 | 0.02 | 0.02 | 0.03 | 0.03 | 0.03 |
| Ca | 1.80 | 1.87 | 1.83 | 1.90 | 1.87 | 1.96 | 1.95 | 1.93 | 1.88 | 1.89 |
| [^B]Na | 0.11 | 0.07 | 0.10 | 0.05 | 0.07 | 0.02 | 0.03 | 0.04 | 0.06 | 0.06 |
| ∑ M4 | 2.00 | 2.00 | 2.00 | 2.00 | 2.00 | 2.00 | 2.00 | 2.00 | 2.00 | 2.00 |
| [^A]Na | 0.43 | 0.50 | 0.45 | 0.39 | 0.32 | 0.19 | 0.23 | 0.18 | 0.27 | 0.25 |
| K | 0.18 | 0.17 | 0.18 | 0.16 | 0.19 | 0.07 | 0.08 | 0.07 | 0.15 | 0.15 |
| ∑ A | 0.61 | 0.68 | 0.63 | 0.54 | 0.51 | 0.26 | 0.32 | 0.25 | 0.42 | 0.40 |
| sum cations | 15.61 | 15.68 | 15.63 | 15.54 | 15.51 | 15.26 | 15.32 | 15.25 | 15.42 | 15.40 |
| F | 0.147 | 0.135 | 0.147 | 0.136 | 0.137 | 0.120 | 0.142 | 0.132 | 0.153 | 0.136 |
| Cl | 0.006 | 0.008 | 0.009 | 0.012 | 0.017 | 0.017 | 0.021 | 0.020 | 0.012 | 0.017 |
| OH | 1.85 | 1.86 | 1.84 | 1.85 | 1.85 | 1.86 | 1.84 | 1.85 | 1.84 | 1.85 |
| log(F/OH) | -0.89 | -0.92 | -0.96 | -1.00 | -0.94 | -0.92 | -0.96 | -0.91 | -0.93 | -0.95 |
| log(Cl/OH) | -2.18 | -2.05 | -2.22 | -2.13 | -2.06 | -2.17 | -2.03 | -2.11 | -2.13 | -2.20 |

Supplementary Table III-2 continued

| Rock type ^a | HG | HG | HG | HG | HG | HG | HG | HG | HG | HG |
|-----------------------------------|-------|-------|-------|-------|-------|-------|-------|-------|-------|-------|
| Spot | a128 | a129 | a130 | a131 | a132 | a133 | a141 | a142 | a143 | a144 |
| Group ^b | III | III | III | II | I | I | II | II | II | II |
| Chemical composition (oxides wt%) | | | | | | | | | | |
| SiO ₂ | 46.04 | 43.91 | 44.75 | 42.28 | 41.54 | 41.2 | 41.78 | 41.36 | 41.33 | 42.3 |
| Al ₂ O ₃ | 7.75 | 9.33 | 9.25 | 10.74 | 11.94 | 11.87 | 10.71 | 11.45 | 11.7 | 10.65 |
| TiO ₂ | 1.79 | 1.99 | 1.98 | 2.72 | 2.91 | 3.04 | 2.59 | 2.84 | 2.89 | 2.82 |
| FeO ^c | 13.47 | 14.67 | 14.21 | 15.34 | 13.36 | 12.98 | 14.99 | 14.62 | 14.67 | 14.65 |
| MnO | 0.28 | 0.25 | 0.28 | 0.23 | 0.28 | 0.23 | 0.28 | 0.3 | 0.25 | 0.26 |
| MgO | 13.09 | 12.13 | 12.41 | 11.3 | 12.14 | 12.36 | 11.59 | 11.71 | 11.49 | 11.89 |
| CaO | 11.85 | 11.69 | 11.75 | 11.49 | 11.37 | 11.54 | 11.42 | 11.37 | 11.48 | 11.16 |
| Na ₂ O | 1.24 | 1.39 | 1.3 | 1.74 | 2.2 | 2.18 | 1.81 | 2.09 | 1.97 | 1.79 |
| K ₂ O | 0.77 | 1.02 | 1.05 | 0.89 | 0.8 | 0.82 | 0.93 | 0.85 | 0.83 | 0.9 |
| F | 0.301 | 0.297 | 0.321 | 0.296 | 0.300 | 0.318 | 0.309 | 0.319 | 0.321 | 0.300 |
| Cl | 0.047 | 0.070 | 0.063 | 0.042 | 0.019 | 0.016 | 0.044 | 0.027 | 0.025 | 0.026 |
| -O=F+Cl | 0.137 | 0.141 | 0.149 | 0.134 | 0.131 | 0.138 | 0.140 | 0.140 | 0.141 | 0.132 |
| Total | 96.49 | 96.61 | 97.21 | 96.93 | 96.73 | 96.42 | 96.31 | 96.80 | 96.82 | 96.61 |
| H ₂ O ^d | 1.86 | 1.84 | 1.85 | 1.84 | 1.85 | 1.84 | 1.82 | 1.83 | 1.83 | 1.85 |
| Total _{calc} | 98.35 | 98.44 | 99.06 | 98.77 | 98.58 | 98.26 | 98.14 | 98.63 | 98.65 | 98.46 |
| Mg# ^e | 0.634 | 0.596 | 0.609 | 0.568 | 0.618 | 0.629 | 0.580 | 0.588 | 0.583 | 0.591 |
| Cations based on 23 oxygen atoms | | | | | | | | | | |
| Si | 6.86 | 6.59 | 6.66 | 6.36 | 6.22 | 6.19 | 6.32 | 6.22 | 6.22 | 6.35 |
| [⁴]Al | 1.14 | 1.41 | 1.34 | 1.64 | 1.78 | 1.81 | 1.68 | 1.78 | 1.78 | 1.65 |
| ∑ T | 8.00 | 8.00 | 8.00 | 8.00 | 8.00 | 8.00 | 8.00 | 8.00 | 8.00 | 8.00 |
| [⁶]Al | 0.22 | 0.24 | 0.28 | 0.27 | 0.32 | 0.29 | 0.23 | 0.25 | 0.29 | 0.24 |
| Ti | 0.20 | 0.22 | 0.22 | 0.31 | 0.33 | 0.34 | 0.29 | 0.32 | 0.33 | 0.32 |
| Fe ^{3+f} | 0.15 | 0.24 | 0.19 | 0.24 | 0.23 | 0.21 | 0.31 | 0.29 | 0.27 | 0.31 |
| Mg | 2.91 | 2.71 | 2.75 | 2.53 | 2.71 | 2.77 | 2.61 | 2.63 | 2.58 | 2.66 |
| [^c]Fe ²⁺ | 1.52 | 1.57 | 1.56 | 1.65 | 1.41 | 1.39 | 1.55 | 1.51 | 1.54 | 1.47 |
| ∑ M1,2,3 | 5.00 | 5.00 | 5.00 | 5.00 | 5.00 | 5.00 | 5.00 | 5.00 | 5.00 | 5.00 |
| [^B]Fe ²⁺ | 0.01 | 0.02 | 0.02 | 0.04 | 0.03 | 0.03 | 0.03 | 0.04 | 0.04 | 0.06 |
| Mn | 0.04 | 0.03 | 0.04 | 0.03 | 0.04 | 0.03 | 0.04 | 0.04 | 0.03 | 0.03 |
| Ca | 1.89 | 1.88 | 1.87 | 1.85 | 1.82 | 1.86 | 1.85 | 1.83 | 1.85 | 1.80 |
| [^B]Na | 0.07 | 0.06 | 0.07 | 0.08 | 0.11 | 0.08 | 0.08 | 0.09 | 0.08 | 0.12 |
| ∑ M4 | 2.00 | 2.00 | 2.00 | 2.00 | 2.00 | 2.00 | 2.00 | 2.00 | 2.00 | 2.00 |
| [^A]Na | 0.29 | 0.34 | 0.30 | 0.43 | 0.53 | 0.55 | 0.45 | 0.52 | 0.49 | 0.41 |
| K | 0.15 | 0.20 | 0.20 | 0.17 | 0.15 | 0.16 | 0.18 | 0.16 | 0.16 | 0.17 |
| ∑ A | 0.44 | 0.54 | 0.50 | 0.60 | 0.68 | 0.71 | 0.63 | 0.68 | 0.65 | 0.58 |
| sum cations | 15.44 | 15.54 | 15.50 | 15.60 | 15.68 | 15.71 | 15.63 | 15.68 | 15.65 | 15.58 |
| F | 0.142 | 0.141 | 0.151 | 0.141 | 0.142 | 0.151 | 0.148 | 0.152 | 0.153 | 0.142 |
| Cl | 0.012 | 0.018 | 0.016 | 0.011 | 0.005 | 0.004 | 0.011 | 0.007 | 0.006 | 0.007 |
| OH | 1.85 | 1.84 | 1.83 | 1.85 | 1.85 | 1.84 | 1.84 | 1.84 | 1.84 | 1.85 |
| log(F/OH) | -0.95 | -0.92 | -0.95 | -0.99 | -0.98 | -1.01 | -1.03 | -1.00 | -0.99 | -1.00 |
| log(Cl/OH) | -2.11 | -2.20 | -2.09 | -2.26 | -2.17 | -2.27 | -2.20 | -2.22 | -2.27 | -2.16 |

Supplementary Table III-2 continued

| Rock type ^a | HG | HG | HG | HG |
|-----------------------------------|-------|-------|--------|-------|
| Spot | a145 | a153 | a154 | a155 |
| Group ^b | III | III | II | I |
| Chemical composition (oxides wt%) | | | | |
| SiO ₂ | 44.1 | 45.7 | 42.3 | 41.76 |
| Al ₂ O ₃ | 9.59 | 7.82 | 11.15 | 11.59 |
| TiO ₂ | 2.29 | 1.7 | 2.97 | 3.04 |
| FeO ^c | 14.56 | 13.92 | 15.38 | 13.16 |
| MnO | 0.32 | 0.28 | 0.29 | 0.23 |
| MgO | 12.43 | 13.27 | 11.64 | 12.67 |
| CaO | 11.45 | 11.7 | 11.61 | 11.43 |
| Na ₂ O | 1.86 | 1.29 | 1.83 | 2.06 |
| K ₂ O | 0.81 | 0.72 | 0.91 | 0.89 |
| F | 0.319 | 0.305 | 0.315 | 0.303 |
| Cl | 0.038 | 0.042 | 0.034 | 0.024 |
| -O=F+Cl | 0.143 | 0.138 | 0.140 | 0.133 |
| Total | 97.62 | 96.61 | 98.29 | 97.02 |
| H ₂ O ^d | 1.86 | 1.86 | 1.86 | 1.86 |
| Total _{calc} | 99.48 | 98.47 | 100.15 | 98.89 |
| Mg# ^e | 0.603 | 0.630 | 0.574 | 0.632 |
| Cations based on 23 oxygen atoms | | | | |
| Si | 6.54 | 6.80 | 6.27 | 6.22 |
| [⁴]Al | 1.46 | 1.20 | 1.73 | 1.78 |
| ∑ T | 8.00 | 8.00 | 8.00 | 8.00 |
| [⁶]Al | 0.22 | 0.17 | 0.22 | 0.26 |
| Ti | 0.26 | 0.19 | 0.33 | 0.34 |
| Fe ^{3+f} | 0.25 | 0.30 | 0.31 | 0.27 |
| Mg | 2.75 | 2.94 | 2.57 | 2.81 |
| [^C]Fe ²⁺ | 1.52 | 1.41 | 1.56 | 1.32 |
| ∑ M1,2,3 | 5.00 | 5.00 | 5.00 | 5.00 |
| [^B]Fe ²⁺ | 0.03 | 0.03 | 0.04 | 0.05 |
| Mn | 0.04 | 0.04 | 0.04 | 0.03 |
| Ca | 1.82 | 1.86 | 1.85 | 1.82 |
| [^B]Na | 0.11 | 0.07 | 0.08 | 0.10 |
| ∑ M4 | 2.00 | 2.00 | 2.00 | 2.00 |
| [^A]Na | 0.43 | 0.30 | 0.44 | 0.50 |
| K | 0.15 | 0.14 | 0.17 | 0.17 |
| ∑ A | 0.58 | 0.44 | 0.62 | 0.67 |
| sum cations | 15.58 | 15.44 | 15.62 | 15.67 |
| F | 0.150 | 0.143 | 0.148 | 0.143 |
| Cl | 0.010 | 0.011 | 0.009 | 0.006 |
| OH | 1.84 | 1.85 | 1.84 | 1.85 |
| log(F/OH) | -0.99 | -0.97 | -0.85 | -0.99 |
| log(Cl/OH) | -2.16 | -2.18 | -2.11 | -2.13 |

Supplementary Table III-3 Composition of biotites from the Liujiawa pluton (wt%)

| Rock type ^a | GN | GN | GN | GN | GN | GN | GN | GN | GN | GN |
|--|-------|-------|-------|-------|-------|-------|-------|--------|--------|--------|
| Spot | 1 | 2 | 3 | 4 | 5 | 6 | 75 | 76 | 77 | 78 |
| Chemical composition (oxides wt%) ^e | | | | | | | | | | |
| SiO ₂ | 36.07 | 34.60 | 36.29 | 36.34 | 36.45 | 36.51 | 36.66 | 37.08 | 36.33 | 36.80 |
| Al ₂ O ₃ | 13.68 | 13.65 | 13.79 | 13.91 | 13.92 | 13.64 | 13.71 | 13.82 | 13.83 | 13.72 |
| TiO ₂ | 4.49 | 4.55 | 4.52 | 4.83 | 4.64 | 4.77 | 4.70 | 4.79 | 4.82 | 4.87 |
| FeO ^b | 18.43 | 18.51 | 18.19 | 18.34 | 18.24 | 18.79 | 18.37 | 18.57 | 18.82 | 18.62 |
| MnO | 0.09 | 0.11 | 0.07 | 0.09 | 0.12 | 0.22 | 0.18 | 0.13 | 0.12 | 0.13 |
| MgO | 12.73 | 12.41 | 12.25 | 12.43 | 12.40 | 12.10 | 12.54 | 12.56 | 12.48 | 12.75 |
| CaO | 0.00 | 0.02 | 0.03 | b.d.l | b.d.l | 0.01 | 0.07 | 0.02 | 0.01 | b.d.l |
| Na ₂ O | 0.23 | 0.15 | 0.13 | 0.15 | 0.12 | 0.14 | 0.18 | 0.18 | 0.18 | 0.21 |
| K ₂ O | 9.09 | 8.85 | 9.04 | 9.19 | 8.99 | 9.26 | 9.18 | 9.24 | 9.33 | 9.16 |
| F | 0.489 | 0.436 | 0.478 | 0.479 | 0.464 | 0.461 | 0.471 | 0.459 | 0.482 | 0.438 |
| Cl | 0.114 | 0.112 | 0.124 | 0.118 | 0.114 | 0.113 | 0.131 | 0.119 | 0.128 | 0.124 |
| -O=F+Cl | 0.232 | 0.209 | 0.229 | 0.228 | 0.221 | 0.220 | 0.228 | 0.220 | 0.232 | 0.212 |
| Total | 95.18 | 93.18 | 94.68 | 95.64 | 95.24 | 95.81 | 95.96 | 96.74 | 96.29 | 96.61 |
| H ₂ O ^c | 3.67 | 3.60 | 3.67 | 3.70 | 3.70 | 3.71 | 3.71 | 3.76 | 3.71 | 3.76 |
| Total _{calc} | 98.85 | 96.78 | 98.35 | 99.34 | 98.95 | 99.51 | 99.67 | 100.50 | 100.00 | 100.37 |
| Mg# ^d | 0.552 | 0.544 | 0.545 | 0.547 | 0.548 | 0.534 | 0.549 | 0.546 | 0.542 | 0.550 |
| Cations based on 22 oxygen atoms | | | | | | | | | | |
| Si | 5.49 | 5.40 | 5.54 | 5.50 | 5.53 | 5.53 | 5.53 | 5.55 | 5.48 | 5.52 |
| [⁴]Al | 2.46 | 2.51 | 2.46 | 2.48 | 2.47 | 2.44 | 2.44 | 2.44 | 2.46 | 2.42 |
| [⁶]Al | 0.00 | 0.00 | 0.02 | 0.00 | 0.02 | 0.00 | 0.00 | 0.00 | 0.00 | 0.00 |
| Ti | 0.51 | 0.53 | 0.52 | 0.55 | 0.53 | 0.54 | 0.53 | 0.54 | 0.55 | 0.55 |
| Mn | 0.01 | 0.01 | 0.01 | 0.01 | 0.01 | 0.03 | 0.02 | 0.02 | 0.02 | 0.02 |
| Mg | 2.89 | 2.89 | 2.79 | 2.81 | 2.80 | 2.73 | 2.82 | 2.80 | 2.81 | 2.85 |
| Fe ²⁺ | 2.35 | 2.42 | 2.32 | 2.32 | 2.31 | 2.38 | 2.32 | 2.32 | 2.38 | 2.34 |
| Na | 0.07 | 0.05 | 0.04 | 0.04 | 0.04 | 0.04 | 0.05 | 0.05 | 0.05 | 0.06 |
| K | 1.77 | 1.76 | 1.76 | 1.77 | 1.74 | 1.79 | 1.77 | 1.76 | 1.80 | 1.75 |
| Ca | 0.00 | 0.00 | 0.00 | 0.00 | 0.00 | 0.00 | 0.01 | 0.00 | 0.00 | 0.00 |
| sum cations | 15.55 | 15.59 | 15.47 | 15.49 | 15.46 | 15.49 | 15.50 | 15.48 | 15.54 | 15.51 |
| F | 0.24 | 0.22 | 0.23 | 0.23 | 0.22 | 0.22 | 0.22 | 0.22 | 0.23 | 0.21 |
| Cl | 0.03 | 0.03 | 0.03 | 0.03 | 0.03 | 0.03 | 0.03 | 0.03 | 0.03 | 0.03 |
| OH | 3.73 | 3.75 | 3.74 | 3.74 | 3.75 | 3.75 | 3.74 | 3.75 | 3.74 | 3.76 |
| log(F/OH) | -1.20 | -1.24 | -1.21 | -1.21 | -1.23 | -1.23 | -1.22 | -1.24 | -1.21 | -1.26 |
| log(Cl/OH) | -2.10 | -2.10 | -2.07 | -2.09 | -2.11 | -2.11 | -2.05 | -2.09 | -2.06 | -2.08 |

^a Rock type: GN = gabbro; PD = two-pyroxene diorite; CD = clinopyroxene diorite; HG = hornblende gabbro;

^b Total iron reported as FeO;

^c H₂O calculated assuming F+Cl+OH=4 in the structural formula based on 22 oxygen atoms;

^d Mg# = molar Mg/(Mg+Fe);

^e b.d.l. = below detection limit.

Supplementary Table III-3 continued

| Rock type ^a | GN | GN | GN | GN | GN | GN | GN | GN | GN | GN |
|--|-------|-------|--------|--------|--------|-------|-------|-------|-------|-------|
| Spot | 79 | 101 | 104 | 105 | 106 | 107 | 108 | 133-1 | 133-2 | 134-1 |
| Chemical composition (oxides wt%) ^e | | | | | | | | | | |
| SiO ₂ | 36.33 | 36.95 | 36.77 | 36.62 | 36.53 | 36.39 | 36.26 | 36.85 | 36.97 | 37.05 |
| Al ₂ O ₃ | 13.84 | 13.70 | 13.75 | 13.95 | 14.08 | 13.11 | 13.82 | 13.95 | 13.98 | 13.64 |
| TiO ₂ | 4.67 | 4.79 | 4.83 | 4.72 | 4.11 | 4.62 | 4.33 | 4.01 | 3.96 | 3.95 |
| FeO ^b | 19.17 | 18.22 | 18.61 | 18.83 | 18.61 | 19.41 | 18.67 | 18.42 | 18.14 | 18.26 |
| MnO | 0.09 | 0.08 | 0.09 | 0.14 | 0.09 | 0.10 | 0.17 | 0.06 | 0.09 | 0.13 |
| MgO | 12.18 | 12.25 | 12.56 | 12.62 | 13.01 | 11.55 | 12.33 | 12.34 | 12.29 | 12.71 |
| CaO | b.d.1 | 0.02 | 0.01 | b.d.1 | 0.01 | 0.06 | 0.09 | 0.09 | 0.08 | 0.03 |
| Na ₂ O | 0.16 | 0.16 | 0.19 | 0.16 | 0.16 | 0.10 | 0.07 | 0.07 | 0.05 | 0.05 |
| K ₂ O | 9.15 | 9.30 | 9.30 | 9.33 | 9.33 | 9.42 | 9.34 | 9.45 | 9.43 | 9.39 |
| F | 0.470 | 0.486 | 0.471 | 0.469 | 0.520 | 0.492 | 0.512 | 0.416 | 0.411 | 0.429 |
| Cl | 0.120 | 0.125 | 0.123 | 0.131 | 0.128 | 0.113 | 0.109 | 0.119 | 0.124 | 0.125 |
| -O=F+Cl | 0.225 | 0.233 | 0.226 | 0.227 | 0.248 | 0.232 | 0.240 | 0.202 | 0.201 | 0.209 |
| Total | 95.95 | 95.84 | 96.47 | 96.72 | 96.32 | 95.13 | 95.48 | 95.59 | 95.32 | 95.56 |
| H ₂ O ^c | 3.70 | 3.71 | 3.73 | 3.74 | 3.70 | 3.65 | 3.67 | 3.73 | 3.73 | 3.72 |
| Total _{calc} | 99.65 | 99.55 | 100.21 | 100.46 | 100.02 | 98.78 | 99.15 | 99.31 | 99.05 | 99.29 |
| Mg# ^d | 0.531 | 0.545 | 0.546 | 0.544 | 0.555 | 0.515 | 0.541 | 0.544 | 0.547 | 0.554 |
| Cations based on 22 oxygen atoms | | | | | | | | | | |
| Si | 5.50 | 5.57 | 5.52 | 5.49 | 5.50 | 5.58 | 5.52 | 5.58 | 5.61 | 5.61 |
| [⁴]Al | 2.47 | 2.43 | 2.43 | 2.47 | 2.50 | 2.37 | 2.48 | 2.42 | 2.39 | 2.39 |
| [⁶]Al | 0.00 | 0.01 | 0.00 | 0.00 | 0.00 | 0.00 | 0.00 | 0.07 | 0.10 | 0.04 |
| Ti | 0.53 | 0.54 | 0.55 | 0.53 | 0.47 | 0.53 | 0.50 | 0.46 | 0.45 | 0.45 |
| Mn | 0.01 | 0.01 | 0.01 | 0.02 | 0.01 | 0.01 | 0.02 | 0.01 | 0.01 | 0.02 |
| Mg | 2.75 | 2.75 | 2.81 | 2.82 | 2.92 | 2.64 | 2.80 | 2.79 | 2.78 | 2.87 |
| Fe ²⁺ | 2.43 | 2.30 | 2.34 | 2.36 | 2.34 | 2.49 | 2.37 | 2.33 | 2.30 | 2.31 |
| Na | 0.05 | 0.05 | 0.05 | 0.05 | 0.05 | 0.03 | 0.02 | 0.02 | 0.01 | 0.01 |
| K | 1.77 | 1.79 | 1.78 | 1.79 | 1.79 | 1.84 | 1.81 | 1.83 | 1.82 | 1.81 |
| Ca | 0.00 | 0.00 | 0.00 | 0.00 | 0.00 | 0.01 | 0.01 | 0.02 | 0.01 | 0.00 |
| sum cations | 15.51 | 15.45 | 15.50 | 15.53 | 15.57 | 15.51 | 15.53 | 15.52 | 15.50 | 15.52 |
| F | 0.23 | 0.23 | 0.22 | 0.22 | 0.25 | 0.24 | 0.25 | 0.20 | 0.20 | 0.21 |
| Cl | 0.03 | 0.03 | 0.03 | 0.03 | 0.03 | 0.03 | 0.03 | 0.03 | 0.03 | 0.03 |
| OH | 3.74 | 3.74 | 3.74 | 3.74 | 3.72 | 3.73 | 3.73 | 3.77 | 3.77 | 3.76 |
| log(F/OH) | -1.22 | -1.21 | -1.22 | -1.23 | -1.18 | -1.19 | -1.18 | -1.28 | -1.28 | -1.26 |
| log(Cl/OH) | -2.08 | -2.07 | -2.08 | -2.05 | -2.06 | -2.11 | -2.12 | -2.09 | -2.07 | -2.07 |

Supplementary Table III-3 continued

| Rock type ^a | GN | GN | GN | GN | GN | GN | GN | GN | GN | GN |
|--|--------|-------|-------|-------|-------|-------|-------|-------|-------|-------|
| Spot | 134 -2 | 137 | 138 | 139 | 140 | 147 | 148 | 149 | 150 | 151 |
| Chemical composition (oxides wt%) ^e | | | | | | | | | | |
| SiO ₂ | 36.74 | 36.81 | 36.65 | 36.56 | 37.08 | 37.09 | 36.85 | 36.57 | 36.30 | 36.83 |
| Al ₂ O ₃ | 13.78 | 13.57 | 13.65 | 13.58 | 13.37 | 13.70 | 13.59 | 13.44 | 13.66 | 13.37 |
| TiO ₂ | 3.93 | 4.78 | 4.67 | 3.93 | 3.96 | 5.00 | 4.92 | 4.73 | 4.66 | 4.81 |
| FeO ^b | 18.09 | 18.94 | 18.15 | 17.56 | 18.57 | 18.53 | 18.27 | 18.08 | 18.36 | 18.37 |
| MnO | 0.10 | 0.05 | 0.06 | 0.13 | 0.10 | 0.07 | 0.09 | 0.08 | 0.10 | 0.04 |
| MgO | 12.45 | 11.87 | 11.99 | 12.75 | 12.40 | 11.59 | 11.59 | 12.01 | 11.83 | 12.08 |
| CaO | 0.02 | 0.05 | 0.05 | b.d.1 | 0.09 | 0.05 | 0.02 | 0.03 | 0.07 | 0.08 |
| Na ₂ O | 0.10 | 0.16 | 0.14 | 0.20 | 0.13 | 0.07 | 0.19 | 0.14 | 0.13 | 0.13 |
| K ₂ O | 9.36 | 9.37 | 9.30 | 9.37 | 9.15 | 9.30 | 9.27 | 9.33 | 9.13 | 9.22 |
| F | 0.427 | 0.390 | 0.397 | 0.438 | 0.368 | 0.431 | 0.437 | 0.434 | 0.462 | 0.401 |
| Cl | 0.124 | 0.110 | 0.112 | 0.126 | 0.129 | 0.107 | 0.105 | 0.104 | 0.110 | 0.113 |
| -O=F+Cl | 0.208 | 0.189 | 0.192 | 0.213 | 0.184 | 0.206 | 0.207 | 0.206 | 0.219 | 0.194 |
| Total | 94.91 | 95.90 | 94.96 | 94.43 | 95.17 | 95.75 | 95.13 | 94.75 | 94.60 | 95.25 |
| H ₂ O ^c | 3.70 | 3.74 | 3.72 | 3.68 | 3.73 | 3.73 | 3.71 | 3.69 | 3.67 | 3.72 |
| Total _{calc} | 98.61 | 99.64 | 98.68 | 98.10 | 98.90 | 99.48 | 98.83 | 98.44 | 98.27 | 98.97 |
| Mg ^{#d} | 0.551 | 0.528 | 0.541 | 0.564 | 0.543 | 0.527 | 0.531 | 0.542 | 0.535 | 0.540 |
| Cations based on 22 oxygen atoms | | | | | | | | | | |
| Si | 5.60 | 5.57 | 5.58 | 5.59 | 5.64 | 5.60 | 5.60 | 5.59 | 5.56 | 5.60 |
| [⁴]Al | 2.40 | 2.42 | 2.42 | 2.41 | 2.36 | 2.40 | 2.40 | 2.41 | 2.44 | 2.40 |
| [⁶]Al | 0.07 | 0.00 | 0.03 | 0.04 | 0.04 | 0.04 | 0.04 | 0.01 | 0.02 | 0.00 |
| Ti | 0.45 | 0.54 | 0.54 | 0.45 | 0.45 | 0.57 | 0.56 | 0.54 | 0.54 | 0.55 |
| Mn | 0.01 | 0.01 | 0.01 | 0.02 | 0.01 | 0.01 | 0.01 | 0.01 | 0.01 | 0.01 |
| Mg | 2.83 | 2.68 | 2.72 | 2.91 | 2.81 | 2.61 | 2.63 | 2.74 | 2.70 | 2.74 |
| Fe ²⁺ | 2.31 | 2.40 | 2.31 | 2.25 | 2.36 | 2.34 | 2.32 | 2.31 | 2.35 | 2.33 |
| Na | 0.03 | 0.05 | 0.04 | 0.06 | 0.04 | 0.02 | 0.06 | 0.04 | 0.04 | 0.04 |
| K | 1.82 | 1.81 | 1.81 | 1.83 | 1.78 | 1.79 | 1.80 | 1.82 | 1.78 | 1.79 |
| Ca | 0.00 | 0.01 | 0.01 | 0.00 | 0.01 | 0.01 | 0.00 | 0.00 | 0.01 | 0.01 |
| sum cations | 15.52 | 15.49 | 15.47 | 15.55 | 15.51 | 15.40 | 15.42 | 15.47 | 15.46 | 15.46 |
| F | 0.21 | 0.19 | 0.19 | 0.21 | 0.18 | 0.21 | 0.21 | 0.21 | 0.22 | 0.19 |
| Cl | 0.03 | 0.03 | 0.03 | 0.03 | 0.03 | 0.03 | 0.03 | 0.03 | 0.03 | 0.03 |
| OH | 3.76 | 3.79 | 3.78 | 3.76 | 3.79 | 3.77 | 3.76 | 3.76 | 3.75 | 3.78 |
| log(F/OH) | -1.26 | -1.31 | -1.30 | -1.25 | -1.33 | -1.26 | -1.25 | -1.25 | -1.22 | -1.29 |
| log(Cl/OH) | -2.07 | -2.13 | -2.12 | -2.06 | -2.06 | -2.14 | -2.15 | -2.15 | -2.12 | -2.11 |

Supplementary Table III-3 continued

| Rock type ^a | GN | GN | GN | GN | GN | GN | GN | GN | GN | GN |
|--|-------|-------|-------|-------|--------|--------|-------|--------|-------|-------|
| Spot | 173 | 184 | 185 | 201 | 27 | 29/1 | 29/2 | 29/3 | 29/4 | 29/5 |
| Chemical composition (oxides wt%) ^e | | | | | | | | | | |
| SiO ₂ | 36.51 | 36.51 | 36.52 | 36.86 | 37.11 | 36.83 | 36.92 | 37.09 | 36.88 | 35.96 |
| Al ₂ O ₃ | 13.65 | 13.48 | 13.79 | 13.72 | 13.96 | 13.65 | 13.56 | 13.67 | 13.74 | 13.53 |
| TiO ₂ | 4.49 | 4.58 | 4.02 | 4.44 | 4.94 | 4.72 | 4.62 | 4.58 | 4.47 | 4.47 |
| FeO ^b | 19.31 | 18.32 | 17.76 | 17.61 | 18.34 | 18.65 | 18.70 | 18.75 | 17.89 | 18.84 |
| MnO | 0.06 | 0.10 | 0.08 | 0.12 | 0.10 | 0.12 | 0.11 | 0.08 | 0.09 | 0.08 |
| MgO | 11.77 | 12.20 | 12.67 | 12.25 | 12.14 | 12.62 | 12.46 | 12.64 | 12.54 | 12.27 |
| CaO | 0.03 | 0.02 | 0.02 | 0.04 | b.d.1 | b.d.1 | b.d.1 | 0.01 | 0.01 | b.d.1 |
| Na ₂ O | 0.08 | 0.28 | 0.15 | 0.15 | 0.21 | 0.22 | 0.16 | 0.21 | 0.16 | 0.18 |
| K ₂ O | 9.45 | 9.25 | 9.12 | 9.38 | 9.17 | 9.48 | 9.36 | 9.26 | 9.36 | 9.31 |
| F | 0.427 | 0.453 | 0.481 | 0.476 | 0.421 | 0.469 | 0.467 | 0.468 | 0.477 | 0.487 |
| Cl | 0.103 | 0.123 | 0.133 | 0.121 | 0.127 | 0.136 | 0.127 | 0.136 | 0.124 | 0.133 |
| -O=F+Cl | 0.203 | 0.219 | 0.232 | 0.228 | 0.206 | 0.228 | 0.225 | 0.228 | 0.229 | 0.235 |
| Total | 95.66 | 95.09 | 94.50 | 94.94 | 96.30 | 96.68 | 96.26 | 96.65 | 95.51 | 95.02 |
| H ₂ O ^c | 3.71 | 3.69 | 3.66 | 3.69 | 3.76 | 3.73 | 3.72 | 3.74 | 3.70 | 3.65 |
| Total _{calc} | 99.37 | 98.78 | 98.17 | 98.63 | 100.06 | 100.42 | 99.99 | 100.39 | 99.21 | 98.66 |
| Mg ^{#d} | 0.521 | 0.543 | 0.560 | 0.554 | 0.541 | 0.547 | 0.543 | 0.546 | 0.555 | 0.537 |
| Cations based on 22 oxygen atoms | | | | | | | | | | |
| Si | 5.56 | 5.56 | 5.57 | 5.60 | 5.57 | 5.53 | 5.56 | 5.56 | 5.58 | 5.51 |
| [⁴]Al | 2.44 | 2.42 | 2.43 | 2.40 | 2.43 | 2.42 | 2.41 | 2.41 | 2.42 | 2.44 |
| [⁶]Al | 0.01 | 0.00 | 0.05 | 0.06 | 0.03 | 0.00 | 0.00 | 0.00 | 0.02 | 0.00 |
| Ti | 0.51 | 0.53 | 0.46 | 0.51 | 0.56 | 0.53 | 0.52 | 0.52 | 0.51 | 0.52 |
| Mn | 0.01 | 0.01 | 0.01 | 0.01 | 0.01 | 0.02 | 0.01 | 0.01 | 0.01 | 0.01 |
| Mg | 2.67 | 2.77 | 2.88 | 2.77 | 2.71 | 2.82 | 2.80 | 2.82 | 2.83 | 2.80 |
| Fe ²⁺ | 2.46 | 2.34 | 2.27 | 2.24 | 2.30 | 2.34 | 2.36 | 2.35 | 2.26 | 2.41 |
| Na | 0.02 | 0.08 | 0.04 | 0.04 | 0.06 | 0.07 | 0.05 | 0.06 | 0.05 | 0.05 |
| K | 1.83 | 1.80 | 1.78 | 1.82 | 1.76 | 1.82 | 1.80 | 1.77 | 1.81 | 1.82 |
| Ca | 0.00 | 0.00 | 0.00 | 0.01 | 0.00 | 0.00 | 0.00 | 0.00 | 0.00 | 0.00 |
| sum cations | 15.52 | 15.51 | 15.50 | 15.46 | 15.43 | 15.54 | 15.51 | 15.51 | 15.49 | 15.56 |
| F | 0.21 | 0.22 | 0.23 | 0.23 | 0.20 | 0.22 | 0.22 | 0.22 | 0.23 | 0.24 |
| Cl | 0.03 | 0.03 | 0.03 | 0.03 | 0.03 | 0.03 | 0.03 | 0.03 | 0.03 | 0.03 |
| OH | 3.77 | 3.75 | 3.73 | 3.74 | 3.77 | 3.74 | 3.74 | 3.74 | 3.74 | 3.73 |
| log(F/OH) | -1.26 | -1.23 | -1.21 | -1.21 | -1.28 | -1.23 | -1.23 | -1.23 | -1.21 | -1.20 |
| log(Cl/OH) | -2.15 | -2.07 | -2.03 | -2.08 | -2.07 | -2.03 | -2.06 | -2.03 | -2.07 | -2.03 |

Supplementary Table III-3 continued

| Rock type ^a | GN | GN | GN | GN | GN | GN | GN | GN | GN | GN |
|--|--------|--------|--------|--------|--------|-------|--------|--------|-------|-------|
| Spot | 29/7 | 29/9 | 29/10 | 29/11 | 29/12 | 29/13 | 29/14 | 29/15 | 43 | 44 |
| Chemical composition (oxides wt%) ^e | | | | | | | | | | |
| SiO ₂ | 36.98 | 37.26 | 37.04 | 37.23 | 37.21 | 36.72 | 37.98 | 37.91 | 36.47 | 36.34 |
| Al ₂ O ₃ | 13.83 | 13.86 | 13.89 | 13.83 | 13.55 | 12.82 | 13.96 | 13.72 | 13.83 | 13.79 |
| TiO ₂ | 4.30 | 4.62 | 4.57 | 4.62 | 4.64 | 4.43 | 4.54 | 4.41 | 4.85 | 4.88 |
| FeO ^b | 18.34 | 17.98 | 18.44 | 18.03 | 18.00 | 18.13 | 17.92 | 18.03 | 17.82 | 17.57 |
| MnO | 0.13 | 0.07 | 0.12 | 0.11 | 0.06 | 0.05 | 0.09 | 0.09 | 0.09 | 0.10 |
| MgO | 12.97 | 12.81 | 12.69 | 12.47 | 12.90 | 12.58 | 12.86 | 13.16 | 12.15 | 12.20 |
| CaO | 0.01 | b.d.1 | 0.01 | b.d.1 | b.d.1 | 0.04 | 0.01 | b.d.1 | b.d.1 | b.d.1 |
| Na ₂ O | 0.10 | 0.16 | 0.16 | 0.19 | 0.20 | 0.15 | 0.18 | 0.19 | 0.14 | 0.14 |
| K ₂ O | 9.44 | 9.44 | 9.43 | 9.43 | 9.50 | 8.97 | 9.43 | 9.59 | 9.08 | 9.13 |
| F | 0.484 | 0.441 | 0.463 | 0.480 | 0.468 | 0.475 | 0.463 | 0.481 | 0.442 | 0.441 |
| Cl | 0.139 | 0.133 | 0.124 | 0.127 | 0.128 | 0.123 | 0.132 | 0.130 | 0.129 | 0.121 |
| -O=F+Cl | 0.235 | 0.216 | 0.223 | 0.231 | 0.226 | 0.228 | 0.225 | 0.232 | 0.215 | 0.213 |
| Total | 96.49 | 96.55 | 96.72 | 96.29 | 96.42 | 94.27 | 97.34 | 97.49 | 94.79 | 94.50 |
| H ₂ O ^c | 3.73 | 3.77 | 3.75 | 3.74 | 3.74 | 3.65 | 3.80 | 3.79 | 3.69 | 3.69 |
| Total _{calc} | 100.22 | 100.32 | 100.47 | 100.02 | 100.17 | 97.92 | 101.14 | 101.28 | 98.49 | 98.19 |
| Mg ^{#d} | 0.558 | 0.559 | 0.551 | 0.552 | 0.561 | 0.553 | 0.561 | 0.565 | 0.549 | 0.553 |
| Cations based on 22 oxygen atoms | | | | | | | | | | |
| Si | 5.55 | 5.57 | 5.54 | 5.58 | 5.58 | 5.63 | 5.62 | 5.61 | 5.55 | 5.55 |
| [⁴]Al | 2.44 | 2.43 | 2.45 | 2.42 | 2.39 | 2.32 | 2.38 | 2.39 | 2.45 | 2.45 |
| [⁶]Al | 0.00 | 0.01 | 0.00 | 0.03 | 0.00 | 0.00 | 0.05 | 0.00 | 0.03 | 0.03 |
| Ti | 0.48 | 0.52 | 0.51 | 0.52 | 0.52 | 0.51 | 0.50 | 0.49 | 0.56 | 0.56 |
| Mn | 0.02 | 0.01 | 0.02 | 0.01 | 0.01 | 0.01 | 0.01 | 0.01 | 0.01 | 0.01 |
| Mg | 2.90 | 2.85 | 2.83 | 2.79 | 2.88 | 2.87 | 2.83 | 2.90 | 2.76 | 2.78 |
| Fe ²⁺ | 2.30 | 2.25 | 2.31 | 2.26 | 2.26 | 2.32 | 2.22 | 2.23 | 2.27 | 2.24 |
| Na | 0.03 | 0.05 | 0.05 | 0.05 | 0.06 | 0.04 | 0.05 | 0.06 | 0.04 | 0.04 |
| K | 1.81 | 1.80 | 1.80 | 1.80 | 1.82 | 1.75 | 1.78 | 1.81 | 1.76 | 1.78 |
| Ca | 0.00 | 0.00 | 0.00 | 0.00 | 0.00 | 0.01 | 0.00 | 0.00 | 0.00 | 0.00 |
| sum cations | 15.53 | 15.49 | 15.51 | 15.47 | 15.51 | 15.47 | 15.45 | 15.51 | 15.43 | 15.44 |
| F | 0.23 | 0.21 | 0.22 | 0.23 | 0.22 | 0.23 | 0.22 | 0.23 | 0.21 | 0.21 |
| Cl | 0.04 | 0.03 | 0.03 | 0.03 | 0.03 | 0.03 | 0.03 | 0.03 | 0.03 | 0.03 |
| OH | 3.73 | 3.76 | 3.75 | 3.74 | 3.75 | 3.74 | 3.75 | 3.74 | 3.75 | 3.76 |
| log(F/OH) | -1.21 | -1.26 | -1.23 | -1.22 | -1.23 | -1.21 | -1.24 | -1.22 | -1.25 | -1.25 |
| log(Cl/OH) | -2.02 | -2.05 | -2.07 | -2.06 | -2.06 | -2.07 | -2.05 | -2.06 | -2.05 | -2.08 |

Supplementary Table III-3 continued

| Rock type ^e | GN | GN | GN | GN | GN | PD | PD | PD | PD | PD |
|--|-------|-------|--------|--------|--------|--------|-------|-------|-------|-------|
| Spot | 48 | 54 | 55 | 64 | 65 | 5 | 6 | 7 | 8 | 26 |
| Chemical composition (oxides wt%) ^e | | | | | | | | | | |
| SiO ₂ | 36.73 | 37.23 | 37.47 | 37.43 | 37.38 | 38.10 | 37.09 | 37.60 | 36.65 | 35.81 |
| Al ₂ O ₃ | 13.72 | 13.66 | 13.74 | 13.99 | 14.04 | 14.11 | 13.85 | 13.60 | 13.46 | 13.79 |
| TiO ₂ | 3.19 | 4.13 | 4.14 | 4.79 | 4.82 | 3.77 | 3.92 | 4.05 | 3.86 | 5.48 |
| FeO ^b | 19.05 | 18.36 | 18.36 | 18.87 | 17.94 | 17.61 | 17.44 | 17.84 | 17.92 | 18.58 |
| MnO | 0.11 | 0.11 | 0.09 | 0.08 | 0.08 | 0.27 | 0.34 | 0.41 | 0.40 | 0.33 |
| MgO | 12.88 | 12.71 | 13.09 | 12.49 | 12.42 | 13.44 | 12.71 | 12.96 | 12.59 | 12.16 |
| CaO | 0.06 | 0.01 | 0.02 | 0.02 | 0.05 | 0.05 | b.d.1 | 0.04 | 0.01 | 0.02 |
| Na ₂ O | 0.10 | 0.07 | 0.10 | 0.14 | 0.19 | 0.07 | 0.07 | 0.06 | 0.07 | 0.09 |
| K ₂ O | 9.11 | 9.35 | 9.47 | 9.42 | 9.38 | 9.55 | 9.40 | 9.18 | 9.43 | 9.01 |
| F | 0.430 | 0.453 | 0.456 | 0.417 | 0.402 | 0.502 | 0.534 | 0.532 | 0.543 | 0.453 |
| Cl | 0.130 | 0.124 | 0.123 | 0.109 | 0.112 | 0.130 | 0.123 | 0.156 | 0.152 | 0.047 |
| -O=F+Cl | 0.210 | 0.219 | 0.220 | 0.200 | 0.195 | 0.241 | 0.253 | 0.259 | 0.263 | 0.201 |
| Total | 95.30 | 95.98 | 96.83 | 97.55 | 96.62 | 97.36 | 95.23 | 96.17 | 94.83 | 95.57 |
| H ₂ O ^c | 3.70 | 3.73 | 3.77 | 3.81 | 3.79 | 3.79 | 3.68 | 3.71 | 3.63 | 3.72 |
| Total _{calc} | 99.00 | 99.72 | 100.60 | 101.36 | 100.41 | 101.15 | 98.90 | 99.88 | 98.46 | 99.29 |
| Mg ^{#d} | 0.546 | 0.552 | 0.560 | 0.541 | 0.553 | 0.576 | 0.565 | 0.564 | 0.556 | 0.538 |
| Cations based on 22 oxygen atoms | | | | | | | | | | |
| Si | 5.59 | 5.61 | 5.59 | 5.56 | 5.58 | 5.63 | 5.61 | 5.63 | 5.60 | 5.44 |
| [⁴]Al | 2.41 | 2.39 | 2.41 | 2.44 | 2.42 | 2.37 | 2.39 | 2.37 | 2.40 | 2.47 |
| [⁶]Al | 0.05 | 0.03 | 0.01 | 0.01 | 0.05 | 0.08 | 0.08 | 0.03 | 0.02 | 0.00 |
| Ti | 0.37 | 0.47 | 0.46 | 0.53 | 0.54 | 0.42 | 0.45 | 0.46 | 0.44 | 0.63 |
| Mn | 0.01 | 0.01 | 0.01 | 0.01 | 0.01 | 0.03 | 0.04 | 0.05 | 0.05 | 0.04 |
| Mg | 2.92 | 2.85 | 2.91 | 2.76 | 2.77 | 2.96 | 2.87 | 2.89 | 2.87 | 2.75 |
| Fe ²⁺ | 2.43 | 2.31 | 2.29 | 2.34 | 2.24 | 2.18 | 2.21 | 2.24 | 2.29 | 2.36 |
| Na | 0.03 | 0.02 | 0.03 | 0.04 | 0.05 | 0.02 | 0.02 | 0.02 | 0.02 | 0.03 |
| K | 1.77 | 1.80 | 1.80 | 1.78 | 1.79 | 1.80 | 1.82 | 1.76 | 1.84 | 1.75 |
| Ca | 0.01 | 0.00 | 0.00 | 0.00 | 0.01 | 0.01 | 0.00 | 0.01 | 0.00 | 0.00 |
| sum cations | 15.59 | 15.50 | 15.53 | 15.48 | 15.45 | 15.50 | 15.48 | 15.45 | 15.53 | 15.47 |
| F | 0.21 | 0.22 | 0.22 | 0.20 | 0.19 | 0.23 | 0.26 | 0.25 | 0.26 | 0.22 |
| Cl | 0.03 | 0.03 | 0.03 | 0.03 | 0.03 | 0.03 | 0.03 | 0.04 | 0.04 | 0.01 |
| OH | 3.76 | 3.75 | 3.75 | 3.78 | 3.78 | 3.73 | 3.71 | 3.71 | 3.70 | 3.77 |
| log(F/OH) | -1.26 | -1.24 | -1.24 | -1.29 | -1.30 | -1.20 | -1.16 | -1.17 | -1.15 | -1.24 |
| log(Cl/OH) | -2.05 | -2.07 | -2.08 | -2.14 | -2.12 | -2.06 | -2.07 | -1.97 | -1.97 | -2.50 |

Supplementary Table III-3 continued

| Rock type ^a | PD | PD | PD | PD | PD | PD | PD | PD | PD | PD |
|--|-------|-------|--------|--------|-------|-------|--------|-------|-------|-------|
| Spot | 27 | 28 | 30 | 43 | 44 | 45 | 46 | 103 | 104 | 105 |
| Chemical composition (oxides wt%) ^e | | | | | | | | | | |
| SiO ₂ | 35.56 | 36.62 | 37.43 | 37.63 | 36.59 | 37.27 | 37.48 | 36.00 | 36.52 | 35.52 |
| Al ₂ O ₃ | 13.95 | 13.83 | 13.63 | 13.81 | 13.66 | 13.85 | 13.87 | 13.84 | 13.58 | 14.13 |
| TiO ₂ | 5.52 | 4.88 | 4.73 | 4.03 | 4.23 | 4.27 | 4.36 | 4.38 | 4.29 | 5.09 |
| FeO ^b | 18.47 | 18.01 | 18.05 | 17.57 | 17.32 | 17.36 | 17.25 | 17.71 | 17.95 | 18.78 |
| MnO | 0.34 | 0.29 | 0.27 | 0.40 | 0.41 | 0.31 | 0.29 | 0.26 | 0.28 | 0.32 |
| MgO | 11.87 | 12.67 | 13.15 | 13.25 | 12.74 | 12.89 | 13.33 | 12.07 | 12.57 | 11.63 |
| CaO | 0.03 | b.d.1 | 0.04 | 0.01 | b.d.1 | 0.01 | 0.01 | 0.02 | b.d.1 | 0.01 |
| Na ₂ O | 0.14 | 0.12 | 0.09 | 0.09 | 0.08 | 0.10 | 0.09 | 0.13 | 0.13 | 0.16 |
| K ₂ O | 9.00 | 9.32 | 9.52 | 9.56 | 9.41 | 9.34 | 9.67 | 9.46 | 9.48 | 8.91 |
| F | 0.486 | 0.489 | 0.501 | 0.514 | 0.493 | 0.517 | 0.493 | 0.495 | 0.531 | 0.497 |
| Cl | 0.033 | 0.087 | 0.090 | 0.118 | 0.135 | 0.142 | 0.098 | 0.093 | 0.097 | 0.063 |
| -O=F+Cl | 0.212 | 0.226 | 0.231 | 0.243 | 0.238 | 0.250 | 0.230 | 0.230 | 0.245 | 0.223 |
| Total | 95.19 | 96.09 | 97.27 | 96.75 | 94.84 | 95.79 | 96.72 | 94.23 | 95.17 | 94.89 |
| H ₂ O ^c | 3.69 | 3.73 | 3.77 | 3.75 | 3.67 | 3.71 | 3.76 | 3.64 | 3.66 | 3.66 |
| Total _{calc} | 98.88 | 99.82 | 101.04 | 100.49 | 98.51 | 99.50 | 100.48 | 97.87 | 98.83 | 98.55 |
| Mg# ^d | 0.534 | 0.556 | 0.565 | 0.573 | 0.567 | 0.570 | 0.579 | 0.548 | 0.555 | 0.525 |
| Cations based on 22 oxygen atoms | | | | | | | | | | |
| Si | 5.42 | 5.51 | 5.56 | 5.61 | 5.57 | 5.60 | 5.58 | 5.53 | 5.56 | 5.44 |
| [⁴]Al | 2.51 | 2.45 | 2.39 | 2.39 | 2.43 | 2.40 | 2.42 | 2.47 | 2.44 | 2.55 |
| [⁶]Al | 0.00 | 0.00 | 0.00 | 0.03 | 0.02 | 0.05 | 0.02 | 0.04 | 0.00 | 0.00 |
| Ti | 0.63 | 0.55 | 0.53 | 0.45 | 0.48 | 0.48 | 0.49 | 0.51 | 0.49 | 0.59 |
| Mn | 0.04 | 0.04 | 0.03 | 0.05 | 0.05 | 0.04 | 0.04 | 0.03 | 0.04 | 0.04 |
| Mg | 2.70 | 2.84 | 2.91 | 2.94 | 2.89 | 2.89 | 2.96 | 2.76 | 2.85 | 2.66 |
| Fe ²⁺ | 2.36 | 2.27 | 2.24 | 2.19 | 2.20 | 2.18 | 2.15 | 2.28 | 2.28 | 2.40 |
| Na | 0.04 | 0.03 | 0.02 | 0.03 | 0.02 | 0.03 | 0.03 | 0.04 | 0.04 | 0.05 |
| K | 1.75 | 1.79 | 1.80 | 1.82 | 1.83 | 1.79 | 1.84 | 1.86 | 1.84 | 1.74 |
| Ca | 0.00 | 0.00 | 0.01 | 0.00 | 0.00 | 0.00 | 0.00 | 0.00 | 0.00 | 0.00 |
| sum cations | 15.46 | 15.49 | 15.50 | 15.51 | 15.51 | 15.46 | 15.52 | 15.52 | 15.53 | 15.47 |
| F | 0.23 | 0.23 | 0.24 | 0.24 | 0.24 | 0.25 | 0.23 | 0.24 | 0.26 | 0.24 |
| Cl | 0.01 | 0.02 | 0.02 | 0.03 | 0.03 | 0.04 | 0.02 | 0.02 | 0.03 | 0.02 |
| OH | 3.76 | 3.74 | 3.74 | 3.73 | 3.73 | 3.72 | 3.74 | 3.73 | 3.72 | 3.74 |
| log(F/OH) | -1.20 | -1.21 | -1.20 | -1.19 | -1.20 | -1.18 | -1.21 | -1.19 | -1.16 | -1.19 |
| log(Cl/OH) | -2.64 | -2.23 | -2.22 | -2.10 | -2.03 | -2.01 | -2.18 | -2.19 | -2.17 | -2.36 |

Supplementary Table III-3 continued

| Rock type ^a | PD | PD | PD | PD | PD | PD | CD | CD | CD | CD |
|--|-------|-------|-------|-------|-------|-------|-------|-------|-------|-------|
| Spot | 106 | 107 | a156 | a157 | a164 | a165 | 44 | 45 | 46 | 47 |
| Chemical composition (oxides wt%) ^e | | | | | | | | | | |
| SiO ₂ | 36.34 | 35.46 | 36.59 | 36.73 | 36.59 | 36.52 | 35.76 | 36.17 | 36.86 | 36.27 |
| Al ₂ O ₃ | 13.84 | 13.80 | 13.60 | 13.50 | 13.93 | 14.14 | 13.72 | 13.90 | 13.89 | 13.94 |
| TiO ₂ | 4.56 | 5.25 | 3.99 | 4.58 | 4.54 | 4.80 | 3.93 | 4.22 | 4.03 | 3.82 |
| FeO ^b | 18.39 | 18.69 | 17.00 | 17.57 | 18.13 | 18.43 | 19.74 | 19.85 | 19.14 | 18.91 |
| MnO | 0.31 | 0.29 | 0.26 | 0.31 | 0.32 | 0.28 | 0.21 | 0.21 | 0.25 | 0.20 |
| MgO | 12.91 | 11.75 | 12.70 | 12.30 | 12.37 | 12.24 | 11.04 | 11.21 | 11.62 | 11.40 |
| CaO | b.d.1 | b.d.1 | 0.05 | 0.09 | 0.03 | 0.03 | 0.02 | 0.01 | 0.01 | 0.01 |
| Na ₂ O | 0.09 | 0.14 | 0.11 | 0.08 | 0.06 | 0.09 | 0.11 | 0.06 | 0.14 | 0.04 |
| K ₂ O | 9.38 | 8.95 | 8.98 | 9.14 | 9.06 | 8.89 | 9.16 | 9.14 | 9.40 | 9.43 |
| F | 0.530 | 0.484 | 0.494 | 0.460 | 0.476 | 0.442 | 0.620 | 0.599 | 0.588 | 0.632 |
| Cl | 0.104 | 0.071 | 0.130 | 0.115 | 0.085 | 0.084 | 0.154 | 0.125 | 0.123 | 0.140 |
| -O=F+Cl | 0.247 | 0.220 | 0.237 | 0.220 | 0.220 | 0.205 | 0.296 | 0.280 | 0.275 | 0.298 |
| Total | 96.20 | 94.66 | 93.67 | 94.65 | 95.38 | 95.75 | 94.16 | 95.21 | 95.78 | 94.50 |
| H ₂ O ^c | 3.70 | 3.65 | 3.64 | 3.68 | 3.71 | 3.74 | 3.53 | 3.60 | 3.64 | 3.56 |
| Total _{calc} | 99.89 | 98.32 | 97.31 | 98.34 | 99.09 | 99.49 | 97.69 | 98.81 | 99.42 | 98.06 |
| Mg# ^d | 0.556 | 0.528 | 0.571 | 0.555 | 0.549 | 0.542 | 0.499 | 0.502 | 0.520 | 0.518 |
| Cations based on 22 oxygen atoms | | | | | | | | | | |
| Si | 5.48 | 5.45 | 5.61 | 5.60 | 5.54 | 5.51 | 5.54 | 5.54 | 5.59 | 5.58 |
| [⁴]Al | 2.46 | 2.50 | 2.39 | 2.40 | 2.46 | 2.49 | 2.46 | 2.46 | 2.41 | 2.42 |
| [⁶]Al | 0.00 | 0.00 | 0.07 | 0.02 | 0.03 | 0.03 | 0.05 | 0.05 | 0.07 | 0.10 |
| Ti | 0.52 | 0.61 | 0.46 | 0.53 | 0.52 | 0.54 | 0.46 | 0.49 | 0.46 | 0.44 |
| Mn | 0.04 | 0.04 | 0.03 | 0.04 | 0.04 | 0.04 | 0.03 | 0.03 | 0.03 | 0.03 |
| Mg | 2.90 | 2.69 | 2.91 | 2.79 | 2.79 | 2.76 | 2.55 | 2.56 | 2.63 | 2.61 |
| Fe ²⁺ | 2.32 | 2.40 | 2.18 | 2.24 | 2.30 | 2.33 | 2.56 | 2.54 | 2.43 | 2.43 |
| Na | 0.03 | 0.04 | 0.03 | 0.02 | 0.02 | 0.03 | 0.03 | 0.02 | 0.04 | 0.01 |
| K | 1.80 | 1.75 | 1.76 | 1.78 | 1.75 | 1.71 | 1.81 | 1.78 | 1.82 | 1.85 |
| Ca | 0.00 | 0.00 | 0.01 | 0.02 | 0.01 | 0.00 | 0.00 | 0.00 | 0.00 | 0.00 |
| sum cations | 15.55 | 15.47 | 15.45 | 15.44 | 15.46 | 15.44 | 15.49 | 15.46 | 15.48 | 15.48 |
| F | 0.25 | 0.23 | 0.24 | 0.22 | 0.23 | 0.21 | 0.30 | 0.29 | 0.28 | 0.31 |
| Cl | 0.03 | 0.02 | 0.03 | 0.03 | 0.02 | 0.02 | 0.04 | 0.03 | 0.03 | 0.04 |
| OH | 3.72 | 3.75 | 3.73 | 3.75 | 3.75 | 3.77 | 3.66 | 3.68 | 3.69 | 3.66 |
| log(F/OH) | -1.17 | -1.20 | -1.19 | -1.23 | -1.22 | -1.25 | -1.08 | -1.10 | -1.12 | -1.08 |
| log(Cl/OH) | -2.14 | -2.31 | -2.04 | -2.10 | -2.24 | -2.24 | -1.96 | -2.06 | -2.07 | -2.00 |

Supplementary Table III-3 continued

| Rock type ^a | CD | CD | CD | CD | CD | CD | CD | CD | CD | CD |
|--|-------|-------|-------|-------|-------|-------|-------|-------|-------|-------|
| Spot | 55 | 56 | 57 | 58 | 59 | 60 | 61 | 62 | 63 | 64 |
| Chemical composition (oxides wt%) ^e | | | | | | | | | | |
| SiO ₂ | 36.29 | 36.50 | 35.96 | 36.49 | 35.74 | 36.58 | 37.22 | 37.92 | 37.04 | 36.89 |
| Al ₂ O ₃ | 14.29 | 14.33 | 14.01 | 13.71 | 13.77 | 13.82 | 13.69 | 13.60 | 13.44 | 13.56 |
| TiO ₂ | 3.48 | 3.45 | 3.75 | 4.47 | 5.00 | 4.22 | 4.12 | 3.98 | 3.94 | 4.19 |
| FeO ^b | 18.51 | 18.33 | 19.04 | 18.11 | 18.70 | 18.25 | 17.58 | 17.88 | 17.11 | 18.37 |
| MnO | 0.20 | 0.19 | 0.21 | 0.22 | 0.25 | 0.19 | 0.23 | 0.25 | 0.20 | 0.23 |
| MgO | 11.96 | 12.12 | 11.28 | 12.12 | 10.89 | 12.05 | 12.54 | 12.90 | 12.68 | 11.73 |
| CaO | 0.02 | b.d.1 | 0.04 | 0.01 | b.d.1 | b.d.1 | 0.03 | b.d.1 | 0.05 | 0.01 |
| Na ₂ O | 0.05 | 0.11 | 0.08 | 0.13 | 0.12 | 0.12 | 0.14 | 0.14 | 0.13 | 0.13 |
| K ₂ O | 9.52 | 9.27 | 9.16 | 9.27 | 9.20 | 9.29 | 8.89 | 8.85 | 9.03 | 9.14 |
| F | 0.697 | 0.676 | 0.663 | 0.608 | 0.593 | 0.653 | 0.665 | 0.704 | 0.658 | 0.654 |
| Cl | 0.138 | 0.127 | 0.138 | 0.110 | 0.117 | 0.119 | 0.113 | 0.097 | 0.105 | 0.139 |
| -O=F+Cl | 0.325 | 0.313 | 0.310 | 0.281 | 0.276 | 0.302 | 0.306 | 0.318 | 0.300 | 0.307 |
| Total | 94.83 | 94.78 | 94.02 | 94.97 | 94.10 | 94.97 | 94.92 | 96.01 | 94.06 | 94.73 |
| H ₂ O ^c | 3.55 | 3.58 | 3.53 | 3.62 | 3.57 | 3.60 | 3.62 | 3.65 | 3.59 | 3.58 |
| Total _{calc} | 98.38 | 98.36 | 97.55 | 98.58 | 97.67 | 98.57 | 98.53 | 99.66 | 97.65 | 98.31 |
| Mg# ^d | 0.535 | 0.541 | 0.514 | 0.544 | 0.509 | 0.541 | 0.560 | 0.563 | 0.569 | 0.532 |
| Cations based on 22 oxygen atoms | | | | | | | | | | |
| Si | 5.55 | 5.57 | 5.56 | 5.56 | 5.52 | 5.57 | 5.63 | 5.67 | 5.65 | 5.63 |
| [⁴]Al | 2.45 | 2.43 | 2.44 | 2.44 | 2.48 | 2.43 | 2.37 | 2.33 | 2.35 | 2.37 |
| [⁶]Al | 0.12 | 0.14 | 0.11 | 0.02 | 0.03 | 0.05 | 0.07 | 0.06 | 0.07 | 0.07 |
| Ti | 0.40 | 0.40 | 0.44 | 0.51 | 0.58 | 0.48 | 0.47 | 0.45 | 0.45 | 0.48 |
| Mn | 0.03 | 0.02 | 0.03 | 0.03 | 0.03 | 0.03 | 0.03 | 0.03 | 0.03 | 0.03 |
| Mg | 2.73 | 2.76 | 2.60 | 2.75 | 2.51 | 2.73 | 2.83 | 2.87 | 2.88 | 2.67 |
| Fe ²⁺ | 2.37 | 2.34 | 2.46 | 2.31 | 2.42 | 2.32 | 2.22 | 2.23 | 2.18 | 2.34 |
| Na | 0.01 | 0.03 | 0.02 | 0.04 | 0.03 | 0.03 | 0.04 | 0.04 | 0.04 | 0.04 |
| K | 1.86 | 1.80 | 1.81 | 1.80 | 1.81 | 1.80 | 1.72 | 1.69 | 1.76 | 1.78 |
| Ca | 0.00 | 0.00 | 0.01 | 0.00 | 0.00 | 0.00 | 0.00 | 0.00 | 0.01 | 0.00 |
| sum cations | 15.51 | 15.49 | 15.47 | 15.46 | 15.41 | 15.45 | 15.38 | 15.38 | 15.41 | 15.41 |
| F | 0.34 | 0.33 | 0.32 | 0.29 | 0.29 | 0.31 | 0.32 | 0.33 | 0.32 | 0.32 |
| Cl | 0.04 | 0.03 | 0.04 | 0.03 | 0.03 | 0.03 | 0.03 | 0.02 | 0.03 | 0.04 |
| OH | 3.63 | 3.64 | 3.64 | 3.68 | 3.68 | 3.66 | 3.65 | 3.64 | 3.66 | 3.65 |
| log(F/OH) | -1.03 | -1.05 | -1.05 | -1.10 | -1.10 | -1.07 | -1.06 | -1.04 | -1.06 | -1.06 |
| log(Cl/OH) | -2.01 | -2.04 | -2.00 | -2.11 | -2.08 | -2.08 | -2.10 | -2.17 | -2.13 | -2.01 |

Supplementary Table III-3 continued

| Rock type ^a | CD | CD | CD | CD | CD | CD | CD | CD | CD | CD |
|--|-------|-------|-------|-------|-------|--------|-------|-------|-------|-------|
| Spot | 65 | 66 | 67 | 111 | 112 | 113 | 114 | 164 | 165 | 166 |
| Chemical composition (oxides wt%) ^e | | | | | | | | | | |
| SiO ₂ | 37.51 | 36.85 | 37.33 | 37.18 | 36.75 | 37.77 | 37.66 | 37.11 | 36.71 | 37.78 |
| Al ₂ O ₃ | 14.04 | 13.98 | 14.19 | 13.70 | 13.61 | 13.92 | 13.80 | 13.87 | 13.81 | 13.57 |
| TiO ₂ | 3.08 | 3.71 | 3.13 | 4.42 | 4.06 | 3.99 | 3.96 | 3.25 | 4.05 | 3.57 |
| FeO ^b | 17.10 | 18.02 | 17.66 | 18.44 | 18.40 | 18.55 | 18.51 | 18.30 | 19.14 | 19.08 |
| MnO | 0.22 | 0.20 | 0.20 | 0.25 | 0.23 | 0.23 | 0.19 | 0.24 | 0.21 | 0.24 |
| MgO | 13.33 | 12.59 | 13.29 | 12.09 | 12.25 | 12.27 | 12.22 | 12.08 | 11.37 | 12.05 |
| CaO | 0.04 | 0.01 | 0.02 | b.d.1 | b.d.1 | b.d.1 | 0.02 | b.d.1 | b.d.1 | 0.01 |
| Na ₂ O | 0.12 | 0.20 | 0.17 | 0.14 | 0.12 | 0.07 | 0.13 | 0.09 | 0.13 | 0.21 |
| K ₂ O | 9.24 | 9.46 | 9.33 | 9.17 | 9.13 | 9.19 | 9.16 | 9.27 | 8.88 | 9.11 |
| F | 0.702 | 0.642 | 0.696 | 0.657 | 0.561 | 0.626 | 0.662 | 0.694 | 0.623 | 0.680 |
| Cl | 0.076 | 0.105 | 0.089 | 0.097 | 0.118 | 0.102 | 0.103 | 0.127 | 0.134 | 0.138 |
| -O=F+Cl | 0.313 | 0.294 | 0.313 | 0.298 | 0.263 | 0.287 | 0.302 | 0.321 | 0.292 | 0.317 |
| Total | 95.15 | 95.46 | 95.80 | 95.85 | 94.96 | 96.44 | 96.11 | 94.69 | 94.75 | 96.10 |
| H ₂ O ^c | 3.63 | 3.63 | 3.64 | 3.64 | 3.64 | 3.69 | 3.65 | 3.57 | 3.59 | 3.63 |
| Total _{calc} | 98.78 | 99.08 | 99.44 | 99.49 | 98.60 | 100.12 | 99.76 | 98.26 | 98.34 | 99.73 |
| Mg# ^d | 0.581 | 0.555 | 0.573 | 0.539 | 0.543 | 0.541 | 0.541 | 0.540 | 0.514 | 0.530 |
| Cations based on 22 oxygen atoms | | | | | | | | | | |
| Si | 5.65 | 5.58 | 5.60 | 5.60 | 5.60 | 5.65 | 5.65 | 5.66 | 5.61 | 5.68 |
| [⁴]Al | 2.35 | 2.42 | 2.40 | 2.40 | 2.40 | 2.35 | 2.35 | 2.34 | 2.39 | 2.32 |
| [⁶]Al | 0.14 | 0.07 | 0.12 | 0.04 | 0.04 | 0.10 | 0.09 | 0.15 | 0.10 | 0.09 |
| Ti | 0.35 | 0.42 | 0.35 | 0.50 | 0.46 | 0.45 | 0.45 | 0.37 | 0.47 | 0.40 |
| Mn | 0.03 | 0.03 | 0.03 | 0.03 | 0.03 | 0.03 | 0.02 | 0.03 | 0.03 | 0.03 |
| Mg | 2.99 | 2.84 | 2.98 | 2.72 | 2.78 | 2.73 | 2.73 | 2.74 | 2.59 | 2.70 |
| Fe ²⁺ | 2.15 | 2.28 | 2.22 | 2.32 | 2.34 | 2.32 | 2.32 | 2.33 | 2.45 | 2.40 |
| Na | 0.04 | 0.06 | 0.05 | 0.04 | 0.04 | 0.02 | 0.04 | 0.03 | 0.04 | 0.06 |
| K | 1.78 | 1.83 | 1.79 | 1.76 | 1.77 | 1.75 | 1.75 | 1.80 | 1.73 | 1.75 |
| Ca | 0.01 | 0.00 | 0.00 | 0.00 | 0.00 | 0.00 | 0.00 | 0.00 | 0.00 | 0.00 |
| sum cations | 15.48 | 15.53 | 15.53 | 15.41 | 15.47 | 15.40 | 15.41 | 15.46 | 15.40 | 15.43 |
| F | 0.33 | 0.31 | 0.33 | 0.31 | 0.27 | 0.30 | 0.31 | 0.33 | 0.30 | 0.32 |
| Cl | 0.02 | 0.03 | 0.02 | 0.02 | 0.03 | 0.03 | 0.03 | 0.03 | 0.03 | 0.04 |
| OH | 3.65 | 3.67 | 3.65 | 3.66 | 3.70 | 3.68 | 3.66 | 3.63 | 3.66 | 3.64 |
| log(F/OH) | -1.04 | -1.08 | -1.04 | -1.07 | -1.14 | -1.09 | -1.07 | -1.04 | -1.09 | -1.05 |
| log(Cl/OH) | -2.27 | -2.13 | -2.20 | -2.17 | -2.09 | -2.15 | -2.15 | -2.04 | -2.03 | -2.01 |

Supplementary Table III-3 continued

| Rock type ^a | CD | CD | CD | CD | CD | CD | CD | CD | CD | CD |
|--|-------|--------|-------|-------|-------|--------|-------|-------|-------|-------|
| Spot | 167 | 168 | 169 | 170 | a78 | a83 | a88 | a89 | a95 | a96 |
| Chemical composition (oxides wt%) ^e | | | | | | | | | | |
| SiO ₂ | 37.65 | 37.82 | 37.09 | 37.29 | 36.78 | 37.59 | 36.60 | 36.69 | 36.24 | 36.36 |
| Al ₂ O ₃ | 13.57 | 13.89 | 13.46 | 13.47 | 13.75 | 13.81 | 13.89 | 13.85 | 13.68 | 13.74 |
| TiO ₂ | 3.62 | 4.43 | 4.24 | 4.00 | 4.77 | 4.35 | 4.38 | 4.43 | 4.48 | 4.62 |
| FeO ^b | 18.27 | 18.72 | 18.11 | 18.00 | 18.37 | 18.12 | 18.62 | 18.56 | 17.47 | 17.55 |
| MnO | 0.19 | 0.22 | 0.22 | 0.19 | 0.22 | 0.17 | 0.21 | 0.23 | 0.26 | 0.24 |
| MgO | 12.67 | 11.58 | 12.11 | 11.86 | 12.10 | 12.44 | 11.68 | 11.38 | 12.44 | 12.09 |
| CaO | 0.01 | 0.04 | 0.02 | 0.01 | 0.04 | 0.02 | b.d.1 | 0.01 | b.d.1 | 0.01 |
| Na ₂ O | 0.07 | 0.17 | 0.14 | 0.11 | 0.19 | 0.13 | 0.10 | 0.11 | 0.15 | 0.10 |
| K ₂ O | 9.27 | 9.20 | 9.06 | 9.20 | 9.20 | 9.64 | 9.27 | 9.36 | 9.09 | 8.77 |
| F | 0.661 | 0.562 | 0.598 | 0.637 | 0.581 | 0.604 | 0.541 | 0.585 | 0.603 | 0.611 |
| Cl | 0.142 | 0.125 | 0.109 | 0.103 | 0.094 | 0.095 | 0.129 | 0.114 | 0.116 | 0.115 |
| -O=F+Cl | 0.310 | 0.265 | 0.276 | 0.291 | 0.266 | 0.276 | 0.257 | 0.272 | 0.280 | 0.283 |
| Total | 95.82 | 96.49 | 94.87 | 94.58 | 95.82 | 96.69 | 95.17 | 95.05 | 94.24 | 93.92 |
| H ₂ O ^c | 3.63 | 3.71 | 3.63 | 3.60 | 3.67 | 3.70 | 3.65 | 3.62 | 3.60 | 3.59 |
| Total _{calc} | 99.45 | 100.20 | 98.50 | 98.19 | 99.49 | 100.40 | 98.81 | 98.68 | 97.84 | 97.51 |
| Mg ^{#d} | 0.553 | 0.524 | 0.544 | 0.540 | 0.540 | 0.550 | 0.528 | 0.522 | 0.559 | 0.551 |
| Cations based on 22 oxygen atoms | | | | | | | | | | |
| Si | 5.66 | 5.66 | 5.64 | 5.68 | 5.55 | 5.61 | 5.57 | 5.59 | 5.55 | 5.57 |
| [⁴]Al | 2.34 | 2.34 | 2.36 | 2.32 | 2.45 | 2.39 | 2.43 | 2.41 | 2.45 | 2.43 |
| [⁶]Al | 0.07 | 0.11 | 0.05 | 0.10 | 0.00 | 0.04 | 0.07 | 0.08 | 0.01 | 0.05 |
| Ti | 0.41 | 0.50 | 0.49 | 0.46 | 0.54 | 0.49 | 0.50 | 0.51 | 0.52 | 0.53 |
| Mn | 0.02 | 0.03 | 0.03 | 0.02 | 0.03 | 0.02 | 0.03 | 0.03 | 0.03 | 0.03 |
| Mg | 2.84 | 2.58 | 2.74 | 2.69 | 2.72 | 2.77 | 2.65 | 2.59 | 2.84 | 2.76 |
| Fe ²⁺ | 2.30 | 2.34 | 2.30 | 2.29 | 2.32 | 2.26 | 2.37 | 2.37 | 2.24 | 2.25 |
| Na | 0.02 | 0.05 | 0.04 | 0.03 | 0.05 | 0.04 | 0.03 | 0.03 | 0.04 | 0.03 |
| K | 1.78 | 1.76 | 1.76 | 1.79 | 1.77 | 1.84 | 1.80 | 1.82 | 1.77 | 1.71 |
| Ca | 0.00 | 0.01 | 0.00 | 0.00 | 0.01 | 0.00 | 0.00 | 0.00 | 0.00 | 0.00 |
| sum cations | 15.45 | 15.37 | 15.41 | 15.39 | 15.44 | 15.46 | 15.45 | 15.43 | 15.45 | 15.37 |
| F | 0.31 | 0.27 | 0.29 | 0.31 | 0.28 | 0.29 | 0.26 | 0.28 | 0.29 | 0.30 |
| Cl | 0.04 | 0.03 | 0.03 | 0.03 | 0.02 | 0.02 | 0.03 | 0.03 | 0.03 | 0.03 |
| OH | 3.65 | 3.70 | 3.68 | 3.67 | 3.70 | 3.69 | 3.71 | 3.69 | 3.68 | 3.67 |
| log(F/OH) | -1.06 | -1.14 | -1.11 | -1.08 | -1.13 | -1.11 | -1.15 | -1.12 | -1.10 | -1.09 |
| log(Cl/OH) | -2.00 | -2.07 | -2.12 | -2.14 | -2.19 | -2.19 | -2.05 | -2.10 | -2.09 | -2.09 |

Supplementary Table III-3 continued

| Rock type ^a | CD | CD | CD | CD | CD |
|--|-------|--------|--------|--------|--------|
| Spot | a103 | a104 | a115 | a117 | a118 |
| Chemical composition (oxides wt%) ^e | | | | | |
| SiO ₂ | 36.84 | 36.97 | 37.85 | 37.44 | 37.53 |
| Al ₂ O ₃ | 14.09 | 14.06 | 13.94 | 14.08 | 13.85 |
| TiO ₂ | 4.11 | 3.94 | 3.48 | 4.24 | 3.92 |
| FeO ^b | 19.54 | 19.44 | 17.57 | 18.09 | 18.25 |
| MnO | 0.28 | 0.25 | 0.24 | 0.24 | 0.22 |
| MgO | 11.42 | 11.77 | 13.05 | 12.51 | 12.76 |
| CaO | b.d.1 | b.d.1 | 0.01 | 0.01 | b.d.1 |
| Na ₂ O | 0.08 | 0.11 | 0.05 | 0.07 | 0.11 |
| K ₂ O | 9.33 | 9.47 | 9.74 | 9.63 | 9.59 |
| F | 0.590 | 0.573 | 0.697 | 0.585 | 0.630 |
| Cl | 0.119 | 0.147 | 0.088 | 0.130 | 0.155 |
| -O=F+Cl | 0.275 | 0.274 | 0.313 | 0.276 | 0.300 |
| Total | 96.13 | 96.46 | 96.40 | 96.75 | 96.72 |
| H ₂ O ^c | 3.65 | 3.67 | 3.66 | 3.70 | 3.67 |
| Total _{calc} | 99.79 | 100.13 | 100.07 | 100.45 | 100.39 |
| Mg ^{#d} | 0.510 | 0.519 | 0.570 | 0.552 | 0.555 |
| Cations based on 22 oxygen atoms | | | | | |
| Si | 5.57 | 5.57 | 5.65 | 5.59 | 5.61 |
| [⁴]Al | 2.43 | 2.43 | 2.35 | 2.41 | 2.39 |
| [⁶]Al | 0.08 | 0.07 | 0.10 | 0.07 | 0.04 |
| Ti | 0.47 | 0.45 | 0.39 | 0.48 | 0.44 |
| Mn | 0.04 | 0.03 | 0.03 | 0.03 | 0.03 |
| Mg | 2.58 | 2.64 | 2.90 | 2.78 | 2.84 |
| Fe ²⁺ | 2.47 | 2.45 | 2.19 | 2.26 | 2.28 |
| Na | 0.02 | 0.03 | 0.01 | 0.02 | 0.03 |
| K | 1.80 | 1.82 | 1.85 | 1.83 | 1.83 |
| Ca | 0.00 | 0.00 | 0.00 | 0.00 | 0.00 |
| sum cations | 15.46 | 15.50 | 15.49 | 15.47 | 15.50 |
| F | 0.28 | 0.27 | 0.33 | 0.28 | 0.30 |
| Cl | 0.03 | 0.04 | 0.02 | 0.03 | 0.04 |
| OH | 3.69 | 3.69 | 3.65 | 3.69 | 3.66 |
| log(F/OH) | -1.12 | -1.13 | -1.05 | -1.13 | -1.09 |
| log(Cl/OH) | -2.08 | -1.99 | -2.22 | -2.05 | -1.97 |

Supplementary Table III-4 continued

| Rock type ^e | CD | CD | CD | CD | CD | CD | CD | CD | CD | CD | CD | CD | CD | CD | CD | CD | CD | CD | CD | CD |
|-------------------------------|-----------------------------------|-------|-------|-------|-------|-------|-------|--------|-------|-------|-------|-------|-------|--------|--------|-------|----|----|----|----|
| Spot | 68 | 72 | 79 | 97 | 62 | 74 | 75 | 78 | 81 | 84 | 86 | 88 | 92 | 94 | 105 | 113 | | | | |
| Group ^b | II | II | II | II | II | II | II | II | II | II | II | II | II | II | II | II | | | | |
| | Chemical composition (oxides wt%) | | | | | | | | | | | | | | | | | | | |
| P ₂ O ₅ | 40.99 | 40.97 | 41.56 | 40.87 | 41.67 | 41.02 | 41.35 | 41.72 | 40.89 | 41.02 | 41.05 | 40.53 | 41.85 | 42.07 | 41.55 | 41.55 | | | | |
| SiO ₂ | 0.43 | 0.21 | 0.13 | 0.31 | 0.19 | 0.18 | 0.18 | 0.20 | 0.31 | 0.28 | 0.17 | 0.22 | 0.16 | 0.22 | 0.25 | 0.21 | | | | |
| SO ₃ | 0.20 | 0.15 | 0.09 | 0.14 | 0.18 | 0.39 | 0.41 | 0.16 | 0.06 | 0.22 | 0.08 | 0.15 | 0.13 | 0.12 | 0.14 | 0.20 | | | | |
| CaO | 54.74 | 55.07 | 54.99 | 54.84 | 54.75 | 55.12 | 54.55 | 55.39 | 55.11 | 54.88 | 55.60 | 54.41 | 55.37 | 55.28 | 55.43 | 55.49 | | | | |
| MnO | 0.03 | 0.00 | 0.00 | 0.05 | 0.06 | 0.02 | 0.03 | 0.10 | 0.04 | 0.05 | 0.05 | 0.12 | 0.02 | 0.14 | 0.02 | 0.05 | | | | |
| FeO ^f | 0.36 | 0.09 | 0.00 | 0.08 | 0.21 | 0.10 | 0.13 | 0.12 | 0.06 | 0.24 | 0.03 | 0.25 | 0.10 | 0.14 | 0.51 | 0.02 | | | | |
| Na ₂ O | 0.02 | 0.01 | 0.04 | 0.00 | 0.11 | 0.12 | 0.09 | 0.09 | 0.00 | 0.08 | 0.00 | 0.07 | 0.03 | 0.01 | 0.02 | 0.01 | | | | |
| K ₂ O | 0.00 | 0.00 | 0.01 | 0.00 | 0.00 | 0.00 | 0.01 | 0.00 | 0.02 | 0.09 | 0.00 | 0.06 | 0.00 | 0.00 | 0.00 | 0.02 | | | | |
| F | 3.583 | 3.794 | 3.760 | 3.720 | 3.926 | 3.467 | 3.499 | 3.659 | 3.864 | 3.890 | 3.912 | 3.683 | 3.527 | 3.861 | 3.778 | 3.812 | | | | |
| Cl | 0.171 | 0.058 | 0.039 | 0.104 | 0.094 | 0.202 | 0.207 | 0.136 | 0.056 | 0.135 | 0.100 | 0.214 | 0.220 | 0.099 | 0.138 | 0.227 | | | | |
| -O=F+Cl | 1.55 | 1.61 | 1.59 | 1.59 | 1.67 | 1.51 | 1.52 | 1.57 | 1.64 | 1.67 | 1.67 | 1.60 | 1.53 | 1.65 | 1.62 | 1.66 | | | | |
| Total | 98.98 | 98.74 | 99.03 | 98.52 | 99.53 | 99.12 | 98.95 | 100.01 | 98.77 | 99.21 | 99.32 | 98.11 | 99.87 | 100.29 | 100.21 | 99.93 | | | | |
| H ₂ O ^f | 0.02 | -0.06 | -0.02 | -0.04 | -0.11 | 0.07 | 0.06 | 0.01 | -0.09 | -0.12 | -0.12 | -0.06 | 0.05 | -0.07 | -0.04 | -0.09 | | | | |
| Total _{calc} | 99.00 | 98.68 | 99.01 | 98.49 | 99.42 | 99.19 | 99.00 | 100.03 | 98.68 | 99.10 | 99.20 | 98.05 | 99.92 | 100.23 | 100.16 | 99.85 | | | | |
| | Cations based on 25 oxygen atoms | | | | | | | | | | | | | | | | | | | |
| Ca | 9.97 | 10.07 | 9.99 | 10.04 | 9.91 | 10.02 | 9.91 | 9.98 | 10.08 | 10.00 | 10.13 | 10.03 | 9.98 | 9.92 | 9.99 | 10.02 | | | | |
| Mn | 0.00 | 0.00 | 0.00 | 0.01 | 0.01 | 0.00 | 0.00 | 0.01 | 0.01 | 0.01 | 0.01 | 0.02 | 0.00 | 0.02 | 0.00 | 0.01 | | | | |
| Fe | 0.05 | 0.01 | 0.00 | 0.01 | 0.03 | 0.01 | 0.02 | 0.02 | 0.01 | 0.03 | 0.00 | 0.04 | 0.01 | 0.02 | 0.07 | 0.00 | | | | |
| Na | 0.01 | 0.00 | 0.01 | 0.00 | 0.04 | 0.04 | 0.03 | 0.03 | 0.00 | 0.03 | 0.00 | 0.02 | 0.01 | 0.00 | 0.01 | 0.00 | | | | |
| K | 0.00 | 0.00 | 0.00 | 0.00 | 0.00 | 0.00 | 0.00 | 0.00 | 0.00 | 0.02 | 0.00 | 0.01 | 0.00 | 0.00 | 0.00 | 0.00 | | | | |
| P | 5.90 | 5.92 | 5.97 | 5.91 | 5.96 | 5.89 | 5.93 | 5.94 | 5.91 | 5.90 | 5.91 | 5.91 | 5.96 | 5.97 | 5.92 | 5.93 | | | | |
| Si | 0.07 | 0.04 | 0.02 | 0.05 | 0.03 | 0.03 | 0.03 | 0.03 | 0.05 | 0.05 | 0.03 | 0.04 | 0.03 | 0.04 | 0.04 | 0.04 | | | | |
| S | 0.03 | 0.02 | 0.01 | 0.02 | 0.02 | 0.05 | 0.05 | 0.02 | 0.01 | 0.03 | 0.01 | 0.02 | 0.02 | 0.02 | 0.02 | 0.03 | | | | |
| sum cations | 16.03 | 16.05 | 16.01 | 16.04 | 16.00 | 16.05 | 15.98 | 16.03 | 16.07 | 16.06 | 16.09 | 16.09 | 16.01 | 15.98 | 16.05 | 16.03 | | | | |
| X(FAp) | 0.96 | 1.02 | 1.01 | 1.01 | 1.05 | 0.93 | 0.94 | 0.97 | 1.04 | 1.05 | 1.05 | 1.00 | 0.94 | 1.02 | 1.01 | 1.02 | | | | |
| X(ClAp) | 0.02 | 0.01 | 0.01 | 0.02 | 0.01 | 0.03 | 0.03 | 0.02 | 0.01 | 0.02 | 0.01 | 0.03 | 0.03 | 0.01 | 0.02 | 0.03 | | | | |
| X(HAp) | 0.01 | -0.03 | -0.01 | -0.02 | -0.06 | 0.04 | 0.03 | 0.01 | -0.05 | -0.07 | -0.07 | -0.03 | 0.03 | -0.04 | -0.02 | -0.05 | | | | |

Supplementary Table III-4 continued

| Rock type ^a | CD | HG | HG | HG | HG | HG | HG | HG | HG | HG | HG | HG | HG | HG | HG | HG | HG | HG | HG | HG | HG | HG | HG | |
|-------------------------------|-----------------------------------|--------|--------|--------|-------|-------|-------|-------|-------|-------|-------|-------|-------|-------|--------|-------|----|----|----|----|----|----|----|--|
| Spot | 115 | 9 | 11 | 12 | 13 | 14 | 15 | 16 | 17 | 18 | 24 | 25 | 26 | 27 | 53 | 55 | | | | | | | | |
| Group ^b | II | II | II | II | II | II | II | II | II | II | II | II | II | II | II | II | II | II | II | II | II | II | II | |
| | Chemical composition (oxides wt%) | | | | | | | | | | | | | | | | | | | | | | | |
| P ₂ O ₅ | 41.60 | 41.78 | 42.06 | 41.88 | 41.38 | 42.06 | 41.57 | 41.78 | 41.00 | 41.79 | 41.33 | 41.40 | 41.22 | 41.22 | 41.97 | 41.69 | | | | | | | | |
| SiO ₂ | 0.24 | 0.11 | 0.08 | 0.12 | 0.13 | 0.15 | 0.13 | 0.09 | 0.11 | 0.14 | 0.10 | 0.11 | 0.13 | 0.05 | 0.11 | 0.12 | | | | | | | | |
| SO ₃ | 0.25 | 0.12 | 0.07 | 0.12 | 0.14 | 0.15 | 0.11 | 0.14 | 0.14 | 0.10 | 0.15 | 0.15 | 0.14 | 0.11 | 0.07 | 0.10 | | | | | | | | |
| CaO | 55.14 | 55.90 | 55.27 | 55.31 | 54.98 | 54.86 | 55.09 | 55.30 | 55.16 | 54.67 | 54.91 | 54.71 | 54.76 | 55.02 | 55.40 | 54.81 | | | | | | | | |
| MnO | 0.07 | 0.01 | 0.04 | 0.03 | 0.11 | 0.06 | 0.02 | 0.04 | 0.10 | 0.09 | 0.00 | 0.10 | 0.03 | 0.07 | 0.07 | 0.09 | | | | | | | | |
| FeO ^c | 0.00 | 0.13 | 0.18 | 0.11 | 0.04 | 0.14 | 0.10 | 0.12 | 0.13 | 0.17 | 0.53 | 0.35 | 0.42 | 0.26 | 0.00 | 0.21 | | | | | | | | |
| Na ₂ O | 0.05 | 0.03 | 0.03 | 0.07 | 0.01 | 0.02 | 0.07 | 0.04 | 0.04 | 0.04 | 0.00 | 0.03 | 0.05 | 0.03 | 0.00 | 0.02 | | | | | | | | |
| K ₂ O | 0.00 | 0.00 | 0.01 | 0.00 | 0.00 | 0.00 | 0.00 | 0.01 | 0.00 | 0.01 | 0.01 | 0.00 | 0.01 | 0.00 | 0.00 | 0.01 | | | | | | | | |
| F | 3.803 | 3.158 | 3.184 | 3.320 | 3.396 | 3.455 | 2.951 | 3.062 | 3.140 | 2.825 | 2.826 | 3.074 | 2.919 | 3.347 | 3.362 | 3.410 | | | | | | | | |
| Cl | 0.042 | 0.596 | 0.585 | 0.530 | 0.445 | 0.441 | 0.517 | 0.567 | 0.583 | 0.724 | 0.628 | 0.516 | 0.695 | 0.561 | 0.619 | 0.548 | | | | | | | | |
| -O=F+Cl | 1.61 | 1.46 | 1.47 | 1.52 | 1.53 | 1.55 | 1.36 | 1.42 | 1.45 | 1.35 | 1.33 | 1.41 | 1.39 | 1.54 | 1.56 | 1.56 | | | | | | | | |
| Total | 99.59 | 100.36 | 100.05 | 99.98 | 99.10 | 99.77 | 99.21 | 99.73 | 98.94 | 99.21 | 99.16 | 99.02 | 98.98 | 99.14 | 100.06 | 99.44 | | | | | | | | |
| H ₂ O ^d | -0.04 | 0.14 | 0.13 | 0.07 | 0.04 | 0.03 | 0.24 | 0.18 | 0.12 | 0.25 | 0.27 | 0.18 | 0.20 | 0.03 | 0.03 | 0.02 | | | | | | | | |
| Total ^{alc} | 99.55 | 100.50 | 100.17 | 100.06 | 99.14 | 99.80 | 99.45 | 99.91 | 99.06 | 99.46 | 99.43 | 99.20 | 99.18 | 99.17 | 100.09 | 99.45 | | | | | | | | |
| | Cations based on 25 oxygen atoms | | | | | | | | | | | | | | | | | | | | | | | |
| Ca | 9.96 | 10.05 | 9.95 | 9.97 | 10.00 | 9.89 | 9.99 | 9.99 | 10.08 | 9.91 | 9.98 | 9.96 | 9.98 | 10.03 | 9.98 | 9.94 | | | | | | | | |
| Mn | 0.01 | 0.00 | 0.01 | 0.00 | 0.02 | 0.01 | 0.00 | 0.01 | 0.01 | 0.01 | 0.00 | 0.01 | 0.00 | 0.01 | 0.01 | 0.01 | | | | | | | | |
| Fe | 0.00 | 0.02 | 0.03 | 0.02 | 0.01 | 0.02 | 0.01 | 0.02 | 0.02 | 0.02 | 0.07 | 0.05 | 0.06 | 0.04 | 0.00 | 0.03 | | | | | | | | |
| Na | 0.02 | 0.01 | 0.01 | 0.02 | 0.00 | 0.01 | 0.02 | 0.01 | 0.01 | 0.01 | 0.00 | 0.01 | 0.02 | 0.01 | 0.00 | 0.01 | | | | | | | | |
| K | 0.00 | 0.00 | 0.00 | 0.00 | 0.00 | 0.00 | 0.00 | 0.00 | 0.00 | 0.00 | 0.00 | 0.00 | 0.00 | 0.00 | 0.00 | 0.00 | | | | | | | | |
| P | 5.94 | 5.94 | 5.98 | 5.96 | 5.95 | 5.99 | 5.96 | 5.96 | 5.92 | 5.98 | 5.94 | 5.95 | 5.94 | 5.94 | 5.98 | 5.97 | | | | | | | | |
| Si | 0.04 | 0.02 | 0.01 | 0.02 | 0.02 | 0.03 | 0.02 | 0.02 | 0.02 | 0.02 | 0.02 | 0.02 | 0.02 | 0.02 | 0.02 | 0.02 | | | | | | | | |
| S | 0.03 | 0.01 | 0.01 | 0.02 | 0.02 | 0.02 | 0.01 | 0.02 | 0.02 | 0.01 | 0.02 | 0.02 | 0.02 | 0.02 | 0.01 | 0.01 | | | | | | | | |
| sum cations | 16.00 | 16.05 | 16.00 | 16.01 | 16.02 | 15.95 | 16.03 | 16.02 | 16.08 | 15.98 | 16.04 | 16.02 | 16.04 | 16.06 | 16.00 | 16.00 | | | | | | | | |
| X(FAp) | 1.01 | 0.84 | 0.85 | 0.88 | 0.91 | 0.92 | 0.79 | 0.82 | 0.85 | 0.76 | 0.76 | 0.83 | 0.79 | 0.90 | 0.89 | 0.91 | | | | | | | | |
| X(ClAp) | 0.01 | 0.08 | 0.08 | 0.08 | 0.06 | 0.06 | 0.07 | 0.08 | 0.08 | 0.10 | 0.09 | 0.07 | 0.10 | 0.08 | 0.09 | 0.08 | | | | | | | | |
| X(HAp) | -0.02 | 0.08 | 0.07 | 0.04 | 0.02 | 0.02 | 0.14 | 0.10 | 0.07 | 0.14 | 0.15 | 0.10 | 0.11 | 0.02 | 0.02 | 0.01 | | | | | | | | |

Supplementary Table III-4 continued

| Rock type ^a | HG | HG | HG | HG | HG | HG | HG | HG | HG | HG | HG | HG | HG | HG | HG | HG | HG | HG |
|-----------------------------------|-------|-------|-------|-------|-------|-------|-------|-------|-------|-------|----|----|----|----|----|----|----|----|
| Spot | 117 | 118 | 119 | 120 | 121 | 136 | 137 | 138 | 139 | 140 | | | | | | | | |
| Group ^b | II | II | II | II | II | II | II | II | II | II | II | II | II | II | II | II | II | II |
| Chemical composition (oxides wt%) | | | | | | | | | | | | | | | | | | |
| P ₂ O ₅ | 41.65 | 41.53 | 41.10 | 41.01 | 41.36 | 41.63 | 41.15 | 41.28 | 41.87 | 41.85 | | | | | | | | |
| SiO ₂ | 0.09 | 0.13 | 0.11 | 0.12 | 0.10 | 0.09 | 0.11 | 0.10 | 0.11 | 0.10 | | | | | | | | |
| SO ₃ | 0.12 | 0.09 | 0.10 | 0.09 | 0.03 | 0.12 | 0.12 | 0.08 | 0.07 | 0.10 | | | | | | | | |
| CaO | 55.24 | 54.68 | 54.99 | 54.87 | 54.67 | 54.59 | 54.74 | 54.64 | 54.69 | 54.88 | | | | | | | | |
| MnO | 0.08 | 0.12 | 0.08 | 0.08 | 0.05 | 0.04 | 0.20 | 0.00 | 0.08 | 0.06 | | | | | | | | |
| FeO ^c | 0.10 | 0.04 | 0.06 | 0.06 | 0.12 | 0.05 | 0.10 | 0.04 | 0.09 | 0.00 | | | | | | | | |
| Na ₂ O | 0.04 | 0.02 | 0.04 | 0.05 | 0.00 | 0.04 | 0.05 | 0.03 | 0.00 | 0.01 | | | | | | | | |
| K ₂ O | 0.01 | 0.00 | 0.00 | 0.01 | 0.00 | 0.00 | 0.01 | 0.01 | 0.01 | 0.02 | | | | | | | | |
| F | 3.282 | 3.299 | 3.328 | 2.951 | 3.278 | 3.002 | 2.990 | 3.053 | 3.049 | 3.001 | | | | | | | | |
| Cl | 0.546 | 0.466 | 0.418 | 0.651 | 0.534 | 0.685 | 0.583 | 0.619 | 0.588 | 0.578 | | | | | | | | |
| -O=F+Cl | 1.51 | 1.49 | 1.50 | 1.39 | 1.50 | 1.42 | 1.39 | 1.43 | 1.42 | 1.39 | | | | | | | | |
| Total | 99.65 | 98.88 | 98.73 | 98.50 | 98.65 | 98.83 | 98.66 | 98.44 | 99.17 | 99.21 | | | | | | | | |
| H ₂ O ^d | 0.08 | 0.08 | 0.07 | 0.19 | 0.07 | 0.17 | 0.19 | 0.15 | 0.18 | 0.20 | | | | | | | | |
| Total _{calc} | 99.73 | 98.96 | 98.81 | 98.69 | 98.72 | 98.99 | 98.85 | 98.59 | 99.34 | 99.41 | | | | | | | | |
| Cations based on 25 oxygen atoms | | | | | | | | | | | | | | | | | | |
| Ca | 10.00 | 9.96 | 10.05 | 10.05 | 9.99 | 9.94 | 10.01 | 10.00 | 9.91 | 9.94 | | | | | | | | |
| Mn | 0.01 | 0.02 | 0.01 | 0.01 | 0.01 | 0.01 | 0.03 | 0.00 | 0.01 | 0.01 | | | | | | | | |
| Fe | 0.01 | 0.01 | 0.01 | 0.01 | 0.02 | 0.01 | 0.01 | 0.01 | 0.01 | 0.00 | | | | | | | | |
| Na | 0.01 | 0.01 | 0.01 | 0.02 | 0.00 | 0.01 | 0.02 | 0.01 | 0.00 | 0.00 | | | | | | | | |
| K | 0.00 | 0.00 | 0.00 | 0.00 | 0.00 | 0.00 | 0.00 | 0.00 | 0.00 | 0.00 | | | | | | | | |
| P | 5.96 | 5.97 | 5.94 | 5.94 | 5.97 | 5.99 | 5.94 | 5.97 | 6.00 | 5.99 | | | | | | | | |
| Si | 0.01 | 0.02 | 0.02 | 0.02 | 0.02 | 0.02 | 0.02 | 0.02 | 0.02 | 0.02 | | | | | | | | |
| S | 0.02 | 0.01 | 0.01 | 0.01 | 0.00 | 0.01 | 0.02 | 0.01 | 0.01 | 0.01 | | | | | | | | |
| sum cations | 16.03 | 16.00 | 16.06 | 16.06 | 16.01 | 15.98 | 16.04 | 16.01 | 15.97 | 15.98 | | | | | | | | |
| X(FAp) | 0.88 | 0.89 | 0.90 | 0.80 | 0.88 | 0.81 | 0.81 | 0.82 | 0.82 | 0.80 | | | | | | | | |
| X(ClAp) | 0.08 | 0.07 | 0.06 | 0.09 | 0.08 | 0.10 | 0.08 | 0.09 | 0.08 | 0.08 | | | | | | | | |
| X(HAp) | 0.04 | 0.05 | 0.04 | 0.11 | 0.04 | 0.09 | 0.11 | 0.09 | 0.10 | 0.11 | | | | | | | | |

Supplementary Table III-5 Summary of estimation of C_K/C_{Na} in melts*

| Rock | Bulk Comp. ** | | Orthopyroxene† | | Clinopyroxene | | Plagioclase | | Amphibole | | Melt | | C_K/C_{Na} | | | | |
|------|---------------|---------|----------------|---------|---------------|--------|-------------|---------|-----------|---------|-------|--------|--------------|---------|-----|-----|------|
| | K_2O | Na_2O | K_2O | Na_2O | Prop. ‡ | K_2O | Na_2O | Prop. § | K_2O | Na_2O | Prop. | K_2O | | Na_2O | | | |
| GN | 2.14 | 3.24 | 0.00 | 0.00 | 12 | 0.00 | 0.40 | 14 | 0.30 | 6.00 | 25 | 0.85 | 0.50 | 1 | 4.3 | 3.5 | 0.80 |
| PD | 1.86 | 3.40 | 0.00 | 0.00 | 10 | 0.02 | 0.40 | 6 | 0.16 | 6.20 | 25 | 0.21 | 0.04 | 2 | 3.2 | 3.2 | 0.65 |
| CD | 2.52 | 3.63 | – | – | – | 0.02 | 0.40 | 4 | 0.16 | 6.20 | 20 | 1.21 | 0.61 | 18 | 3.9 | 3.9 | 0.65 |

* The melts are supposed to have been equilibrated with biotites, and are estimated by subtracting the minerals phases which crystallized prior to biotite from the bulk rock composition; compositions are in wt%;

** Bulk compositions are unpublished data of the authors;

† Compositions of orthopyroxene, clinopyroxene, plagioclase and amphibole are average values;

‡ Proportions of minerals are derived from point counting (wt%, also see Supplementary Table III-1);

§ Half of total plagioclase is supposed to have crystallized prior to biotite

Curriculum Vitae

LEBENS LAUF

Name: Chao Zhang
Birth: 09/Feb/1982, in Zhenjiang (Jiangsu Province, PR China)

Contact

Institut für Mineralogie
Callinstr. 3
30167 Hannover
Phone: +49 (0)511 762-5517
Fax: +49 (0) 511 762-3045
Email: c.zhang@mineralogie.uni-hannover.de

Education

| | |
|-------------------|---|
| 2008/10 – 2012/04 | Doctor study in Petrology, Institut für Mineralogie, Gottfried Wilhelm Leibniz Universität Hannover (Germany) |
| 2004/09 – 2008/09 | Master study in Petrology, Faculty of Earth Sciences, China University of Geosciences (China) |
| 2000/09 – 2004/06 | Bachelor study in Geology, Faculty of Earth Sciences, China University of Geosciences (China) |

Research interest

- (1) Petrogenesis of granite and related crust-derived magmas
- (2) Migmatite and crustal anatexis
- (3) Partition of F and Cl between minerals, melt and fluid and their variation with magmatic evolution
- (4) Physicochemical properties of pre-eruption magmas and eruption mechanisms of volcanoes
- (5) Mesozoic magmatism and tectonic transformation in eastern China

Laboratory experience

EPMA, XRF, XRD, Raman, TIMS, LA-ICP-MS, LA-MC-ICP-MS, SHRIMP

Computer skill

Geological applications: Theriak-Domino, Perple_X, QUILF, MELTS, Comagmat, Pele, Minpet
Mathematical applications: Origin, Mathematica
Graphical applications: CorelDraw, Surfer, Grapher, ImageJ

Conference and workshop

2011 Goldschmidt Conference, Prague (Czech)
2011 Sulfur in Magmas and Melts, Workshop of Mineralogical Society of America, Goslar (Germany)
2007 National Symposium on Petrology and Geodynamics, Wuhan (China)

Language skill

Chinese – native tongue
English – fluent
German – basic

Award and scholarship

| | |
|------|--|
| 2004 | Outstanding Bachelor Thesis (granted by Hubei Province Education Department) |
| 2008 | Oversea Graduate Student Scholarship (granted by China Scholarship Council) |
| 2011 | Outstanding PhD Student Research Fund (granted by China University of Geosciences) |
| 2011 | Doktorabschluss Stipendium (granted by DAAD) |

Journal publication

- Zhang C**, Holtz F, Ma C, Wolff P E, Li X. 2012. Tracing the evolution and distribution of F and Cl in plutonic systems from volatile-bearing minerals: A case study from the Liujiawa pluton (Dabie orogen, China). *Contributions to Mineralogy and Petrology*, acceptable after minor revision
- Zhang C**, Ma C, Holtz F. 2012. Partial melting of hydrous continental lower crust: discussion on the petrogenesis of C-type adakites from the Dabie orogen. *Geological Journal of China Universities*, 18(1), in press (in Chinese with English abstract)
- Zhang C**, Ma C, Liao Q, Zhang J, She Z. 2011. Implications of subduction and subduction zone migration of the Paleo-Pacific Plate beneath eastern North China, based on distribution, geochronology, and geochemistry of Late Mesozoic volcanic rocks. *International Journal of Earth Sciences*, 100, 1665–1684
- Zhang C**, Ma C, Holtz F. 2011. "Origin of high-Mg adakitic magmatic enclaves from the Meichuan pluton, southern Dabie orogen (central China): Implications for delamination of the lower continental crust and melt-mantle interaction"-Reply. *Lithos*, 125, 839–844
- Zhang C**, Ma C, Holtz F. 2010. Origin of high-Mg adakitic magmatic enclaves from the Meichuan pluton, southern Dabie orogen (central China): Implications for delamination of the lower continental crust and melt-mantle interaction. *Lithos*, 119, 467–484
- Zhang C**, Ma C, Liao Q, Zhang J, Xiao D, Fu L, Wang L. 2009. Geochemistry of Late Mesozoic-Cenozoic volcanic rocks in the Huanghua depression, Bohai Bay: Petrogenesis and implications for tectonic transition. *Acta Petrologica Sinica*, 25(5), 1159–1177 (in Chinese with English abstract)
- Zhang C**, Ma C. 2008. Large-scale Late Mesozoic magmatism in the Dabie Mountain: Constraints from zircon U-Pb dating and Hf isotopes. *Journal of Mineralogy and Petrology*, 28(4), 71–79 (in Chinese with English abstract)
- Zhang C**, Ma C, She Z, Yin K. 2005. Volcanic ash in the clay rocks from upper Shaximiao formation of middle Jurassic, Northeast of Sichuan Basin: evidence from petrology, mineralogy and geochemistry. *Geological Journal of China Universities*, 11(3), 415–424 (in Chinese with English abstract)
- Chen L, Ma C, Zhang J, Mason R, **Zhang C**. 2011. Mafic dykes derived from Early Cretaceous depleted mantle beneath the Dabie orogenic belt: implications for changing lithosphere mantle beneath eastern China. *Geological Journal*, 46, 333–343
- Ding L, Ma C, Li J, Robinson P, Deng X, **Zhang C**, Xu W. 2011. Timing and genesis of the adakitic and shoshonitic intrusions in the Laoniushan complex, southern margin of the North China Craton: Implications for post-collisional magmatism associated with the Qinling Orogen. *Lithos*, 126, 212–232
- Sun Y, Ma C, **Zhang C**. 2011. Geochemistry, zircon geochronology and Hf isotopes of Lujiazhai granites from the Dabie Orogen: Evidence for the Neoproterozoic magmatism along the northeastern margin of Yangtze Block. *Earth Science Frontiers*, 18(2), 85–99 (in Chinese with English abstract)
- Chen L, Ma C, She Z, Mason R, Zhang J, **Zhang C**. 2009. Petrogenesis and tectonic implications of A-type granites in the Dabie orogenic belt, China: geochronological and geochemical constraints. *Geological Magazine*, 146(5), 638–651
- Liu Y, Ma C, **Zhang C**, Shen Z, Zhang J. 2009. Petrogenesis of Yueshan pluton: Zircon U-Pb dating and Hf isotope evidence. *Geological Science and Technology Information*, 28(5), 22–30 (in Chinese with English abstract)
- Wang L, Ma C, Zhang J, Chen L, **Zhang C**. 2008. Petrological and geochemical characteristics and petrogenesis of the Early Cretaceous Taohuashan-Xiaomoshan granites in northeastern Hunan Province. *Geological Journal of China Universities*, 14(3), 334–349 (in Chinese with English abstract)
- Jian W, Yin K, Luo C, Yao L, **Zhang C**. 2008. Slip zone characteristics of Anlesi Landslide in Wanzhou of Three Gorges Reservoir area. *Earth Science*, 33(5), 672–678 (in Chinese with English abstract)
- Ma C, Shen Z, Zhang J, **Zhang C**. 2006. Crustal roots, orogenic heat and magmatism. *Earth Science Frontiers*, 13(2), 130–139 (in Chinese with English abstract)
- Tao J, **Zhang C**, Ma C, Yang K, Zhou H. 2006. Geochemistry and petrogenesis of Cretaceous high Sr and low Y granitoids pluton in Fangshan Area, Beijing. *Geological Science and Technology Information*, 25(2), 11–18 (in Chinese with English abstract)
- Jian W, Yin K, Ma C, Liu L, **Zhang C**. 2005. Characteristics of incompetent beds in Jurassic red clastic rocks in Wanzhou. *Rocks and Soil Mechanics*, 26(6), 901–914 (in Chinese with English abstract)

Conference abstract

- Zhang C**, Holtz F, Ma C. 2011. Hydration crystallization process in mafic-felsic mixing magmatic system: A case study from the Dabie orogen (East-central China). *Mineralogical Magazine*, 75, 2249 (Goldschmidt 2011, Prague)
- Zhang C**, Ma C, Holtz F, Wolff P E, Li X. 2011. Tracing the evolution and distribution of F and Cl in plutonic systems from volatile-bearing minerals: A case study from the Liujiawa pluton (Dabie orogen, China). Workshop (Mineralogical Society of America): Sulfur in Magmas and Melts. Goslar (Germany), August 20–24, 2011
- Zhang C**, Ma C. 2008. Framework of Mesozoic magmatism and crust-mantle interaction in the Dabie Mountain and middle-lower Yangtze River belt, central China. *Geochimica et Cosmochimica Acta*, 72(12S), A1077 (Goldschmidt 2008, Vancouver)
- Zhang C**, Ma C, Liao Q. 2007. Geochemistry of the Mesozoic-Cenozoic volcanic rocks in the Huanghua depression. 2007 National Symposium on Petrology and Geodynamics, Wuhan, China (in Chinese)
- Zhang C**, Ma C. 2006. The Late Mesozoic tectono-magmatic event in the Luotian dome, central Dabie orogen. 2006 National Symposium on Petrology and Geodynamics, Nanjing, China (in Chinese)